



HAL
open science

Combinatorial diversity of two-pore-domain k^+ channels and its involvement in migraine

Perrine Royal

► **To cite this version:**

Perrine Royal. Combinatorial diversity of two-pore-domain k^+ channels and its involvement in migraine. Molecular biology. Université Côte d'Azur, 2018. English. NNT: 2018AZUR4114. tel-02177132

HAL Id: tel-02177132

<https://theses.hal.science/tel-02177132>

Submitted on 8 Jul 2019

HAL is a multi-disciplinary open access archive for the deposit and dissemination of scientific research documents, whether they are published or not. The documents may come from teaching and research institutions in France or abroad, or from public or private research centers.

L'archive ouverte pluridisciplinaire **HAL**, est destinée au dépôt et à la diffusion de documents scientifiques de niveau recherche, publiés ou non, émanant des établissements d'enseignement et de recherche français ou étrangers, des laboratoires publics ou privés.

THÈSE DE DOCTORAT

La diversité combinatoire des canaux
potassiques à deux domaines pore et son
implication dans la migraine

Perrine ROYAL

Institut de Biologie de Valrose

**Présentée en vue de l'obtention
du grade de docteur en Sciences de la vie
d'Université Côte d'Azur**
Dirigée par : Guillaume Sandoz
Soutenue le : 17 décembre 2018

Devant le jury, composé de :
Michel Fink, PhD, Cisbio Bioassays
Michel Lazdunski, Pr., IPMC
Florian Lesage, PhD, IPMC
Pierre Paoletti, PhD, IBENS
Guillaume Sandoz, PhD, iBV
Stephen Tucker, Pr., Université d'Oxford
Michel Vivaudou, PhD, IBS

LA DIVERSITÉ COMBINATOIRE DES CANAUX POTASSIQUES À DEUX DOMAINES PORE ET SON IMPLICATION DANS LA MIGRAINE

Jury

Président du jury

Pr. Michel LAZDUNSKI, Professeur, IPMC

Rapporteurs

Pr. Stephan TUCKER, Professeur in Biophysics, University of Oxford

Dr Michel VIVAUDOU, DR, IBS

Examineurs

Dr Michel FINK, Scientific Content Manager, Cisbio Bioassays

Dr Florian LESAGE, DR & Directeur adjoint, IPMC

Dr Pierre PAOLETTI, DR & Directeur du département de Biologie, ENS



LA DIVERSITÉ COMBINATOIRE DES CANAUX POTASSIQUES À DEUX DOMAINES PORE ET SON IMPLICATION DANS LA MIGRAINE

Résumé

Le maintien d'un potentiel de membrane de repos négatif est à la base de l'excitabilité neuronale. Ce potentiel négatif est généré par un courant de fuite de potassium induit par les canaux potassiques à deux domaines pore (K_{2P}). Ils se sont révélés impliqués dans de nombreux mécanismes physiologiques et physiopathologiques tels que la dépression, la neuroprotection contre les ischémies, l'anesthésie, la migraine et la perception de la douleur. L'hétéromultimérisation est un mécanisme couramment utilisé dans la nature pour augmenter la diversité fonctionnelle des complexes protéiques. Par exemple, avec 15 gènes classés en 6 sous-familles, les canaux K_{2P} pourraient générer 120 combinaisons et, en théorie, chacune d'elles posséderait des caractéristiques bien distinctes. Ici, nous avons d'abord étudié la capacité des membres de la même sous-famille K_{2P} (sous-famille TREK) à s'assembler pour former des hétéromères fonctionnels dotés de nouvelles propriétés. En alliant l'optopharmacologie, une technique de précipitation de molécules uniques (SiMPull) et une technique de co-localisation à l'échelle de la molécule unique à la membrane plasmique, nous avons déterminé l'existence ainsi que la stœchiométrie des complexes créés entre TREK1, TREK2 et TRAAK. Nous avons caractérisé fonctionnellement les hétérodimères et avons constaté qu'ils formaient tous des canaux sélectifs au potassium rectifiant vers l'extérieur avec une sensibilité à la tension et aux pH variables. Ayant constaté que l'hétéromérisation est possible dans la même sous-famille, nous nous demandons si cela peut être fait entre membres de familles différentes et quelles pourraient en être les conséquences pathophysiologiques. Nous avons trouvé que TREK1 et TREK2 sont capable d'hétéromériser avec le canal plus distant TRESK, un canal K_{2P} impliqué dans la migraine. Chez l'homme, la mutation TRESK-MT, une délétion de 2 paires de base (F139WfsX24) qui induit la formation de TRESK-MT1, un dominant négatif de TRESK, a été corrélé à la migraine. De manière surprenante, nous avons découvert que cette délétion induit un site alternatif de traduction (fsATI), menant à la formation d'un second fragment de TRESK, TRESK-MT2 qui s'assemble spécifiquement avec TREK1 et TREK2. Cet assemblage induit l'extinction des courants TREK, ce qui va augmenter l'excitabilité des neurones trijumeaux, une composante clé dans l'induction

de la migraine, à l'origine du phénotype migraineux observé. Ensemble, ces résultats démontrent que l'hétéromérisation des canaux K_{2P} n'est pas rare et doit être considérée pour comprendre leurs fonctions pathophysiologiques. Enfin, les analyses génétiques des mutations liées à des pathologies devraient désormais prendre en compte les fsATI.

Mots-clefs : canaux potassiques, hétéromérisation, SiMPull, migraine, fsATI

COMBINATORIAL DIVERSITY OF TWO-PORE-DOMAIN K^+ CHANNELS AND ITS INVOLVEMENT IN MIGRAINE

Abstract

Maintenance of a negative resting membrane potential underlies the basis of neuronal excitability. This negative potential is generated by a potassium leak current mediated by two-pore-domain potassium channels (K_{2P}). Over the years, they have been shown to be involved in many physiological and pathophysiological mechanisms such as depression, neuroprotection, anesthesia, migraine and pain perception. Heteromultimerization is a mechanism commonly used to increase the functional diversity of protein complexes. For example, with 15 genes classified in 6 subfamilies, the K_{2P} channel family can potentially generate 120 combinations and, in theory, each of them would show different functional properties. Here, we first investigated the ability of the members from the same K_{2P} subfamily (TREK subfamily) to assemble and form functional heteromeric channels with novel properties. Using single molecule pulldown (SiMPull) from HEK cell lysates, subunit counting in the plasma membrane of living cells and opto-pharmacology, we show that the TREK channel members TREK1, TREK2, and TRAAK readily co-assemble. We functionally characterized the heterodimers and found that all combinations form outwardly rectifying potassium-selective channels but with variable voltage sensitivity and pH regulation. Having found that heteromerization is possible within the same subfamily we wonder if it can happen between members from different subfamilies with lower sequence homology and what could be the pathophysiological consequences. We found that TREK1 and TREK2 are able to heterodimerize with the distantly-related TRESK, a two-pore-domain K^+ channel implicated in migraine. Notably, in humans, TRESK-MT, a 2 bp



frameshift mutation (F139WfsX24), which induced the formation of TRESK-MT1 a dominant negative for TRESK, was found to perfectly segregate with typical migraine in a large pedigree. Strikingly, we found that the 2 bp frameshift mutation induced an alternative translation initiation (fsATI) which leads to the translation of a second TRESK fragment, termed TRESK-MT2. We show that by co-assembling with and inhibiting TREK1 and TREK2, TRESK-MT2 increases trigeminal sensory neuron excitability, a key component of migraine induction, leading to a migraine-like phenotype. Together these findings demonstrate that K_{2P} heteromerization is not rare and needs to be considered to understand their pathophysiological functions and that genetic analysis of disease-related mutations should consider fsATI as a distinct class of mutations.

Key words: potassium channels, heteromerization, SiMPull, migraine, fsATI

Table des matières

Résumé	3
Abstract	4
Thanks	9
Abbreviations	13
Illustrations	16
Tables	17
Equation	17
I. Introduction	18
A. The resting membrane potential	18
B. Potassium channels: structure and function	19
1. The pore	20
2. Voltage-gated potassium channels	22
3. Inwardly rectifying potassium channels	27
4. K_{2P} channels	28
5. Gating	29
C. K_{2P} channels family	33
1. Generalities	34
2. Electrophysiological properties	34
3. Structure	35
4. Up and down state and opening mechanism	37
5. TWIK family	39
6. TASK family	41
7. THIK family	43
8. TALK family	44
9. TREK family	44
10. TRESK CHANNEL	54
D. K_{2P} channels and pain perception	58
E. Pathophysiology of migraine	64
1. Generalities	64
2. Anatomy of the trigeminovascular pain pathway	65
3. Activation and sensitization of the trigeminovascular pathway	67
4. Aura	70
5. Channel dysfunction in migraine	71
6. Roles for signal molecules and receptors in trigeminal ganglia	78
7. Treatments	81

F.	Alternative translation initiation.....	82
	Another mechanism resulting in two proteins translated from one mRNA	85
G.	Heteromerization and subunits assembly.....	85
	1. How heteromerization occurs.....	86
	2. K_{2P} heteromerization	88
II.	Problematics.....	92
III.	Material and methods	93
	A. Molecular Biology	93
	B. Immunocytochemistry.....	93
	C. Western Blot.....	93
	D. SiMPull assay (adapted from Jain et al., 2012)	94
	1. Principle	94
	2. Surface passivation and construction of flow chambers.....	94
	3. Sample preparation.....	94
	4. Antibody immobilization.....	95
	5. Single molecule imaging and spot counting	95
	E. Subunit counting with <i>X. laevis</i> Oocytes.....	95
	F. Neuron extraction	96
	G. Electrophysiology	96
	1. Oocytes.....	96
	2. HEK cells.....	97
	3. Neurons.....	97
	H. Behavior: Assessment of rodents allodynia.....	97
IV.	Article I.....	102
	A. Introduction.....	102
	Tools.....	102
	B. Article I: Heteromerization within the TREK channel subfamily produces a diverse family of highly regulated potassium channels.	103
	C. Discussion and conclusions	114
V.	Article II.....	115
	A. Introduction.....	115
	TREK-TRESK association, how the story started	115
	B. Article II: Migraine-associated TRESK mutations increase neuronal excitability through alternative translation initiation and inhibition of TREK	116
	C. Discussion and conclusions	172
VI.	Discussion	173
	A. Pathologies linked to K_{2P} heteromerization	173

1.	About the formation of heteromers.....	173
2.	Pathophysiological involvement of the heteromers	175
B.	Physiological implications of TRESK and TREKs as background K ⁺ channels ..	176
1.	Functional expression of TRESK and TREK1/TREK2 in TG neurons.....	176
2.	TREKs and TRESK involvement in pain sensation	176
C.	TREK channels to treat migraine.....	177
VII.	Perspectives	178
A.	Frameshift induced alternative translation initiation as a new mechanism for genetic diseases	178
1.	Database analysis of frameshift mutants.....	178
2.	KCNQ1	179
B.	SiMPull: toward an automatization	180
1.	Advantages of TIRF microscopy	180
2.	Transition from coverslips to beads.....	181
VIII.	Conclusions	183
IX.	Annexes.....	184
A.	Annex 1: Article	184
Ci-VSP stoichiometry and assembling.....	184	
B.	Annex 2: Patent.....	199
C.	Technical annex	239
Screening of protein-protein interaction's modulators.....	239	
X.	Bibliography.....	240

Thanks

I am really honored and would like to thank the Pr. Michel Lazdunski, to accept to preside my thesis committee. I would also like to thank the Pr. Stephen Tucker and Dr Michel Vivaudou to review my work and the Dr Michel Fink, Dr Florian Lesage and Dr Pierre Paoletti to examine my work. I am really impressed and happy to have all of you reunited in my thesis committee.

I will now thank all the people that surrounded me during my PhD, without whom I would never have reached the end. First of all, I will never be grateful enough to Dr. Guillaume Sandoz, who supervised my thesis. Since 2013 when we first met, starting from the ground, he always trusted me and we built a very strong relationship based on a lot of work, the will to go through everything, we started together and always succeed. He taught me so many things about electrophysiology, K_{2P} channels, but especially a way to analyze and to build scientific thinking. I would never have learned so many skills in another team. Dr. Guillaume Sandoz let me manipulated and innovated in the lab, as well as in other labs from Sophia-Antipolis to Spain. I don't have enough words to express how thankful I am.

I would also like to thank Brigitte Wdziekonski, our substitution mom in the lab. First for all the job you have done for me, from cells to molecular biology, as well as slides for single molecule pull down and product orders. Secondly for as the time you spend talking with me about life, will, carrier. You have always been here to support me, even in the worse times, thank you.

Thanks to the former members of the lab. Dr. Yannick Comoglio, you taught me a lot in the lab, all your skills and your knowledges about the containing of the fridges and chemicals cabinet. Dr Rayan Arant for the very interesting discussions we used to have. Dr. Thomas Besson especially for the train trips we were making together every day for few months.

A special thanks to Dr. Céline Nicolas, who not only taught me how to deal with the mice, but also helped me in some life decisions throughout my PhD. I wish we'll share some more of your home office days for lunch discussion! Arnaud, thank you for having been the best intern ever. You made me think about how to transfer my knowledges. Dr. Olena Butenko, it was a great pleasure to work with you for few months, and to show you some part of our beautiful country. Pablo, thanks for all the patience you

gave to me, thanks for all the time we spend out of the lab, talking about future, past and so much more. I am glad to have had the opportunity to work with you for two years, and I wish you the best for your PhD.

Thanks to all the members of the 4th floor for their smiles, nice words, skills and will they gave me at some point. Especially the youth, with whom I've been sharing more than good times in the lab. Anthony, Pierre, Raphaël and other PhD students and post-doc at the iBV, Torsten and Morgane among others.

A special thanks to another PhD student, Clément Verkest. Thank of you, I've been able to learn new skills with animals, and concretized the animal experimentation side of the article. You have been so patient with me, and very professional. I wish you the best for your carrier. Another PhD student in Spain, Alba Andrea, allowed me to work first on trigeminal neurons, then on infected rats, to finalize the article. We spent so many hours enclosed together with rats, thank you for your kindness and you determination.

Back to the iBV, I would like to thank the members of the imaging facility, Sebastien Schaub, who helped me to set the single molecule pulldown technique at first, then Magali Mondin, to have taught me how to use the spinning disk microscope. Sama Rekima, for the histology part, and thank to the sterilization team Santhi, Mouna and Dominique for the time you make us win.

Now I would like to thank to all the people who shared my weakly life for these three years. My friends, you have always been here, even the days when I was not in the best mood. You helped me to get through this PhD, with the smile. Marie, you were, you are, and will always be the best friend I will ever have. Nana, you were far, but the few times we saw each other were among the best during these years, you are in my soul. Remy, you supported me for so long, even in the worst days, you gave me many hopes and made me understand so much about me, I have no words to explain how grateful I will always be, you brought me a family of friends. My sister, Roxanne, I'm sorry for all the times where I could not come with you because I had to work , I swear, I will make some efforts now that everything is over. Dr. Titouan Royal, my brother, I'm so proud of you, thank for giving me the will to survive and reinforce me when we were younger!

One last thank for my Mom, you have been so patient, every days, you supported me, and you gave trust in me since the first days of school. I wish I could one day give you back all the feelings you gave me.

Pulvis et umbra sumus, Horace

Abbreviations

4-AP	4-aminopyridine
5-HT	Serotonin
AA	Arachidonic acid
ADP	Adenosine-di-phosphate
AKAP	A-kinase-anchoring protein
AMPA	α -amino-3-hydroxy-5-methylisoxazol-4-propionate receptor
AP	Action potential
ASIC	Acid-sensing ion channel
AT2R	Angiotensin receptor type II
ATI	Alternative translation initiation
ATP	Adenosine-tri-phosphate
cAMP	Cyclic adenosine monophosphate
Ca _v	Voltage-gated calcium channel
CGRP	Calcitonin gene related peptide
CNS	Central nervous system
COP1	Coatomerprotein complex 1
DAG	Diacylglycerol
DRG	Dorsal root ganglion
DRN	Dorsal raphe nucleus
FRET	Förster Resonance Energy Transfer
GABA	γ -aminobutyric acid
GFP	Green fluorescent protein
GHK	Goldman, Hodgkin and Huxley
GPCR	G protein coupled receptor
IsoK	Symmetric K ⁺ concentration
K2P	Two-pore-domain potassium channel
KCNE1	K ⁺ voltage-gated channel subfamily member E1
KI	Knock-in

KO	Knock-out
LPA	Lysophosphatidic acid
MAP2	Microtubule-associated protein 2
Nav	Voltage-gated sodium channel
NGF	Nerve growth factor
NK1R	Neurokinin 1 receptor
NMDA	N-Methyl D-Aspartate
NMDAR	N-methyl-D-aspartate
NO	Nitrous oxide
NSAID	Nonsteroidal anti-inflammatory drug
NTG	Nitroglycerin
P	Pore domain
P0	Open probability
PA	Phosphatidic acid
PD	Phosphatase domain
PGE2	Prostaglandine E2
pHext	Extracellular pH
pHint	Intracellular pH
PIP2	Phosphatidyl inositol diphosphate
PKA	Proteine kinase A
PKC	Proteine kinase C
PLC	Phospholipase C
PLD2	Phospholipase D2
PUFA	Polyunsaturated fatty acid
RNA	Ribonucleic acid
SiMPull	Single molecule pull down
SP	Substance P
SSRI	Serotonin selective reuptake inhibitor
TEA	Tetraethylammonium

TG	Trigeminal ganglion
TIRF	Total internal reflection fluorescence
TRP	Transient receptor potential channel
TTX	Tetrodotoxine
VSD	Voltage-sensing domain

Illustrations

Figure 1: Potassium channels structure	20
Figure 2: The transmembrane part of KcsA	22
Figure 3: BK channels and its auxiliary subunits are pivotal in neuronal excitability. 26	
Figure 4: IV curves and structure of Kir channels.....	28
Figure 5 : Structure and conformational change of the potassium channel.....	30
Figure 6: Cartoon model of K _{2P} 2.1 (TREK-1).	31
Figure 7: Dendrogram of the K _{2P} potassium channel family and their characteristic functional features.....	33
Figure 8: Background potassium currents described by the GHK equation.	35
Figure 9: Cartoon showing the topology of a two-pore-domain potassium channel K _{2P} and its assembly in dimer.....	36
Figure 10: The structure of K _{2P} -channels.	37
Figure 11: Cartoon model of TRAAK gating and mechanosensitivity.....	38
Figure 12: Up and down states of TREK2.....	39
Figure 13 : Differential distribution of mRNA coding for TASK-1 and TASK-3 in the rat CNS.....	42
Figure 14: TASK channels regulations.	42
Figure 15: Polymodal activation of TREK1 by physical and chemical stimuli.....	45
Figure 16: TREK1 is involved in the therapeutic effect of 5-HT reuptake inhibitors via a negative feedback induced on the serotonergic neurons	48
Figure 17: Top view of the extracellular side of homodimeric TREK1 (A) and TREK2 (B) channels.	51
Figure 18: Partners, regulatory domains and alternative variants of TREK1	53
Figure 19: Regulation of the TRESK channel by calcineurin and phosphorylations. 58	
Figure 20:TREK1 is involved in several polymodal pain perception.....	60
Figure 21: Lysophosphatidic acid (LPA) and two-pore-domain K (K _{2P}) channels. Representation of K _{2P} channels in the membrane.....	61
Figure 22: Migraine step by step	66
Figure 23: Pathways and brain regions involved in the transmission of migraine.	69
Figure 24: Diagram showing the various mechanisms involved in migraine at different sites in the nociceptive pathway	71
Figure 25: Functional roles of the proteins coded by known FHM genes within a glutamatergic synapse..	73
Figure 26: A schematic representation outlining some of the predicted mechanisms contributing to migraine pathogenesis.....	76
Figure 27: Schematic topology of the human TRESK subunits showing the position variants.....	77

Figure 28 : Main potential targets of currently utilized preventive drugs and those under-investigation for migraine..	81
Figure 29 : $K_{2P}2.1$ Channel may be inhibitory or excitatory, depending at which start codon translation is initiated.	84
Figure 30: Alternative translation start sites and variants of alternative open reading frames within eukaryotic mRNA.	84
Figure 31: Co-translational assembly of protein complexes	87
Figure 32: Schematic diagrams for passive conductance and $G_{\beta\gamma}$ -dependent glutamate release	90
Figure 33: Schematic diagram of the SiMPull principle of HA- $K_{2P}X$ with another K_{2P} subunit.	94
Figure 34: Electronic Von Frey aesthesiometer apparatus with the grid and plastic boxes.	99
Figure 35: Drawing of the mouse paw.	99
Figure 36: Procedure used for targeting rat trigeminal ganglia.	100
Figure 37: Cartoon of the subunit counting with <i>X. laevis</i> oocytes.	105
Figure 38: Interacting K_{2P} partners.	115
Figure 39: TREK1-PCS for functional heteromerization study.	115
Figure 40: MDCK cells expressing mCherry-KCNQ1del572-576-GFP.	179
Figure 41: Translation of a second protein is not at the origin of a dominant negative effect on KCNQ1.	180
Figure 42: Schematic representation of the SiMBeads.	182
Figure 43: Interaction with inhibitors can make a loss of fluorescent spots observed in SiMPull.	243

Tables

Table 1: Summary of studies investigating the effect of altered K^+ channel expression and function on acute, neuropathic, and inflammatory pain phenotypes.	63
Table 2: Heterodimers of two-pore-domain potassium (K_{2P}) channels	91

Equation

Equation de Nernst.	19
---------------------	----

I. Introduction

When the principal concepts of electrophysiology were developed (Hodgkin and Huxley, 1952), the importance of K^+ currents for cellular excitability has been revealed. Nevertheless, at this point, the molecular entities responsible for K^+ current through the membrane were not known. Ion channels are fundamental elements for the signalization in the nervous system. They generate electric signals in neurons, regulate neurotransmitters secretion and switch electric signals toward sensorial stimuli as nociceptive stimuli, to which neurons are submitted. Ion channels properties also are linked with long term modifications in signalization, at the origin of the nervous system plasticity.

During the last 40 years, new techniques such as electrophysiology, biochemistry and molecular biology made up a revolution in the study of these channels. In 1970, only few voltage sensitive ion channels were known, along with some neurotransmitters receptors. Nowadays the number of classified ion channels has been largely increased (more than 300). To understand the role of each of these channels in the body and more specifically in the nervous system, the study of their structure, their subcellular localization along with their electrophysiological and pharmacological properties is fundamental.

Nevertheless, among this diversity, principles have emerged. Thus, many channels are built on a same model, where they delimitate a central pore in which ions can get through the plasma membrane. Furthermore, we can sort these channels in families, in which we have a well describe model for the molecular structure and function.

A. The resting membrane potential

All prokaryote and eukaryote cells have plasma membranes. The plasma membrane (also known as the cell membrane) is the outermost cell surface, which separates the cell from the external environment. The plasma membrane is composed primarily of lipids, especially phospholipids, and proteins. The lipids occur in a bilayer. We observe, for each eukaryotic cell at rest in our body, a resting membrane potential (RMP) which is negative. This RMP can be explained by the difference of the unequal distribution of ions across the membrane and the relative permeability for the different ions. K^+ concentration being more important inside the cell, the situation for Na^+ , Ca^{2+}

is opposite. These gradients of concentration, are due to a differential membrane permeability for the different ions and their passive transport by diffusion. Their movement is motivated by the concentration and also, as ion is a charged particle, by the existence of a transmembrane electric field. Thus, for each ion specie, the equilibrium condition will not be obtained by equalization of concentrations as it is the case in the simple diffusion of a neutral solute, but is obtained by an electrochemical gradient across the membrane. The membrane potential for the equilibrium of an ion is given by the Nernst equation.

$$E_{ion} = \frac{R * T}{z * F} * Ln \frac{[ion]_{ext}}{[ion]_{int}}$$

Equation de Nersnt in which R is the universal gas constant: $R = 8.314472(15) \text{ J K}^{-1} \text{ mol}^{-1}$, T is the temperature in kelvin, F is the Faraday constant, the number of coulombs per mole of electrons: $F = 96\,485 \text{ C.mol}^{-1}$, z is the number of electrons transferred in the cell reaction.

At rest the membrane is principally permeable to K^+ and therefore the RMP is close to E_k . This K^+ permeability at rest is due to K_{2P} channels along with some other K^+ channels. Two-pore-domain potassium channels are leaky meaning they are opened at resting membrane potential and let the potassium to reach out of a cell. This leak current of potassium is maintained until the equilibrium state is reached (E_k).

This state is mandatory for the cellular health. In mammal, more than 80 genes have been found to encode for potassium channels. They are involved in a wide diversity of physiological functions and their dysfunction lead to many pathologies (Shieh et al., 2000). These dysfunctions can either be genetically or acquired due to autoimmune diseases. The pathologies involving the ion channels are called channelopathies.

B. Potassium channels: structure and function

Potassium channels are ubiquitously expressed by nearly all kingdoms of life and provide a wide range of functions. The x-ray crystallographic structure of KcsA was the first prokaryotic potassium channel structure characterized (Doyle et al., 1998). Since, the mechanism of gating and functionality of potassium channels has been well studied. K^+ channels are made of transmembrane helices, anchoring the lipid bilayer, and pore domains. According to their structure (see Figure 1) and function, they are sorted in four major classes:

- The voltage-gated (K_v), and calcium-sensitive (K_{Ca}), made of either six or seven transmembrane domains,
- the inwardly rectifying (K_{ir}), with two transmembrane domains,
- the two-pore-domain (K_{2P}), made of four transmembrane domains.

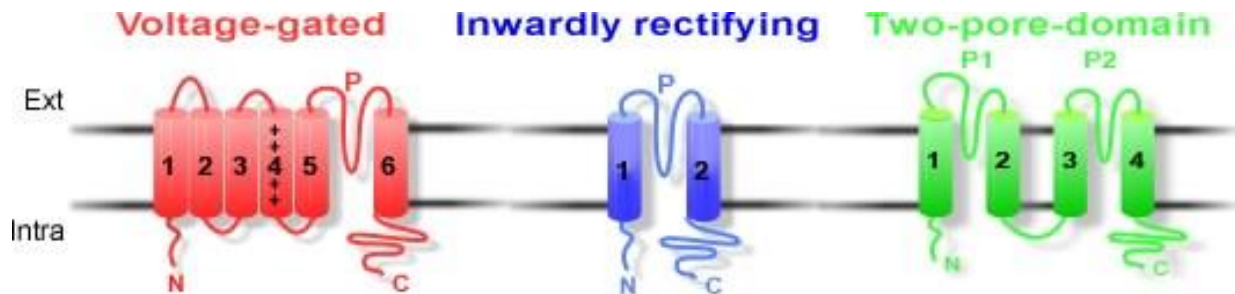


Figure 1: Potassium channel structures. Voltage-gated channels (red) possess 6 transmembrane domains and one pore domain (P). Some of them present a 7th transmembrane segment. The inward rectifier channels possess 2 transmembrane domains and one pore domain (P). The two-pore-domain potassium channels possess 4 transmembrane domains and 2 pore domains (P1 and P2).

To be functional, potassium channels have to be associated in a complex of 2 or 4 subunits called alpha (α), forming the pore. This complex can be made of the same subunits, forming homomers, or of different subunits, called heteromers. Ancillary subunits, named beta (β), sometimes combine with the channel (α subunit) to change its biophysical properties.

These α -subunits possess a sequence called P loop, highly conserved among species and mandatory to form the selectivity filter of potassium channel. Four pore-forming domains comprise a pore through which the potassium moves. Intra and extracellular domains possess several regulation sites, which can play a role on the gating or the conductivity of the channel.

In this part I will first describe the general architecture of the pore, describe the different potassium channel families and give some explanation about their general gating and more precisely about K_{2P} gating.

1. The pore

The ions move into a pore formed by four pore-forming domains which is conserved among the K^+ channels. Doyle et al. described in 1998 the structure of the pore-forming domain of a K^+ channel from *Streptomyces Lividans* (Doyle et al., 1998). The pore forming domain consists of the outer helix, loop regions, pore helix, selectivity

filter and inner helix. The inner and outer helices represent the intern cavity. The pore helix (P) plays a structural role in the filter stabilization. The active site of K⁺ channels is made of the selectivity filter (SF). This last is made of a conserved signature sequence TxGY/FG (Heginbotham et al., 1994). K⁺ ions are conducted very efficiently in this selectivity filter, at near diffusion-limited rates (10⁷ ions channel⁻¹.s⁻¹) (Kuang et al., 2015). K⁺ channels are highly selective and more permeant for K⁺ than sodium ions (1000 K⁺ for 1 Na⁺).

Selectivity and conductivity

The potassium enters into the central water-filled cavity (Sc) through the intracellular side via the helical bundle of KcsA channel (see Figure 2). Then passes the selectivity filter (SF) (from S4 to S1) to reach the extracellular entryway (S0 and Sext), following the electrochemical gradient. Hydration state of the potassium ions changes during these steps, going from hydrated in the Sc, dehydrated in the SF, to end-up hydrated in the Sext (Doyle et al., 1998).

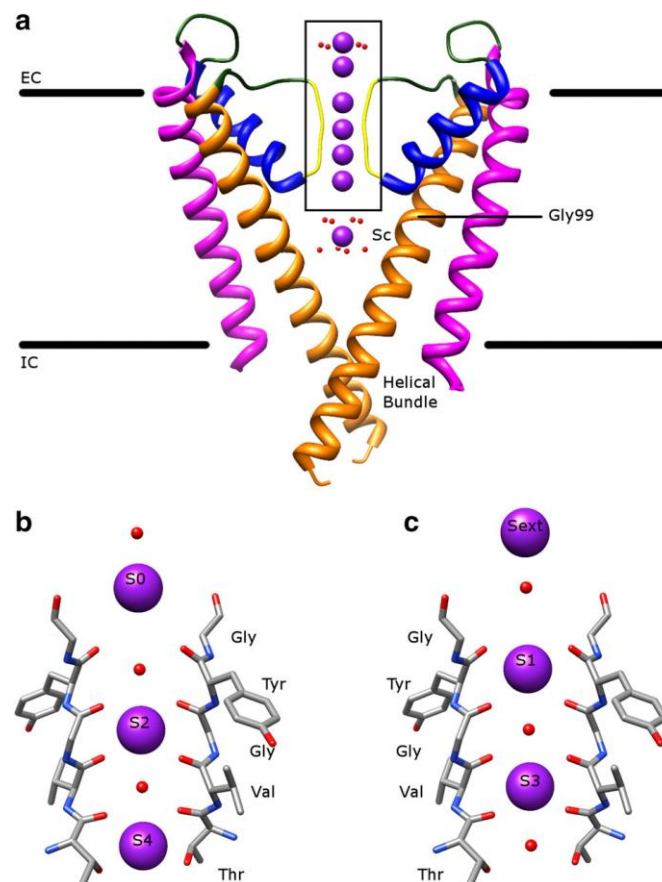


Figure 2: The transmembrane part of KcsA. a. The atomic structure of KcsA in the conductive state (PDB: 1K4C) viewed along the membrane plane. The pore-forming domain consists of the outer helix (magenta), loop regions (green), pore helix (blue), SF (yellow), and inner helix (orange). The conducted K^+ ions are represented by purple balls with surrounding water molecules in red. EC is extracellular and IC is intracellular. b, c. The enlarged view of the boxed area in (a) containing the SF and the extracellular entryway. The different states of occupation are depicted. For clarity, only two monomers opposite to each other are shown (from Kuang et al., 2015).

The filter has two states of occupation of its four potassium binding sites. The K^+ binding sites are formed by the carbonyl oxygens of the SF signature sequence TVGYG and the side chain of threonine. These four sites are not all occupied at the same time by ions, indeed there would be alternation between a molecule of water and a K^+ ion. There are two conformations: 2,4 (S1/H₂O, S2/ K^+ , S3/H₂O, S4/ K^+) and the 1, 3 (S1/ K^+ , S2/H₂O, S3/ K^+ , S4/H₂O) (Figure 2b and 2c respectively). The conduction mechanism consists of a concerted exchange between the two configurations until the arrival of a third ion on one side of the filter, causing the output of a K^+ ion on the other side. This structure of the SF minimizes the transfer energy, thus maximizes ionic conduction velocity (Bernèche and Roux, 2001). This mechanism called knock-on, may not be the only one. In 2104, Köpfer et al proposed another conduction mode, the direct coulomb knock-on, where the ions would preferentially occupy S2 and S3, going out to the extracellular site when another ion arrives at S1 (Köpfer et al., 2014).

Selectivity could be explained by the tridimensional structure of this region. Hydrated ions or smaller ones cannot be well addressed into the channel. However, under physiological conditions, two K^+ ions residing in the SF prevent Na^+ ion conduction (Valiyaveetil et al., 2006).

2. Voltage-gated potassium channels

The action potential generated by neurons involves several types of voltage-gated ion channels. Whereas voltage-gated sodium channels are opened for a short period followed by a quick inactivation, the voltage-gated potassium channels (K_v) are activated and remain open for a longer period (Hodgkin and Huxley, 1952).

The majority of K_v channels opens when the membrane is depolarized and closes when the membrane is hyperpolarized and inactivates for maintained depolarization. They are made of 6 transmembrane domains and one P loop. To be functional, they need to form tetramers. All subunits possess a voltage sensitive domain (VSD, S1 to

S4, S4 being the sensor). S5 and S6 delimitate the pore domain. S4 is composed by positively charged residues such as lysine or arginine every 3 amino acids, allowing a conversion of electric energy toward a mechanic one, rearranging S5 and S6 domains leading to the channel opening (Mannuzzu et al., 1996).

Inactive at resting membrane potential, they will open when the activation threshold is reached during a depolarization. K⁺ massive efflux will result in the repolarization of the membrane to the resting membrane potential.

The 40 mammalian members of this family are sorted in 12 subfamilies depending on their sequence homology.

2.a) Shaker TYPE

The first channel to have been cloned in *Drosophila melanogaster* by the Jan's lab (Papazian et al., 1987). Its name is given by the loss of function of the gene KCNA1 coding for this protein, leading to a shaking phenotype in the fly's paw. In human they are encoded by 8 genes KCNA1-8 coding for the protein Kv1.1-8.

These channels have been found in the brain, the heart, the skeletal muscle, the lung, the retina and pancreas. They are sensitive to 4-aminopyridine (4-AP) and some toxins (Browne et al., 1994; Gutman et al., 2005; Scheffer et al., 1998).

In sensory neurons of the trigeminal somatosensory system, Kv1.1 and Kv1.2 underlie the excitability brake current of cold thermoreceptor neurons. The slow-inactivating outward K⁺ current produced by Kv1 is involved during the action potential phase of repolarization. It prevents the unspecific activation by cold. Mutations in the channel Kv1.1 (Maylie et al., 2002) give rise to truncated forms of the protein which destabilize the open state and thus are associated to disease (González et al., 2017).

2.b) Shab, Shaw, Shal

Shab or KV2.1-2, Shaw or Kv3.1-4 and Shal or Kv4.1-3 are expressed in the brain, smooth muscle, lung, heart, testis and pancreas. They have been found by sequence homology in the drosophila. As Shaker channels, they are inhibited by tetraethylammonium (TEA) and 4-aminopyridine (4-AP) (Gutman et al., 2005).

2.c) KCNQs

These five channels named $K_v7.1-5$ (or KCNQ1 to KCNQ5) are expressed in the brain, the heart, inner ear, skull muscle and pancreas. In neurons, they show a slow activation when associated with β -subunits and thus are involved in the fast after hyperpolarization phase, right after the action potential.

KCNQ channels are involved in pathologies affecting heart and brain. Mutations in the $K_v7.1$ channel, expressed in the heart results in a modification of the potassium current leading to long QT syndrome which is characterized by a prolonged QT interval, resulting in a heart beating abnormally and an increased risk of arrhythmias and sudden death.

2.d) Ether-a-gogo

As the Shaker family, this family was first discovered in drosophila mutants that showed a shaking phenotype in the paw, under ether anesthesia. They are three subfamilies, called eag (or $K_v10.1-2$), erg (for eag related gene or $K_v11.1-3$) and elk (for eag-like K^+ channels or $K_v12.1-3$). They produce a current with a slow activation. In the heart and the brain, they are involved in the action potential repolarization. As KCNQ1, mutations in human erg channel $K_v11.1$ are involved in long QT syndrome, via its involvement in ventricular repolarization.

2.e) "Modifier" subunits

Four of the K_v families (K_v5 , 6, 8, and 9) encode subunits that act as modifiers. Although these do not produce functional channels on their own, they are able to assemble with K_v2 family subunits forming heterotetrameric channels with unique properties increasing the functional diversity within K_v2 channel family. They modulate the activation and/or inactivation phase of the channels.

2.f) Ancillary subunits and partners of K_v channels

A variety of other peptides has also been shown to associate with K_v tetramers and modify their properties, including several β subunits (which associate with K_v1 and K_v2 channels), KCHIP1 (K_v4), calmodulin (K_v10), and minK (K_v11).

2.g) K_{ca} channels, activated by calcium

These tetrameric channels are activated by an intracellular increase of calcium concentration and voltage for some. This family can be divided in two distinct

subfamilies. The first is made of BK channels, for big K⁺ conductance (Wei et al., 1994) and the channels possess 7 TM. As Kv channels, the BK channels are voltage-dependent. The second is made of 6 TM channels and is divided in SK channels (slow conductance) and IK channel for intermediate conductance, both insensitive to potential.

(1) BK channels

These channels are both calcium and voltage dependent. Each of the subunit is composed of 7 TM, with a S4 domain sensitive to potential, and another transmembrane domain called S0, making the N-terminus to be on the extracellular side. The calcium sensor is localized in the C-terminus and rely on hydrophobic negatively charged residues that bound the calcium (Schreiber and Salkoff, 1997). The calcium binding shifts the IV curve toward more hyperpolarized potential favoring BK activation (Sun et al., 1999).

BK channels are ubiquitous in the SNC and are involved in the rapid/medium phase of the hyperpolarization after an action potential. Their sensitivity to calcium involves them in many physiological functions notably in the nervous system, BK channels have been involved in neurotransmitter release (Faber and Sah, 2003).

Ancillary subunits

Most of the BK channels are associated with a β or γ subunits. β subunits are made of 2 transmembrane domains. Four different β subunits (β 1– β 4) have been cloned and identified in mammals. They act on the calcium and voltage sensitivity of the BK channels, as well as the activation and their pharmacology (see Figure 3 below).

In the nervous system, BK channels have been involved in neurotransmitter release. In the cells where they are expressed, depending on the α and β subunit assembling, the resulting currents and functions will not be the same.

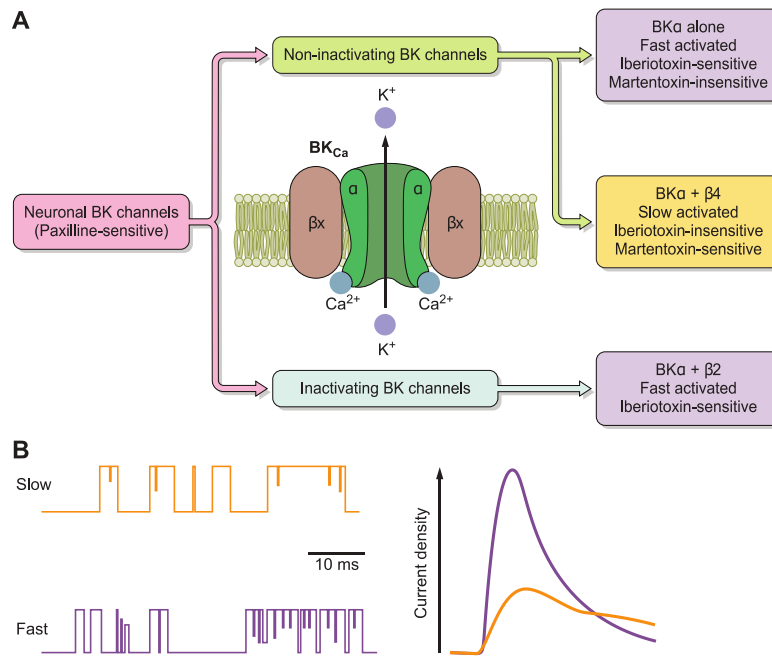


Figure 3: BK channels and its ancillary subunits are pivotal in neuronal excitability. A: diagram chart of BK neuronal channels, pharmacology of scorpion toxins, and general gating features. B: illustration of single-channel recordings and current densities for fast and slow activated neuronal BK from (Latorre et al., 2016).

In trigeminal ganglia, the combination of BK channel with β_4 subunit modulates glutamate release, and CGRP release is inhibited by activation of this combined channels (Samengo et al., 2014).

The four γ subunits are encoded by LRRC genes and also play on biophysical and pharmacological properties of BK channels (Yan and Aldrich, 2010). In testes, γ_2 (LRRC52) increases BK current and is linked to fertility deficit (Zeng et al., 2015).

(2) SK channels

SK channels or $K_{Ca2.1-3}$ possess a small conductance to potassium from where they have been named. They are made of 6 TM and one pore domain. Unlike BK channel, they are not voltage sensitive and do not directly interact with the calcium but are modulated by calmodulin that directly acts on the C-terminus domain (Maylie et al., 2004).

They are expressed throughout the central nervous system. Their activation limit the firing frequency of action potential (Faber and Sah, 2007), playing a role in medium afterhyperpolarization following an action potential and in synaptic plasticity (Stackman et al., 2002).

(3) IK channels

IK or $K_{Ca3.1}$ channel (or SK4) for intermediate conductance is not sensitive to membrane potential. They share the same sensitivity to intracellular calcium concentration as SK channels via calmodulin binding in the C-terminus. In cancer types, this channel has been found to be important in cell proliferation (Thurber et al., 2017).

3. Inwardly rectifying potassium channels

K_{ir} channels have diverse physiological functions in the cell, depending on their type and location, and are modulated by various mediators, such as ions, phospholipids, and proteins binding (for review see Hibino et al., 2010). The fifteen members can be divided into seven subfamilies based on their mediators and the properties of ion conduction. They have the ability to form *in vivo* homo or hetero tetramers. These seven subfamilies can be classified into four main groups:

- Classical K_{ir} channels ($K_{ir}2.1-4$) are constitutively activated, are involved for instance in cardiac myocytes where $K_{ir}2.1$ and $K_{ir}2.2$ heteromer stabilizes membrane potential close to E_k (Zobel et al., 2003).
- G protein-gated K_{ir} ($K_{ir}3.1-4$) are regulated by G-protein coupled receptors (GPCR). In the brain, GIRK channels expressed in hippocampal neurons will generate post-synaptic inhibitory potentials induced by $GABA_B$ receptor activation (Lüscher et al., 1997) in concert with TREK channels (Sandoz et al., 2012).
- ATP-sensitive K^+ channels ($K_{ir}6.1-2$), linked to cellular metabolism. K_{ATP} are inhibited by ATP, but in complex with sulfonylurea receptor in presence of ADP, they will be activated. They regulate the membrane potential of pancreatic β cells thus modulating insulin secretion (Ashcroft and Rorsman, 1989).
- K^+ transport channels ($K_{ir}1.1$, $K_{ir}4.1-2$, $K_{ir}5$, and $K_{ir}7$). Mostly expressed in the apical membrane of epitheliums where they are involved in Na^+ and K^+ homeostasis.

One characteristic of these channels is the inward rectification resulting from the pore block by the magnesium ion (Mg^{2+}) on the intracellular side for depolarized membrane potential (Figure 4). The same allosteric block is observed with

polyamines. The rectification will be weaker or stronger depending on the expressed α subunit.

Another characteristic of these channels is their structure. Each subunit being made of two TM, they need to form tetramers to be functional. They can either homo- or heteromerize.

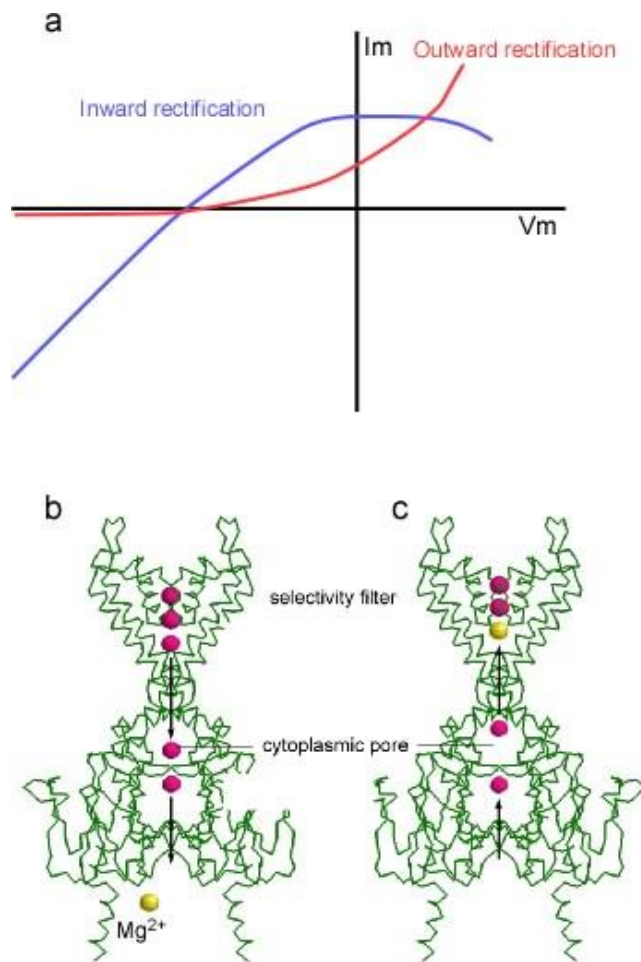


Figure 4: IV curves and structure of Kir channels. a. Outward rectification is characterized by a current intensity that increases with the values of depolarized potentials (red). Inward rectification is characterized by a decrease in the outgoing current with the values of depolarized potentials (blue). b, c. Representation of the blocking of the K_{IR} channels by the magnesium ion. When the membrane potential is lower than potassium reversion potential, K^+ ions (pink) can get through (b). When the membrane potential exceeds the potential potassium equilibrium Mg^+ ion (yellow) blocks the pore of the channel, thus preventing the outward current (c). Modified from Hsieh et al., 2015.

4. K_{2P} channels

K_{2P} channels are made up of two subunits, each contains 2 pairs of transmembrane segments, each flanking a pore domain (in the order: TM1, P1, TM2, TM3, P2, TM4). At rest, the activity of these channels drives the membrane potential toward the K^+

equilibrium potential and therefore reduces cellular excitability. Fifteen members of the K_{2P} channel family have been cloned in mammals which can be divided into 6 subfamilies based on sequence homology and biophysical properties (Figure 7 see below page 36). The members of the TREK channel subfamily, TREK1, TREK2 and the more distant TRAAK channels, are widely expressed in the nervous system. The TREK channels display low basal activity but can be stimulated by various stimuli including an increase in temperature, mechanical stretch and cell swelling, intracellular acidification, arachidonic acid and other polyunsaturated fatty acids (PUFAs), external alkalization, lysophospholipids and phosphatidylinositol-4,5-bisphosphate, and pharmacological agents such as volatile anesthetics and riluzole. TRESK channel is the only member of the TRESK subfamily. It has a sensitivity to intracellular calcium.

My thesis project focused exclusively on K_{2P} channels, especially TREK and TRESK subfamilies. I will develop extensively the properties and characteristics of these channels in the chapters following the chapter 5 "Gating".

5. Gating

Voltage dependent K^+ channels usually have three states: resting, activated, and inactivated. The channels are usually closed in the resting state, and opened after a stimulus activation, followed by turning to the nonconductive state.

There are three types of mechanisms in K^+ channels to describe the gating one for the activation and two for the inactivation.

Activation will rely on the intracellular helices –the bundle crossing gating–, inactivation involves the selectivity filter –SF gating. The two gates will be coupled differentially in K_v channels and two-pore-domain potassium channels. A third mode of gating, N-type or ball-and-chain inactivation, reflects block of the open pore by a portion of the amino terminal of the same protein (Loots and Isacoff, 1998). In fact, the blockage is caused by a "ball" of a N-terminal sequence which binds to the inner vestibule within the channel. This blockage causes inactivation of the channel by stopping the flow of ion. This mechanism is responsible of the fast inactivation of K_v channels and has not been reported in K_{2P} channels.

(1) Bundle crossing gating

The voltage sensing for activation relies mainly on the membrane potential and is called the bundle-crossing gating. The voltage dependence of voltage-gated channels is mediated by the mobile charge-containing fourth transmembrane segment, S4, in the voltage sensor domain (VSD, S1 to S4 see the structure below Figure 5). When the channel is closed, there is a physical block by the inner helices, prohibiting the ion to get through from the intracellular side (Loots and Isacoff, 2000). Following a depolarization, the positively-charged residues on the S4 domains move toward the exoplasmic surface of the membrane, thanks of a hinge glycine residue, inducing a conformational change of the activation gate allowing opening of the channel (Figure 6 and Blunck et al., 2006).

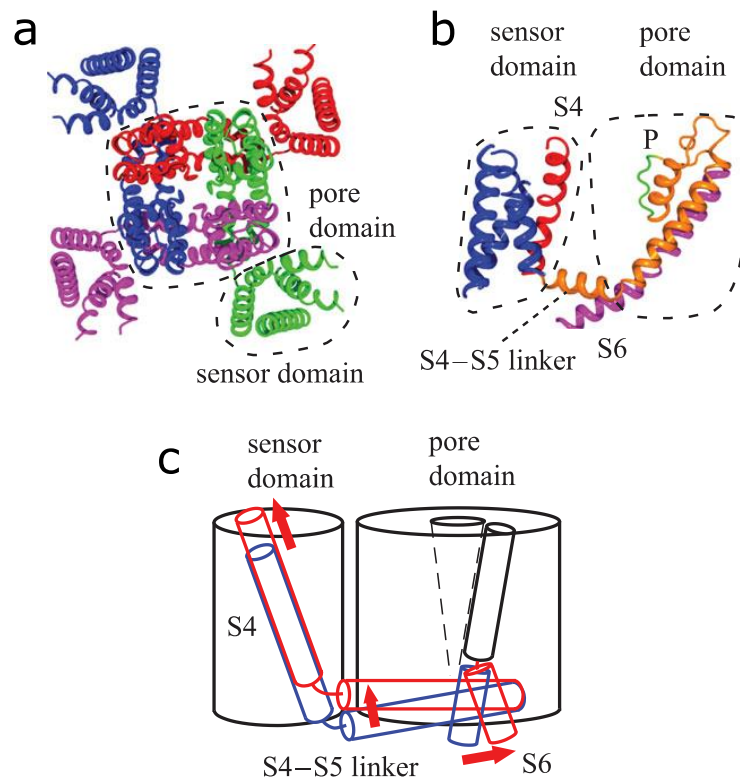


Figure 5 : Structure and conformational change of the potassium channel. (a) Crystal structure of Kv1.2 potassium channel (PDB accession number: 2A79). Each subunit is in a different colour. The pore domain is surrounded by four sensor domains. **(b)** Structure of a single subunit showing the position of S4 (red), selectivity filter (P), and gate-forming S6 (magenta). **(c)** Schematic representation of the conformational change that occurs on gating. Blue and red represent the position in the resting and activated state, respectively (from Yoshimura and Sokabe, 2010).

In K_{2P} , it remains poorly understood how stimuli such as phospholipids, G-protein receptor stimulation or pressure can regulate the channel activation. However, the questioning about a bundle crossing mechanism is opened in K_{2P} . Ben-Abu et al. have

demonstrated that chimera constructs between a K_v subunit, and the P1 region of a drosophila version of a K_{2P} channel possess a more stable activation gate than K_v channels. Activation of this construct by voltage could rely on the action of the voltage-sensor on the K_{2P} activation gate, suggesting that inner helices could be involved in K_{2P} channel gating (Ben-Abu et al., 2009).

(2) SF gating

The SF gating is involved in the inactivation and occurs near the selectivity filter region. This mechanism is also called C-type inactivation. It has been highlighted using the pore inhibitor tetraethylammonium (TEA) along with its dependence on extracellular K^+ and its sensitivity to mutation of residues on the SF vicinity. Structural work on KcsA channel shows that when removing the K^+ , the channel undergoes a conformational change (from conductive to nonconductive state), leading to a reduction in the number of bound ions at the SF. This mechanism has been observed on prolonged depolarization-promoted opening Kv channel and has been linked to the slow inactivation process.

This mechanism has been found in K_{2P} channels, there is a gating control in the selectivity filter via changes of conformation in helical transmembrane domains. Several subfamilies of K_{2P} channels possess a pH sensitivity, given by residues such as histidine, in the vicinity of the selectivity filter (see the cartoon model in Figure 6, Bagriantsev et al., 2011; Cohen et al., 2008; Sandoz et al., 2009). Another argument that pH sensing is similar to C-type inactivation of K_v channels supporting this view is that a high external K^+ concentration known to slow C-type inactivation alters pH inhibition of human (Cohen et al., 2008) and mouse TREK1 (Sandoz et al., 2009), and pH activation of TREK2 (Sandoz et al., 2009).

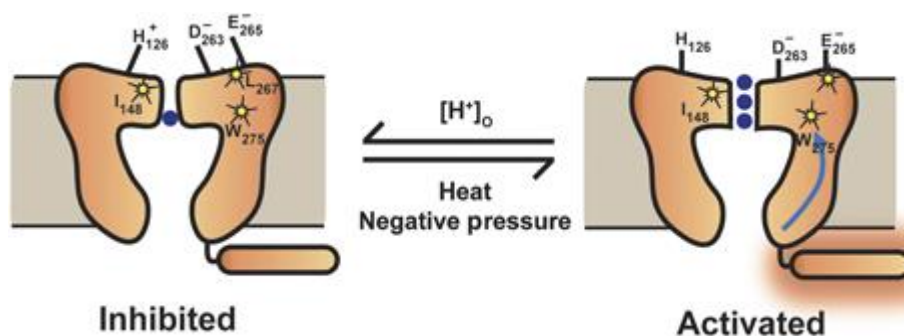


Figure 6: Cartoon model of $K_{2P}2.1$ (TREK-1) C-type-like gating by extracellular acidosis, heat, and pressure. Low-activity (inhibited) state and a high-activity (activated) state that involves a C-type-like gate. As suggested earlier (Sandoz et al,

2009), external acidification causes structural rearrangements in the pore triggered by electrostatic interactions between the protonated extracellular pH-sensing His126, and the negatively charged region in the P2-loop, which includes Asp263 and Glu265. Authors propose that Ile148, Leu267, and Trp275 (indicated with stars) are crucial elements of the C-type-like gate. As suggested elsewhere (Honore, 2007), temperature and mechanical stress have their sensing elements located in the intracellular C-terminal domain. Activated C-terminal domain (indicated with the orange halo) induces movements of the M4 transmembrane segment and affects channel activity through the C-type gate. The blue arrow indicates the putative pathway. For clarity, only one of the two cytoplasmic C-termini is depicted (from Bagriantsev et al., 2011).

Furthermore, Tucker and Baukowitz have shown in 2011 using quaternary ammonium (QA) derivatives – known to be allosteric blockers of potassium channels selectivity filter – that the selectivity filter regulation in K_{2P} does not rely on the physical closure observed in the bundle crossing mechanism, since QA are still able to access the selectivity filter, no matter the protonation state of the channel (Piechotta et al., 2011).

Since 2012, Dan Minor's team is deeply trying to understand the mechanism by which, the Carboxy-terminal tail (C-tail) and the selectivity filter can be coupled (Bagriantsev et al., 2011, 2012, Lolicato et al., 2014, 2018; Pope et al., 2018). Mutations in the selectivity filter abolish intracellular regulation by the C-tail and *vice versa*. Furthermore, mutation in the TM4 helix or between TM4 and C-tail induce a loss of the coupling. The main conclusion is that the gating of TREK1 involves C-type like gate, but also involves TM4 flexibility. Zhuo and collaborators provide a role of a glycine hinge G312 in M4 involved in the allosteric regulation of the C-tail (Zhuo et al., 2016). In 2017, Minor group identified a druggable K_{2P} site that stabilizes the C-type gate 'leak mode' (Lolicato et al., 2018).

(3) Hydrophobic gating in K_{2P}

In line with these experiments, playing with hydrophobic residues, Lesage's team has shown in TWIK1 that mutation of leucine located in the M2 domain (possessing a hydrophobic side chain) L146 to aspartic acid (a negatively charged residue) would increase the usually low current (Chatelain et al., 2012).

More recently, an explanation has been provided by Tucker's team. They presented a new mechanism in TWIK1 channel termed hydrophobic gating (Aryal et al., 2014). Molecular dynamic studies revealed that the region represents a hydrophobic barrier, leading to a dehydration of the pore region, thus decreasing the ionic conduction, to finally downregulate TWIK activity. Replacing these hydrophobic residues to positively

charged residues such as arginine will increase the observed current. In conclusion, amino acids composition of the intern cavity will play a role on ion efflux.

C. K_{2P} channels family

Mammalian K_{2P} channels all share the same topology and a main role which is to establish and maintain the resting membrane potential. The 15 members have been cloned in mammalian and are classified (see Figure 7) depending on their sequence homology and their functional characteristics in 6 subfamilies. Surprisingly, even though they share the same function, apart from the pore domain, the sequence is poorly conserved between members, leading to particular characteristics.

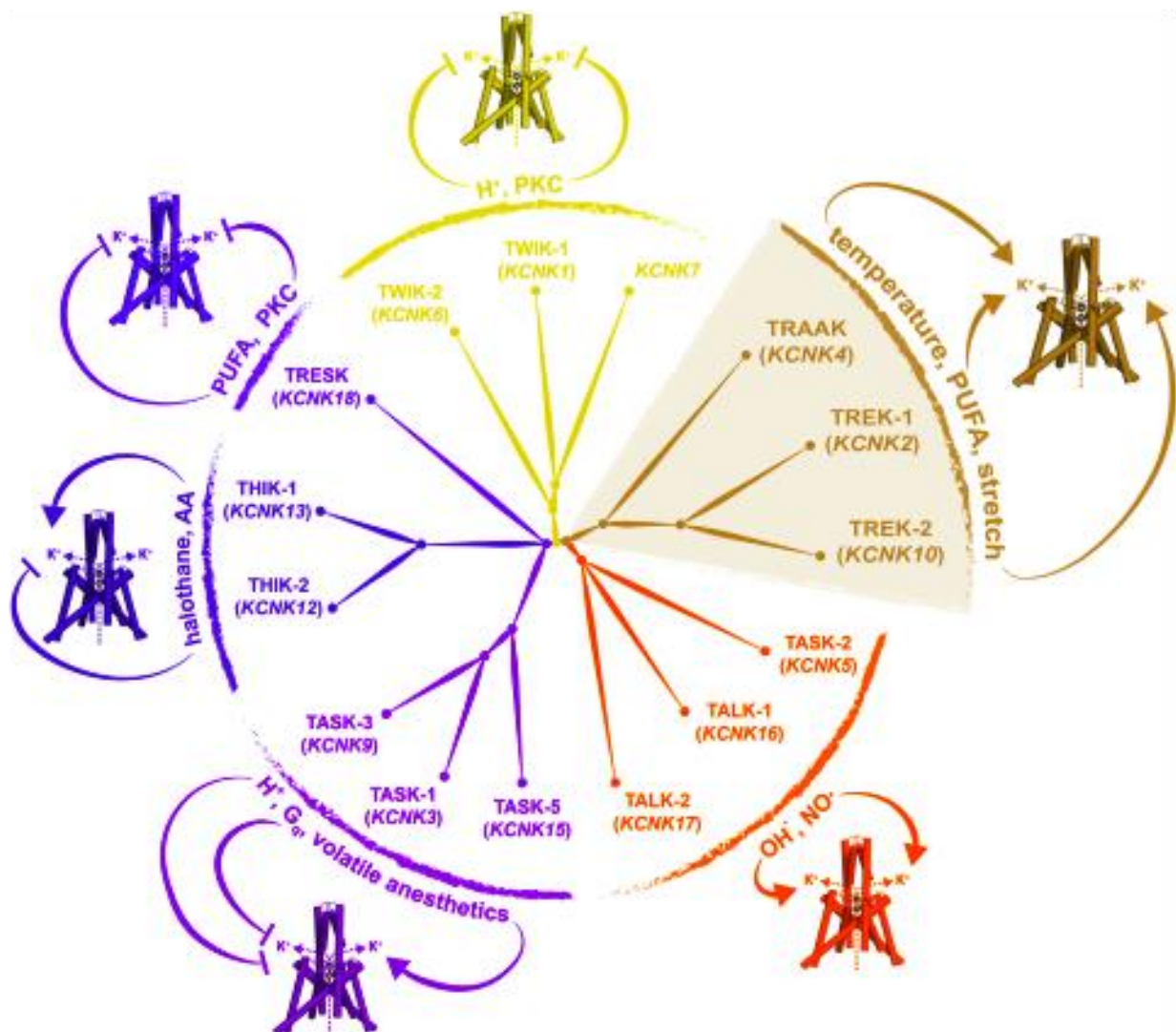


Figure 7: Dendrogram of the K_{2P} potassium channel family and their characteristic functional features. The effects of different stimuli on the currents of the channels within each K_{2P} subfamily are indicated. PUFA, polyunsaturated fatty acids; PKC, protein kinase C; AA, arachidonic acid. TWIK ("Tandem of P domains in a Weak Inwardly rectifying

potassium (K^+) channel") TREK ("TwikRElated K^+ channel") TASK (Twik-related Acid-Sensitive K^+ channel) TALK (Twik-related ALkalin pH activated K^+ channel) THIK (Twik-related Halothane Inhibited K^+ channel) TRESK (Twik-RElated Spinal cord K^+ channel) from (Decher et al., 2017a).

1. Generalities

This family of potassium channels is the last one to have been uncovered and cloned. The first mammalian one, TWIK1, was cloned in 1996 in Nice (Lesage et al., 1996). TWIK is the acronym for Tandem of pore domains in a Weak Inwardly rectifying potassium (K^+) channel. The channel was at the origin of the leak current described by Hodgkin and Huxley in 1952 in squid giant axon.

Leak potassium channels have been described as being constitutively open at rest. However, these channels are polymodal and respond to a wide range of stimuli, such as pH, temperature, membrane stretch, fatty acids and anesthetics (Lesage and Lazdunski, 2000).

They are ubiquitous, and thus play a role in the brain, the cardiovascular system, immune system and the somatosensory system. They exhibit the functional properties expected for K^+ leaky channels: opening near the physiological voltage range to pass K^+ selective currents, showing few or no voltage/time dependency.

2. Electrophysiological properties

In the 50', Hodgkin and Katz have postulated that the cell membrane at rest is permeable to potassium (Hodgkin and Katz, 1949). General assumptions were made to establish the Goldman-Hodgkin-Katz (GHK) flux equation:

- The membrane is a homogeneous substance
- The electrical field is constant so that the transmembrane potential varies linearly across the membrane
- The ions access the membrane instantaneously from the intra- and extracellular solutions
- The permeant ions do not interact
- The movement of ions is affected by both concentration and voltage differences

Allowing one to predict the current/voltage plot of potassium shown in Figure 8. Most K_{2P} channels lack voltage sensitivity, and any kind of activation or inactivation kinetic. The rectification can thus be approximated by GHK equation in asymmetric K^+

conditions, which rely on the electrochemical gradient of K^+ ion, for most of K_{2P} channels (Duprat et al., 1997).

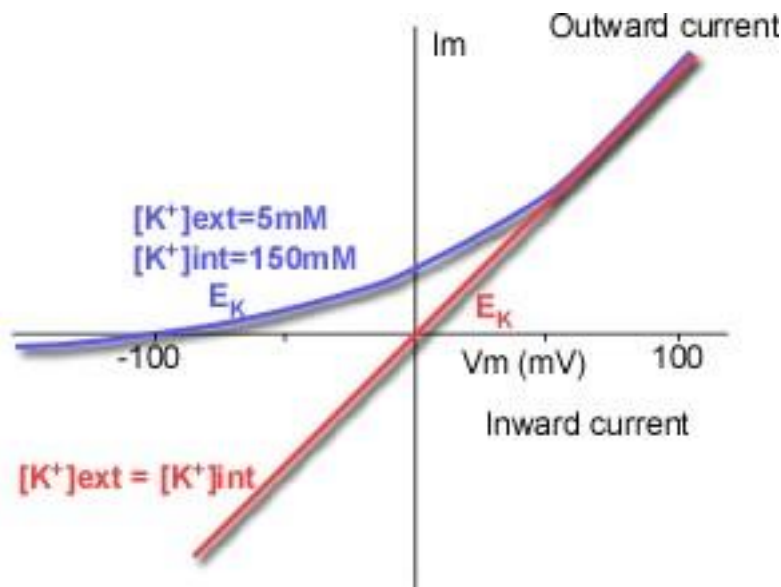


Figure 8: Background potassium currents described by the GHK equation. In physiological condition the current-potential curve (IIV curve) in blue crosses the x-axis at potential value close to the equilibrium potential of the K^+ ion ($E_K = -80mV$). In symmetrical K^+ solution, IV curve (red) crosses the x-axis at $0mV$.

If membrane potential is over the potassium potential equilibrium, the electrochemical gradient is in favor of a potassium output. Otherwise, there will be a potassium entry. The IV curve will thus be characterized by an outward rectification in physiological conditions. This outward rectification has important implications in the role of K_{2P} in the central and peripheral nervous system by i) stabilizing the resting membrane potential, and ii) enabling action potential (AP) generation in absence of K_v channels by repolarization of the membrane after AP thank of their conductance (MacKenzie et al., 2015).

However, some K_{2P} channels such as TREK1 or TASK3 do not respect this equation (Fink et al., 1996). TREK1 for instance possesses a voltage- and time-dependant activation due to an increased open probability for depolarized potential (Schewe et al., 2016).

3. Structure

K_{2P} channels are characterized by the presence of two pore forming regions and four trans-membrane (TM) regions named TM1 to TM4 (or M1 to M4) in each channel subunit and, unlike other classes of K^+ channels, are functional as dimers (not

tetramers, see Figure 9) (Lesage et al., 1996; Levitz et al., 2016). TM1 and TM2 are linked together via an extracellular loop containing two alpha helices termed C1 and C2 and a pore domain named P1. The second extracellular loop joins together TM3 and TM4 and contains the second pore domain P2.

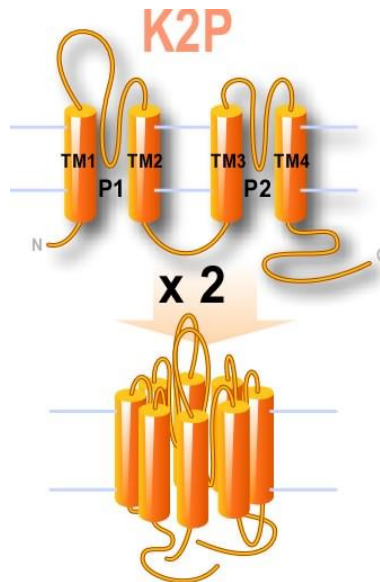


Figure 9: Cartoon showing the topology of a two-pore-domain potassium channel K₂P and its assembly in dimer.

TWIK1 and TRAAK crystallographic structures have been released in 2012 and gave clues about the understanding of structure-function relationships in K₂P channels (Brohawn et al., 2012; Miller and Long, 2012). C1 and C2 form an extracellular cap, of about 35 Å that could be involved in dimerization. In TWIK1 channel and other K₂P (TREK1, TREK2...) two subunits are connected via a covalent disulfide bound that may help in the structure stabilization (Lesage et al., 1996). TM2 and TM4 helices flanking the channel pore pass through the membrane obliquely. The more external helices, cross the membrane vertically (Renigunta et al., 2015).

Crystallographic model of TRAAK revealed in 2012 by Brohawn et al. gave new clues about the path taken by the ions in the selectivity filter (Brohawn et al., 2012). There is a lateral window made of helix M2 of one subunit and helix M4 of another subunit that gives a direct access to the intern cavity in the intracellular side. These helices also act on the conductivity and ion selectivity.

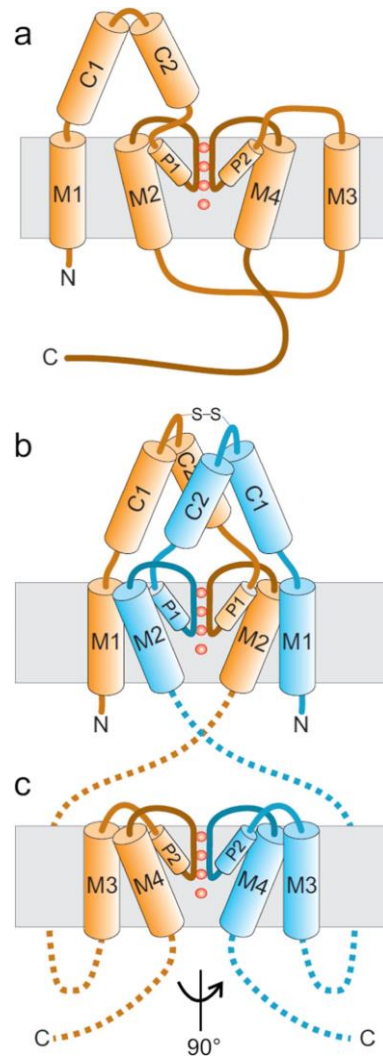


Figure 10: The structure of K_{2P} -channels. a. Topology of K_{2P} -channels. b. Sketch of the structure of the N-terminal part of the two subunits (including the M1, C1, C2, P1 and M2 domains). c. Sketch of the structure of the C-terminal part of the two subunits (including the M3, P2 and M4 domains). The helices are not drawn to scale. For clarity, the pore helices are relatively small (from Renigunta et al., 2015).

More recently, TREK2 structure has been characterized (Dong et al., 2015), allowing one to better understand the gating mechanism of K_{2P} channels.

4. Up and down state and opening mechanism

Two states, termed “up” and “down,” are known from x-ray structural crystallographic studies and have been suggested to differ in conductance. However, the structural details of the gating behavior are largely unknown. According to MacKinnon group, in the up configuration, TRAAK channel offers to potassium a passage open and direct between the cytoplasm and the extracellular environment (Brohawn et al., 2012,

2014). In the down state, the passage of ions is blocked by the phospholipid chain of the plasma membrane.

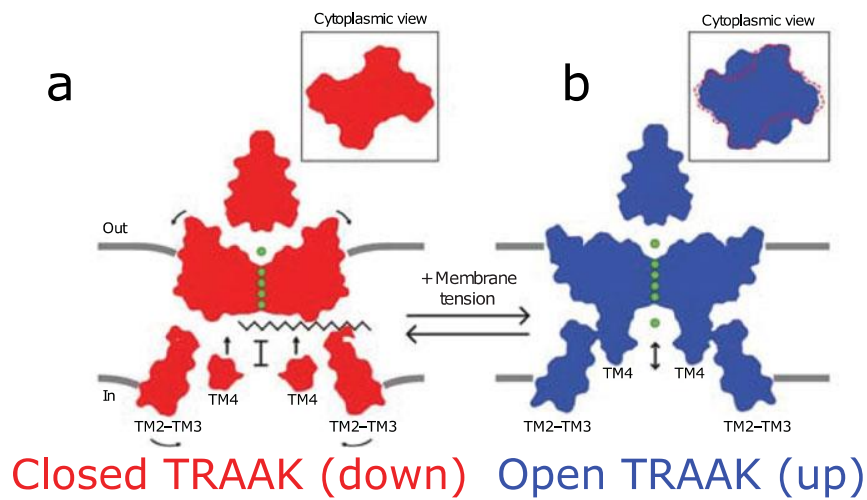


Figure 11: Cartoon model of TRAAK gating and mechanosensitivity. The down conformation (red) is a closed channel state and the up conformation (blue) is an open channel state. In the down conformation, a lipid acyl chain accesses the central cavity through intra membrane openings to block ion (green) conduction. In the up conformation, lipid is sealed from the cavity to permit ion conduction. Shape changes upon opening can explain the mechanosensitivity of TRAAK and TREK channels. Area expansion and reduced mid plane bending create an energy difference between channel states that promotes force activation, from (Brohawn et al., 2014).

The down state suggested to be the closed one, has been conflictual. Indeed, Minor's group determined the down state using a constitutively activated TRAAK channel as the opened and activated state (Lolicato et al., 2014). Subsequent structure of TREK2 channel, provided an insight into the relevance of up and down states (Dong et al., 2015; McClenaghan et al., 2016) and its involvement in mechanosensitivity.

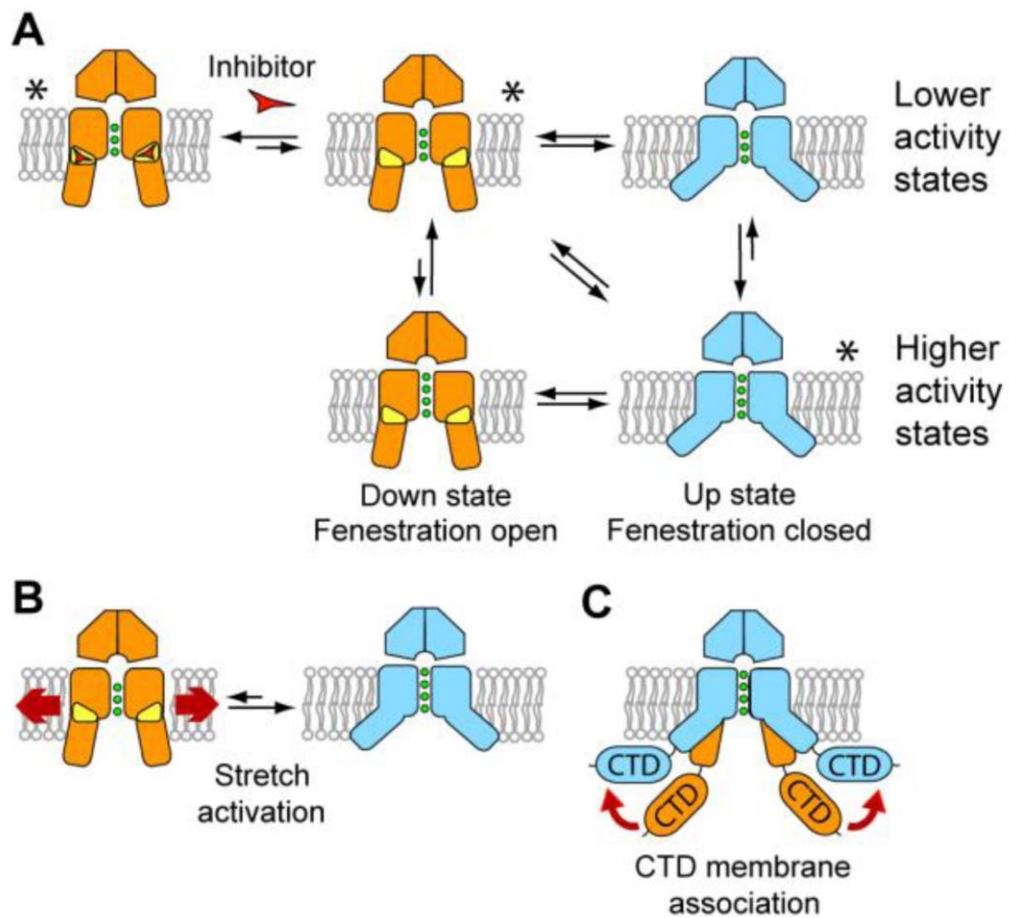


Figure 12: The down state, lower conductivity conformations are shown in orange, with the fenestrations indicated in yellow. The up state conformations are shown in blue. Inhibitors such as norfluoxetine are represented by a red triangle. (A) Overall scheme for K_{2P} channel gating. Higher and lower conductivity states are shown for both conformations as the filter may gate independently of these larger changes, though with a different probability. Conformations for which we have crystal structures are indicated with an asterisk. (B) Schematic of activation of TREK channels by mechanical stretch. The direct interaction of TREK-2 with lipids in the membrane may allow lateral forces to facilitate conversion from the down to the up state which is fluoxetine insensitive. (C) Association of the C-terminal domain (CTD) with the membrane. The diverse cytoplasmic C-terminal extensions of K_{2P} channels provide an additional site for modulation of channel activity. This regulation could operate in part though association of the CTD with the membrane after post-translational or pH changes that would favor the more active up state (from Dong et al., 2015).

Membrane tension can provide the channel energy to switch from one configuration to another (Brohawn, 2015). The transition between the two open conformations, "open-down" stabilized by pH and "open-up" stabilized by the pressure, would be more energetically favorable than the transition from a closed conformation to an open conformation (McClenaghan et al., 2016).

5. TWIK family

TWIK1 was the first K_{2P} channel to be cloned in mammalian in 1996 in Nice (Lesage et al., 1996). TWIK is the acronym for Tandem of pore domains in a Weak Inwardly rectifying potassium (K^+) channel. TWIK channel family is made up of 3 members, TWIK1, TWIK2 and KCNK7. In heterologous expression system, they produce very small or no currents. This is partially due to their subcellular localization. Indeed, KCNK7 is especially found in the endoplasmic reticulum (Salinas et al., 1999), while TWIK1 is located in recycling vesicle (Feliciangeli et al., 2010).

TWIK1 is expressed in the central nervous system (hippocampus, thalamus, and cerebellum) and in periphery in the heart, lungs, and kidneys (Arrighi et al., 1998). TWIK1 channels are selectively expressed in DRG neurons and show a reduction of expression after neuropathic injury. The maintenance of this reduction weeks after the injury suggest a major role for TWIK1 in the maintenance of chronic neuropathic pain (Mao et al., 2017; Pollema-Mays et al., 2013). However, TWIK1 only provides a small background current when expressed in heterologous expression systems, and seems to be in majority retained in intracellular compartment (Feliciangeli et al., 2010; Lesage et al., 1996).

Human TWIK2 also generate currents with very small amplitude in heterologous system (Patel et al., 2000). However, the rat homologous TWIK2 channel creates 15 times more current. Beside this difference, they possess the same particular electrophysiological properties. Its role is not well known and its tissue distribution could be linked to its silent activity.

As TWIK2, KCNK7 does not generate any current when expressed in heterologous system, in which it is retained in the endoplasmic reticulum (Salinas et al., 1999). Nothing is known about the function and the pathophysiological implication of this channel in human, where it is expressed in dorsal root ganglia and cerebellum (Medhurst et al., 2001).

Would TWIK1 role in pain rely on the formation of heteromers in the brain with other K_{2P} channels?

Astrocytes express TWIK1. These cells show a passive conductance resulting in a low membrane resistance. This resistance seems to implicate leak potassium current, but the responsible are not yet identified. Indeed, it was hypothesized by Zhou et al that

TREK1 and TWIK1 independently participate in this passive conductance (Zhou et al., 2009), however, the same group suggested that mice KO for TWIK1 did not show significant differences in astrocytic membrane passive conductance. Independently, Park group showed that passive conductance membrane in astrocytes that expressed TWIK1 specific shRNA was completely reduced (Hwang et al., 2014). Furthermore, they have shown that TWIK1/TREK1 heteromeric channels were formed, and these last carry the passive conductance in astrocytes along with a fast glutamate release upon G $\beta\gamma$ binding (Hwang et al., 2014). This last characteristic of the pore leading to the transport of glutamate upon activation however remains unknown. We have tested the ability of TWIK1 and TREK to heteromerize and did not observed this association in our assay.

6. TASK family

TASK1 and TASK3 are two pore domains K⁺ channels that are pH sensitive. The current they generate show little time-dependence and weak rectification while TASK5 is found to be inactive in heterologous expression system. TASK1 and TASK3 are both inhibited by extracellular acidification (Duprat et al., 1997) and local anesthetics (Maingret et al., 2001). They also are inhibited by hormones and transmitters that act via G_{q/11}-coupled receptors, such as muscarinic M3 receptors. They are activated by volatile anesthetics (halothane and isoflurane). These channels are non-sensitive to TEA and 4-AP as well as Barium and Cesium that usually block K⁺ channel.

These two channels are highly expressed in the central nervous system. TASK5 is also found in the brain, in the central auditory system nervous system, but is thought to be non-functional, however it may works in association with an ancillary subunit (Karschin et al., 2001).

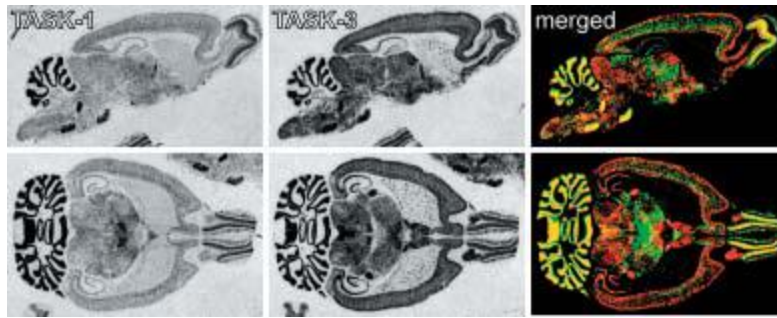


Figure 13 : Differential distribution of mRNA coding for TASK-1 and TASK-3 in the rat CNS. Sagittal (top) and horizontal (bottom) sections from rat brain were hybridized with radioactive probes specific for TASK-1 and TASK-3 (Talley and others 2001). On the left are grayscale images of the resulting film autoradiograms. To generate the colored panels shown on the right, the grayscale images were converted to a single color (TASK-1: green, TASK-3: red) and the respective images were merged. Only regions with moderate-to-high signal intensity were included. Areas of overlapping expression are shown in yellow. Particularly evident in this regard are granule cells in the cerebellum and olfactory bulb, and brainstem motoneurons (Talley et al., 2003)

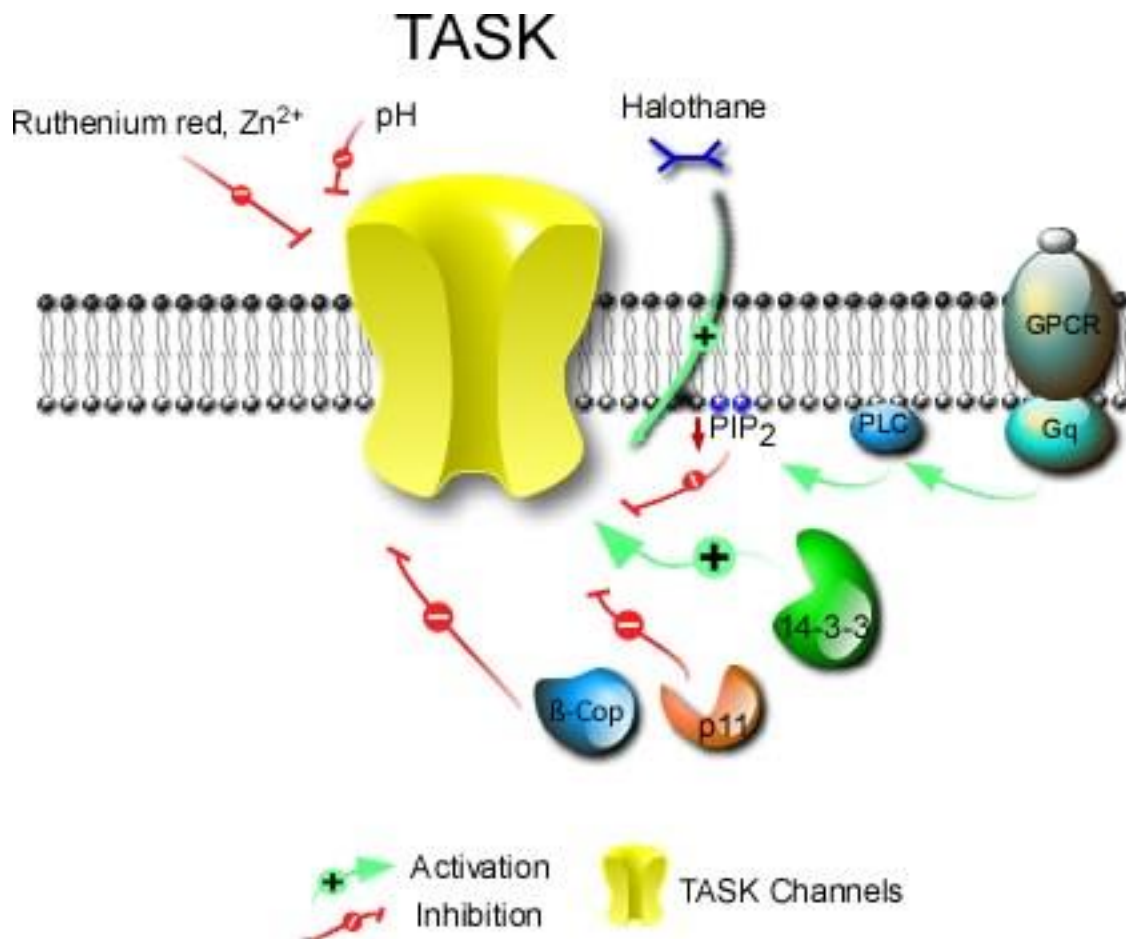


Figure 14: TASK channels regulations.

TASK currents can be inhibited in two ways by protein G coupled receptors. Notably, after G_q activation, the activation of phospholipase C (PLC) induces depletion in PIP₂ in plasma membrane reducing channel activity (Chemin et al., 2003; Czirják and

Enyedi, 2002). It was also postulated that the direct interaction between the achannel and $G_{\alpha q}$ can inhibit the channel (Chen et al., 2006). Alternatively, the expression level of these channel can be regulated via the membrane trafficking, see Figure 14. TASK1 and 3 have interaction sites (C and N terminal) with the β COP protein. This subunit of the COP-1 complex is responsible for the retention of proteins in the endoplasmic reticulum. When addressing channels to the membrane, this interaction is displaced by competitive binding with 14-3-3 protein in the C-terminal region (Rajan et al., 2002). A subunit of the annexin II complex, P11, also appears to be involved in the transport of the channel to the plasma membrane in the presence of 14-3-3 (Girard et al., 2002).

6.a) Role of TASK1 and TASK3 in cerebellar granule (CG) neurons culture and apoptosis

In 1999 Watkins and Mathie identified in CG neurons a novel K^+ conductance termed $I_{K(SO)}$ which is involved in apoptosis during development. This K^+ current is outwardly rectifying. This non-inactivating current, $I_{K(SO)}$ can be inhibited by cholinergic agonists, acting through pertussis toxin-resistant muscarinic receptors, but it does not resemble previously characterized muscarine-sensitive K^+ currents (Watkins and Mathie, 1996). Inhibition of this current depolarized the neuron, suggesting its role in excitability of CG neurons. Later on, the laboratory of Professor Michel Lazdunski provided an explanation: the current properties are identical to TASK1 and TASK3. Results suggested that homomultimeric TASK1, TASK3, and possibly the heteromultimeric TASK1/TASK3 channels, are contributing to $I_{K(SO)}$ and thus may directly influence GN K^+ -dependent cell death in culture (Lauritzen et al., 2003).

6.b) Role of TASK1 and TASK3 in nociception

KO mice for TASK1 and TASK3 highlighted their role in nociception (see chapter K_{2P} and pain perception) (Linden et al., 2006).

7. THIK family

THIK1 and THIK2 were both found to be expressed in the rat brain. While THIK2 was expressed in most brain region, with the highest expression level in the cerebellar granule cell layer and the olfactory bulb, as well as in the cortex and the hypothalamus, THIK1 expression is rather weak and restricted to some nuclei and brain regions. This differential expression is poorly overlapping (Rajan et al., 2001).

In heterologous expression system, THIK2, in contrast to THIK1, did not produce any measurable currents. However, by using a trafficking mutant (three arginines in the N-terminus of human THIK2 channel, replaced by three alanines), Renigunta et al determined the functional characteristics of hTHIK2 in heterologous system (Renigunta et al., 2014). Blin et al have shown in 2014 that THIK1, by co-assembling with THIK2, form heteromeric channels, with new functional properties (Blin et al., 2014).

8. TALK family

TASK2, TALK1 and TALK2 are members of this subfamily. These channels are activated by an alkalization of the extracellular pH (Decher et al., 2001; Girard et al., 2001). This regulation could be linked to basic residues in the extracellular P loop, interacting with the selectivity filter; substitution of these sensors by a non-charged amino acid such as an alanine led TALK channels to be constitutively opened in a wide range of pH.

Due to their expression in the pancreas, TALK1 channel plays a potential role in type 2 diabete (Duprat et al., 2005; Vierra et al., 2017).

9. TREK family

TREK (TWIK-related K⁺) potassium channels are mechano-sensitive ion channels which are members of the two pore domain (K_{2P}) potassium channel family (Fink et al., 1996; Lesage et al., 2000). They contribute to background potassium conductances in many neurons and other cell types. Their activity can be regulated by a number of different physical and chemical stimuli which include membrane stretch, membrane depolarization, heat, arachidonic acid and other polyunsaturated fatty acids (see Figure 15 below and Honoré, 2007; Mathie, 2010; Noël et al., 2011). There are three members of the TREK subfamily, TREK1 (K_{2P}2.1; KCNK2), TREK2 (K_{2P}10.1; KCNK10) and TRAAK (K_{2P}4.1, KCNK4) which share many structural and functional properties. However, it does not mean that tweens all the time act alike, indeed, they do not share the same pH sensitivity (Sandoz et al., 2009 and see below, chapter 9.c Regulations). Recent evidences showed that all three channels subunits can co-assemble to each other to form functional heterodimeric channels

(Blin et al., 2016; Lengyel et al., 2016; Levitz et al., 2016). This co-assembly has been addressed during my thesis (Chapter G. K_{2P} heteromerization, page 94)



Figure 15: Polymodal activation of TREK1 by physical and chemical stimuli from Dedman et al., 2009.

9.a) TREK family expression

TREK1 is the second K_{2P} channel to have been cloned (Fink et al., 1996), followed by TRAAK (Fink et al., 1998) and TREK2 (Bang et al., 2000) in the Lazdunski's lab. They share more than 70% of homology within the family.

TREK1, TREK2 and TRAAK are highly expressed in the central nervous system. Human TREK1 (hTREK1) expression is abundant in tissues such as the brain, the spinal cord, the heart, the kidneys, the ovaries and the small intestine (Fink et al., 1996). More specifically, TREK1 is strongly expressed in the amygdala, basal ganglia, cortex and hippocampus. TREK1 is also found in peripheral tissues such as the gastrointestinal tract, and in mechanosensitive neurons innervating the bladder and colon where it is involved in detection and transduction of skin and organ deformation (La and Gebhart, 2011).

In the peripheral nervous system, TREK channels have a strong expression in somatosensory neurons such as large and small diameter neurons of the dorsal root

ganglia. I will discuss in another chapter about the involvement of these channels in the perception of mechanical, thermal and chemical stimuli (Alloui et al., 2006; Kang et al., 2005; Medhurst et al., 2001; Noël et al., 2009; Pereira et al., 2014).

9.b) Pathologies involving TREK

(1) Cancers

Due to the important changes of pH homeostasis in cancer, the role of pH-sensitive two-pore-domains potassium channels must be investigated. If TRAAK is not involved in cancers, TREK1 and TREK2 have been identified in 2013 in several cancer types (Williams et al., 2013) either overexpressed or with an attenuated expression. TREK1 blockers or RNAi can inhibit cellular proliferation and tumor progression (Voloshyna et al., 2008). Furthermore, TREK1 could serve as a biomarker in prostate cancer (Zhang et al., 2015).

However, it has also been shown that an overexpression of TREK1 in another cell type in pancreatic cancer can inhibit the proliferation. Using a pharmaceutical activator of TREK1, BL-1249, the authors have been able to inhibit cancer cell migration (Sauter et al., 2016).

(2) Arrhythmias and heart diseases

In atrial and ventricular cardiomyocytes, leak potassium currents play a critical role in maintaining the membrane potential and in regulating the action potential duration. Some K_{2P} as TREK are also expressed in these cells and play a role in this current.

TREK1 is thought to be the actor of SAK current observed in cardiac cells. SAK current is involved in the repolarization and possesses the same characteristic properties as TREK1 current (pH-, mechano- and arachidonic acid sensitivity, for review see Decher et al., 2017a). In human ventricular arrhythmia, TREK1 mutant I267T with an increased stretch sensitivity was found to play a pro-arrhythmic role (Decher et al., 2017b).

(3) Depression

Depression is a very complex and polygenic psychiatric disorder. It's a heterogeneous disease and not all patients respond in the same way to treatments. In 2006, using

TREK1 KO mice, the Lazdunski lab has demonstrated the direct involvement of TREK1 in this pathology (Heurteaux et al., 2006).

It appears that TREK1 KO mice have the same resistant depression phenotype (in the several performed tests: Porsolt forced swim test, the tail suspension test, the conditioned suppression of motility test and the learned helplessness test) than the mice treated with antidepressants such as fluoxetine or paroxetine (Heurteaux et al., 2006). In KO mice, serotonergic (5-hydroxytryptaminergic neurons) neurons of the dorsal raphe nucleus (DRN), that do not express TREK1 anymore, have a greater activity inducing a wider release of serotonin to the targeted structures such as hippocampus. These mice appear to be insensitive to selective serotonin reuptake inhibitors (SSRIs) (e.g. Fluoxetine) and prove the potential therapeutic effect of TREK1 inhibition in depression (Heurteaux et al., 2006). TREK2 has also been found to be inhibited by SSRIs (Park et al., 2016), TRAAK remains insensitive (Thümmler et al., 2007). Dong and collaborators shown in 2015 how fluoxetine was acting on TREK2 via lateral window between TM2 and TM4 (see chapter I.C.4. Up and down state p.40).

Serotonin release in 5-hydroxytryptaminergic neurons activates the 5-HT_{1A} receptors, inducing an inhibition of the production of adenosine cyclic monophosphate (cAMP), which increases the activity of TREK1. To increase the activity of the channel will reduce the excitability of the neuron and decrease the release of 5-HT. Using antidepressants (SSRIs, fluoxetine ...), or in KO mice, the channel is no longer capable of decreasing the activity of 5-hydroxytryptaminergic neurons; thus resulting in an overall increase in 5-HT release by the DRN neurons because negative feedback is no longer present (Heurteaux et al., 2006).

In 2010, Mazella et al. demonstrated that a peptide, the spadin that results from the post-translational modification of the Sortilin/NTSR-3 (NeuroTenSinReceptor-3) receptor (Mazella et al., 2010), could be a specific blocker of TREK1 channel. This block was postulated to provide the same antidepressant like phenotype (Mazella et al., 2010) as fluoxetine and TREK1 invalidation (KO). More recently, spadin analogs were found to be more efficient at TREK1 inhibition (Djillani et al., 2017 and for review see Djillani et al., 2018).

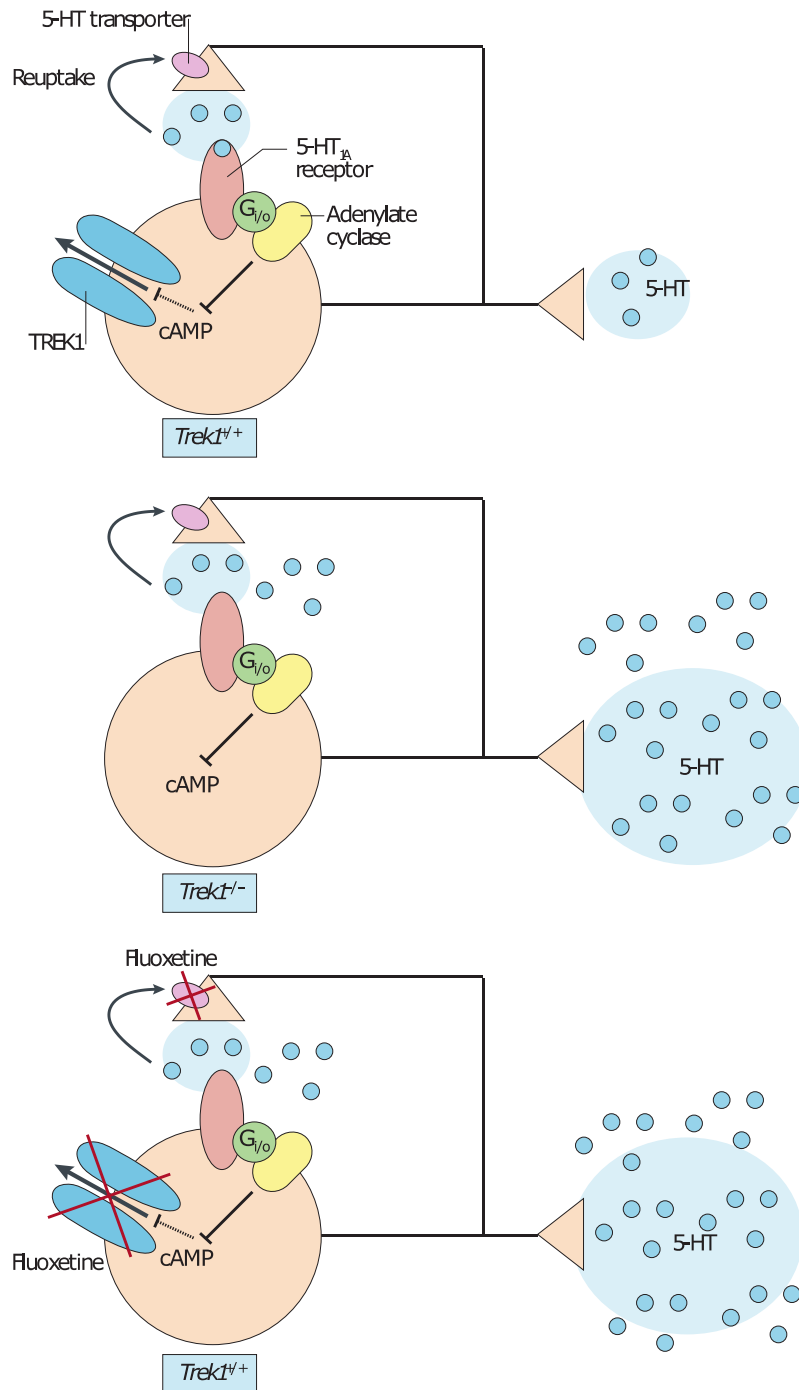


Figure 16: TREK1 is involved in the therapeutic effect of 5-HT reuptake inhibitors via a negative feedback induced on the serotonergic neurons from Honoré, 2007.

It is worth to note that recently an activator of TREK1, ostruthin, has been found to be involved in anti-depressive and anxiolytic effect in mice (Joseph et al., 2018). This botanical compound increases whole-cell TREK1 channel current in heterologous system and the author propose a possible mechanism for the anxiolytic activity

through the TREK1 activation in the lateral septum, since this last is known to be involved in the anxiety and depression-like behaviors.

(4) Cerebral ischemia and neuroprotection

In the brain, ischemia elicits hypoxia and hypoglycemia that induce neuronal excitotoxicity due to glutamate and damaging brain and resulting in disability and death. Many studies have suggested that K_{2P} channels contribute to the ability of astrocytes to protect neurons against ischemia. Heurteaux and collaborator demonstrated in 2004 that mice lacking TREK1 channel were more vulnerable to ischemia. Via injection of lysophospholipids, they even increased the survival rate of WT mice (Heurteaux et al., 2004). The concomitant effect of the lysophospholipids release and the intracellular pH acidosis could have a synergistic effect on TREK1 and TRAAK currents in neurons. This hyperpolarization will finally lead to a decreased in excitability and will ultimately protect from glutamate release (Heurteaux, 2007).

Interestingly, ischemia is one of the symptoms resulting from circulating nitrogen bubbles in decompression sickness. Bubbles in this pathology alter the vascular endothelium while circulating and result in neurological damage. In mice, it has been shown that the presence of TREK1 potassium was neuroprotective in decompression sickness (Vallee et al., 2012). Conversely, it has also been shown that acute fluoxetine treatment increases the survival rate. This is a paradox because fluoxetine is a blocker of TREK1 channels. More recently Vallee used spadin to block TREK1. This last where more sensitive to pathogenic decompression. Nevertheless, mice which had both blocked TREK1 channels and fluoxetine treatment were better protected. They concluded that the preventive effect of such an acute dose of fluoxetine is enhanced when TREK1 is inhibited, and furthermore, increased the survival rate (Vallée et al., 2016).

9.c) Regulations

(1) Mechanosensitivity

TREK channels are activated by shear stress, membrane stress and negative membrane pressure (Bang et al., 2000; Honoré, 2007; Patel et al., 1998). This sensitivity is conserved in excised membrane patch, suggesting an intrinsic regulation in the channel (Berrier et al., 2013). The C-terminus is involved in this regulation

(Maingret et al., 1999) since mutation in it modify its sensitivity. The curvature of the membrane was found to play a role on TREK channels activation (Patel et al., 1998).

This mechano-sensitivity has been studied in triple KO mice for TREK1, TREK2 and TRAAK. These mice, as expected, shown an increased mechanical allodynia at very low threshold in von Frey assessment (Alloui et al., 2006).

(2) Thermosensitivity

Increase in the temperature can activate TREK and TRAAK channels (Kang et al., 2005; Maingret et al., 1999) and this regulation may involve the C-terminus (Maingret et al., 1999) or more specifically a coupling between the C-type gate and the selectivity filter (Bagriantsev et al., 2011, 2012).

This thermosensitivity has been studied in mice lacking TREK1 and TRAAK channels. These last are more sensitive to temperatures under 17°C or over 46°C (Alloui et al., 2006; Noël et al., 2009). TREK2 would be more involved in the sensitivity of less harming temperature (Pereira et al., 2014). This role in thermosensitivity is even more important when we consider the expression of TREK channels in neurons that also express TRPV1 and TRPM8 (Yamamoto et al., 2009). These last are involved in the depolarization of the sensor neurons after a hot or cold stimulus. By their action, TREK channels could counterbalance the effect and abolish the signal transduction by a hyperpolarization of the membrane (Alloui et al., 2006; Noël et al., 2009).

(3) Sensitivity to pH

TREK1, TREK2 and TRAAK are regulated by intra- and extracellular pH. TREK2, unlike TREK1 and TRAAK, is activated by extracellular acidification (Sandoz et al., 2009). Beside to be oppositely regulated, TREK1 and TREK2 share the same pH sensor i.e. a conserved histidine localized in the first extracellular domain (H126 for TREK1 and H151 pour TREK2). TREK1 protonation of this histidine induces an electrostatic attraction with two negatively charged residues in the P2 (D263 and E265), while the protonation of the histidine 151 in TREK2 induces an electrostatic repulsion with a positively charged arginine (R293) in the P2 loop (Sandoz et al., 2009).

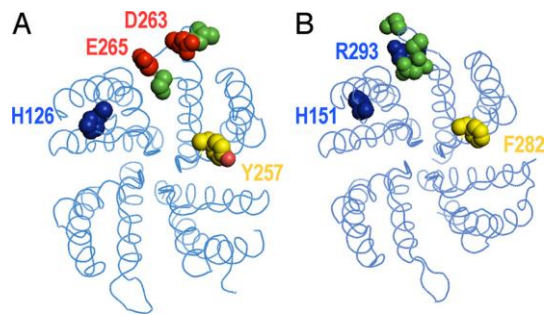


Figure 17: Top view of the extracellular side of homodimeric TREK1 (A) and TREK2 (B) channels. Cytoplasmic Nter and Cter domains are not shown. Studied residues are colored in only one monomer. pH-sensing histidines are indicated. Positively charged residues are in blue and negatively charged residues in red. Neutral residues are depicted in green and aromatics F282 and Y272 are in yellow along with the oxygen atom in red in Y272.

TREK are also regulated by internal pH. TRAAK is activated at intracellular alkaline pH unlike TREK1 and TREK2 which are both activated by intracellular acid pH via the glutamate residue 306 (Honoré et al., 2002). This regulation could have a role during ischemia (Lesage and Barhanin, 2011).

(4) Sensitivity to lipids

Polyunsaturated fatty acids (PUFA) such as arachidonic acid (AA) are activators of TREK channels (Patel et al., 1998). They increase TREK currents up to 20 times (Maingret et al., 2000) and this sensitivity is involved in the neuroprotection in ischemic condition (Heurteaux et al., 2004)

Lysophosphatidic acid (LPA) is present in the membrane of cells and participate in pathophysiological conditions through its involvement in signaling pathways after coupling with G protein-coupled receptors. This lysophospholipid would have an indirect effect, through its insertion in the plasma membrane, and would thus rely on the mechanosensitivity of TREK channels (Lesage et al., 2000; Maingret et al., 2000).

PIP2 (phosphatidylinositol-4,5-biphosphate), phosphatidic acid (PA) and phosphatidylserine (PS) are able to activate TREK1 channel (Chemin et al., 2005; Lopes et al., 2005). TREK1 bares in its C-terminus a positively charged motif (R297, K301, K302, K304 and R311). It will create electrostatic bounds with the negatively charged phospholipid PIP2 in the bilayer (Sandoz et al., 2011), stabilizing the channel in an active form.

A depletion in PIP2 after G_q protein coupled receptor activation will inhibit TREK1 current (Chemin et al., 2003; Sandoz et al., 2011). Also, in 2007, it was reported that PIP2 could have an antagonism effect on TREK1 (Chemin et al., 2007). This dual regulation has recently been addressed using Bioluminescence Resonance Energy Transfert assay (BRET). They proposed a controversial model where PIP2 directly compete with anionic lipids agonism such as PA (Cabanos et al., 2017).

Specificity of action

All members of TREK subfamily are able to be activated by phosphatidic acid (PA). PA is extremely short-lived and will quickly be degraded by conversion into DAG. Our group has shown that phosphatidic acid (PA), produced by phospholipase D 2 (PLD2) from phosphatidylcholine, is able to activate TREK1 and TREK2 channels. This specificity of mechanism is linked to the direct coupling between PLD2 and TREK channels, in their C-terminus. This interaction allows the existence of a PA rich micro-domain in which the channel is included inducing its activation (Comoglio et al., 2014).

(5) Regulation by protein G coupled receptors (GPCR)

The complex gating of TREK1 is regulated by various receptors and second messenger pathways. TREK1 and TREK2 currents both are down-regulated by the stimulation of both G_s - and G_q -coupled membrane receptors (Kang et al., 2006; Lesage et al., 2000; Patel et al., 1998). Several GPCR are able to regulate TREK channels. Notably G_i , G_s and G_q types.

Activation of G_s leads to an increase of cAMP production via activation of adenylyl cyclase (AC). Activated protein kinase A (PKA) will then phosphorylate the serine 333 on TREK1 (Maingret et al., 2000), and serine 359 of TREK2 (Lesage et al., 2000). This pathway is involved in regulation by serotonin through 5HT4 receptor.

Activation of G_i , instead leads to a decrease of cAMP, followed by a downregulation of the activity of protein kinase A. This will dephosphorylate the serine 333 and leads to increase TREK current (Lesage et al., 2000). This regulation is observed by Sandoz after $GABA_B$ receptor activation by baclofen, a $GABA_B$ receptor agonist (Sandoz et al., 2012). Using a photoswitched tethered ligand approach, he shown that this activation

led to activation of the endogenous TREK1 current in CA1 neurons (Sandoz et al., 2012).

GABA_B receptor activation as also been suggested to be involved in hippocampal astrocytes via direct interaction of TREK1 and G_{βγ}. This direct interaction through N-terminus of TREK1 would make TREK1 channel glutamate-permeable (Woo et al., 2012). TREK2 is also activated by G_i pathway (Deng et al., 2009).

Activation of G_q is linked to TREK1 inhibition by three different manners. First, activation of phospholipase C (PLC) hydrolyses PIP₂ and as seen earlier, would induce a C-tail uncoupling from the membrane (Sandoz et al., 2011). This is observed in mGluR1 and 5 regulation. Also PKC induces this uncoupling via the phosphorylation of serine 300, after serine 333 phosphorylation (Murbartián et al., 2005). Finally, TREK1 could directly been linked to DAG (Chemin et al., 2003).

TRAAK also possesses in the C-terminus residues that can be phosphorylated by PKA and PKC (Chemin et al., 2003; Fink et al., 1998), but is unaffected by such stimuli.

(6) Protein partners

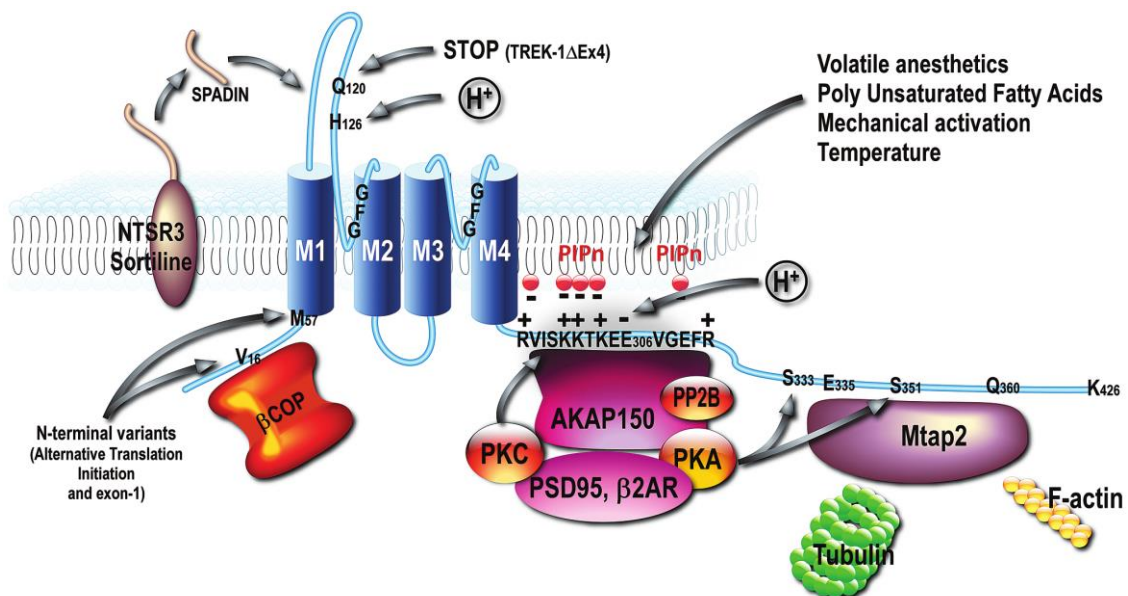


Figure 18: Partners, regulatory domains and alternative variants of TREK1 channel, from Noël et al., 2011.

- A-kinase-anchoring protein AKAP150

AKAP150 (A kinase anchoring protein) is a scaffold protein that interacts with the proximal C-terminal (pCT) domain of TREK1 (R297 to R311), which is also one involved in the stimulation by PIP2. Its binding to a key regulatory domain of TREK1 transforms low-activity TREK1 channels at rest into robust leak conductance insensitive to AA, stretch and acidification (Sandoz and Lesage, 2008; Sandoz et al., 2006).

- Microtubule-associated protein 2 MAP2

MAP2 is a partner of TREK1 and TREK-2 (Sandoz et al., 2008). MAP2 is a scaffold protein located in dendritic spines. The interaction of MAP2 with TREK1 occurs at the C-terminal domain at a site between positions 335 and 360. This site contains 4 positively charged amino acids (K342, K347, R348, K349), essential for the association between the two proteins. MAP2 increases the channel density at the membrane involving tubulin in this effect (Sandoz et al., 2008). AKAP150 and MAP2 can bind TREK1 at the same time, thus placing the channel in a microdomain comprising elements of the cytoskeleton, regulatory proteins, kinases, ion channels and GPCR.

- Coatmerprotein complex 1 COP1

The β subunit of this protein (β -COP1) can directly interact with TREK1 N-terminus. β -COP1 is involved in the transport from Golgi apparatus to plasma membrane. Expression of this β -COP1 increases TREK1 expression at the plasma membrane and thus its current density (Kim et al., 2010).

- Neurotensine 3 receptor (NTSR3)

This receptor is involved in intracellular trafficking in Golgi apparatus. It directly interacts with TREK1, increasing its expression at the plasma membrane. However, another regulation has been mentioned earlier. Due to a post translational maturation, an N-terminus peptide is cleaved from NTSR3, the spadin. This peptide linked to the TREK1/NTSR3 will lead to its endocytosis, decreasing TREK1 current (Mazella et al., 2010).

TRESK channel (K_{2P}18.1) is the last K_{2P} channel to be discovered (Sano et al., 2003). This channel is distant in sequence homology from the other subunits. It is particularly different in its structure because it has a very long intracellular loop greater than 120 amino acids and a small C-terminal part. Originally cloned in the spinal cord from which it derives its name, TRESK is mainly expressed in the trigeminal ganglia (TG) and dorsal root ganglia (DRG) (Kang and Kim, 2006; Sano et al., 2003; Yoo et al., 2009). It represents the most abundantly expressed K_{2P} channel in those structures in which it is a major component of the background potassium conductance (Dobler et al., 2007).

10.a) TRESK channel structure, pharmacology, and electrophysiological properties

The TWIK-related spinal cord potassium (TRESK) channel is encoded by the KCNK18 gene (Enyedi and Czirják, 2015; Sano et al., 2003). The general properties and structure of TRESK are similar to those of other K_{2P} channels; however, the protein shares only a 19% homology in amino acid sequence amongst its K_{2P} relatives, indicative of sub-family status (Enyedi and Czirják, 2015; Enyedi et al., 2012). The main differences with other K_{2P} channel is its huge intracellular loop between TM2 and TM3 and a small C-terminus.

The leak current induced by its expression shows an outwardly rectification, that is, unlike TREK currents, not dependent to voltage. This channel possesses the same general properties as K_{2P} channels: poor sensitivity to extracellular tetraethylammonium (TEA, external application) and 4-aminopyridine and is inhibited by barium and quinidine (Kang et al., 2004a; Sano et al., 2003).

TRESK channel is also activated by clinical concentrations of volatile anesthetics such as halothane and isoflurane (Liu et al., 2004). However, the sensitivity of TRESK-KO mice to these anesthetics is unaffected, minimizing its involvement in anesthesia (Chae et al., 2010).

10.b) Tissue expression

TRESK is expressed in human brain. In the central nervous system, such as dorsal root ganglia, trigeminal ganglia, cerebellum, the cortex and sympatic and

parasympatic ganglia (Yoo et al., 2009). Peripherally, it is found mainly in the testis and the thymus and spleen of rat and mouse (Kang et al., 2004a).

10.c) Regulation

(1) Mechanosensitivity

It has been shown in 2013, by Gasull's team, that like TREK channels, TRESK current was able to be modulated by membrane stretch and shear stress. This mechanism would not be linked to C-terminus interaction with the membrane, but more by conformational change of the structure in the membrane (Callejo et al., 2013).

(2) Sensitivity to pH

The murine TRESK channel is activated by acid pH (pH 6) and inhibited by basic pH (pH 9). The same histidine responsible for the pH sensitivity of TASK channels is conserved in murine TRESK channels and a substitution of this histidine for asparagine abolishes this sensitivity (Dobler et al., 2007; Kang and Kim, 2006). In contrast, human homolog does not have this histidine and is therefore not sensitive to pH.

(3) Sensitivity to lipids

Another indication of its involvement in nociception is its activation by lysophosphatidic acid (LPA), a lysophospholipid released in case of tissue damage. In DRGs, LPA activates the TRESK channel via lysophosphatidic acid receptors (LPAR) coupled to the G_q protein. While LPA activates TRPV1 channels leading to depolarization, the hyperpolarization caused by activation of the TRESK channel would counteract the nociceptor signal. With this inhibitory effect in sensory neurons, the TRESK channel appears to be a good candidate for the development of new analgesics (Kollert et al., 2015).

An application of arachidonic acid as well as other PUFAs was found to inhibit TRESK (Sano et al., 2003).

Furthermore, it has recently been shown that hTRESK was activated by a direct interaction of PIP₂ with the intracellular loop. PIP₂ concentration is directly linked to GPCRs activity, and so can be Ca²⁺ intracellular concentration. Therefore the

inhibitory effect of PIP₂ depletion could be counterbalanced depending on the GPCR receptor activation, it seems to be very investigated in a cell specificity manner (Giblin et al., 2018).

I will discuss this lipid regulation in the chapter dedicated to K_{2P} and pain perception.

(4) Partner proteins and calcium dependence

The intracellular loop connecting domains M2 and M3 is the place of important regulation of the channel. The human TRESK channel is constitutively inhibited by phosphorylations at serine 252 by PKA and at a serine cluster (S262, S264 and S267) by Microtubule-Affinity Regulating Kinase (MARK) kinase. S252 phosphorylation promotes the binding of calcineurin, a serine/threonine phosphatase, at the PQIIS site present in the N-terminal intracellular loop (Figure 19 A). An increase in intracellular calcium concentration activates calcineurin which can then bind to the LQLP motif, another interaction site present in the C-terminal part of the loop. The phosphatase activity of calcineurin dephosphorylates the serines, which increases the activity of the TRESK channel (Figure 19 B). The channel then returns to its basal state by rephosphorylation by the PKA and MARK kinases (Enyedi and Czirják, 2015). The constitutively inhibited state of rest is favored by the attachment of the 14-3-3 protein. This protein recognizes the phosphorylated serine 252 and increases the inhibition. Nevertheless, 14-3-3 also has an antagonistic effect. Its binding inhibits MARK kinases, promotes the activated state of TRESK and slows down its return to the basal state (Figure 19 C) (Enyedi and Czirják, 2015).

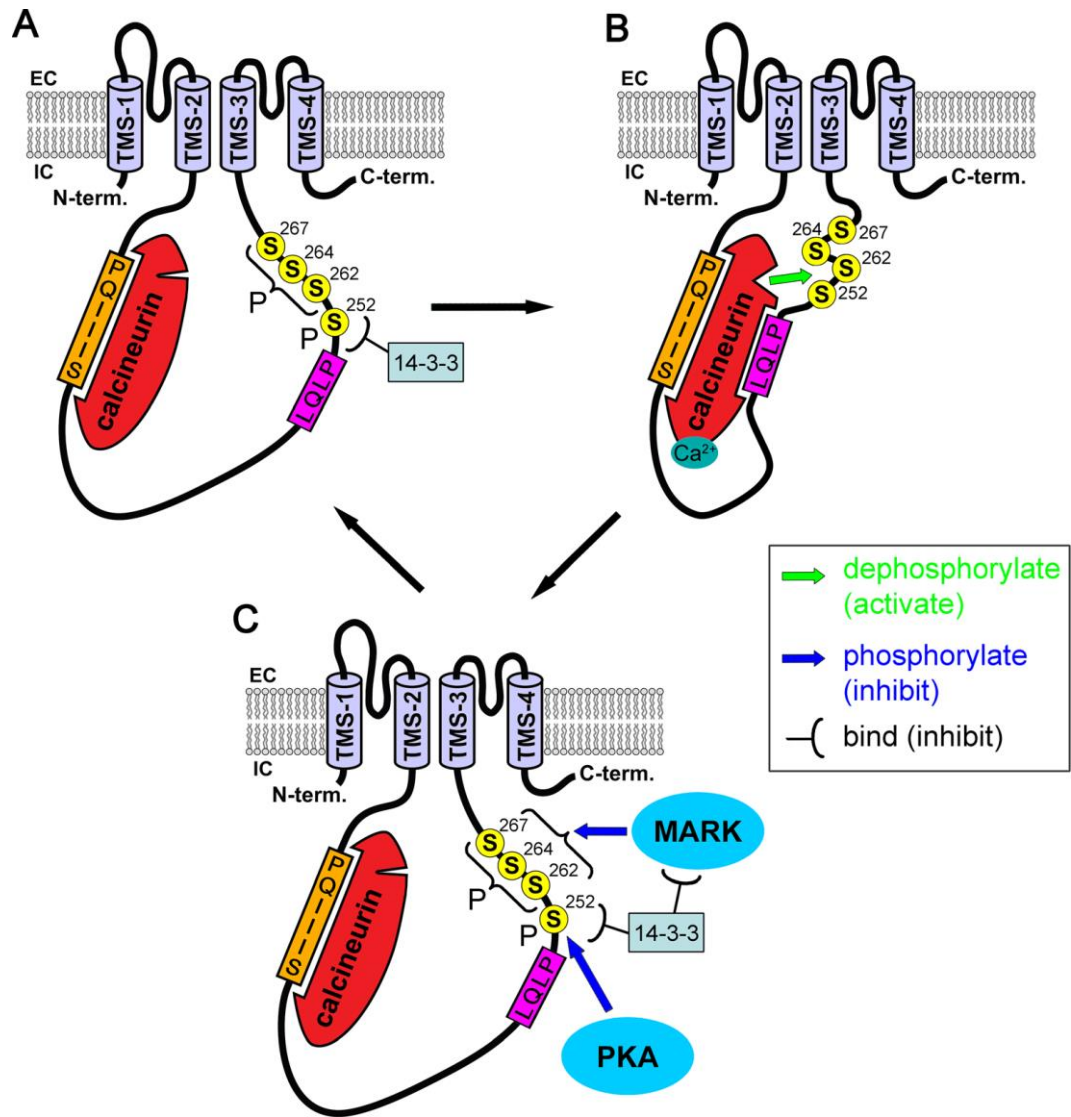


Figure 19: Regulation of the TRESK channel by calcineurin and phosphorylations (from Enyedi and Cziráj, 2015).

D. K_{2P} channels and pain perception

Pain is defined as “an unpleasant sensory and emotional experience associated with actual or potential tissue damage, or described in terms of such damage” (International association for the study of Pain, 1986). As a self-protective mechanism, the sensation of pain alerts us to real or impending injury and triggers appropriate protective responses, showing how important it is to determine and characterize ion channels involved in peripheral tissue. There are different pain-causing signals such as heat, pressure, chemical agents, among others, that will be detected by ion channels and receptors in the peripheral nociceptor. The signal is then processed to the central nervous system via dorsal root ganglion (DRG) or trigeminal ganglion (TG) (Waxman

and Zamponi, 2014). The presence of K_{2P} in DRG neurons and TG (Medhurst et al., 2001), via their role in hyperpolarization, tunes the amount of nociception transmitted to CNS, therefore a pivotal contribution of two-pore-domain potassium (K_{2P}) channels in chronic pain processing is believed.

TASK1 and TASK3. KO animal has been very useful tool to understand the involvement of these channels in pain perception. TASK1 KO mice showed increased sensitivity to thermal nociception in a hot-plate test but not in a tail-flick test (Linden et al., 2006) and a lesser sensitivity to analgesic and sedative effect of a cannabinoid agonist (Linden et al., 2006). These findings suggest that TASK1 channels expressed in supraspinal pathway are involved in the nociceptive behavior.

TRESK. In DRGs, TRESK channel is expressed in nociceptive neurons of small and medium diameter. In models of neuropathic pain induced by nerve damage, the expression of TRESK is significantly reduced, leading to hyperexcitability of the neurons and an increase in the discharge frequency of the action potentials. Mice treated with anti-TRESK RNA (RiboNucleic Acid) become hypersensitive to mechanical stimuli but not to thermal stimuli (Tulleuda et al., 2011).

TREK. As seen in the description of the different K_{2P} subunit made previously, TREK1 has a major role due to its finely tuned regulations. KO animals for TREK1 have been useful to understand the role of TREK1 in sensitivity and mechanical stimulation in neurons expressing TRPV1 (Alloui et al., 2006, Yamamoto et al., 2009). Double KO animals for TREK1 and TRAAK (Noël et al., 2009) and even for TREK2 show defects in mechanical and cold pain responses (Pereira et al., 2014).

TREK channels are involved in several pain stimuli perception, as seen in Figure 20.

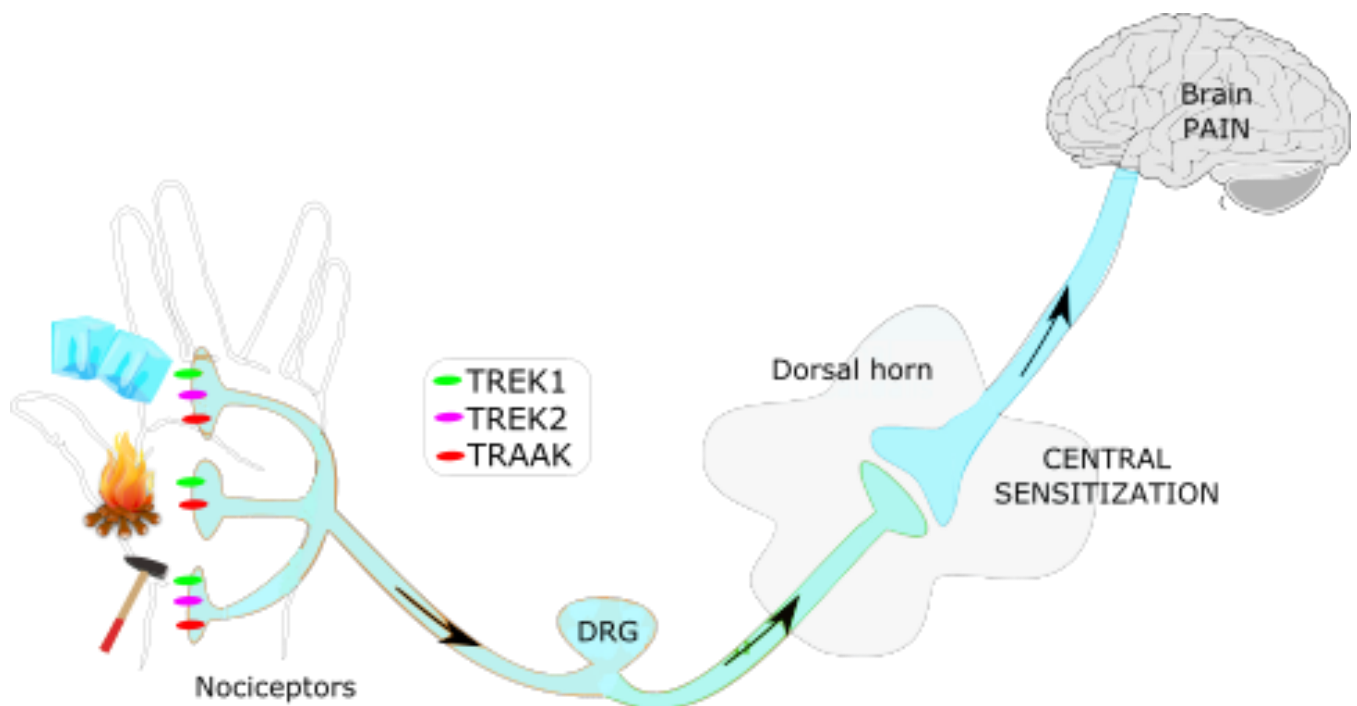


Figure 20: TREK1 is involved in several polymodal pain perception. Thermal and mechanical stimuli are detected by several TREK channels expressed in nociceptors (along with other ASIC, TRP and piezo channels, not shown here). They are primary sensors of a nervous signal that will be sent to the cortex where it will be integrated as a painful signal. DRG for dorsal root ganglion.

Morphine, an opioid extract from poppy used in pain medication, has been shown to increase TREK1 current, *via* direct interaction with G-protein-coupled μ opioid receptor μ OR. This action on TREK1 current leads to analgesic effects without side effect observed with morphine (Devilliers et al., 2013).

Other molecules have been shown to be able to stimulate TREK current in dorsal root ganglion neurons (Dadi et al., 2017; Loucif et al., 2018).

TRESK and TREK1. In the pain pathway, the TREKs and TRESK channels located at C-fibers terminals can counteract the activation of inward-conducting ion channels by pressure, heat or cold, whereas steady Kv currents stabilize resting membrane potential and regulates action potential threshold. As TREKs and TRESK are targets of modulation by receptor agonists, they are likely to play an active role in the regulation of excitability in DRG neurons (Kang and Kim, 2006).

LPA signaling in the nervous system has been linked to neuropathic pain through LPA protein-G coupled receptor (see below, Figure 21). LPA is mainly released from the

membrane during tissue injury. Direct inhibition of TRPV1 by LPA leads to a depolarization and action potential firing in DRG neurons (Nieto-Posadas et al., 2011) (Kollert et al., 2015). TRESK, by its activation via calcium increase following Gq protein activation would counterbalance the depolarizing effect of TRPV1. But the TREK1 inhibition linked to PIP2 depletion after PLC activation would also leads to an excitatory effect on DRG neurons. Therefore the level of expression of each of these channel seems to be the key mechanism in pain signaling after inflammatory process.

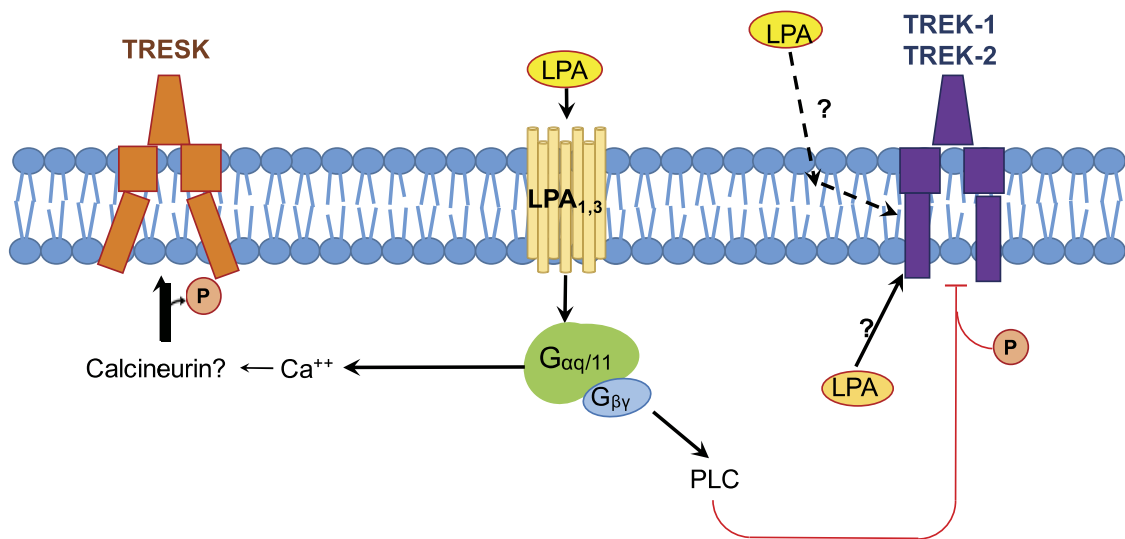


Figure 21: Lysophosphatidic acid (LPA) and two-pore-domain K (K_{2P}) channels. Representation of K_{2P} channels in the membrane. TWIK-related K (TREK)-1, TREK-2 are activated by extracellular LPA through an unknown mechanism that might include effects in membrane physical properties. LPA binding to specific LPA receptor results in the phosphorylation and inactivation of TREK1 and TREK-2 or the dephosphorylation and activation of TWIK-related spinal cord K (TRESK) channels (Chemin et al., 2005; Kollert et al., 2015) from Hernández-Araiza et al., 2018).

To sum up, see the Table 1 below that regroups the studies investing the K_{2P} subunits involved in several pain phenotypes.

Subunit	Manipulation	Expression/excitability	Pain phenotype	Ref.
TWIK1	Nerve injury (SNI)	↓TWIK1 expression	Not determined	(Pollema-Mays et al., 2013)
TASK1	Knockout	↓TASK1 expression	↑Heat	(Linden et al., 2006)
	Inflammation	↓TASK1 expression in DRG	Spontaneous pain	(Marsh et al., 2012)
TASK2	Inflammation	↓TASK2 expression in DRG	Spontaneous pain	(Marsh et al., 2012)
TASK3	Inflammation	↓TASK3 expression in DRG	Not determined	(Marsh et al., 2012)
	Knockout	↓TASK3 expression	↑Cold	(Morenilla-Palao et al., 2014)
TREK1	Knockout	↓TREK1 expression ↑AP firing ↓Inflammatory	Reduced cold hypersensitivity after SNL TREK1 inhibited by PGE2 and cAMP, ↑Mechanical, heat	(Alloui et al., 2006)
TREK2	Knockdown inflammation	↓TREK2 expression in DRG	Spontaneous pain	(Acosta et al., 2014)
	Knockout	↓TREK2 expression	inhibited by PGE2 and cAMP ↑ Mechanical, ↑ perception of nonaversive warm	(Pereira et al., 2014)
TRAAK	Knockout	↓TRAAK expression	↑Mechanical, heat TREK1/TRAAK KO: ↑noxious cold pain but reduced cold sensitivity after oxaliplatin	(Descoeur et al., 2011; Noël et al., 2009)
TRESK	Human dominant-negative mutation	↓TRESK currents	↑Migraine pain	(Lafrenière et al., 2010)
	Nerve injury (axotomy) TRESK knockdown	↓TRESK expression in DRG	↑Mechanical Trend for thermal pain	(Tulleuda et al., 2011)
	Knockout	↓TRESK currents	Not determined	(Dobler et al., 2007)

	TRESK overexpression after spared nerve injury	↑TRESK currents	↓Mechanical allodynia	(Zhou et al., 2013)
--	--	-----------------	-----------------------	---------------------

Table 1: Summary of studies investigating the effect of altered K⁺ channel expression and function on acute, neuropathic, and inflammatory pain phenotypes from Li and Toyoda, 2015.

E. Pathophysiology of migraine

The word migraine derives from the greek word “hemicrania” (imikrania; ημικρανία) which means half the skull (Rose, 1995). Hippocrates described in 400 BC the occurrence of migraine attacks (including the different phenomena accompanying the migraine). In 1988, for the first time, migraine and other headache disorders were comprehensively classified by the International Headache Society in the International Classification of Headache Disorders, nowadays the 3rd edition. Since, the World Health Organization, researchers and clinicians refer to its diagnostic criteria. Hopefully, migraine is no longer treated as in middle age times, with trepanning, a surgical procedure that involves drilling a hole into the skull with one aim being to release evil spirits (Collado-Vázquez and Carrillo).

1. Generalities

Migraine consists of recurrent and disabling headaches, usually accompanied by nausea, vomiting, phonophobia or photophobia, or other autonomic symptoms (International Headache Society, 2004). Although the initiation of a migraine attack is frequently associated with a wide variety of internal and external triggers such as hormonal fluctuations, skipping meals or sensory overload, often the attacks are precipitated by external triggers such as alcohol, lack of sleep, or stress (Kelman, 2007). The neural vascular mechanisms underlying the development of this primary condition remain to be elucidated. In ~20% of cases, attacks are preceded by visual disturbances known as auras that may take the form of scintillating shapes, hallucinations, or black spots. The aura is thought to be associated with the phenomenon of cortical spreading depression (CSD), a wave of neuronal depolarization that slowly propagates over the cortical regions of the brain but this connection has been recently questioned (Borgdorff, 2018; Vgontzas and Burch, 2018).

1.a) Prevalence

Migraine is the most common neurological disorder, the third common disease in the world affecting ~15% of the population (that’s around 1 in 7 people), and occurs three times more often in women than men (Steiner et al., 2013). Chronic migraine affects approximately 2 % of the population (Natoli et al., 2010). Migraine often starts at

puberty and most affects people between 35 and 45 years. However, younger can also be affected, about 4 % of pre pubertal children suffer from migraine. Finally, the estimated proportion of time spent with migraine during an average person's life is 5.3%.

Patients suffering from migraine are more susceptible to depression; in France, about 10 % of the patient suffering from migraine suffer from severe depression. The annual cost for a patient is about 3000 €. The financial burden of migraine on France economy is estimated at 242 M€ annually (Aly et al., 2018).

1.b) Sensitivity alteration as path to migraine?

The symptoms that accompany migraine from the prodromal stage through the headache phase suggest that multiple neuronal systems function abnormally. The migraine brain is altered structurally and functionally, hypersensitive to fluctuations in homeostasis, less able to adapt and subject to recurrence of headache. Furthermore, data supporting the activation and sensitization of the trigeminovascular system include the progressive development of cephalic and whole-body cutaneous allodynia during a migraine attack (Louter et al., 2013). Here, I will mainly focus on the role of the trigeminovascular pathway.

Disrupted and dysregulated systems of peripheral nerve excitation are at the origin of most pathological states of head pain. This excitation is tightly controlled by coordinated plasmalemmal¹ ion channels whose main function is to control the degree of neuronal action potential depending on the strength of the external trigger (Du and Gamper, 2013).

2. Anatomy of the trigeminovascular pain pathway

The trigeminal is the primary nerve that carries pain impulses from the mouth, teeth, head, face, ears, and neck to the central nervous system via the fifth cranial nerve. The trigeminal system consists of afferent nerve fibers innervating the pial and dural meningeal vessels surrounding the brain, arising from trigeminal ganglion, and efferent

¹ Plasmalemma or cell membrane

projections synapsing with second order neurons in the trigeminal nucleus caudalis (TNC) (Liu et al., 2008).

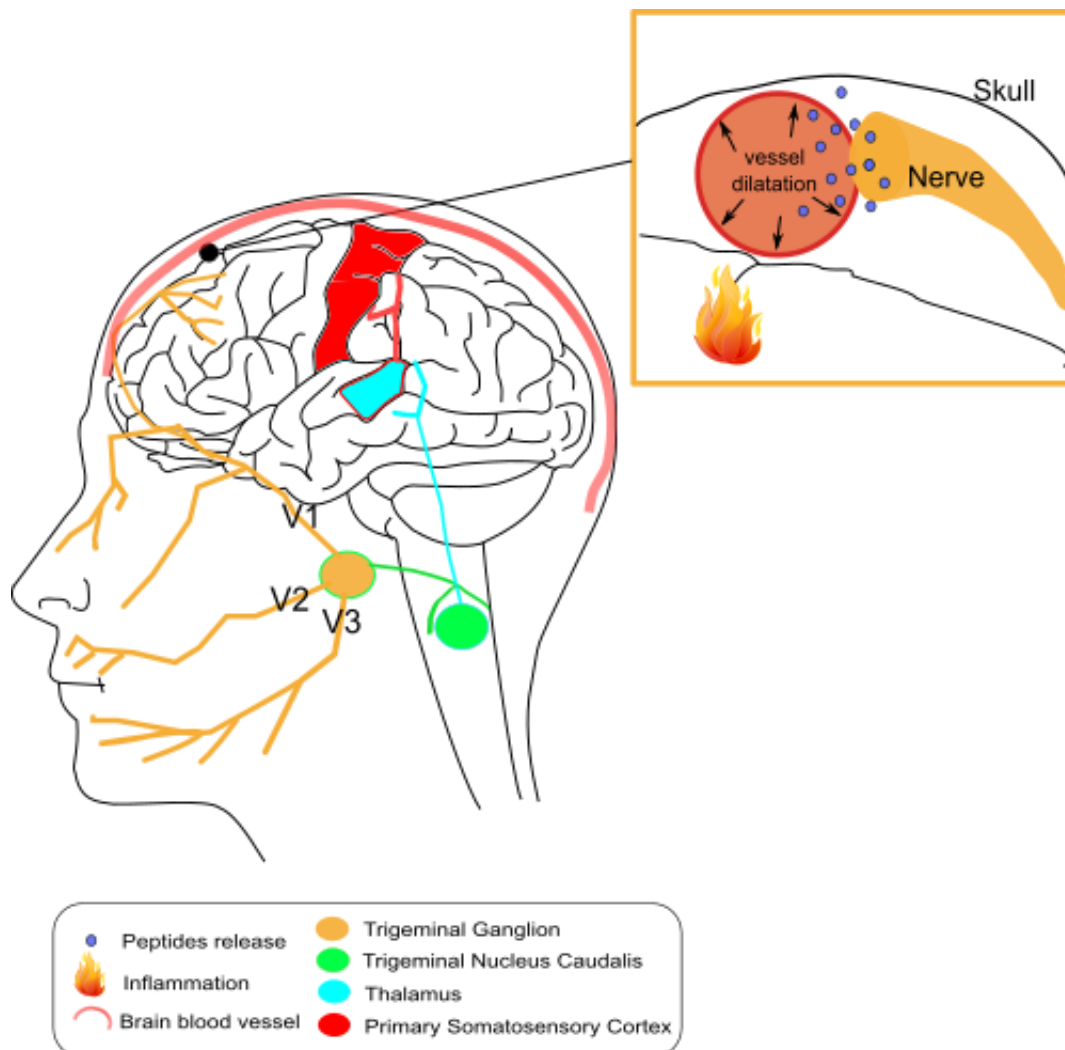


Figure 22: Migraine step by step. Migraine is triggered when a wave of electricity which starts in the trigeminal nerve on the side of the face stimulates the release of peptides such as CGRP and other substances that cause inflammation and makes other nerves more sensitive to pain. In the inset on the right, the depolarizing wave enters the brain and ripples across the surface of the brain – and together with CGRP causes blood vessels to dilate. Sensitization of the nerves progresses from peripheral nerve cells on the skin to central neurons in the brain.

2.a) Peripheral innervation of the trigeminovascular system

The headache phase of the migraine attack is thought to initiate as an activation of nociceptors innervating pial, arachnoid and dural blood vessels. The nociceptive innervation of intracranial vasculature and meninges consists of unmyelinated (C-fibers) and thinly myelinated (A δ fibers) axons containing vasoactive neuropeptides such as substance P and calcitonin gene-related peptide (CGRP). The cell body being

in the trigeminal ganglion, axons reach the dura mainly through the ophthalmic branch of the trigeminal nerve (V1) and to a lesser extent to other divisions. Dura is also innervated by neurons on the upper cervical dorsal root ganglia.

2.b) Central projections of meningeal primary afferents

The projections from upper cervical nerve roots and trigeminal ganglion converge at trigeminal nucleus caudalis (TNC), which explains the distribution of migraine headache in anterior and posterior part of head and upper neck. Fibers from TNC travel to ventroposterior medial nucleus of thalamus and to sensory cortex. Other fibers also project to several subcortical areas such as reticular formation, cerebellum, and midbrain. Nociceptive information is also transmitted to limbic system, which explains emotional response in migraine headache (see Figure 23).

3. Activation and sensitization of the trigeminovascular pathway

3.a) Cortical spreading depression

The transient phenomenon of cortical spreading depression (CSD) is a wave of propagating excitation, leading to neuronal and glial depolarization. The wave starts in visual cortical areas to slowly (from 2 to 6 mm/min) move forward the cortex (Lauritzen, 1994). After this event, a long-lasting depression (hyperpolarization) is observed in the neuronal and glial neurophysiological activity, suggesting the CSD seems to propagate via non synaptic mechanisms (Leao, 1944). The initial wave of CSD represents a massive depolarization of glial cells and neurons, accompanied by a large increase in extracellular K^+ , a reduction in extracellular Na^+ , and significant fluxes of other ions including protons, Cl^- , Mg^{2+} and Zn^{2+} .

Kramer and collaborators in 2016 (Kramer et al., 2016) have demonstrated that glutamate-induced toxicity is at the origin of this CSD after the alteration of the neuronal environment by noxious stimuli. Glutamate activates cation currents, through NMDA receptors, leading to disruption of ion gradients. The depolarization, which is usually counterbalanced by Na^+/K^+ pumps, is not quickly enough recovered, thus is followed by a long-lasting inhibition of spontaneous neuronal activity. Studies in animals indicate that CSD can activate pain pathways, but the role of CSD as a

potential trigger for migraine headache remains uncertain. Moskowitz team proved in rodent that the CSD provokes a trigeminovascular activation (Bolay et al., 2002).

To trigger CSD, experimentations on animal models were made. It rely on local mechanical and electrical stimulations, as well as KCl, CaCl₂ injections, along with glutamate receptor agonists. Most often, an extracellular K⁺ increase is a critical step to initiate cortical spreading depression. This CSD can be inhibited by glutamate receptor antagonists, suggesting a role for glutamate receptors within the brain in this paradigm.

3.b) Peripheral and central sensitization

Sensitization occurs after neurogenic inflammation when neurons become more responsive to both nociceptive and non-nociceptive stimuli, namely decrease in thresholds of response, increase in magnitude of response, expansion of receptive field, and apparition of spontaneous activity.

Sensitive neurons involved in pain react differently as they are activated. Thus a same stimulation, will create an amplified reaction, or neurons would be activated by a usually indifferent stimulation.

Perivascular peripheral nociceptor sensitization (terminations close to meningeal vessels) could explain the pulsatile nature of the headache, reflecting an abnormal sensitivity to cephalic pulsations normally non-algogenic.

Sensitization of central nociceptors in the caudal TNC could be responsible for cutaneous allodynia (that is, the occurrence of pain triggered by a normally painless stimulus) observed by some patients in the periorbital area. Contralateral and/or localized periorbital allodynia in the limbs could be a reflection of neural sensitization at the thalamic stage (see Figure 23 below).

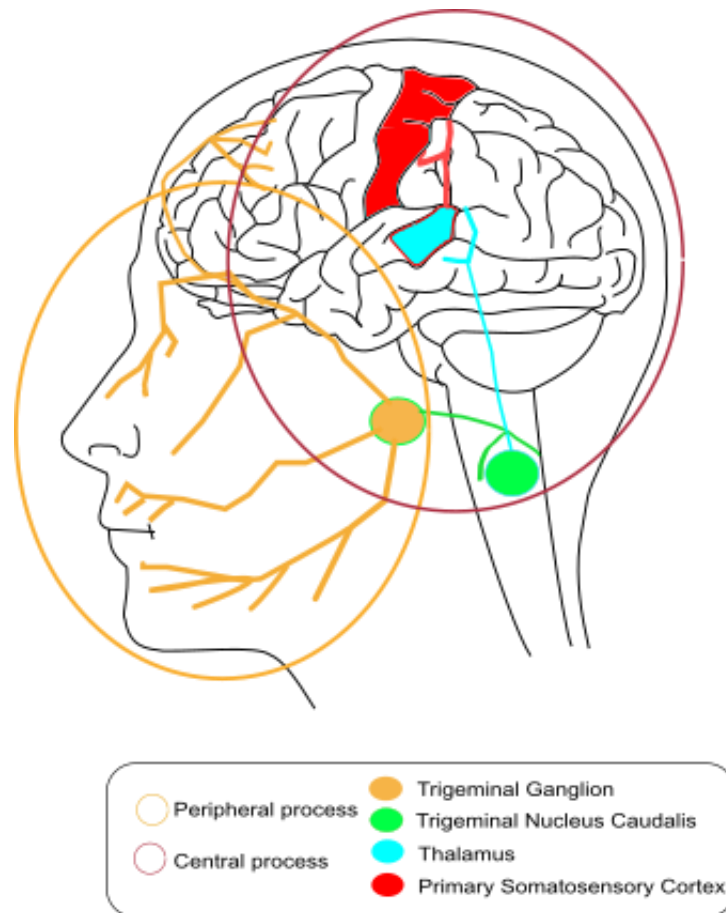


Figure 23: Pathways and brain regions involved in the transmission of migraine. Primary afferent neurons, with their cell bodies in the trigeminal ganglion (orange) (innervate mouth and face), couple over to secondary neurons in the trigeminal nucleus caudalis (spinal nucleus of the trigeminal complex) (green). The axons of the second order neurons project to the thalamus (blue). Third order neurons, with their bodies in the thalamus, project to the somatosensory cortex (red), responsible for the sensory aspect of pain.

(1) Primary afferent neurons (peripheral)

In migraine, the peripheral sensitization correspond to primary afferent nociceptive neurons exhibiting an increased responsiveness to mechanical or thermal stimuli at the original site of inflammation. A decreased activation threshold makes the neurons responsive to previously ineffective stimulus intensities. Furthermore, this sensitization can be manifested by a spontaneous activity, in the absence of any external stimulus. This sensitization is translated by the throbbing characteristic of the migraine. Indeed, sensitization of the nociceptive neurons innervating the meninges creates an intracranial hypersensitivity (Olesen et al., 2009).

One presumed factor that cause local release of sensitizing chemicals (i.e CGRP, substance P, and serotonin) from the peripheral terminals of meningeal nociceptors is the CSD. This last leads to a release of K^+ and glutamate, two excitatory agents. The

resulting component is a vasodilatation and plasma extravasation (Charles and Brennan, 2009). See the Figure 24 below for more details on the pathways.

(2) TNC and higher-order neurons (central)

The trigeminal nerve is connected to the brain stem and can actually affect many pathways of the entire nervous system. It acts like a gatekeeper, allowing or blocking nerve flow in the spinal column. The central sensitization is this state when, nociceptive neurons located in the dorsal horn and the spinal cord show an increased excitability, accompanied by a reinforced synaptic strength. Thus, the sensitized nociceptors become more responsive to innocuous sensory signals arriving from outside the inflammatory site. The resulting symptom of this central sensitization is a phenomenon of allodynia (See Figure 24 below).

This central sensitization is linked to two distinct mechanisms. The initiation of the sensitization is provided by the release of excitatory amino acid glutamate and neuropeptides from the C-fiber nociceptors. When the periphery is activated, leading to discharge of action potentials, calcium input into the central terminals of C-fibers nociceptors causes them to release the neuropeptides in the dorsal horn. Activation of these C-fibers leads to depolarization of the dorsal horn neurons.

The second mechanism that leads to the maintenance of the sensitization in the spinal cord neurons is due to the release of neurotransmitters. It induces a cascade of signaling pathway leading to activation of numerous receptors. This high activity of nociceptors is at the origin of a long term alterations of gene regulation, which in turn leads to an increased number of receptors, to ultimately enhance transmission (for review see de Tommaso and Scirucchio, 2016).

4. Aura

As seen earlier, CSD is a slowly propagating wave of neuronal and glial depolarization. This last provides the explanation for aura during migraine attacks even though the direct evidence from patient still lacks. Blood flow imaging provides the most reliable evidence for a dysregulation in cerebral blood vessel involved in the aura. Thus, any incidence on the blood viscosity, release of vasoactive substances, or platelet dysregulation will have an impact in blood circulation in dural blood vessel (Dalkara et

al., 2010). The correlation between CSD and aura has been recently questioned and reviewed by Piet Borgdorff (Borgdorff, 2018).

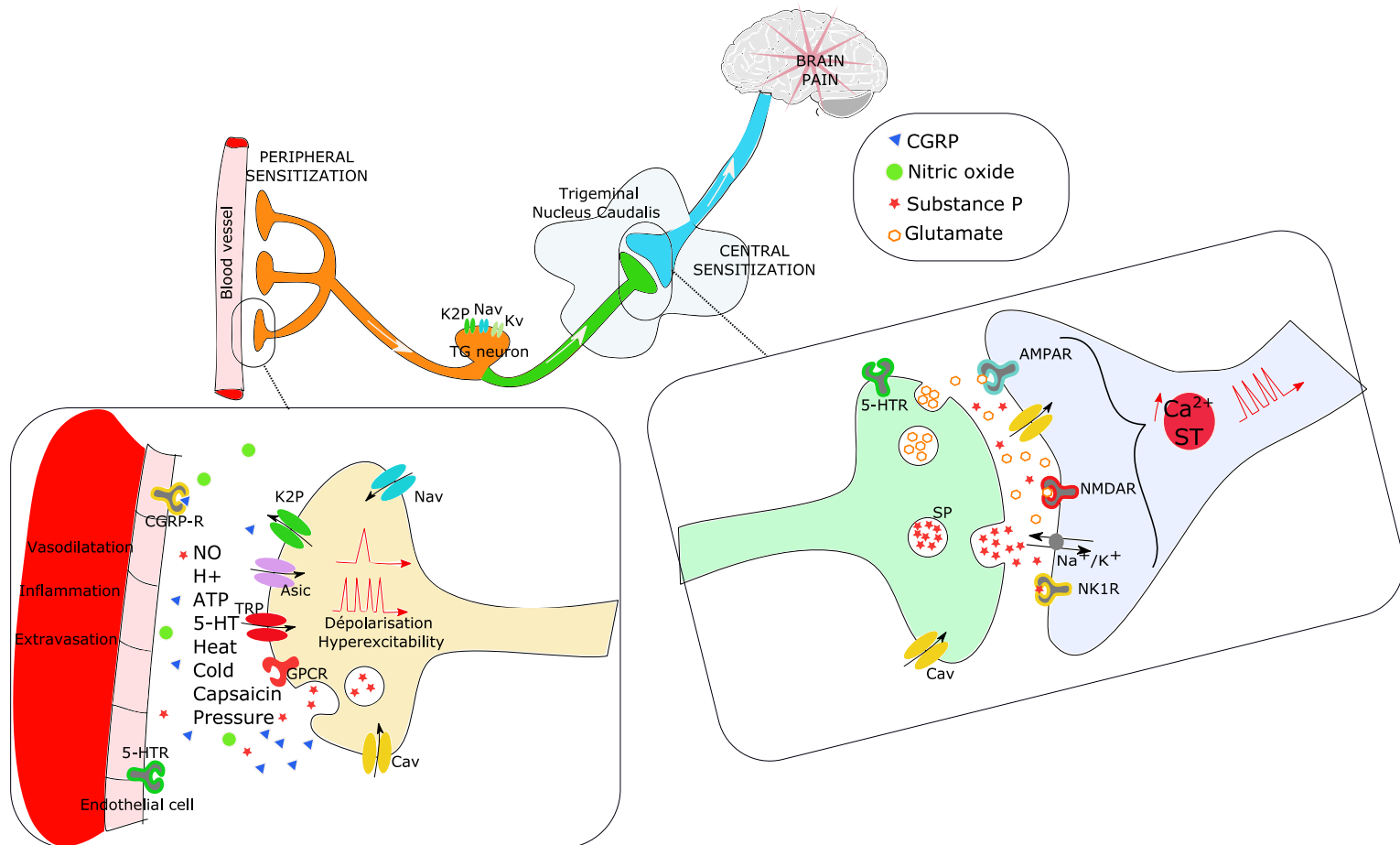


Figure 24: Pathway of trigeminal pain signal transmission in migraine with emphasis on mechanisms of sensitization. Extracellular inflammatory agents sensitize and activate afferent nociceptive neurons, inducing a depolarization and thus increases neuron excitability. The signal will be transmitted centrally with the release of glutamate and substance P, activation the transduction signaling pathways through several receptors. AMPAR=α-amino-3-hydroxy-5-methyl-4-isoxazolepropionic acid receptor, ASIC=acid sensing ion channel, TRP=transient receptor potential channel, NMDAR=N-methyl-D-aspartate receptor.

5. Channel dysfunction in migraine

Some uncommon forms of migraine are linked to mutations of genes coding for ion channels or pump. I will discuss here about the importance of CACNA1A gene, ATP1A2 gene, and SCN1A gene in three types of familial hemiplegic migraine and TRESK in a familial form of migraine with or without aura. Nevertheless even though TRP channels mutations have not directly been identified in migraine phenotype, their

localization, function and regulation properties made them perfect candidates for a role in migraine sensitization and inflammatory process (Albury et al., 2017).

5.a) TRP channels as a target to cure migraine

Transient receptor potential (TRP) channels are expressed in primary sensory neurons of trigeminal ganglion and dural afferents including those containing CGRP which mediates neurogenic inflammatory responses. Activation of TRP channels promotes excitation of nociceptive afferent fibers and potentially leads to nociceptive responses, allodynia and hyperalgesia. In addition to pain, allodynia to mechanical and cold stimuli can result from sensitization of both peripheral afferents and of central pain pathways (as seen earlier). In the TRP family, TRP vanilloid 1 (TRPV1) and TRP Ankyrin 1 (TRPA1) are highly expressed in nociceptive neurons.

5.b) Familial hemiplegic migraines and channelopathies

Familial Hemiplegic Migraine (FHM) is a subtype of migraine with aura transmitted in an autosomal-dominant fashion. Attacks are similar to those of common migraines, however they have a hemiparesis characteristic.

Familial hemiplegic migraine type 1 (FHM-1) is a Mendelian subtype of migraine with aura that is caused by missense mutations in the CACNA1A gene that encodes the $\alpha 1A$ subunit of neuronal $Ca_v2.1$ calcium channels. This voltage-gated neuronal channel is expressed throughout the mammalian nervous system at presynaptic terminals and plays a role in controlling neurotransmitter release. Within over the twenty different mutations, Ferrari's group used FMH1 mutant mice such as knock-in mouse carrying the human version of the R192Q mutation, to study the functional consequences of mutations in CACNA1A (van den Maagdenberg et al., 2004). They have shown that this gain-of-function effect led to a lowered threshold for CSD, explaining the increased susceptibility of the migraine brain. In fact, neurons carrying one of the mutant will be more sensitive to smaller depolarizations than wild type channels, leading to an increased calcium uptake resulting in an excess release of glutamate (Wessman et al., 2007).

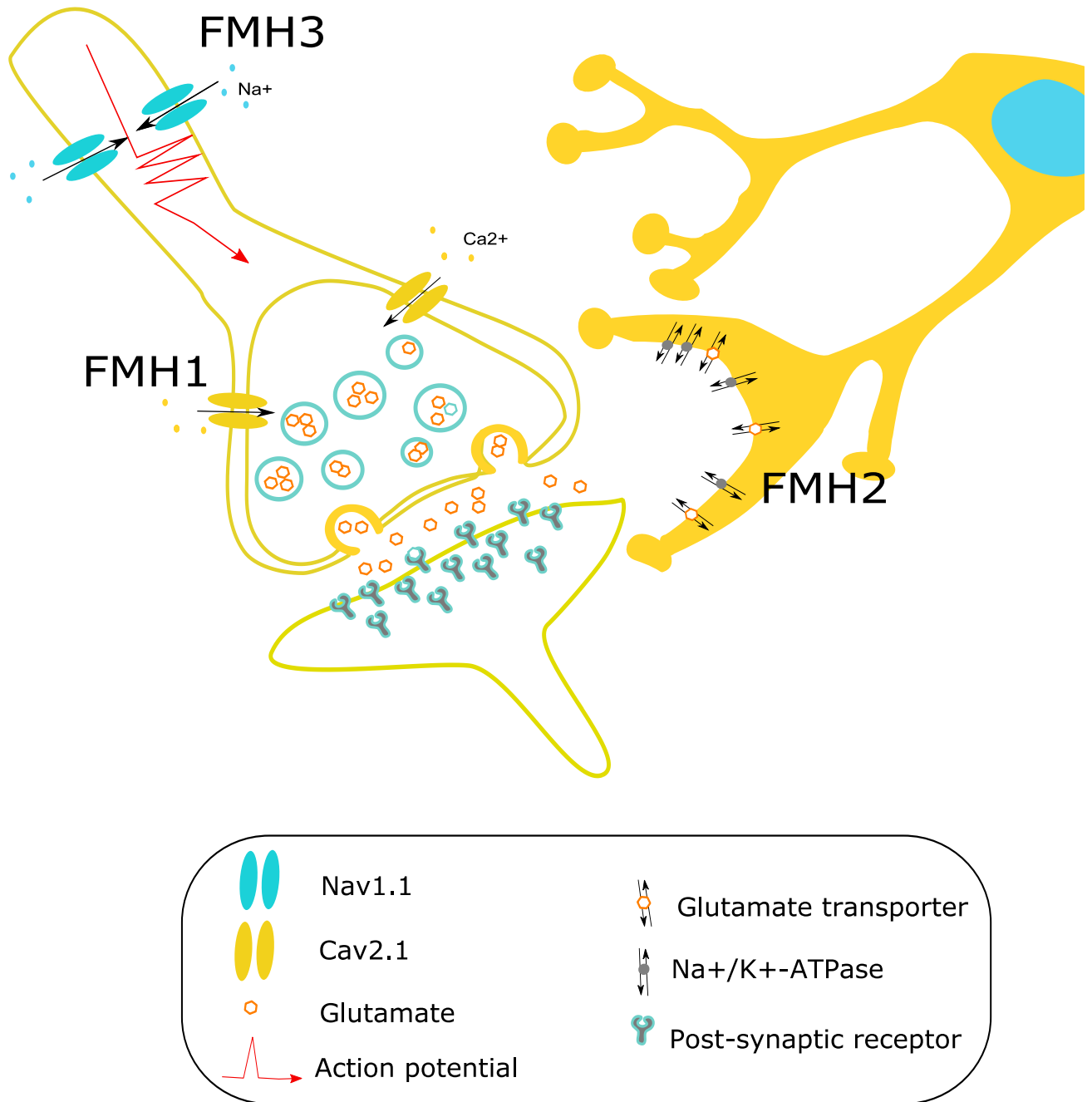


Figure 25 : Functional roles of the proteins coded by known FHM genes within a glutamatergic synapse. When an action potential reaches the presynaptic terminal, the voltage-gated calcium channels open and let Ca²⁺ ions enter the excitatory neuron, leading to the release of glutamate into the synaptic cleft. The CACNA1A (FHM1) gene encodes the $\alpha 1$ subunit of Cav2.1 channels, and FHM mutations within this gene cause a gain-of-function phenotype and thus increase release of glutamate. ATP1A2 encodes an $\alpha 2$ subunit of a Na⁺ /K⁺ -ATPase expressed on astrocytes, which clears extracellular potassium and produces a Na⁺ gradient that is used in the uptake of glutamate from the synaptic cleft by glutamate transporters. Mutations slow the clearance of glutamate and K⁺ ions. Mutations in SCN1A, encoding the $\alpha 1$ subunit of the neuronal voltage-gated sodium channel Nav1.1, fit well with this pathophysiological model of FHM. Nav1.1 channels are essential in the generation and propagation of action potentials, and the FHM mutation seems to cause accelerated recovery of the channel from fast inactivation. Thus, the neurons can fire at a higher frequency than they do normally (in inhibitory interneurons).

More recently, using the same mouse model of hemiplegic migraine, the role and expression of CGRP receptor were studied. Trigeminal neurons of this KI mouse were shown to release more CGRP, creating a neuronal sensitization. However, they have shown that there is no change in CGRP receptor expression in KI mice, making the huge release of CGRP as the main contributor to trigeminal pain sensitization in this animal model (Vilotti et al., 2016).

The FMH type II (FMH2) relies on more than 50 different mutations in the gene ATP1A2 encoding for the Na⁺/K⁺ -ATPase α 2 subunit (which is a pump and not a channel). In primarily astrocytes where it is expressed, this protein is known to maintain the sodium and potassium gradients across cellular membranes via ATP hydrolysis. By adjusting ion concentrations across the membrane, the gradient provides the basis for electrical excitation in neurons. An increase in sodium concentration, increases the calcium concentration resulting in the release of glutamate (such as in FMH1). The result of these combined mechanisms is a prolonged recovery time after excitation, making the brain more susceptible to CSD (Gritz and Radcliffe, 2013).

The final known mutated gene coding for a channel involved in FMH is SCN1A, coding for a voltage-gated sodium channel Nav1.1 (Dichgans et al., 2005). This last is also relevant in epilepsy, with a hundred of mutations linked to several kinds of epilepsy. Six mutations have been found in causing pure FMH type III (three other mutations are also linked to epilepsy). These last lead to an overall gain of function such as increased non-inactivated depolarization-induced persistent sodium currents; resulting in enhanced sodium influx. In the brain, this channel causes an increased firing of inhibitory GABAergic neurons where it is expressed. The subsequent extracellular increase of potassium could, as in FMH type II, trigger cortical spreading depression (Dichgans et al., 2005).

5.c) TRESK and migraine

Given the functional role of TRESK in neuronal electrochemical excitability and its local expression in both DRG and TG, it is conceivable that the TRESK channel interacts with the nociceptive pathways during migraine pathogenesis. Some evidence exists for this in rat model, which have demonstrated that down-regulation of TRESK expression increases sensitivity to painful stimuli, whereas TRESK overexpression in

DRG neurons was shown to attenuate injury-induced pain sensitization (Tulleuda et al., 2011, Zhou et al., 2017).

(1) Frameshift mutation F139Wfsx24

A study conducted by Lafrenière et al. identified a rare dominant-negative frameshift mutation (F139Wfsx24, ExAC: allele frequency 0.0006, meaning 0,06% of the population) in the KCNK18 gene, using a large, multigenerational pedigree genome-wide linkage approach (Lafrenière et al., 2010). The 2-bp deletion in KCNK18 was found to segregate wholly amongst migraineurs with typical migraine with or without aura. The mutant allele leads to a truncated non-functional TRESK subunit that suppresses conduction of the wild-type dimer through a dominant-negative interaction. This inhibition was supposed to increase trigeminal ganglion neuron excitability leading to migraine (see the Figure 26 for the involvement of TRESK in migraine and Lafrenière et al., 2010; Liu et al., 2013).

This observation supports a role for KCNK18 in migraine, as a genetic switch for neurogenic dysfunction linked to migraine and defined a possible relationship between TRESK dysfunction and its contribution migraine with aura.

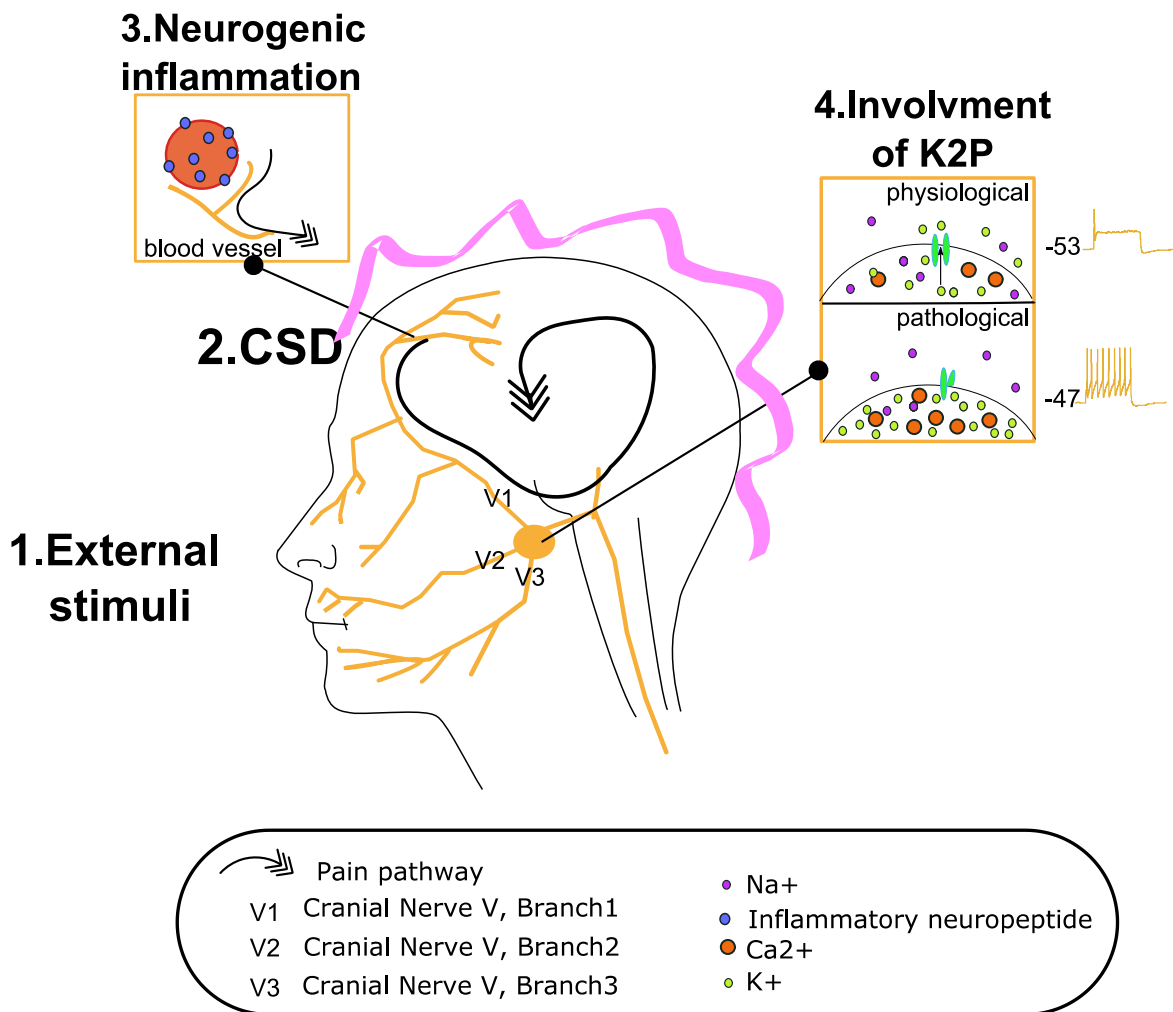


Figure 26: A schematic representation outlining some of the predicted mechanisms contributing to migraine pathogenesis. 1. Various endogenous and exogenous triggers may simultaneously disturb the subcortical aminergic sensory modulatory systems within the brain to ultimately activate the first division of the trigeminal nervous system (V1/2/3). 2 Stimulation of these fibres ignites the transmission of nociceptive information and initiates a CSD wave—causing Cortical Hyperexcitability. 3. As a response, Cortical Hyperexcitability enhances somatotopic activity—which results in an increase in the release of endogenous bio-regulators, i.e. glutamate, neuropeptides. These factors induce a regional sterile neurogenic inflammation, leading to an increase in pain trafficking. 3. Mutations in the *KCNK18* gene and consequent K2Ps dysfunction further exacerbate cortical hyperexcitability and pain transmission. Up: under normal circumstances, the fully functioning TRESK protein effectively controls potassium conductance and stabilises the negative resting membrane potential (excitability adjustment and depolarisation counteraction) through the transport of potassium, which subsequently regulates both Na⁺ and Ca²⁺ ions (potassium equilibrium potential). Dysfunction in the TRESK protein (bottom) disrupts this potassium equilibrium potential through prohibiting potassium efflux, ultimately lowering the action potential threshold of the neuron, enhancing the transmission of nociceptive information and the release of various neurotransmitters, adapted from Albury et al., 2017).

Consistently, TRESK overexpression could inhibit nociceptor hyperexcitability and neuropeptides release. Thus reversing the pain syndrome (Guo and Cao, 2014; Zhou et al., 2013, 2017).

(2) TRESK polymorphism and migraine phenotype

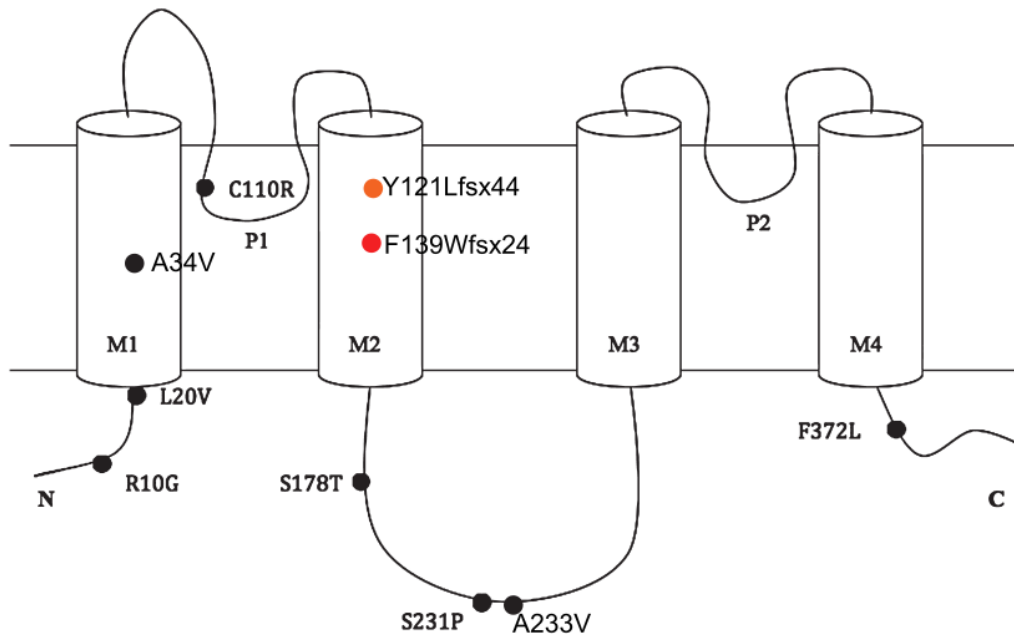


Figure 27: Schematic topology of the human TRESK subunits showing the position variants.

Gene mutations have been investigated in a large cohort of migraine patients and controls. Several missense variants (R10G, A34V, C110R, S231P and A233V, see Figure 26) in addition to the 2 pb deletion, were found: some had no functional effect, some were able to induce the formation of a non-functional channel and some lead to non-functional channel that inhibit the wild-type channel activity (Andres-Enguix et al., 2012). The C110R variant, which leads to a dominant negative of TRESK, was found in migraineurs and healthy subjects. The authors admitted that the presence of one non-functional variant with a dominant negative function is not sufficient to develop a migraine phenotype.

Another study, led in an Australian population, revealed that single-nucleotide polymorphisms in the KCNK18 gene have no association with migraine, suggesting the rare occurrences of migraine pain phenotypes linked to genetic polymorphism (Maher et al., 2013).

More recently, a group has been interested in the prevalence of KCNK18 gene mutations in an Italian population. They assessed the functionality of these mutations *in silico*, to determine the mechanism of the damaging effect (Rainero et al., 2014). Once again, while some mutations were dramatic for the wild type channel function,

others were barely damaging. Their conclusion was that the precise role of this gene in migraine predisposition deserves further study.

The involvement of TRESK channel variants in migraine then became controversial: one mutant TRESK-MT, with a dominant negative effect on wild-type (WT) TRESK leads to an increase of trigeminal (TG) neuron excitability (Liu et al., 2013), the other one, TRESK-C110R with the same dominant negative effect on WT-TRESK current does not increase TG neuron excitability and is not selectively expressed in migraineurs.

In our study, we found out the major difference between these two mutants. TRESK-MT is able to co-assemble and inhibit TREK channels, while TRESK-C110R is not. By inhibiting TRESK, TREK1 and 2, TRESK-MT will induce an increase of TG excitability whereas TRESK-C110R and its dominant regulation of WT-TRESK is not sufficient to induce an increase in excitability. This solved the controversial lack of effect of TRESK-C110R on TG neurons excitability and migraine phenotype.

Furthermore we demonstrated how a new mechanism by which a frameshift mutation will induce the translation of a new peptide, involved in a pathology.

6. Roles for signal molecules and receptors in trigeminal ganglia

6.a) Glutamate

Has seen before, glutamate is thought to play a specific role in the cortical spreading depression. Yet, it seems like the glutamate release, as well as CGRP release is mediated by P/Q calcium channels and the activation of 5-HT receptors. Calcium channels mediate a fraction of depolarization-associated glutamate release from cultured trigeminal neurons. Furthermore, it is suggested that activation of 5-HT₁ receptor is at the origin of an inhibition of glutamate release (Xiao et al., 2008).

6.b) Serotonin

Earlier it was suggested that probably the fluctuating serotonin levels lead to pH variations in the brain causing migraine, since serotonin also called as 5-hydroxytryptamine (5-HT), is a basic amine. In the brain, normal levels of endogenous

serotonin (5-HT) prevents migraine headache. It has been found that most of the neurons present in the dorsal raphe (site of emergence of trigeminal nerve) and trigeminal ganglia are serotonergic.

Serotonin receptors have been found on the trigeminal nerve and cranial vessels. By its role on cerebral vasculature and its action in central pain control, serotonin is a good candidate for the pathogenesis of migraine. The use of tricyclic antidepressants, which block serotonin reuptake, for prophylactic treatment of migraine also supports its role. However, its role is still inconclusive as selective serotonin reuptake inhibitors do not have the same prophylactic effect as tricyclic antidepressants (Ruthirago et al., 2017).

The 5-HT₁ receptors are coupled to Gi/Go and mediate cellular effects through decreasing cellular levels of cAMP. Targeting the peripheral 5HT_{1B} receptors with triptans (serotonergic agonist, see below) plays on vasodilatation and plasma extravasation by a vasoconstrictive effect. While targeting the 5HT_{1D} receptors will inhibit the release of vasoactive neuropeptides within trigeminal endings (Kilinc et al., 2017).

6.c) Neuropeptides: Substance P and CGRP

Substance P and CGRP are produced from a subset of trigeminal afferents. Substance P (neurokinin1) is also released by peptidergic C fibers. This neuropeptide is made of 11 amino acids, and also provides a vasodilator effect. Calcitonin gene-related peptide (CGRP) is a 37-amino-acid neuropeptide, first identified in 1982. It belongs to a family of peptides which includes calcitonin, adrenomedullin and amylin. Localization studies have shown a wide distribution of CGRP immunoreactive structures in the peripheral nervous system and in the CNS. The concomitant effect of these two peptides will favor the neurogenic inflammation.

(1) Role of calcium channel in CGRP release

Voltage-dependent calcium channels, Cav2.1 a P/Q-type calcium channels, are localized in trigeminal presynaptic nerve terminals in the dura and the TNC where they have a prominent role in trigeminovascular nociception. As said earlier, release of glutamate in the cortex, which may trigger cortical spreading depression (sometimes manifest as aura symptoms) and/or migraine pain by activating the trigeminovascular

system, is controlled predominantly by P/Q-type channels (for review, see Moskowitz et al., 2004).

(2) CGRP receptor

The calcitonin receptor-like receptor (CGRP-R in the cartoon) is a heterotrimer, each subunit possesses 7 transmembrane domains, is supplemented by a small single transmembrane peptide, named receptor activity-modifying protein (RAMP1) that forms the CGRP-specific ligand binding site. In addition, a small intracellular protein component, called receptor component protein (RCP), is necessary for linking the receptor to the intracellular signal-transduction machinery, which operates mainly through G protein G_s and adenylate cyclase, resulting in elevated cAMP levels. RAMPs proteins enable expression of CLR on the cell surface, determine the glycosylation state of the receptor, and determine the relative affinity of this receptor for CGRP.

(3) Role of CGRP and substance P in migraine

CGRP is a neuropeptide that exists in trigeminal ganglia nerves and a potent vasodilator of cerebral blood vessels. CGRP is believed to mediate vasodilatory mechanism of neurogenic inflammation and the transmission of trigeminovascular nociceptive signal from intracranial vessels to central nervous system. Stimulation of trigeminal ganglion causes the release of CGRP. Infusion of CGRP caused migraine attacks in patients in one study. However, other studies involving intracranial and extracranial arteries yielded conflicting results. The fact that sumatriptan, the serotonin 1B/1D receptor agonist, normalizes the elevated level of CGRP in migraine patients supports its effect in the treatment of migraine by inhibiting CGRP release.

Substance P will have a role in periphery, on the neurogenic inflammation of the dura mater and another role in transmitting the pain signaling via its receptor NK1, expressed in post-synaptic neurons.

6.d) Nitric oxide

Nitric oxide (NO) donors such as glyceryl trinitrate (GTN) or sodium nitroprusside cause headaches as a side effect. This was first observed in workers at explosive factories who experienced headaches frequently. The latter finding initiated extensive research on the role of NO in migraine (Trainor and Jones, 1966). NO is a potent

vasodilator produced by NO synthase in endothelial vascular cells, inflammatory cells or neurons. NO is able by itself to pass through membranes. Via two mechanisms, NO will increase nociceptor excitability:

- NO is able to directly interact with guanylate cyclase, leading to the production of cyclic guanosine monophosphate (Koesling et al., 2004). This would have an inhibitory effect on excitability (Levy and Strassman, 2004).
- In another hand, NO acts as an activator of TRPV1 and TRPA1, leading to a depolarization of the neurons, thus an increase of excitability (Miyamoto et al., 2009).

In our study, we used a NO donor, isosorbide dinitrate (ISDN), to trigger migraine like phenotype in mice and rats (Dallel et al., 2018; Pradhan et al., 2014; Thomsen et al., 1996; Verkest et al., 2018).

7. Treatments

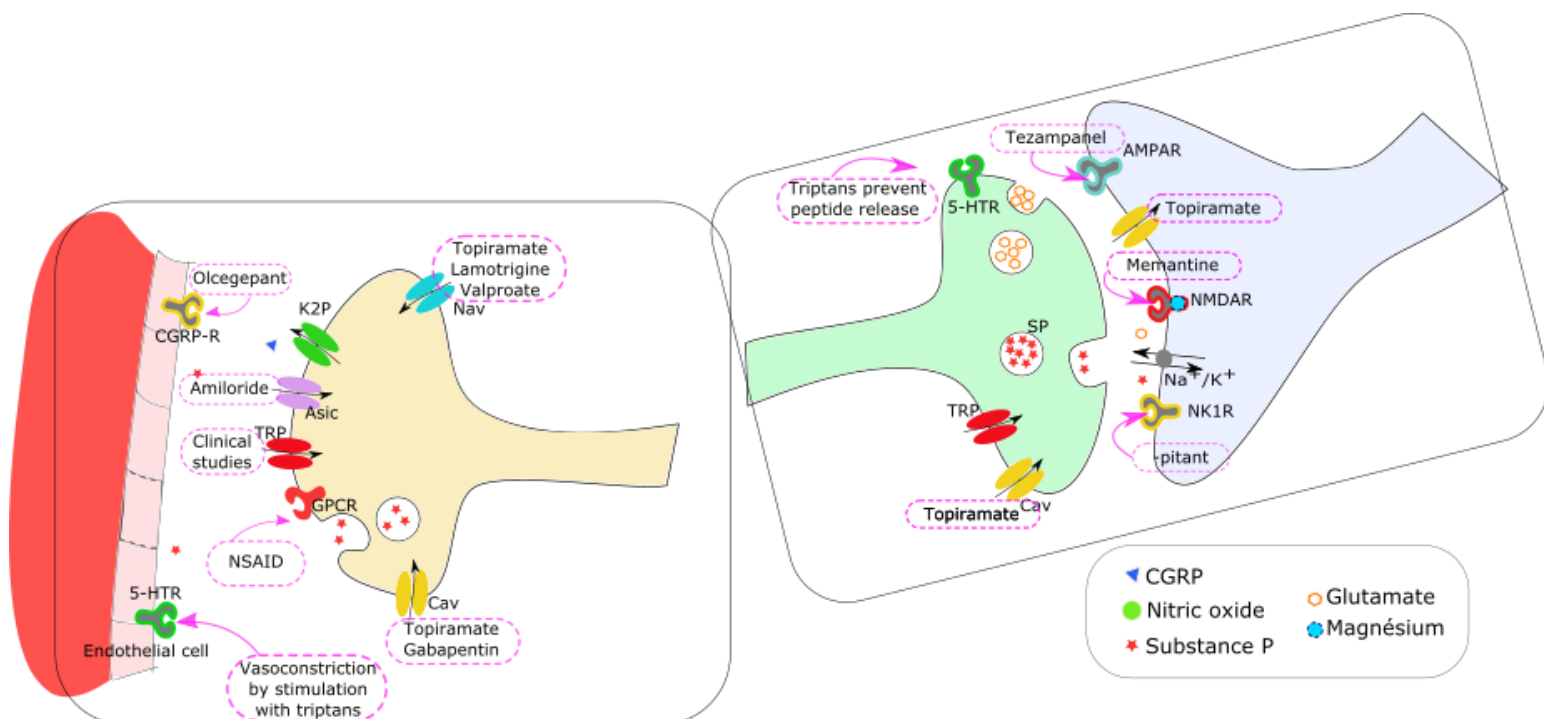


Figure 28 : Main potential targets of currently utilized drugs for migraine. The mechanisms mediating CSD inhibition by several migraine preventive drugs are not completely understood. The inhibitory action is mainly exerted by influencing ion channels and neurotransmission.

Medications used in migraine are not really specific and mainly target glutamatergic transmission (for an inhibition) and blockage of cationic ion channels –Na⁺ and Ca²⁺ voltage dependent channels such as **lamotrigine**, **gabapentin** respectively, or

topiramate that block both. They can also play a role in the potentialisation of GABAergic inhibitive action. Topiramate and **valproate** for instance by blocking Na⁺ channels. Topiramate also blocks kainate receptors (not shown here), receptors for glutamate.

Another glutamate receptor can be targeted to inhibit the transmission of the signal, via NMDA receptor, thank of the inhibitory action of **magnesium**, will reduce glutamatergic transmission. Also, they can be blocked by the **memantine**, a NMDA glutamate receptor inhibitor.

Other molecules target other system such as **triptans** by activating 5-HT receptors will play an inhibitory effect of the signal transduction and in the periphery will lead to a vasoconstriction; or non-steroidal anti-inflammatory drugs (**NSAIDs**) which are the most commonly used therapies for migraine attacks. They will act on the prostaglandin receptors (PGE₂) shown here as a GPCR (red receptor on primary nociceptor). These drugs are taken in acute treatment of migraine. They will also block the cyclooxygenase not shown here and thus, synthesis of prostaglandin. The idea is to target the action of CGRP, by CGRP-R blockage using antagonists like **olcegepant**. Also, targeting the substance P receptor NK1 on the post synaptic neurons with antagonist molecules called **x-pitans** will inhibit the transduction of the signal. Hypothalamus should be taken as a target for treatment. Bold characters refer to the molecules added on the Figure 28 (the different ideas for treatments were taken on the Mayo Clinic Institute's website "Mayo Clinic- Diagnosis and Treatments").

Our idea would be to activate K_{2P} channels, thus leading to a hyperpolarization of the membrane of nociceptors, but also limiting the transmission of the signal in the soma located in trigeminal ganglion neurons.

F. Alternative translation initiation

It is now clear that the number of genes in eukaryotic genomes does not reflect the biological complexity of the organisms. Alternative splicing is known to greatly increase the number of produced proteins. To this diversity, we can also add the different proteins made of alternative translation initiation (ATI). This last occurs when another AUG codon is in phase with the open reading frame and is embedded in a good consensus sequence.

Protein synthesis in eukaryotes is made on a ribosome-scanning model. The translation involves the recruitment of a 40S ribosomal subunit at the 5'-end cap structure of the mRNA, followed by a movement down the RNA using ATP (Kozak, 1999). The translation should start at the AUG codon nearest the 5' end of the mRNA. For most of the eukaryotic mRNA, it is the case: the initiation site is embedded in a sequence context favorable for the ribosome. The favorable Kozak consensus sequence is made of [AG]-XX-ATGG, the nucleotides at position -3 and +4 (here underlined) are the one that defined the strength of the site. However, sometimes, the ribosome reads through this consensus site, and the first ATG will not be used for translation. This “leaky scanning” can occur because of the weak sequence context of the first ATG. It will result in the translation of a downstream ATG (Kozak, 1999). Therefore, the same messenger is able to synthesize several proteins with different N-terminal sequences which would allow specific subcellular localization in relation with the presence or not of a nuclear localization signal (NLS) or a signal peptide in the amino-terminal part of the larger protein.

TREK1 mRNA was found to have an alternative translation initiation (ATI) site i.e an AUG codon in frame which is embedded by a strong Kozak sequence. This ATI leads *in vivo* to the formation of a shorter TREK1 channel, with new properties. Indeed, this TREK1, depleted from its N-terminus, is now selective to sodium in addition to its potassium selectivity (Thomas et al., 2008).

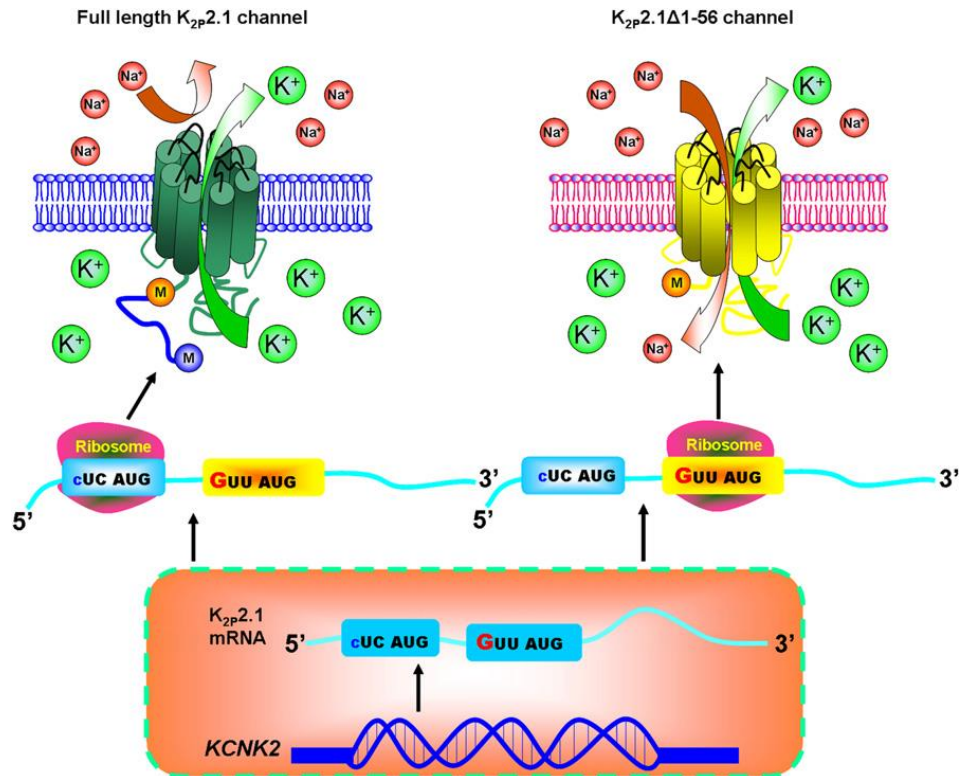


Figure 29 : $K_{2p2.1}$ Channel May Be Inhibitory or Excitatory, Depending at which Start Codon Translation Is Initiated. The first start codon (AUG) at $K_{2p2.1}$ mRNA is flanked by a weak translation initiation sequence (CUC). Ribosome may initiate translation at this site and yield a full-length $K_{2p2.1}$ channel. Alternatively, a ribosome may skim over the first start codon until it comes across the second (AUG) flanked by a stronger translation initiation sequence (GUU) and generates an N-terminal truncated $K_{2p2.1}\Delta 1-56$ channel. The full-length $K_{2p2.1}$ channel is highly selective for K^+ and hyperpolarizes the neurons. In contrast, the $K_{2p2.1}\Delta 1-56$ channel permeates both K^+ and Na^+ and thus excites the neurons. The blue and orange spheres depict the first (M1) and second (M57) methionine residues in the N terminus of the $K_{2p2.1}$ channels, from Yang and Jan, 2008.

Kochetov made a review of the different types of alternative open reading frames. Alternative translation initiation starts can lead to different protein products with modification one N-terminus either extended, either truncated or unrelated proteins (Kochetov, 2008).



Figure 30: Alternative translation start sites and variants of alternative open reading frames within eukaryotic mRNA. uORFs start from AUG codons located within 50 -untranslated region and can be either 50 -UTR-restricted (uORF1, white box), partially overlap with CDS (uORF2, light grey box) or fuse with CDS (i.e. if the uAUG lies in the CDS frame and no

termination codons are located between this uAUG and the annotated start codon; uORF3, gray box). dORFs start from AUG codons located downstream from the annotated start codon in a suboptimal context and can either encode small protein (dAUG is located out of the CDS frame: dORF1, dark grey box), or encode N-end truncated protein variant (dAUG is located in frame with CDS: dORF2, gray box). The annotated ORF (CDS) is marked by black color. Note, the databanks of nucleotide sequences commonly contain an annotation of CDS as a protein-coding sequence solely encoded by the mRNA (Kochetov, 2008) .

Another mechanism resulting in two proteins translated from one mRNA

Internal Ribosome Entry Sites (IRES) are non-canonical translation initiation that have been discovered in picornaviruses by Pelletier & Sonenberg in 1988. These sites can directly recruit ribosomes to initiate translation without scanning from 5' UTR end of the mRNA.

Recently, it has been shown that an IRES sequence upstream of the cofilin mRNA in neurons is mandatory for the translation of this last. Furthermore, this IRES-mediated translation support the growth and the extension of axon in hippocampal cultures (Choi et al., 2018).

This mechanism can also lead to diseases. Voltage-gated calcium channel CACNA1A (also involved in familial hemiplegic migraine) is associated with spinocerebellar ataxia type 6. By using RNA folding stimulation, the authors shown that in mRNA sequence of Cav2.1 C-terminus, there was an IRES sequence, that mediates the expression of this segment, toxic for the cells and involved in neuronal atrophy in animal models (Du et al., 2013).

G. Heteromerization and subunits assembly

Heteromerization is a common mechanism used by nature to increase functional diversity. Potassium channels do not make exception and their huge diversity can further be enhanced by their ability to make heteromeric channels. Heteromers will eventually possess different properties from the homomers, it is thus a way to increase functional diversity without an increased number of genes.

For instance, K_v channels are known to form heteromers among the same subfamily, as seen in the chapter A.1 about voltage-gated potassium channel. Furthermore, some subunits are found functional only in heteromerization state with other

subfamilies (for instance K_v2 with $K_v5,6$ and K_v8). The diverse expression patterns will determine their ability to form heteromers.

1. How heteromerization occurs

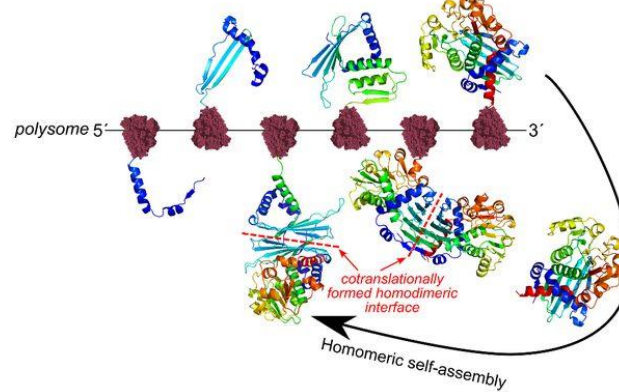
Most cellular processes are carried out by proteins, which, when made of more than two subunits, generally assemble into homomeric, or heteromeric complexes. It was thought for many years that complexes were made in the cytoplasm through random collisions. Recently, Shiber et al provided *in vivo* some evidences that seem to indicate that most protein complexes are assembled co-translationally, while one of the subunit at least is being synthesized by the cell's ribosome machinery (Shiber et al., 2018). This mode of assembly requires less energy and is more efficient. However it remains unclear how the subunits get together into proximity.

To be functional, potassium channel subunits need to be assembled in a protein complex and the interaction between the subunits needs to be strong. The quaternary structure of the protein is defined by the way the subunits will behave together, it involves folding and translocation of the polypeptide. It can be either homomeric (repeated copies of one subunit) or heteromeric (multiple protein subunits, encoded by different genes). They can also be heteromers forms by single chain cleavage.

Co-translational assembly can be explained by two distinct mechanisms. After transcription, several ribosomes can bind to the same mRNA, forming a polysome, allowing the simultaneous translation of several identical proteins. During the translation, two assembly mechanisms can be envisaged. In the first case, a newly synthesized subunit may associate with another copy being translated. It is also possible that the two peptides being synthesized on the same polysome interact even before the end of their translation (Wells et al., 2015).

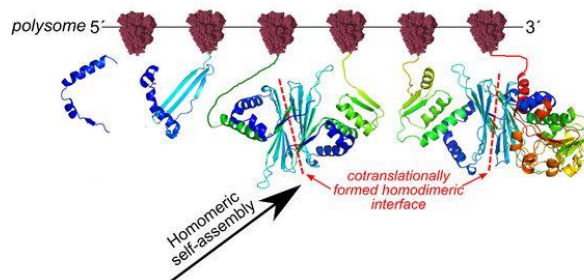
A) Cotranslational homomer assembly

between one nascent chain and one full subunit



B) Cotranslational homomer assembly

between two nascent chains



C) Cotranslational heteromer assembly

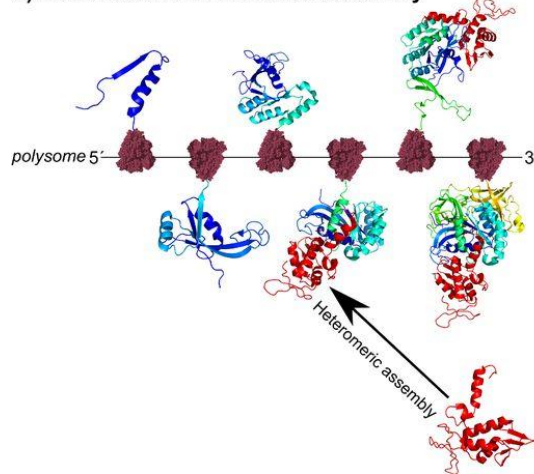


Figure 31: Co-translational assembly of protein complexes. In all panels, moving from left (5') to right (3') on the polysome (i.e. the mRNA bound to multiple ribosomes), we can see increasingly long nascent chains being translated. Homomer assembly can occur in two ways. In (A), a full-length subunit is released and binds to a nascent chain, forming a co-translationally assembled homodimer. In (B), two nascent chains from the same polysome interact with each other. For heteromer assembly (C), a different subunit (red) encoded by a different gene binds to a nascent chain, forming a co-translationally assembled heterodimer. These are hypothetical examples of co-translational assembly based upon PDB ID: 2I99 (homodimer) and PDB ID: 2DCU (heterodimer) (Wells et al., 2015).

The mechanism for heteromerization formation seems to be the same, involving the co-translation (Liu et al., 2016). Their conclusion is the following: physical association of transcripts encoding different subunits provides the spatial proximity required for nascent proteins to interact during biogenesis, and may represent a general

mechanism facilitating assembly of heteromeric protein complexes involved in a range of biological processes.

2. K_{2P} heteromerization

Heteromerization has been observed in K_{2P} channel family, it is found to happen within the same subfamilies, such as TASK1-TASK3 (Kang et al., 2004b), TREK1-TREK2, TREK1-TRAAK and TREK2-TRAAK (Blin et al., 2016; Lengyel et al., 2016; Levitz et al., 2016), and THIK1-THIK2 (Blin et al., 2014). Heterodimerization between different subfamilies has also been reported for TWIK1 (Hwang et al., 2014; Plant et al., 2012) and more recently between TASK1-TALK2. Heterodimerization appears to have a major physiological impact in expanding the functional diversity of K_{2P} channels.

K_{2P} heteromerization remains an open question. For more than fifteen years, this problematic has been explored and only a few number of heteromers were found. Some K_{2P} have an overlapping expression, and despite a poor sequence identity, they are able to heteromerize. Not much is known about the rules that determine rather a subunit will assemble with another and how this mechanism occurs. If the disulfide bridge is very important for assembly and conservation of the cap structure, it is not conserved among K_{2P} family and thus the new structures present in heterodimeric configurations could affect the gating mechanism and, at least in part, explain the new properties.

4.a) Intrafamily heteromerization

The first heteromeric K_{2P} to be characterized is the TASK-1/TASK-3 heteromer (Czirják and Enyedi, 2002). This was possible thanks to the difference in sensitivity that it possesses for ruthenium red. As expected, the complex formed by these two subunits has new biophysical characteristics. TASK-1 is sensitive to extracellular acidification whereas TASK-3 is sensitive to extracellular alkalization. The heteromer has an intermediate pH sensitivity (Kang et al., 2004b, Kim et al., 2009; Papreck et al., 2012).

There are several K_{2P} s that do not produce current in heterologous expression systems. One of the main reasons is their retention in the endoplasmic reticulum (Bichet et al., 2015). One might think that these silent channels can have the same role as silent Kvs. That is, forming heteromers with others K_{2P} to modulate their

function. This is the case of THIK-2. Indeed this subunit, normally retained in the endoplasmic reticulum, may associate with a subunit THIK-1. The newly formed channel can join the plasma membrane and have a current measurable. The heteromer has an intermediate conductance compare to homomers (Blin et al., 2014).

5.a) Interfamily heteromerization

In 2012, by using Fluorescence Resonance Energy Transfert (FRET), it has been demonstrated that TWIK1 is able to interact with TASK1 and TASK3, co-localized in granular cells of the cerebellum. These heteromers associate with the small protein SUMO, involved in the trafficking (Plant et al., 2012). It would have a huge impact in these cells, since SUMOylation would inhibit 50% of the outward potassium conductance. In this study, they used TWIK1-TREK1 interaction as a negative control, showing the absence of interaction between the two subunits. Nevertheless, the SUMOylation model is really controversial (Felicangeli et al., 2007) and has never been observed by other labs.

However, two years after, the formation of heteromers between TREK1-TWIK1 has been shown to be involved in astrocyte passive conductance. In 2009, TWIK1 and TREK1 were shown to support the passive conductance of mature hippocampal astrocytes, using their electrophysiological properties. Hwang et al demonstrated a direct interaction between TREK1 and TWIK1, relying on a disulfide bridge carried by the cysteine on the extracellular cap of the subunits. This heteromer would also be involved in glutamate release in astrocytes after activation of CB1 receptors through $G_{\beta\gamma}$ protein.

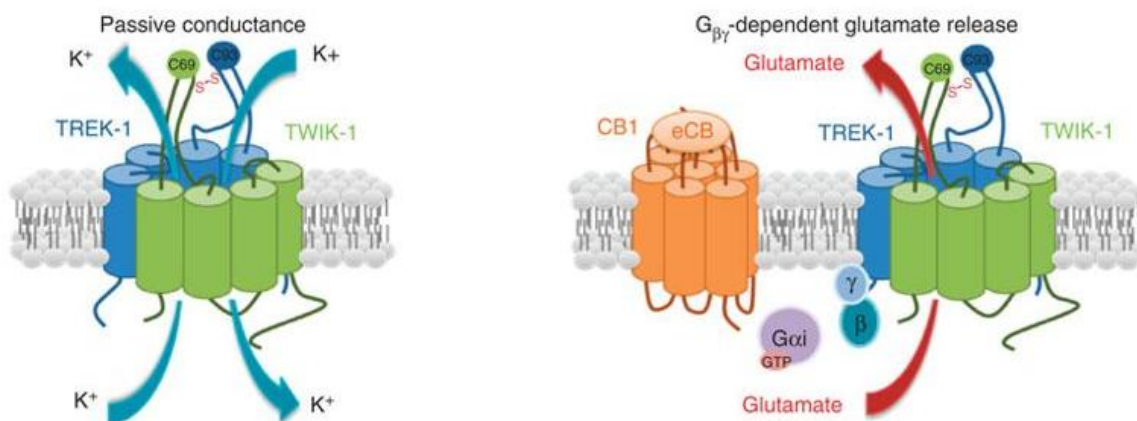


Figure 32: Schematic diagrams for passive conductance (left panel) and $G_{\beta\gamma}$ -dependent glutamate release (right panel). TWIK1 and TREK1 channels are supposed to form a functional heterodimer in astrocytes using a disulfide bridge at cysteine 69 (C69) for TWIK1 and 93 (C93) for TREK1. This heterodimer would be responsible for passive potassium conductance in astrocytes. B. The activation of the CB1 cannabinoid receptor causes these cells to release the $G_{\beta\gamma}$ complex which binds to the TWIK1 and TREK1 channels at their N-terminal portion. This association causes conformational changes in the heterodimer and a dilation of its pore, allowing the passage of glutamate. The heterodimer would therefore be involved in neuronal excitability by being responsible for the rapid release of glutamate by astrocytes after activation of the CB1 receptor (from Hwang et al., 2014).

Contradictory, we found using Single Molecule Pull down that these two channels are unable to heteromerize in heterologous expression system. Similarly to our lab, the Lesage's team failed to observe an association between TREK1 and TWIK1 (Blin et al., 2016). Along with these results, genetic deletion of TREK1 with or without TWIK1 did not change the basic electrophysiological properties of hippocampal astrocytes. Further researches are needed to understand role of TREK1 and TWIK1 in astrocyte physiology.

Recently, heteromerization of two-pore-domain channel TASK1 and TALK2 in living heterologous expression systems has been studied using different fluorescent techniques coupled with TIRF microscopy (Suzuki et al., 2017). They have found out that the new heterodimers were found endogenously in a pancreatic cell line. They further characterized the current formed by this heteromer and revealed that pH and halothane sensitivities were modified compared to the homomeric version of these channels.

The different heteromers found up to now are listed in the Table 2 below.

K _{2P} Dimer	Validation		Disulfide Bond	Physiological Function	Ref.
	<i>In vitro</i>	<i>In vivo</i>			
TASK-1/TASK-3		Co-IP	N.D.	The heterodimeric channels mediate the pH and isoflurane-sensitive K ⁺ currents in hypoglossal motoneurons.	(Berg et al., 2004)
TWIK-1/TASK-1 (or TASK-3)	FRET, Co-IP		N.D.	The heterodimeric channels comprise the acid-sensitive K ⁺ currents and response to halothane in cerebellar granule cells.	(Plant et al., 2012)
TWIK-1/TREK1	Co-IP, BiFC, MY2H	Co-IP, PLA	Dependent	The heterodimeric channels mediate passive conductance and fast glutamate release in cortical astrocytes.	(Cho et al., 2017)
			(TWIK-1 C69/TREK1 C93)		
TWIK-1/TREK-2	Co-IP		Dependent	N.D.	(Cho et al., 2017)
			(TWIK-1 C69)		
TWIK-1/TRAAK	Co-IP		Dependent	N.D.	(Cho et al., 2017)
			(TWIK-1 C69)		
THIK-1/THIK-2	FRET, PLA		N.D.	N.D.	(Blin et al., 2014)
TRAAK/TREK1 (or TREK-2)	SiMPull		N.D.	N.D.	(Blin et al., 2016; Levitz et al., 2016)
	TIRF imaging				
	FRET				
	PLA				
TREK1/TREK-2	Co-IP	Single channel recording	N.D.	N.D.	(Lengyel et al., 2016)
TASK-1/TALK-2	BiFC, FRET, Co-IP	TIRF imaging	N.D.	N.D.	(Suzuki et al., 2017)

Table 2: Heterodimers of two-pore-domain potassium (K_{2P}) channels (Cho et al., 2017) .

II. Problematics

Given the role of two-pore-domain potassium channels in modulating sensory neuron excitability and firing, both in physiological and pathological conditions, we examined the ability of the different K_{2P} subunits expressed in these neuron to form heterodimers and what would be the consequences. These widely conserved phenomenon among plants and humans allows to increase the functional diversity without increasing the number of genes. As said earlier for K_v or K_{ir} channels, this phenomenon occurs among potassium channels, and can even more give a role to non-functional subunits.

However, the study of this mechanism is complex due to the lack of a specific pharmacology and some intrinsic problem of these channels with the classical biochemical experiments. In this context, we needed to use some very precise and new tools to highlight interaction among K_{2P} subunits. We have developed in the lab a technique called single molecule pull-down or SiMPull to study protein complexes at single molecular level. We applied this method to identify a direct interaction between full length K_{2P} channels and mutants.

III. Material and methods

A. Molecular Biology

Channels fused to the green fluorescent protein for expression in HEK 293T were cloned in the vector pcDNA3.1-GFP made in the lab. This mammalian expression vector possesses a multiple cloning site and the CMV promoter to provide a high expression level. For xenopus oocytes single molecule imaging, experiments were done using pGEM-HE vector, allowing a low level of expression on the surface, needed for counting. The channels were fused to green or red fluorescent protein and inserted in the vector. All the HA-tagged channels for SiMPull and Western-Blot were cloned in a commercial pCMV-HA vector.

For electrophysiology channels and mutants were used in a pIRES2-EGFP and/or pIRES2-mCherry vector.

B. Immunocytochemistry

Transfected cells on coverslips were fixed with PBS containing 4% paraformaldehyde for 15 minutes at room temperature (RT), then permeabilized with PBS and 0,1% Triton X-100 (PBST) and blocked for 1h with 5% horse serum (HS) in PBST. Primary and secondary antibodies were diluted in PBST and 5% HS and incubated for 1h at RT. Three 5-min washes with PBST were carried out between each incubation step and at the end of the procedure. Coverslips were mounted in Dako Fluorescent Mounting medium (Dako Corporation, Carpinteria, CA, USA). The following antibodies were used: rabbit anti-TREK1 polyclonal antibodies (Sandoz et al., 2006), goat anti-rabbit IgGs conjugated to Alexa Fluor 488 (Molecular Probes Europe BV, Leiden, The Netherlands). Microscopy analysis and data acquisition were carried out with an Axioplan 2 Imaging Microscope.

C. Western Blot

HEK293 cells were transfected with Lipofectamine (Invitrogen). After 48 hours, cells were washed and immediately lysed in SDS-containing Laemmli's buffer or harvested, then resuspended in a buffer containing (in mM) 100 NaCl, 40 KCl, 20 NEM, 1 EDTA, 20 HEPES-KOH (pH 7.4), 10% glycerol, 1% Triton X-100, and complete protease inhibitor tablets (Roche Diagnostics, Basel, Switzerland) at 4°C. Lysates were

clarified by centrifugation at 20 000 G for 30 min. Proteins were separated on 12% SDS polyacrylamide gel and blotted onto nitrocellulose membrane (Hybond-C extra, Amersham Biosciences, Freiburg, Germany). Detection was carried out using mouse monoclonal antibody clone HA-7 against the HA epitope (Sigma).

D. SiMPull assay (adapted from Jain et al., 2012)

1. Principle

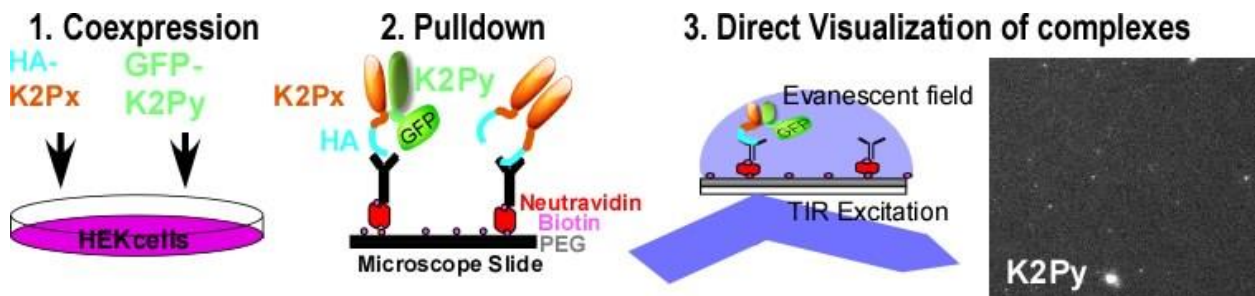


Figure 33: Schematic diagram of the SiMPull principle of HA-K₂P_x with another K₂P subunit. GFP-K₂P_y (1) A K₂P_x subunit labeled HA is co-expressed with a K₂P_y subunit labeled GFP in HEK293T cells. (2) After lysis of the cells, the complexes are put in the presence of anti-HA antibodies previously fixed on a microscope slide. (3) The presence or absence of subunits labeled GFP is revealed through a TIRF microscope. The image on the right shows an example of results obtained with this technical.

2. Surface passivation and construction of flow chambers

To construct the flow chambers, the slides and coverslips are thawed in the dark at room temperature for 10 minutes. A piece of double-sided tape is sandwiched between the slide and the coverslip, excluding a 5 mm channel where the inlet/outlet holes are located. The tape has to stick to both surfaces. The edges are sealed with epoxy glue and allowed to dry for 10 minutes. The volume of the flow channel is about 20 μ L.

3. Sample preparation

The SiMPull is performed on cell lysates as those used for conventional pull-down analysis. The cells are harvested from the coverslip using 500 μ L of PBS without Ca²⁺ during 35 minutes. The samples are centrifuged for 2 minutes at 11 000 rpm at 4°C. Cells were lysed in buffer containing (in mM): 10 Tris pH 7.5, 150 NaCl, 1 EDTA, protease inhibitor cocktail (Thermo Scientific) and 1.5% IGEPAL (Sigma). After 30-60 minute incubation at 4°, lysate was centrifuged for 20 minutes at 16,000 g and the supernatant was collected and kept at 4°C.

4. Antibody immobilization

Coverslips passivated with PEG (~99%)/ biotin-PEG(~1%) and treated with neutravidin were prepared as described above. 15 nM biotinylated anti-HA antibody (abcam, #ab26228) was applied for 20 minutes and then washed out. Antibody dilutions and washes were done in T50 + BSA buffer containing (in mM): 50 NaCl, 10 Tris, pH 7.5.

5. Single molecule imaging and spot counting

Lysate, diluted in T50 + 0.1 mg/mL BSA was then applied to the chamber and washed away following brief incubation (~2 minutes). Single molecules were imaged using a 488 nm Argon laser on a total internal reflection fluorescence microscope with a 100x objective (Olympus). We recorded the emission light after an additional 3x magnification and passage through a double dichroic mirror and an emission filter (525/50 for GFP) with a back-illuminated EMCCD camera (Andor iXon DV-897 BV). Movies of 250 frames were acquired at frame rates of 10–30 Hz. The imaged area was 13 x 13 μm^2 . At least 5 movies were recorded for each condition and data was analyzed using custom software. Multiple independent experiments were performed for each condition. Representative data sets are presented to quantitatively compare conditions tested on the same day.

E. Subunit counting with *X. laevis* Oocytes

Twenty-four hours after RNA injection and expression at 18 °C, *X. laevis* oocytes were enzymatically treated with hyaluronidase (1 mg/mL; Sigma) and neuraminidase (1 unit/mL; Sigma) for 15 min at 4 °C and manually devitellinized to enable close contact of the oocyte's plasma membrane to the coverslip. The coverslips' refractive index ($n = 1.78$) matched the refractive index of the microscope objective front lens (100/NA1.65; Olympus) and the immersion oil (Cargille). GFP was excited with a 488-nm argon laser, and ttTomato was excited with a 532-nm diode-pumped solid-state (DPSS) laser. We recorded the emission light after an additional 3x magnification and passage through a double-dichroic mirror and an emission filter (525/50 for GFP, 592.5/50 for ttTomato) with a back-illuminated EM CCD camera (iXon DV-897 BV). Movies of 500 frames were acquired at frame rates of 10–30 Hz. The imaged area was 13 × 13 μm^2 . For two-color experiments, fluorescence from tdTomato was

measured first, and after almost complete bleaching of tdTomato to prevent Förster/fluorescence resonance energy transfer from green to red chromophores, GFP fluorescence was measured. Occasionally, a few tdTomato molecules did not bleach completely, but even unbleached tdTomato did not affect fluorescence from colocalized GFP significantly. Laser powers were between 0.5 mW and 2 mW, and the diameter of the beam at the sample was 20 μm . Switching the illumination on and off and changing emission filters were done using electromechanical shutters and a motorized filter wheel. The typical time for switching off the 532-nm illumination, changing emission filters, and switching on the 488-nm illumination was 1–2 s.

F. Neuron extraction

All mouse experiments were conducted according to national and international guidelines and have been approved by the local ethical committee (CIEPAL NCE). The C57BL/6 breeders were maintained on a 12 h light/dark cycle with constant temperature (23–24°C), humidity (45–50%), and food and water ad libitum at the animal facility of Valrose. TG tissues were collected from postnatal day 1 mice of either sex and treated with 2 mg/ml collagenase type II (Worthington) for ~2 hours, followed by 2.5 mg/ml trypsin for 15 min. Neurons were dissociated by triturating with fire-polished glass pipettes and seeded on polylysine/laminin coated coverslips. The DMEM-based culture medium contained 10% fetal bovine serum and 2mM GlutaMAX (Invitrogen). Neurons were transfected at 1 day *in vitro* (DIV) using Lipofectamine 2000 (Invitrogen). Transfected neurons were identified by the green fluorescence and patch clamp recordings were performed between DIV 3 and 5.

G. Electrophysiology

1. Oocytes

Oocyte two-electrode voltage clamp electrophysiology was performed in a 0.3-mL perfusion chamber; a single oocyte was impaled with two standard microelectrodes (1–2.5 M Ω resistance) filled with 3 M KCl, and maintained under voltage clamp using a Dagan TEV 200 amplifier in standard ND96 solution [96 mM NaCl, 2 mM KCl, 1.8 mM CaCl₂, 2 mM MgCl₂, 5 mM Hepes (pH 7.4 with NaOH)]. For the high K solution, the NaCl was replaced by KCl. Stimulation of the preparation, data acquisition, and analysis were performed using pClamp software (Molecular Devices). Changes in

extracellular pH were induced by a microperfusion system that allowed local and rapid changes of solutions. Hepes was replaced by MES (5 mM) for buffer solutions with a pH between 6.5 and 5.0.

2. HEK cells

HEK 293T cell electrophysiology was performed 24–72 h after transfection in solution containing 145 mM NaCl, 4 mM KCl, 1 mM MgCl₂, 2 mM CaCl₂, and 10 mM Hepes. Glass pipettes of resistance between 3 MΩ and 6 MΩ were filled with intracellular solution containing 140 mM KCl, 10 mM Hepes, 5 mM EGTA, and 3 mM MgCl₂ (pH 7.4). Cells were patchclamped using an Axopatch 200A (Molecular Devices) amplifier in the whole-cell mode. Currents were elicited by voltage ramps (from –100 to 50 mV, 1 s in duration), and the current density was calculated at 0 mV. For acidic intracellular (5.5 pHi) solutions, Hepes was substituted with MES, and for basic (8.0 pHi) solution, Hepes was substituted with Tris.

3. Neurons

Neuronal excitability was studied in small-diameter TG neurons. Extracellular solution contained (in mM): 135 NaCl, 5 KCl, 2 CaCl₂, 1 MgCl₂, 5 HEPES, 10 glucose, pH 7.4 with NaOH, 310 mOsm. The pipette solution contained the following (in mM): 140 K-gluconate, 10 NaCl, 2 MgCl₂, 5 EGTA, 10 HEPES, 2 ATP-Mg, 0.3 GTP-Na, 1 CaCl₂ pH 7.3 with KOH, 290 mOsm. Recording pipettes had < 4.5 MΩ resistance. Series resistance (<20 MΩ) was not compensated. Signals were filtered at 10 kHz and digitized at 20 kHz. After establishing whole-cell access, membrane capacitance was determined with amplifier circuitry. The amplifier was then switched to current-clamp mode to measure resting membrane potential (V_{rest}). Neurons were excluded from analysis if the V_{rest} was higher than -40 mV or if the input resistance was smaller than 200 MΩ. To test neuronal excitability, neurons were held at V_{rest} and injected with 1 s depolarizing currents in 25 pA incremental steps until at least 1 action potential (AP) was elicited.

H. Behavior: Assessment of rodents allodynia

Administration of nitric oxide (NO) donors provides the most reliable model of migraine induction in humans. Nitric oxide (NO) is a potent endogenous vasodilator with an impressive array of biological actions (Moncada et al., 1991).

This protocol is made to measure the mechanical sensitivity thresholds in mice using an electronic von Frey aesthesiometer (Ugo Basile dynamic plantar aesthesiometer). The von Frey filament is applied against the central edge of the animal hind paw. Paw withdrawal caused by the stimulation is registered as a response. The corresponding force applied is recorded by the system and displayed on the screen of the von Frey unit.

At each paw withdrawal, the Dynamic Plantar Aesthesiometer (DPA) automatically detects and records latency time, and actual force at the time of paw withdrawal reflex. A movable force actuator is positioned below the plantar surface of the animal and the desired force and force speed (ramp) is applied, as preset by the operator. A Von Frey–type 0.5mm filament exerts increasing force, until the animal twitches its paw.

Drug administration

Isosorbide dinitrate (ISDN) was used to a dose of 10 mg/kg. The vehicle control used in these experiments was 0.9% saline. All injections were administered as a 10 ml/kg volume. Animals were tested for baseline responses immediately prior to intraperitoneal (ip) injection with ISND. Animals were tested for mechanical sensitivity every 30 minutes after the first injection and for 3 hours. For chronic experiments, testing occurred every day during 5 days, each was followed by an ip injection of ISDN except for the last one. For the topiramate experiment, mice were injected with topiramate once at a dose of 30 mg/kg, and mechanical nociception thresholds were assessed every 30 minutes during two hours after the injection.

Sensory Sensitivity Testing

To assess mice hind paw mechanical threshold, mice were acclimatized to the plastic box with a metal wire mesh table for 20 min. The mechanical stimulus was delivered to the plantar surface of the hind paw from below the floor of the test chamber by an automated testing device (dynamic plantar aesthesiometer; Ugo Basile Cat. No.

37450). A steel rod of diameter 0.5 mm was pushed against the hind paw with ascending force of 0 to 7.5 g over a period of 10 s. When the animal withdrew its hind paw, mechanical stimulus automatically stopped, and the force at which the animal withdrew its paw was recorded to the nearest 0.1 g. Animals were subjected to three consecutive trials with at least 3–5 min between the trials and averaged to select animals.

Needed :

- Electronic von Frey aesthesiometer (protocol for the test is 7.5 grams in 10 seconds)
- 10 control mice (7 to 12 weeks, male)
- 10 KO mice



Figure 34: Electronic Von Frey aesthesiometer apparatus with the grid and plastic boxes

Solutions:

- A NO donor = Isosorbide dinitrate (ISDN) or Risordan® injectable solution (10 mg/10 mL). You can aliquot a vial and inject 10 mg/kg (about 250 µL) IP.

Requirement:

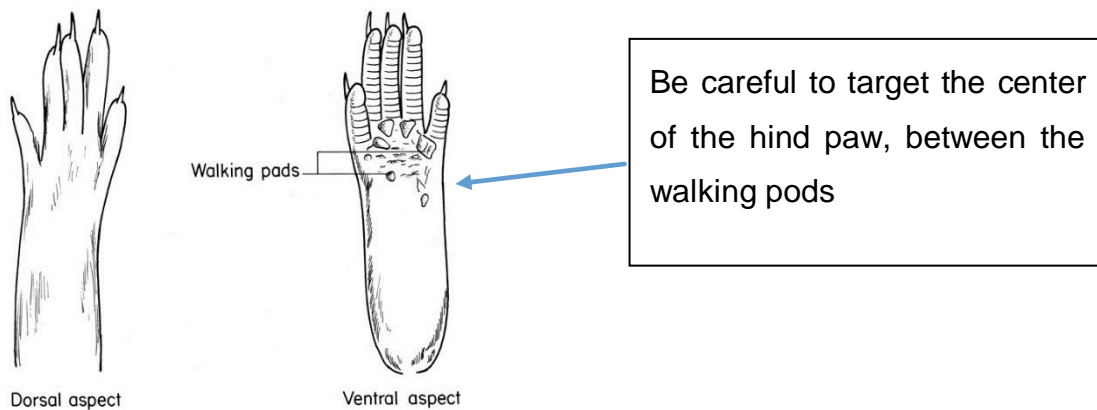


Figure 35: Drawing of the mouse paw.

Before any experimentation, it is mandatory to submit your mice to habituation, to “train” them. To do so, you have to put your mice on the grid, and make them be used to the apparatus. Let them stand for 20 minutes on the grid, in the Plexiglas boxes. And then, try to measure each mice, one by one, on the two hind paw (at least 3 measures/mice for the habituation). Let from 30 seconds to 1 minute between each

stimulation. Record the values of the threshold on a printed excel table for each mouse.

Assessment of rat face mechanical allodynia after virus injection

The procedures of virus trigeminal injections are described by Long *et al.* (Long et al., 2017). Briefly, following general anesthesia with a cocktail of ketamine and xylazine (100 mg/kg and 10 mg/kg respectively in i.p), rats were shaved and place on a warmed surgical plate. The site of injection was determined using a notch between the condylar process and the ipsilateral angular process. The depth of injection was 9 mm. Antibiotics were used 5 days following injections. Viral vector suspension (10 μ L) containing 6 μ g/mL of Polybrene was injected slowly over 1 min. Rats in the experimental group (n=14) received 10 μ L of viral vector containing the MT2 protein sequence, while those in the control group (n=14) received the same amount of EGFP viral vector. Epifluorescence imaging and qPCR were performed to verify successful transduction of trigeminal ganglia by viral vector.

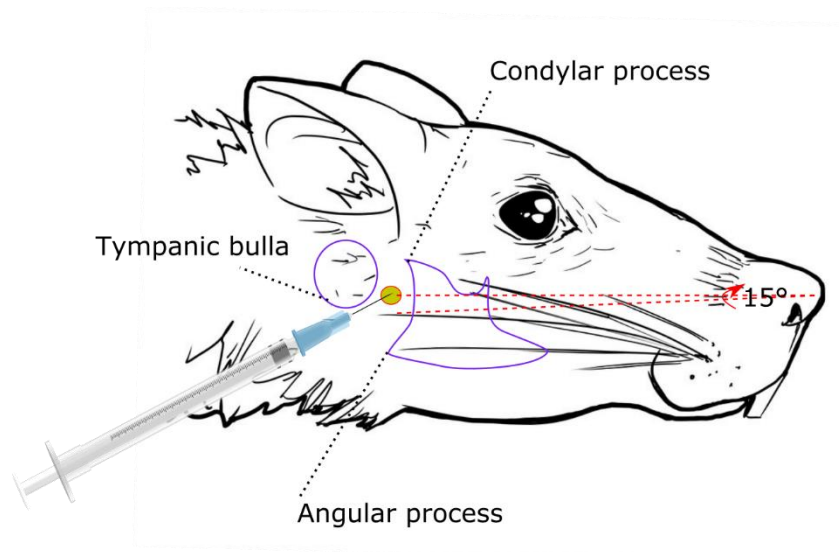


Figure 36: Procedure used for targeting rat trigeminal ganglia. Facial hairs covering the area between the ears and eyes were removed, the tympanic bulla (purple circle) and mandible were palpated and marked. Then, an injection site (yellow circle) was marked between the tympanic bulla and mandible, 2 mm posterior to the posterior notch of the mandible formed by the angular and condylar processes. A needle was inserted through the marked injection site and advance by 9 mm, the direction of injection was 15° upwards. Legend adapted from Long et al., 2017.

The face mechanical sensitivity was measured using calibrated von Frey filaments (Bioseb, France). Unrestrained rats placed in individual plastic boxes on top of a wire surface boxes were trained over one week to stimulation on the periorbital area,

following a progressive protocol, starting with non-noxious filaments during the first 3 days of training. The face withdrawal force threshold (g) was determined by the filament evoking at least 3 responses over five trials, starting with lower force filaments. To test the effect of ISDN, the face mechanical sensitivity was measured every 30 minutes before (basal value) and during three hours after intraperitoneal (i.p.) injection.

A. Introduction

In 2002, heteromerization within K_{ir} potassium channel family was demonstrated to be at the origin of several phenotypes of Andersen's syndrome. $K_{ir2.x}$ subfamily is expressed in cardiomyocytes and is really important as the channels shape of the action potential. Preisig-Muller and collaborators shown that not-only mutations in $K_{ir2.1}$ could have a dominant negative effect on itself, but also on $K_{ir2.2}$ and $K_{ir2.3}$ when they were co-expressed. Thus, the formation of heteromers within this subfamily explains how a mutation in one subunit i) was involved in the inhibition of others subunits and ii) leads to the phenotype complexity of a disease (Preisig-Müller et al., 2002).

Given the different regulations governing TREK subfamily, their overlapping expression and the role of this subfamily in the generation and control of the resting membrane potential in neurons involved in several paradigms, TREK heteromers could have a potential role in physiopathology.

Tools

To first characterized the complexes formed between two subunits, we used to optic techniques. The SiMPull allows one to immuno-precipitate specifically the complexes of interest, in a single molecule manner, and to distinguish the stoichiometry of each complex. Total internal fluorescence microscopy creates an evanescent field of only 200 nm above the sample, to get rid of the background. One subunit is caught on the slide via an antibody that will recognize the HA-tag. The other subunit is fused to a green fluorescent protein and will be illuminated and bleached by the laser (see Chapter SiMPull in Materiel and Method p. 97). Here, using this technique, we proved that TREK1 works as a dimer and is able to interact with TREK2 with no preference, and to a lesser extend with TRAAK.

To prove that these heteromeric channels were formed with a low level of expression as it would be the case *in vivo*, we performed subunit counting in *Xenopus laevis* oocytes (Ulbrich and Isacoff, 2007). It allows to directly visualize on the plasma membrane of oocytes the complexes formed using fluorescent tagged subunits.

Complexes made with only one kind of subunit will be observed in one color, the co-localization of two different subunits will be observed in both channels, and the overlapping image will reveal existence of the complexes.

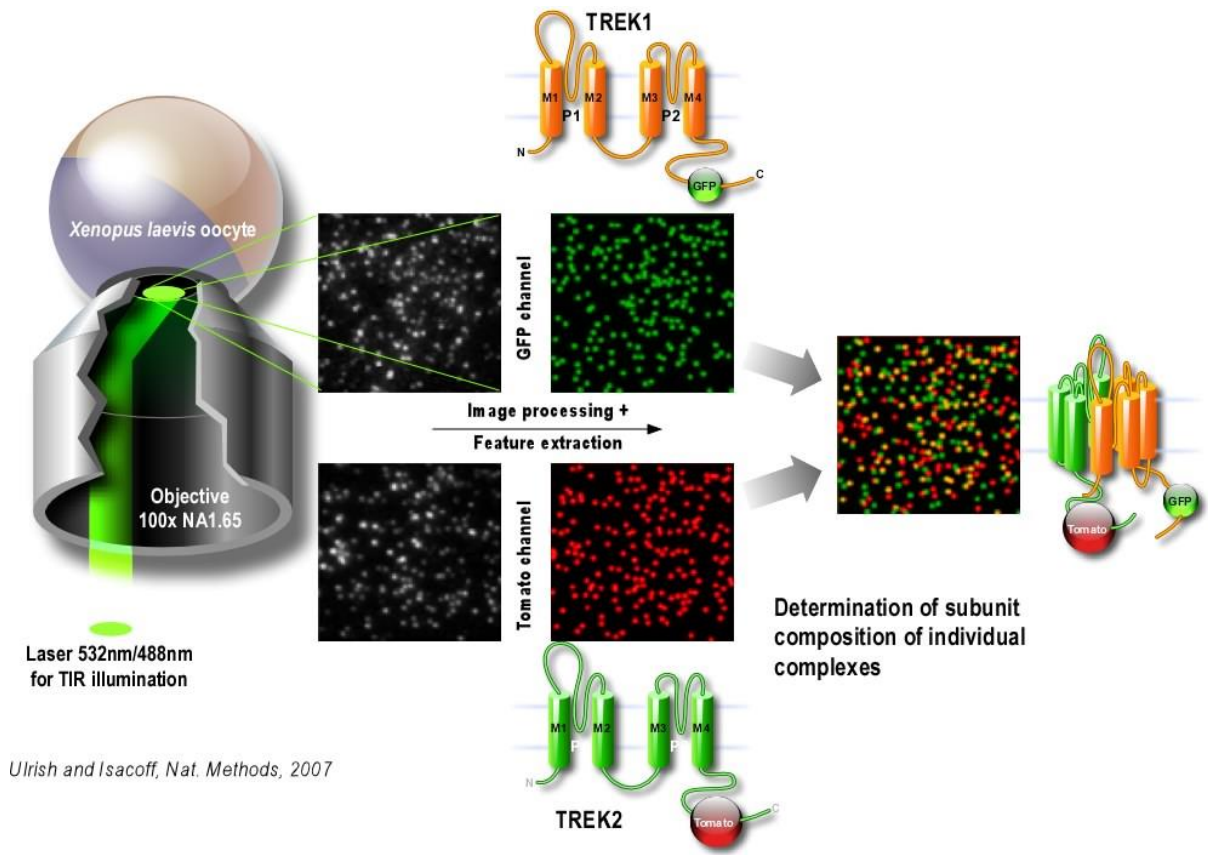


Figure 37: Cartoon of the subunit counting with *X. laevis* oocytes. Each subunit is fused to a fluorescent protein. After RNA injection in oocytes, the membrane is observed with TIRFM. Determination of subunit compositions is made from the two acquired images, in each fluorescent channel.

Transfection of both RNA would lead to the formation of heteromers as well as some homomers. To have a uniform expression of these heteromers only, at the plasma membrane, in order to characterize their currents and not the one formed by homomeric versions of the channels, we built chimeric tandem dimer. For each combination, we made both C-terminus and N-terminus fusion. Since a lot of regulations occurs within the N- or C-terminus domains, we have to take into account the eventual steric hindrance generated by the fusion.

B. Article I: Heteromerization within the TREK channel subfamily produces a diverse family of highly regulated potassium channels.

Heterodimerization within the TREK channel subfamily produces a diverse family of highly regulated potassium channels

Joshua Levitz^{a,1}, Perrine Royal^{b,c,d,e,1}, Yannick Comoglio^{b,c,d,e}, Brigitte Wdziekonski^{b,c,d,e}, Sébastien Schaub^{b,c,d}, Daniel M. Clemens^a, Ehud Y. Isacoff^{a,f}, and Guillaume Sandoz^{b,c,d,e,2}

^aDepartment of Molecular and Cell Biology and Helen Wills Neuroscience Institute, University of California, Berkeley, CA 94720; ^bInstitute of Biology Valrose (iBV), Université Nice Sophia Antipolis, UMR 7277, 06100 Nice, France; ^cCNRS, iBV, UMR 7277, 06100 Nice, France; ^dINSERM, iBV, 06100 Nice, France; ^eLaboratories of Excellence, Ion Channel Science and Therapeutics, Nice, France; and ^fPhysical Bioscience Division, Lawrence Berkeley National Laboratory, Berkeley, CA

Edited by Lily Yeh Jan, University of California, San Francisco, CA, and approved February 26, 2016 (received for review November 17, 2015)

Twik-related K⁺ channel 1 (TREK1), TREK2, and Twik-related arachidonic-acid stimulated K⁺ channel (TRAAK) form the TREK subfamily of two-pore-domain K⁺ (K_{2P}) channels. Despite sharing up to 78% sequence homology and overlapping expression profiles in the nervous system, these channels show major differences in their regulation by physiological stimuli. For instance, TREK1 is inhibited by external acidification, whereas TREK2 is activated. Here, we investigated the ability of the members of the TREK subfamily to assemble to form functional heteromeric channels with novel properties. Using single-molecule pull-down (SiMPull) from HEK cell lysate and subunit counting in the plasma membrane of living cells, we show that TREK1, TREK2, and TRAAK readily coassemble. TREK1 and TREK2 can each heterodimerize with TRAAK, but do so less efficiently than with each other. We functionally characterized the heterodimers and found that all combinations form outwardly rectifying potassium-selective channels but with variable voltage sensitivity and pH regulation. TREK1-TREK2 heterodimers show low levels of activity at physiological external pH but, unlike their corresponding homodimers, are activated by both acidic and alkaline conditions. Modeling based on recent crystal structures, along with mutational analysis, suggests that each subunit within a TREK1-TREK2 channel is regulated independently via titratable His. Finally, TREK1/TRAAK heterodimers differ in function from TRAAK homodimers in two critical ways: they are activated by both intracellular acidification and alkalization and are regulated by the enzyme phospholipase D2. Thus, heterodimerization provides a means for diversifying functionality through an expansion of the channel types within the K_{2P} channels.

potassium channels | single-molecule fluorescence | leak current | combinatorial diversity | heteromerization

Twik-related K⁺ channel 1 (TREK1), TREK2, and Twik-related arachidonic-acid stimulated K⁺ channel (TRAAK) are two-pore-domain K⁺ (K_{2P}) ion channels that belong to the TREK channel subfamily and assemble as dimers to produce an inhibitory, outwardly rectifying potassium current. They are not very active under basal conditions but can be dynamically stimulated by a wide range of stimuli, including mechanical stretch (1), heat (2, 3), phospholipids (4–6), and polyunsaturated fatty acids (1, 7). pH is an especially prominent regulator of these channels. Intracellular acidification stimulates both TREK1 and TREK2 (8, 9), whereas TRAAK is stimulated by intracellular alkalization (10). In contrast, extracellular acidification is able to inhibit TREK1 and TRAAK, but activates TREK2 (11). Members of the TREK channel subfamily are also regulated extensively by intracellular scaffolding and signaling proteins (10). We recently characterized the regulation of these channels by the enzyme phospholipase D2 (PLD2) and found that PLD2 associates with TREK1 and TREK2, but not TRAAK, which localizes these channels to a microdomain rich in phosphatidic acid (PA) that tonically activates the channels (5).

TREK1 and TREK2 share ~65% sequence identity, whereas TREK1 and TRAAK share ~40% (12–14). All three subunits are highly expressed throughout the nervous system (12, 14), where they display distinct but overlapping distributions (15). Due to their ubiquitous expression throughout the brain and based on gene KO studies, these channels are thought to play crucial roles in neuroprotection and anesthesia (16), depression (17), and pain perception (10).

Heteromultimerization is a mechanism commonly used to increase the functional diversity of protein complexes. Heteromerization within the K_{2P} channel family was first described in 2002, with the identification of the TASK1–TASK3 complex (18). In this case, the existence of specific sensitivity to ruthenium red allowed the authors to prove the existence of this heteromer functionally. Recently, it has been found that THIK2 requires heteromerization with THIK1 to be active (19). TREK1 has been reported to heteromerize with TWIK-1 in astrocytes (20), but in another study, TREK1 was shown not to heteromerize with TWIK-1 (21). Physiologically, heteromerization of K_{2P} channels can be extremely functionally relevant in neurons. For example, the TASK1–TASK3 heteromer has been shown to contribute to the standing, outward potassium current in cerebellar granule cells (22), which plays a crucial role in apoptosis (20). Despite the increasing interest in heteromerization of K_{2P}

Significance

The two-pore-domain K⁺ (K_{2P}) family of potassium channels provides basal inhibitory tone to regulate resting membrane potential and excitability of neurons. Although physiological and biochemical studies have indicated that distinct members of the family can heterodimerize, the tendency to do so, rather than homodimerize, and the functional effects of heterodimerization are minimally understood. We find that Twik-related K⁺ channel 1 (TREK1) dimerizes as readily with TREK2 as with itself and also with Twik-related arachidonic-acid stimulated K⁺ channel (TRAAK), although less efficiently. The heterodimers combine functional properties of their constituents in terms of three key modes of regulation: by external pH, internal pH, and phospholipase D2. The unique regulatory properties of TREK1-TREK2 and TREK1-TRAAK heterodimers provide insight into the extracellular and intracellular gating mechanisms of K_{2P} channels.

Author contributions: J.L., P.R., Y.C., E.Y.I., and G.S. designed research; J.L., P.R., Y.C., B.W., and G.S. performed research; S.S. and D.M.C. contributed new reagents/analytic tools; J.L., P.R., Y.C., S.S., D.M.C., and G.S. analyzed data; and J.L., P.R., E.Y.I., and G.S. wrote the paper.

The authors declare no conflict of interest.

This article is a PNAS Direct Submission.

¹J.L. and P.R. contributed equally to this work.

²To whom correspondence should be addressed. Email: sandoz@unice.fr.

This article contains supporting information online at www.pnas.org/lookup/suppl/doi:10.1073/pnas.1522459113/-DCSupplemental.

channels, it is unknown whether members of the TREK channel subfamily are able to complex with each other and what the functional properties are of these potential heteromers.

Here, we show, using single-molecule fluorescence techniques, that TREK1, TREK2, and TRAAK heterodimerize and that the heterodimers reach the plasma membrane. TREK1-TREK2 heterodimers are functional and produce a current with intermediate amplitude and increased outward rectification compared with TREK1 and TREK2 homodimers. Most interestingly, external pH regulation of the TREK1-TREK2 heterodimer is different from TREK1 and TREK2 homodimers. This heterodimer shows minimal activity at pH 7.4 but is activated by both acidic and alkaline conditions. Mutational and structural analysis of the heterodimer indicate that each subunit has a His pH sensor that operates through intrasubunit electrostatic interactions. We also characterized the TREK1-TRAAK heterodimer and found an intermediate current amplitude and regulation by external pH. Surprisingly, TREK1-TRAAK showed biphasic activation in response to either intracellular acidification or alkalization. Finally, we addressed the ability of the intracellular partner protein PLD2 to regulate the TREK1-TRAAK heterodimer and found that only one TREK1 subunit is sufficient to permit current potentiation.

Results

Single-Molecule Analysis of Coassembly of TREK1, TREK2, and TRAAK Channels in Mammalian Cells. To determine the ability of TREK channels to heteromerize, we used the recently developed single-molecule pull-down (SiMPull) assay (23). SiMPull enables direct visualization of Ab-immobilized individual protein complexes on PEG-passivated coverslips to determine the composition and stoichiometry within individual protein complexes by observing fluorophore bleaching steps.

We first confirmed that TREK channels may be immobilized as dimers in SiMPull by expressing a construct containing an N-terminal HA tag followed by a GFP and then TREK1 (HA-GFP-TREK1) in HEK 293T cells. After 24 to 48 h of expression, cells were lysed and single HA-GFP-TREK1 complexes were pulled down using an anti-HA Ab and imaged with total internal reflection fluorescence (TIRF) microscopy (Fig. 1A). In the absence of the HA Ab, there were no fluorescent spots, confirming the specificity of the Ab and the passivation of the

coverslip (Fig. 1A). The majority of fluorescence intensity trajectories (Fig. 1B) showed two-step bleaching ($\sim 53\%$), with the remaining spots bleaching in one step ($\sim 38\%$) or, occasionally, three or more steps ($<10\%$) (Fig. 1C). This distribution agrees with the binomial distribution for a strict dimer based on an estimated GFP maturation probability of $\sim 75\%$ (24). SiMPull experiments with HA-GFP-TREK2 confirmed that these channels also form strict dimers in mammalian cells (Fig. S1A–C).

We next tested the ability of TREK1 to coassemble with its most closely related homolog, TREK2. We coexpressed HA-TREK1 with GFP-TREK1 or GFP-TREK2 and assessed the ability of HA-TREK1 to coimmunoprecipitate the other channels via the anti-HA Ab. In both cases, HA-TREK1 was able to pull down many fluorescent spots via interactions with the GFP-tagged constructs (Fig. 1D). Importantly, when HA-TREK1 was not coexpressed, neither of the GFP-tagged channels was isolated (Fig. 1D and E). HA-TREK1 pulled down both GFP-TREK1 and GFP-TREK2 with comparable efficiency (Fig. 1E), indicating that TREK1 can coassemble with TREK2 without any clear preference for itself. We also found that HA-TREK2 was able to pull down GFP-TREK2 or GFP-TREK1 with comparable efficiency (Fig. S1D and E).

We also extended this study to TRAAK. Strikingly, HA-TREK1 or HA-TREK2 was able to pull down GFP-TRAAK despite only $\sim 40\%$ sequence identity (Fig. S1F and G). The extent of pull-down of GFP-TRAAK with HA-TREK1 or HA-TREK2 showed weaker efficiency compared with GFP-TREK1 (Fig. S1F–I). We next wondered if TREK1 can coassemble with more distant K_2P channels from another subfamily, such as TASK1 or TASK3, which share $\sim 30\%$ sequence identity with TREK1. The number of detected spots for both GFP-TASK1 and GFP-TASK3 was ~ 10 -fold less than the number of spots detected for GFP-TREK1 (Fig. S2A and B). Consistent with previous studies (18, 25), we found that HA-TASK3 pulled down GFP-TASK3 or GFP-TASK1 with similar efficiency (Fig. S2C).

Because SiMPull was used to isolate complexes at high levels of expression, we wanted to determine whether the same interactions would occur at low protein density exclusively on the plasma membrane.

TREK1 and TREK2 Coassemble and Are Targeted to the Plasma Membrane. To determine the ability of the identified TREK1-TREK2 heterodimer to form on the plasma membrane of living cells, we used single-molecule subunit counting of membrane-bound proteins in *Xenopus* oocytes (24). The assay is performed at low levels of expression, minimizing nonspecific interactions.

We first validated the technique by expressing either a C-terminally GFP-tagged TREK1 (TREK1-GFP) or TREK2 (TREK2-GFP) alone and counting GFP bleaching steps to confirm the dimerization of TREK1 and TREK2. For both TREK1-GFP and TREK2-GFP, $\sim 30\%$ of spots bleached in one step, whereas $\sim 70\%$ bleached in two steps (Fig. 2A and B). This observation agrees well with the binomial distribution expected for a dimer with GFP maturation of $\sim 75\%$ and is consistent with results from SiMPull (Fig. 1).

We next applied a two-color, colocalization-based version of subunit counting to test for coassembly between TREK1 and TREK2. When both TREK1-GFP and a C-terminally tdTomato-tagged TREK2 (TREK2-tdTomato) subunits were coexpressed, some spots were only green, some were only red, and the rest were colocalized spots containing both green and red fluorescence (Fig. 2C). Although background colocalization rates for noninteracting membrane proteins have been estimated at $<5\%$ (24), $\sim 25\%$ of the total spots were colocalized in this experiment (114 of 476 spots colocalized). Coexpression of TREK2-GFP and TREK1-tdTomato showed a similar spot distribution with considerable colocalization between the two subunits (105 of 348 spots colocalized). These results confirm that when TREK1 and TREK2 are coexpressed at low densities on the plasma membrane,

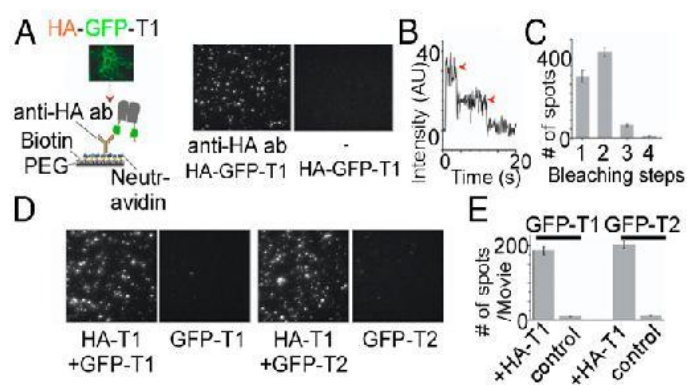


Fig. 1. SiMPull of TREK1 from HEK 293T cells reveals TREK1 homodimers and TREK1-TREK2 heteromers. (A, Left) Schematic of SiMPull of TREK1. HEK 293T cells expressing HA-GFP-TREK1 (HA-GFP-T1) are lysed and then immobilized on a passivated coverslip conjugated to a biotinylated anti-HA Ab. (A, Right) TIRF images of single molecules showing that HA-GFP-TREK1 immobilization is dependent on the anti-HA Ab. (B) Representative trace showing two-step photobleaching (red arrows) of HA-GFP-TREK1. AU, arbitrary units. (C) Summary of photobleaching step distribution for HA-GFP-TREK1. (D) Representative images showing that HA-TREK1 (HA-T1) can pull down GFP-TREK1 (GFP-T1) or GFP-TREK2 (GFP-T2) with comparable efficiency. Controls without HA-TREK1 confirm specificity. (E) Summary of HA-TREK1 pull-down of GFP-TREK1 and GFP-TREK2.

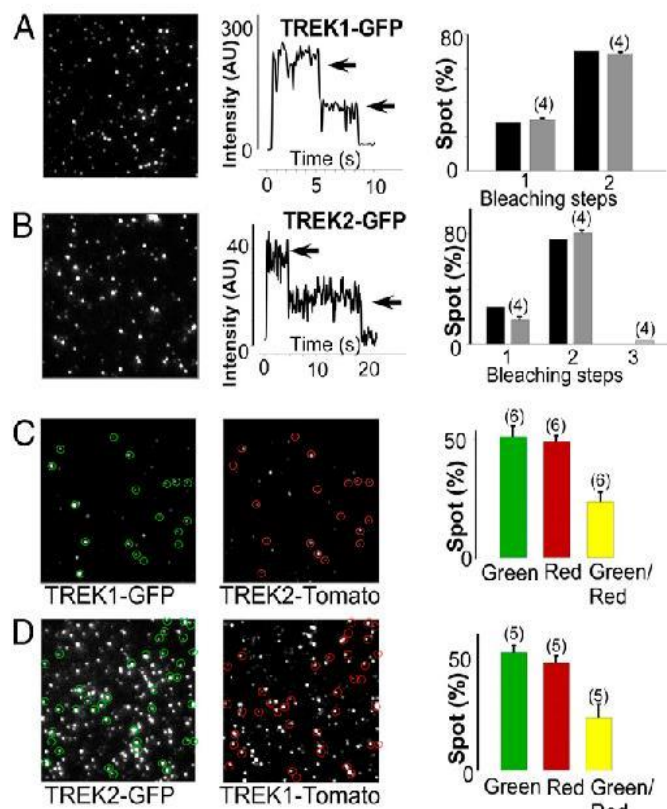


Fig. 2. TREK1 and TREK2 form heterodimers on the plasma membrane of *Xenopus* oocytes. Single-molecule subunit counting of TREK1 (A) and TREK2 (B) confirms strict dimerization. (Left) Images showing the first frame of a movie obtained for TREK1-GFP or TREK2-GFP. (Middle) Representative examples showing the time course of fluorescence photobleaching (gray arrows) from a single spot. (Right) Summary of photobleaching step distribution (gray bars) compared with the predicted distribution for a dimer based on 80% GFP maturation (black bars). (C) Representative TIRF images in the GFP (green) and tdTomato (red) channels for oocytes expressing similar levels of TREK1-GFP and TREK2-tdTomato. A bar graph summarizes the total number of red, green, and colocalized spots (yellow). (D) Similar data to C with TREK2-GFP and TREK1-tdTomato. The numbers of cells tested are indicated in parentheses.

a mix of TREK1 and TREK2 homodimers and TREK1-TREK2 heterodimers exists. We next tested the hypothesis that TREK1-TREK2 heterodimers would have unique functional properties.

Functional Characterization of TREK1-TREK2 and TREK1-TRAAK Heterodimers. To obtain a homogeneous population of heterodimers, we fused TREK1 and TREK2 subunits to produce either a TREK1-TREK2 or TREK2-TREK1 tandem (Fig. 3 A and B). Both tandems formed functional potassium-selective channels (Fig. 3 A and B) with similar basal current amplitudes ($3.13 \pm 0.5 \mu\text{A}$ for TREK1-TREK2 and $3.10 \pm 0.4 \mu\text{A}$ for TREK2-TREK1) that were intermediate between the basal current amplitudes of TREK1 ($5.5 \pm 1 \mu\text{A}$) and TREK2 ($1.8 \pm 0.5 \mu\text{A}$) homodimers (Fig. 3 C and D). TREK1-TREK2 and TREK2-TREK1 had the same channel properties (Fig. 3), indicating that the order of the subunits within the tandem is not important. Importantly, TREK1-TREK1 and TREK2-TREK2 tandem homodimers showed the same amplitude as WT-TREK1 ($P > 0.4$) or WT-TREK2 ($P > 0.2$), respectively, indicating that the tandem construct does not alter basal expression or functional properties (Fig. S3). We also fused TRAAK to TREK1 to produce TREK1-TRAAK and TRAAK-TREK1 tandems that also formed potassium-selective channels with current amplitudes ($1.5 \pm 0.1 \mu\text{A}$ TREK1-TRAAK and $1.4 \pm 0.2 \mu\text{A}$ TRAAK-TREK1) that were intermediate between the amplitudes observed for homodimers of TRAAK ($0.6 \pm 0.1 \mu\text{A}$) and TREK1

($2.4 \pm 0.3 \mu\text{A}$) (Fig. S4). We next examined the functional and regulatory properties of the heterodimeric channels.

TREK1-TREK2 Heterodimers Show Modified Current Rectification. In symmetrical K^+ conditions, TREK-1 and TREK-2 produce outwardly rectifying currents that can be characterized by the ratio $I_{-80\text{mV}}/I_{+80\text{mV}}$, which are 0.68 ± 0.05 and 0.58 ± 0.02 for TREK1 and TREK2, respectively. Interestingly, the rectification was stronger for TREK1-TREK2 and TREK2-TREK1 tandem dimers compared with TREK1 and TREK2 homodimers (0.31 ± 0.05 for TREK1-TREK2 and 0.35 ± 0.02 for TREK2-TREK1). In contrast, the TREK1-TRAAK and TRAAK-TREK1 tandem dimers showed the same rectification as TREK1 and TRAAK homodimers (Fig. S4 E and F).

pH Regulation of TREK1-TREK2 and TREK1-TRAAK Heterodimers. For both TREK1 and TREK2, intracellular acidification increases the potassium current by protonating Glu residues on the post-M4 C-terminal domain (Ctd), which controls channel gating through interaction with the plasma membrane (6, 26). Consistent with previous studies, acidifying the intracellular solution from internal pH (pH_i) 7.4 to pH_i 5.5 increased TREK2 current (I_{TREK2}) by 27 ± 5 -fold, whereas I_{TREK1} showed only an 8 ± 3 -fold increase ($P < 0.01$) (Fig. 4 A and B). We tested the TREK2-TREK1 under the same conditions and observed a 6 ± 0.8 -fold current increase, similar to the increase seen in TREK1 ($P > 0.8$) but significantly

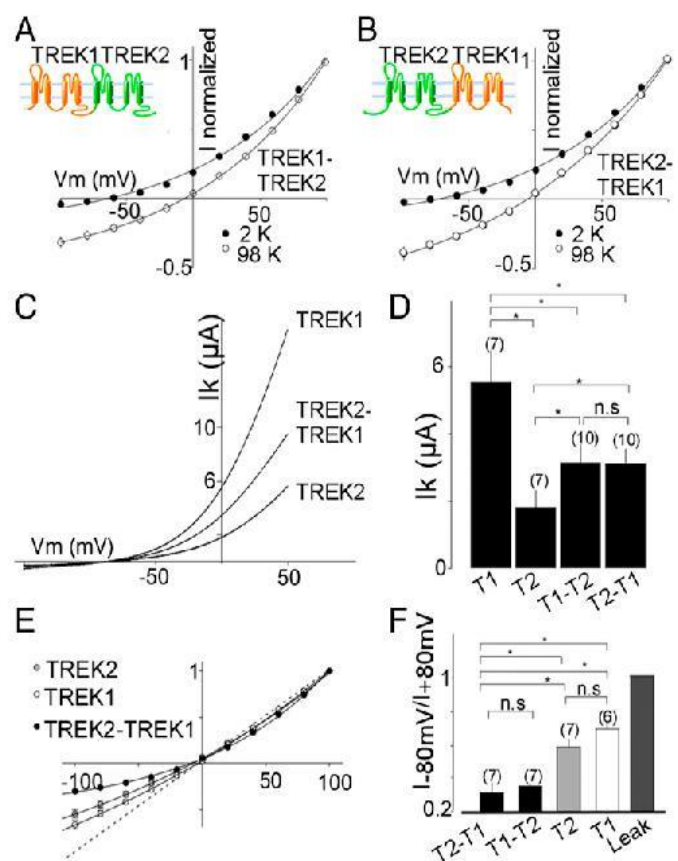


Fig. 3. Functional characterization of TREK1-TREK2 heterodimers. Normalized current–voltage (I – V) curves for TREK1-TREK2 (T1-T2) (A) or TREK2-TREK1 (T2-T1) (B) tandem dimers in the presence of two concentrations of external potassium (2 mM and 98 mM). (C) Representative traces showing TREK1 (T1), TREK2 (T2), and TREK2-TREK1 currents elicited by voltage ramps (from -100 to 50 mV, 1-s duration). (D) Summary of average current amplitudes. (E) Normalized I – V curves for TREK1, TREK2, and TREK2-TREK1 obtained in symmetrical potassium conditions (98 mM). (F) Bar graph representing the ratio (absolute values) of mean current recorded at -80 and $+80$ mV. The numbers of cells tested are indicated in parentheses. Student's t test ($*P < 0.05$). I_k , potassium current; n.s., not significant; V_m , membrane potential.

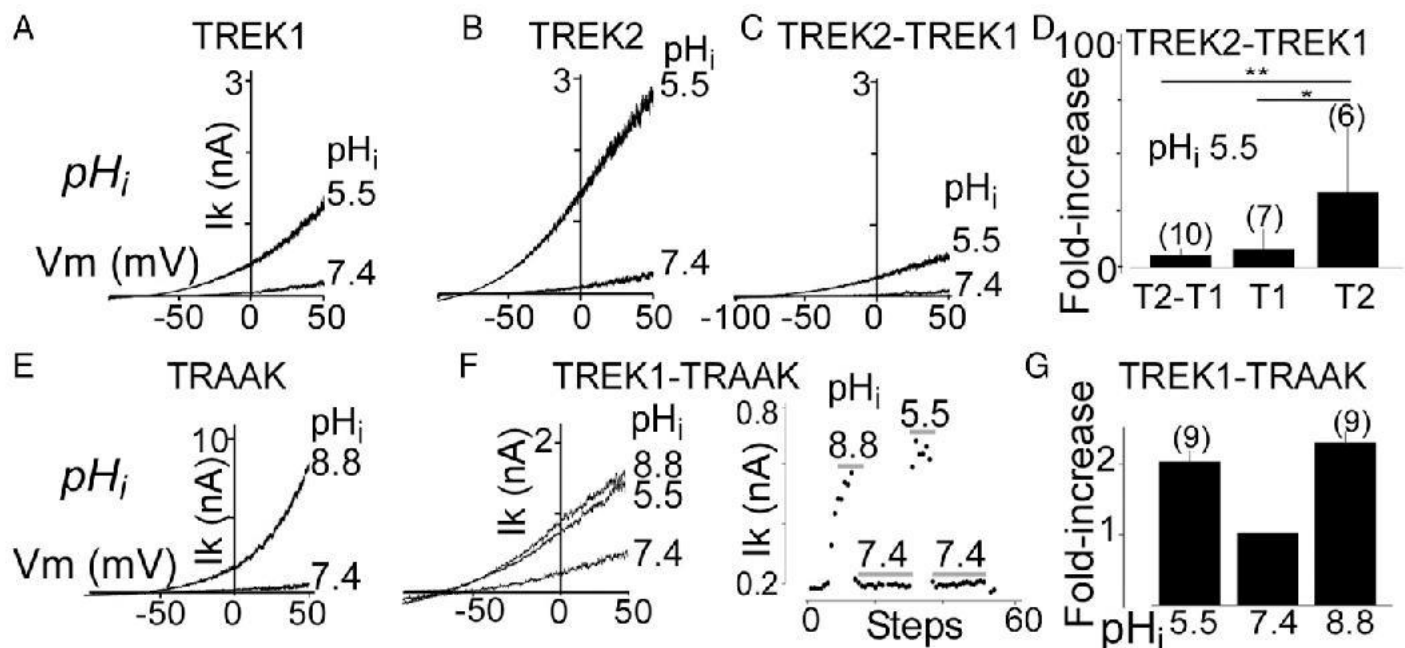


Fig. 4. Regulation of TREK family heterodimers by intracellular pH (pH_i). Representative traces showing the effect of intracellular acidification on TREK1 (T1) (A), TREK2 (T2) (B), and TREK2-TREK1 tandem heterodimers (T2-T1) (C). (D) Bar graph summarizing the current fold increases induced by a pH_i shift from 7.4 to 5.5. Representative traces showing the effect of changes in pH_i on TRAAK homodimers (E) and TREK1-TRAAK tandem heterodimers (F). An example of the response to dynamic changes in pH_i for TREK1-TRAAK is shown in F. Currents were elicited by voltage ramps (from -100 to 50 mV, 1-s duration, 1 step per 5 s). (G) Bar graph summarizing the increase in current induced by pH_i shift from 7.4 to either 5.5 or 8.8 for TREK1-TRAAK. The numbers of cells tested are indicated in parentheses. Student's *t* test ($*P < 0.05$; $**P < 0.01$).

less than what was observed for TREK2 ($P < 0.01$) (Fig. 4 C and D). Unlike TREK1 and TREK2, TRAAK is activated by intracellular alkalinization (Fig. 4E). Using TREK1-TRAAK tandem dimers, we found that these heterodimers are weakly activated by both increases and decreases in pH_i (Fig. 4 F and G).

We next investigated the regulation of TREK heterodimers by external pH (pH_o). Despite the high degree of sequence identity ($\sim 70\%$), TREK1 and TREK2 display an opposite regulation by pH_o (11): TREK1 is inhibited by acidification and activated by alkalinization, whereas TREK2 is activated by acidification and inhibited by alkalinization. TREK1-TREK2 showed unique regulation by pH_o . Acidification from pH_o 8.5–7.4 induced a rapid and large decrease in TREK1-TREK2 current amplitude ($51 \pm 6\%$) that was similar to TREK1 ($71 \pm 6\%$) (Fig. 5A). Further acidification from 7.4 to 6.5 induced a $34 \pm 9\%$ increase in TREK1-TREK2 current, similar to what was observed for TREK2 ($49 \pm 11\%$) (Fig. 5A). We titrated the pH and found that the heterodimer produces its lowest activity at physiological pH 7.4 and that either acidification or alkalinization leads to an increase in current (Fig. 5 B and C). In contrast to TREK2, TRAAK is inhibited by external acidification, but more weakly than TREK1 (11). As expected, TREK1-TRAAK was inhibited by external acidification but the observed inhibition was intermediate in amplitude between what is seen in TREK1 (highly sensitive) and TRAAK (poorly sensitive) (Fig. 5D).

We next probed the atypical regulation of the TREK1-TREK2 heterodimer to determine the mechanism of pH-sensing. TREK1 and TREK2 channels have a homologous pH sensor: a conserved His located in the first extracellular loop [H126 in TREK1 and H151 in TREK2 (11)]. Mutation of both His to either Ala or Lys within the tandem TREK2-TREK1 heterodimer abolished pH sensitivity (Fig. 6 A and B), confirming their roles in pH sensing. Within a heterodimer, mutation of only the pH sensor (H151) of the TREK2 subunit did not fully abolish pH sensitivity but, instead, converted the channel into a TREK1-like “mode”: The tandem heterodimer was potentiated by $68 \pm 13\%$ or $40 \pm 9\%$ by alkalinization from pH 7.2–8 and inhibited by $53.5 \pm 5\%$ and $48 \pm 16\%$ by acidification from pH 7.4–6.5 for H151A and H151K, respectively (Fig. 6 A and B). In addition, H151K, which mimics

the protonated state, increased the basal current of the heterodimer by $39 \pm 7\%$, whereas H151A, which mimics the deprotonated state, induced a basal current decrease of $38.5 \pm 15\%$ (Fig. 6C). This measurement is in agreement with the effects of the H151K mutation ($58 \pm 12\%$ increase in basal current) and

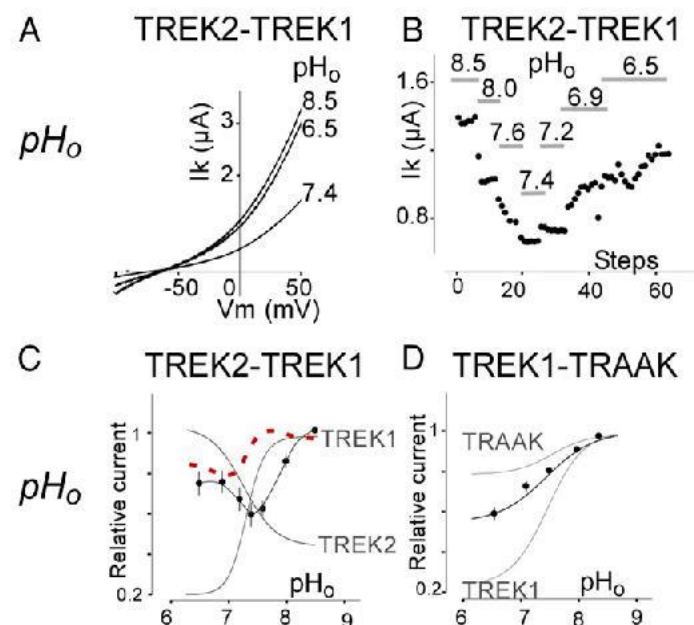


Fig. 5. Regulation of TREK family heterodimers by extracellular pH. (A) Representative traces showing the effect of changes in extracellular pH (pH_o) on TREK2-TREK1 tandem heterodimers. Currents were elicited by voltage ramps (from -10 to 50 mV, 1-s duration). (B) Representative example of dynamic regulation of TREK2-TREK1 tandem heterodimers by changes in pH_o . (C) pH_o dependence of TREK2-TREK1 tandem (black) compared with TREK2 and TREK1 (gray) homodimers. The linear sum of the pH_o dependence of the TREK1 and TREK2 homodimers is shown as a dotted red line. (D) pH_o dependence of TREK1-TRAAK tandem homodimers (black) compared with TREK1 and TRAAK homodimers (gray).

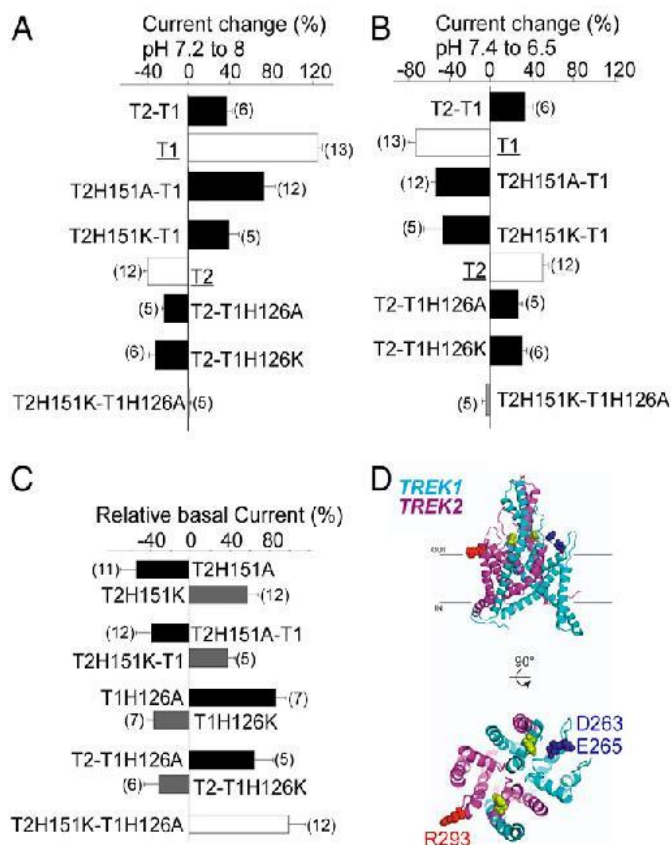


Fig. 6. Mechanism of pH_o sensitivity of TREK2-TREK1 heterodimers. (A) Bar graph showing the percentage of current at pH 8 relative to pH 7.2 for TREK1 (T1), TREK2 (T2), TREK2-TREK1 (T2-T1), and TREK2-TREK1 (T2-T1) mutants. (B) Bar graph showing the percentage of current at pH 7.4 relative to pH 6.5. (C) Bar graph showing the current amplitude of TREK2 (T2) mutants relative to TREK2, TREK1 (T1) mutants relative to TREK1, and TREK2-TREK1 (T2-T1) mutants relative to TREK2-TREK1. (D) Structural model of TREK1-TREK2 heterodimers showing His pH sensors (yellow). The proposed negatively charged interacting residues of TREK1 (cyan) are shown in blue, and the proposed positively charged interacting residues of TREK2 (magenta) are shown in red.

the H151A mutation ($30 \pm 14\%$ decrease in basal current) in TREK2 homodimers (Fig. 6C). Together, these data indicate that the His pH sensors within a heterodimer control basal current and the pH_o response in a subunit-autonomous manner. In agreement with this interpretation, mutation of the pH sensor of the TREK1 subunit within the TREK1-TREK2 heterodimer (H126A or H126K) resulted in TREK2-like pH-sensing behavior (Fig. 6A and B). Consistent with what was seen for TREK1 homodimers, heterodimers with TREK1-H126A showed increased basal current by $68 \pm 15\%$, whereas tandem heterodimers with TREK1-H126K showed decreased basal current by $31.8 \pm 5\%$ (Fig. 6C).

To visualize how extracellular His within the first loop of TREK channels may control the sensitivity to pH_o , we used crystal structures of TREK2 (27) and TREK1 to build a model of the TREK1-TREK2 heterodimer. The model shows that charged residues within the second extracellular loop (negatively charged E265 and D263 in TREK1 and positively charged R293 in TREK2), which were previously identified as potential electrostatic interaction partners (11), are indeed positioned to interact with the His, and that these interactions occur within a subunit (Fig. 6D). This proximity likely explains why pH sensing can operate independently in each subunit.

Regulation of TREK1-TRAAK Heterodimers by PLD2. We recently described how, in both TREK1 and TREK2, interaction of the

intracellular Ctd with the PA-producing enzyme PLD2 results in PA-dependent tonic activation (5). Despite its sensitivity to PA, TRAAK is not regulated by PLD2 because it does not form a channel-enzyme complex. We asked if the TREK1-TRAAK heterodimer, which presumably contains only one PLD2 binding site in the Ctd of the TREK1 subunit, can be regulated by PLD2 coexpression. TRAAK-TREK1 and TREK1-TRAAK tandems were potentiated by coexpression of PLD2 to a similar level as seen for TREK1 (Fig. 7), suggesting that only one Ctd is sufficient to bind PLD2 and produce enough PA for tonic activation.

Discussion

In this study, we analyzed the ability of members of the TREK channel subfamily of K_2P channels to coassemble and found that TREK1, TREK2, and TRAAK are able to heteromerize: TREK1 coassembles with TREK2 as efficiently as it does with itself and also assembles with TRAAK, although less efficiently. In contrast, TREK1 coassembles poorly with members of other K_2P subfamilies, such as TASK channels. The overlapping expression patterns in the mouse brain (7, 28) suggest that heterodimers may form in native tissue. We found that the functional properties of heterodimers are distinct from the functional properties of the homodimers, thereby providing an added mechanism for functional diversity.

Extracellular acidification has previously been shown to inhibit homodimers of TREK1 and activate homodimers of TREK2 (11). We found that TREK1-TREK2 heterodimers display a unique blend of pH sensitivity, with activation by both extracellular acidification and alkalinization, which results in an unusual property of minimal activity at physiological pH_o . Mutations in the pH sensor of the TREK1 subunit of the heterodimer converted the TREK1-TREK2 heterodimeric channel into TREK2-like pH-sensing, whereas mutations in the pH sensor of the TREK2 subunit converted the heterodimeric channel into TREK1-like pH-sensing. Together, these findings reveal that the pH sensors operate individually within each subunit.

Interestingly, extracellular acidification or mutation of the pH sensor His in the first extracellular loop to Lys boosts current in TREK1 and inhibits current in TREK2, whereas mutation to Ala has the opposite effects (11). Moreover, the opposite effect in TREK1 and TREK2 can be accounted for by the opposite charges of the interacting residues in the second extracellular loop: two acidic residues in TREK1 vs. a basic residue in TREK2. These characteristics are consistent with the model that repulsion between the external loops stabilizes the open state of the channel, whereas attraction between the external loops stabilizes the closed state of the channel (11). How could such interactions between the first and second external loops be communicated to the internal gate of the channel? An answer is

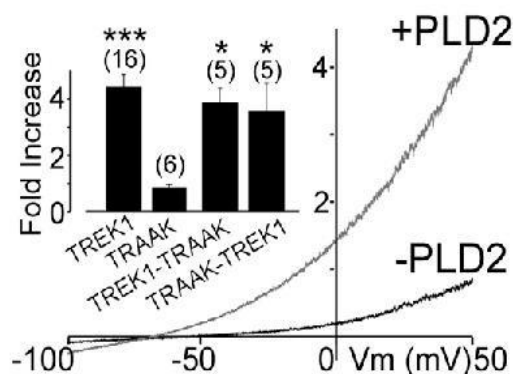


Fig. 7. Potentiation of TREK1-TRAAK heterodimers by PLD2. Representative traces showing effects of PLD2 coexpression on TREK1-TRAAK. (Inset) Summary of current potentiation by coexpression of PLD2. The numbers of cells tested are indicated in parentheses. Student's *t* test (* $P < 0.05$; *** $P < 0.001$).

suggested by the location of the charged residues in the second external loop just “above” the fourth transmembrane helix, which has been shown to serve as an intracellular gate in K₂P channels (29–31), implying an activation rearrangement that propagates through the helix to the intracellular gate.

It is interesting to consider how the proposed pH sensor to gate linkages in the two subunits combines their influences on the gate. Given the opposite effect of titration of the sensor His in TREK1 and TREK2, one would have expected that the effect of pH would have been blunted in the TREK1-TREK2 heterodimer and perhaps that the effect on one of the subunits (e.g., TREK1, which is potentiated at alkaline pH by more than TREK2 is inhibited) would have dominated, leaving a reduced and monotonic effect of pH in the TREK1-TREK2 heterodimer. However, what we observed instead was that the TREK1-TREK2 heterodimer was activated at both low and high pH. This nonlinear influence on gating suggests a more complex process that may involve intersubunit interactions.

TREK subfamily channels are also modulated by pH_i. Whereas TREK1 and TREK2 homodimers are activated by intracellular acidification (32), TRAAK is activated by intracellular alkalization (27). We find that TREK1-TRAAK heterodimers are activated by both increases and decreases in pH_i. This regulation indicates that, as seen with the extracellular His pH_o sensors, the C termini of TREK and TRAAK individually sense pH and influence gating.

The unique sensitivity of TREK1-TREK2 and TREK1-TRAAK heterodimers to changes in extracellular or intracellular pH, respectively, may have important physiological consequences. Deviation from resting pH is associated with heavy activity or metabolic load, as well as with pathological states. Neurons coexpressing TREK1 and TREK2 or TREK1 and TRAAK may form heterodimers that are activated by both acidification and alkalization. This coassembly may endow TREK channels with a neuroprotective function, whereby pH deviation from physiological values increases

the hyperpolarizing outward potassium current to prevent potentially damaging excitation from spreading throughout the network.

In contrast to the complex subunit regulation by pH, we found that another class of regulation, by PLD2, operated in a simple manner. PLD2 has been shown recently to regulate TREK1 and TREK2, but not TRAAK, with specificity defined by the ability of PLD2 to bind to the C termini of TREK1 and TREK2, but not TRAAK (5). We find that TREK1-TRAAK heterodimers are regulated by PLD2 with a similar potency to TREK1, indicating that a channel needs only one PLD2-compatible C-terminal domain to bind PLD2. Thus, whereas the two C termini respond individually to changes in pH_i and the two pH_o sensors respond individually to changes in external pH, a single PLD2 binding site in one C-terminal domain is sufficient to anchor the enzyme, which then can create a PA-rich domain.

Methods

Standard molecular biological, biochemical, and electrophysiological techniques were used as described previously (5) and (*SI Methods*). Electrophysiology was performed 24–72 h after transfection for HEK 293T cells and 24–48 h after injection for *Xenopus* oocytes. For SIMPull experiments, coverslips were prepared as described (23). Single molecules were imaged using a 488-nm argon laser on a TIRF microscope with a 60× objective (Olympus). For subunit counting with *Xenopus laevis* oocytes, oocytes were enzymatically treated with hyaluronidase (1 mg/mL; Sigma) and neuraminidase (1 unit/mL; Sigma) for 15 min at 4 °C and manually devitelinized to enable close contact of the oocyte's plasma membrane to the coverslip.

ACKNOWLEDGMENTS. We thank S. Bharill, M. Ulbrich, and O. Soriani for technical assistance and helpful discussion. The work was supported by a grant (to G.S.) by the Action Thématique et Incitative sur Programme-AVENIR (ATIP-AVENIR) funds and the French National Center for Scientific Research, as well as by grants (to G.S.) from the Fondation NRJ-Institut de France, Agence Nationale de la Recherche (ANR) (Laboratory of Excellence “Ion Channel Science and Therapeutics,” Grant ANR-11-LABX-0015-01), and ANR Dynaselect (Grant ANR-14-CE13-0010); by grants (to E.Y.I.) from the National Science Foundation (Grant IOS-1451027) and NIH (Grant R01NS35549); and by a Chateaubriand fellowship (to J.L.).

- Patel AJ, et al. (1998) A mammalian two pore domain mechano-gated S-like K⁺ channel. *EMBO J* 17(15):4283–4290.
- Maingret F, et al. (2000) TREK-1 is a heat-activated background K⁺ channel. *EMBO J* 19(11):2483–2491.
- Kang D, Choe C, Kim D (2005) Thermosensitivity of the two-pore domain K⁺ channels TREK-2 and TRAAK. *J Physiol* 564(Pt 1):103–116.
- Maingret F, Patel AJ, Lesage F, Lazdunski M, Honoré E (2000) Lysophospholipids open the two-pore domain mechano-gated K⁺ channels TREK-1 and TRAAK. *J Biol Chem* 275(14):10128–10133.
- Comoglio Y, et al. (2014) Phospholipase D2 specifically regulates TREK potassium channels via direct interaction and local production of phosphatidic acid. *Proc Natl Acad Sci USA* 111(37):13547–13552.
- Sandoz G, Bell SC, Isacoff EY (2011) Optical probing of a dynamic membrane interaction that regulates the TREK1 channel. *Proc Natl Acad Sci USA* 108(6):2605–2610.
- Fink M, et al. (1998) A neuronal two P domain K⁺ channel stimulated by arachidonic acid and polyunsaturated fatty acids. *EMBO J* 17(12):3297–3308.
- Maingret F, Patel AJ, Lesage F, Lazdunski M, Honoré E (1999) Mechano- or acid stimulation, two interactive modes of activation of the TREK-1 potassium channel. *J Biol Chem* 274(38):26691–26696.
- Kim Y, Gnatenco C, Bang H, Kim D (2001) Localization of TREK-2 K⁺ channel domains that regulate channel kinetics and sensitivity to pressure, fatty acids and pHi. *Pflugers Arch* 442(6):952–960.
- Noël J, Sandoz G, Lesage F (2011) Molecular regulations governing TREK and TRAAK channel functions. *Channels (Austin)* 5(5):402–409.
- Sandoz G, Douguet D, Chatelain F, Lazdunski M, Lesage F (2009) Extracellular acidification exerts opposite actions on TREK1 and TREK2 potassium channels via a single conserved histidine residue. *Proc Natl Acad Sci USA* 106(34):14628–14633.
- Lesage F, Terrenoire C, Romey G, Lazdunski M (2000) Human TREK2, a 2P domain mechano-sensitive K⁺ channel with multiple regulations by polyunsaturated fatty acids, lysophospholipids, and Gs, Gi, and Gq protein-coupled receptors. *J Biol Chem* 275(37):28398–28405.
- Bang H, Kim Y, Kim D (2000) TREK-2, a new member of the mechanosensitive tandem-pore K⁺ channel family. *J Biol Chem* 275(23):17412–17419.
- Fink M, et al. (1996) Cloning, functional expression and brain localization of a novel unconventional outward rectifier K⁺ channel. *EMBO J* 15(24):6854–6862.
- Talley EM, Solorzano G, Lei Q, Kim D, Bayliss DA (2001) Cns distribution of members of the two-pore-domain (KCNK) potassium channel family. *J Neurosci* 21(19):7491–7505.
- Heurteaux C, et al. (2004) TREK-1, a K⁺ channel involved in neuroprotection and general anesthesia. *EMBO J* 23(13):2684–2695.
- Heurteaux C, et al. (2006) Deletion of the background potassium channel TREK-1 results in a depression-resistant phenotype. *Nat Neurosci* 9(9):1134–1141.
- Czirják G, Enyedi P (2002) Formation of functional heterodimers between the TASK-1 and TASK-3 two-pore domain potassium channel subunits. *J Biol Chem* 277(7):5426–5432.
- Blin S, et al. (2014) Tandem pore domain halothane-inhibited K⁺ channel subunits THIK1 and THIK2 assemble and form active channels. *J Biol Chem* 289(41):28202–28212.
- Woo DH, et al. (2012) TREK-1 and Best1 channels mediate fast and slow glutamate release in astrocytes upon GPCR activation. *Cell* 151(1):25–40.
- Plant LD, et al. (2010) One SUMO is sufficient to silence the dimeric potassium channel K2P1. *Proc Natl Acad Sci USA* 107(23):10743–10748.
- Lauritzen I, et al. (2003) K⁺-dependent cerebellar granule neuron apoptosis. Role of task leak K⁺ channels. *J Biol Chem* 278(34):32068–32076.
- Jain A, et al. (2011) Probing cellular protein complexes using single-molecule pull-down. *Nature* 473(7348):484–488.
- Ulbrich MH, Isacoff EY (2007) Subunit counting in membrane-bound proteins. *Nat Methods* 4(4):319–321.
- Lauritzen I, et al. (2005) Cross-talk between the mechano-gated K2P channel TREK-1 and the actin cytoskeleton. *EMBO Rep* 6(7):642–648.
- Honoré E (2007) The neuronal background K2P channels: Focus on TREK1. *Nat Rev Neurosci* 8(4):251–261.
- Kim Y, Bang H, Gnatenco C, Kim D (2001) Synergistic interaction and the role of C-terminus in the activation of TRAAK K⁺ channels by pressure, free fatty acids and alkali. *Pflugers Arch* 442(1):64–72.
- Sandoz G, et al. (2008) Mtap2 is a constituent of the protein network that regulates twik-related K⁺ channel expression and trafficking. *J Neurosci* 28(34):8545–8552.
- Brohawn SG, del Mármol J, MacKinnon R (2012) Crystal structure of the human K2P TRAAK, a lipid- and mechano-sensitive K⁺ ion channel. *Science* 335(6067):436–441.
- Dong YY, et al. (2015) K2P channel gating mechanisms revealed by structures of TREK-2 and a complex with Prozac. *Science* 347(6227):1256–1259.
- Bagriantsev SN, Peyronnet R, Clark KA, Honoré E, Minor DL, Jr (2011) Multiple modalities converge on a common gate to control K2P channel function. *EMBO J* 30(17):3594–3606.
- Honoré E, Maingret F, Lazdunski M, Patel AJ (2002) An intracellular proton sensor commands lipid- and mechano-gating of the K⁺ channel TREK-1. *EMBO J* 21(12):2968–2976.
- Reiner A, Arrant RJ, Isacoff EY (2012) Assembly stoichiometry of the GluK2/GluK5 kainate receptor complex. *Cell Reports* 1(3):234–240.
- Sali A, Blundell TL (1993) Comparative protein modelling by satisfaction of spatial restraints. *J Mol Biol* 234(3):779–815.
- Humphrey W, Dalke A, Schulten K (1996) VMD: Visual molecular dynamics. *J Mol Graph* 14(1):33–38, 27–28.

Supporting Information

Levitz et al. 10.1073/pnas.1522459113

SI Methods

Molecular Biology, Cell Culture, and Gene Expression. All channel DNA was used in the pIRES2eGFP and pEXO vectors. Capped cRNAs were synthesized in vitro from the linearized plasmid by using T7 RNA polymerase (Ambion). Tandems between TREK1 and TREK2 or TREK1 and TRAAK were generated by PCR.

HEK 293 or 293T cells were maintained in DMEM with 5% FBS on poly-L-lysine-coated glass coverslips in 12-well plates. Cells were transiently cotransfected using Lipofectamine 2000 (Invitrogen) with a total of 1–1.6 μg of DNA total per 18-mm-diameter coverslip.

Defolliculated *Xenopus* oocytes were injected with cRNA (5 ng) encoding mouse TREK1, TREK2, and TRAAK or TREK1-TREK2, TREK1-TREK2, TRAAK-TREK1, and TREK1-TRAAK tandems. They were used for electrophysiological studies 2–4 d after injection. For single-molecule experiments, the amount of injected cRNA required to produce resolvable single channels on the cell's surface was determined empirically.

Electrophysiology. HEK 293 cell electrophysiology was performed 24–72 h after transfection in solution containing 145 mM NaCl, 4 mM KCl, 1 mM MgCl_2 , 2 mM CaCl_2 , and 10 mM Hepes. Glass pipettes of resistance between 3 $\text{M}\Omega$ and 6 $\text{M}\Omega$ were filled with intracellular solution containing 140 mM KCl, 10 mM Hepes, 5 mM EGTA, and 3 mM MgCl_2 (pH 7.4). Cells were patch-clamped using an Axopatch 200A (Molecular Devices) amplifier in the whole-cell mode. Currents were elicited by voltage ramps (from -100 to 50 mV, 1 s in duration), and the current density was calculated at 0 mV. For acidic intracellular (5.5 pH_i) solutions, Hepes was substituted with MES, and for basic (8.0 pH_i) solution, Hepes was substituted with Tris.

Oocyte two-electrode voltage clamp electrophysiology was performed in a 0.3-mL perfusion chamber; a single oocyte was impaled with two standard microelectrodes (1–2.5 $\text{M}\Omega$ resistance) filled with 3 M KCl, and maintained under voltage clamp using a Dagan TEV 200 amplifier in standard ND96 solution [96 mM NaCl, 2 mM KCl, 1.8 mM CaCl_2 , 2 mM MgCl_2 , 5 mM Hepes (pH 7.4 with NaOH)]. For the high K solution, the NaCl was replaced by KCl. Stimulation of the preparation, data acquisition, and analysis were performed using pClamp software (Molecular Devices). Changes in extracellular pH were induced by a microperfusion system that allowed local and rapid changes of solutions. Hepes was replaced by MES (5 mM) for buffer solutions with a pH between 6.5 and 5.0.

SiMPull. For SiMPull experiments, HEK 239T cells were harvested from coverslips by incubating with Ca^{2+} -free PBS buffer for 20–30 min, followed by gentle pipetting. Cells were pelleted and lysed in buffer containing 150 mM NaCl, 1 mM EDTA, protease inhibitor mixture (Thermo Scientific), and 1.5% (vol/vol) IGEPAL (Sigma). After 30–60 min incubation at 4 $^\circ\text{C}$, lysate was centrifuged for 20 min at $16,000 \times g$ and the supernatant was collected. Coverslips passivated with PEG ($\sim 99\%$)/biotin-PEG ($\sim 1\%$) and treated with Neutravidin (Thermo Scientific) were prepared as described (23). Biotinylated anti-HA Ab (15 nM, no. ab26228; Abcam) was applied for 20 min and then washed out. Ab dilutions and washes were done in T50 buffer containing 50 mM NaCl and 10 mM Tris (pH 7.5). Lysate, diluted in standard patch-clamp electrophysiology extracellular recording solutions (*SI Methods, Electrophysiology*) was then applied to the chamber and

washed away following brief incubation (~ 2 min). Single molecules were imaged using a 488-nm argon laser on a TIRF microscope with a 60 \times objective (Olympus). We recorded the emission light after an additional 3 \times magnification and passage through a double-dichroic mirror and an emission filter (525/50 for GFP) with a back-illuminated EM CCD camera (iXon DV-897 BV; Andor). Movies of 500–800 frames were acquired at frame rates of 10–30 Hz. The imaged area was $13 \times 13 \mu\text{m}^2$. At least five movies were recorded for each condition, and data were analyzed using custom software as previously described (24). Multiple independent experiments were performed for each condition. Representative datasets are presented to compare conditions tested on the same day quantitatively. For photobleaching experiments, error bars were calculated using counting statistics as described by Reiner et al. (33).

Subunit Counting with *X. laevis* Oocytes. Twenty-four hours after RNA injection and expression at 18 $^\circ\text{C}$, *X. laevis* oocytes were enzymatically treated with hyaluronidase (1 mg/mL; Sigma) and neuraminidase (1 unit/mL; Sigma) for 15 min at 4 $^\circ\text{C}$ and manually devitellinized to enable close contact of the oocyte's plasma membrane to the coverslip. The coverslips' refractive index ($n = 1.78$) matched the refractive index of the microscope objective front lens (100/NA1.65; Olympus) and the immersion oil (Cargille). GFP was excited with a 488-nm argon laser, and ttTomato was excited with a 532-nm diode-pumped solid-state (DPSS) laser. We recorded the emission light after an additional 3 \times magnification and passage through a double-dichroic mirror and an emission filter (525/50 for GFP, 592.5/50 for ttTomato) with a back-illuminated EM CCD camera (iXon DV-897 BV). Movies of 500 frames were acquired at frame rates of 10–30 Hz. The imaged area was $13 \times 13 \mu\text{m}^2$. For two-color experiments, fluorescence from ttTomato was measured first, and after almost complete bleaching of ttTomato to prevent Förster/fluorescence resonance energy transfer from green to red chromophores, GFP fluorescence was measured. Occasionally, a few ttTomato molecules did not bleach completely, but even unbleached ttTomato did not affect fluorescence from colocalized GFP significantly. Laser powers were between 0.5 mW and 2 mW, and the diameter of the beam at the sample was 20 μm . Switching the illumination on and off and changing emission filters were done using electromechanical shutters and a motorized filter wheel. The typical time for switching off the 532-nm illumination, changing emission filters, and switching on the 488-nm illumination was 1–2 s.

Structural Modeling. The model of the TREK1-TREK2 heterodimer was constructed based on the crystal structures of TREK1 [Protein Data Bank (PDB) ID code 4TWK] and TREK2 (PDB ID code 4BW5) (30). The program Modeler (34) was used to fill in the unresolved regions of each structure separately. The resultant full-length model of TREK2 chain B was then aligned to chain B of the TREK1 dimer structure using Visual Molecular Dynamics (VMD) (35). Finally, the full-length model of TREK1 chain A, the aligned full-length model of TREK2 chain B, and the crystallographic waters and potassium ions from the TREK1 structure were written to a new PDB file with a patch applied to form the disulfide bridge between Cys69 in TREK1 and Cys58 in TREK2 using a custom Tcl script run in VMD. Figures were then generated using PyMOL.

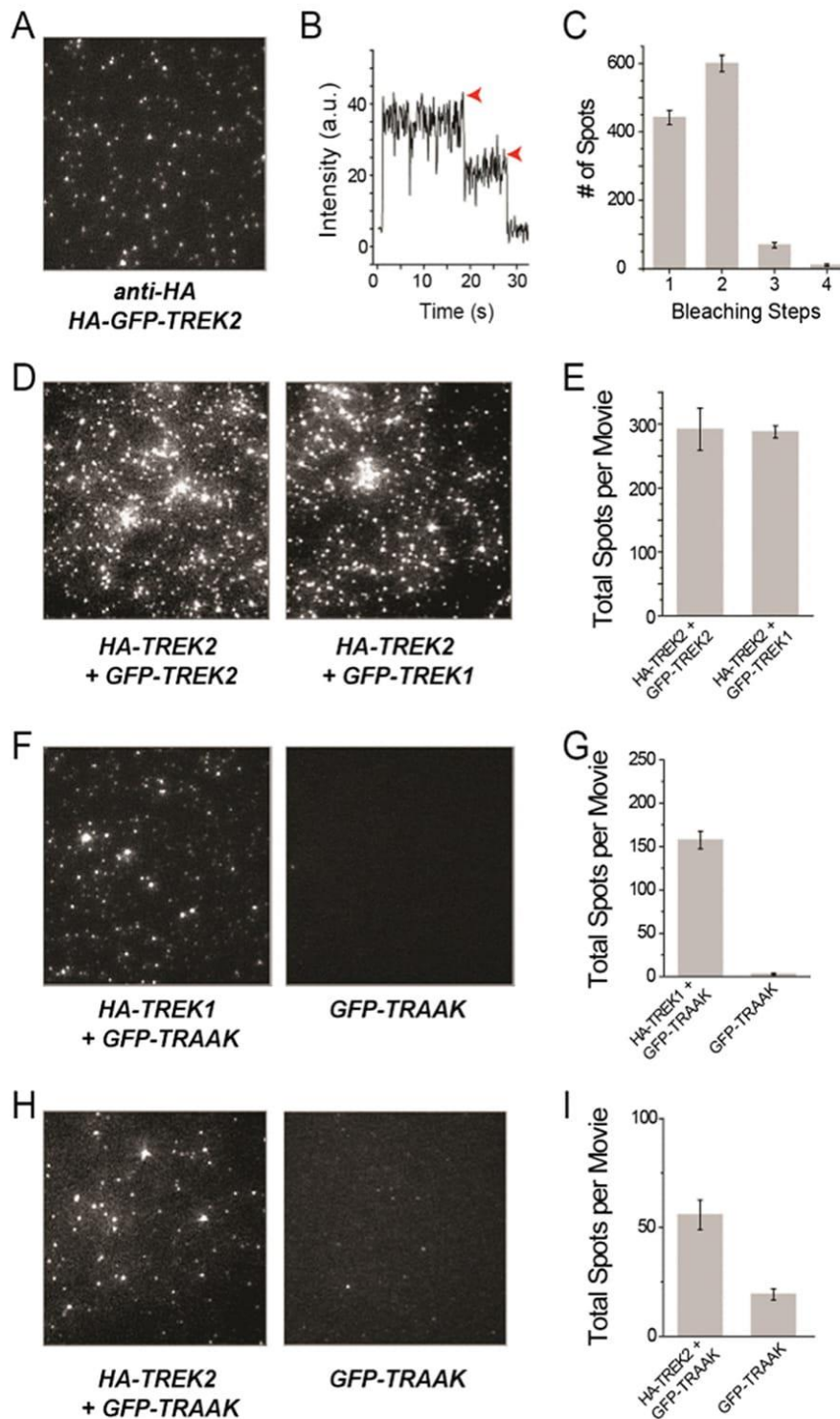


Fig. S1. SIMPull from HEK 293T cells reveals TREK2 homodimers and TREK1/TRAACK and TREK2/TRAACK heteromers. (A) TIRF images of immobilized single molecules of HA-GFP-TREK2. (B) Representative trace showing two-step photobleaching (red arrows) of TREK2. a.u., arbitrary unit. (C) Summary of photobleaching step distribution for HA-GFP-TREK2. (D) Representative images showing that HA-TREK2 is able to pull down GFP-TREK1 or GFP-TREK2 with comparable efficiency. (E) Summary of HA-TREK2 pull-down of GFP-TREK1 and GFP-TREK2. Representative images and summary graphs showing that HA-TREK1 (F and G) or HA-TREK2 (H and I) is able to pull down GFP-TRAACK above background levels, as measured by GFP-TRAACK alone.

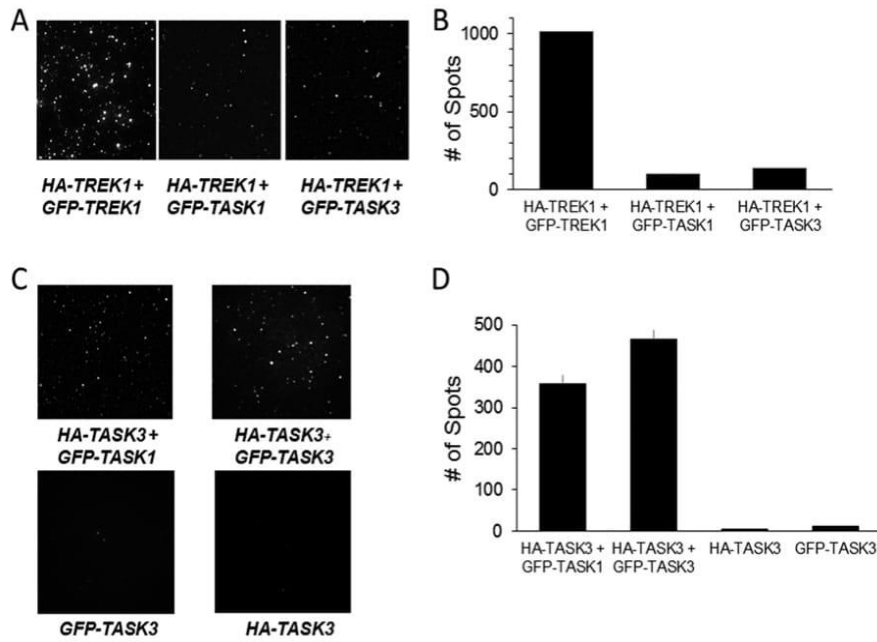


Fig. S2. SIMPull reveals a lack of heteromerization between TREK1 and TASK1 or TASK3, but clear heteromerization between TASK1 and TASK3. (A) TIRF images of immobilized single molecules of HA-TREK1-mediated pull-down of GFP-TREK1 (Left), GFP-TASK1 (Middle), or GFP-TASK3 (Right). (B) Summary of HA-TREK1 pull-down showing much more efficient pull-down of TREK1 compared with TASK1 or TASK3. Dilution factors describe how much lysate was diluted before application onto a coverslip. (C) Representative images showing that HA-TASK3 is able to pull down GFP-TASK1 or GFP-TASK3 with comparable efficiency. (D) Summary of HA-TASK1 pull-down of GFP-TASK1 and GFP-TASK3 compared with controls with GFP-TASK1 or HA-TASK1 alone.

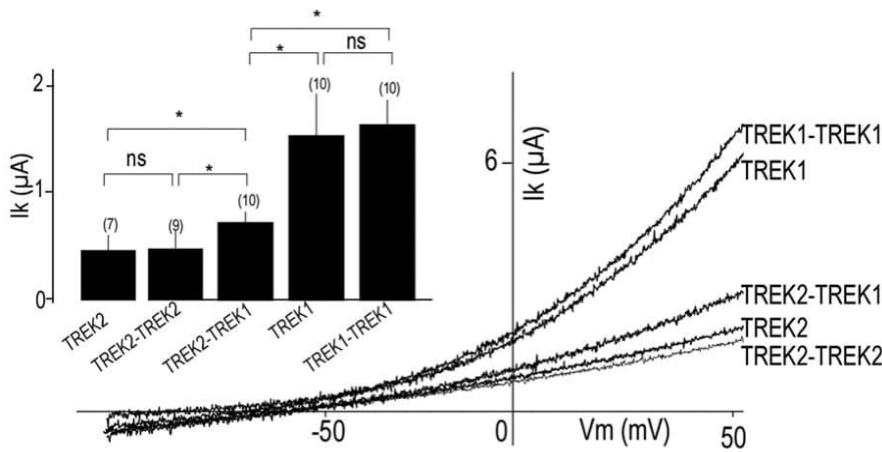


Fig. S3. TREK1-TREK1 and TREK2-TREK2 tandem homodimers show the same amplitude as WT TREK1 and TREK2, respectively. Representative traces showing TREK1, TREK1-TREK1, TREK2, TREK2-TREK2, and TREK2-TREK1 currents. Currents were elicited by voltage-ramps (from -100 to 50 mV, 1 s in duration). (Inset) Bar graph showing average TREK1, TREK1-TREK1, TREK2, TREK2-TREK2, and TREK2-TREK1. The numbers of cells tested are indicated in parentheses. Student's t test ($*P < 0.05$). I_k , potassium current; n.s., not significant; V_m , membrane potential.

C. Discussion and conclusions

In this paper, we have been able to assess the unique sensitivity of TREK1-TREK2 and TREK1-TRAAK heterodimers to changes in both external and internal pH. Changes of pH from resting values are involved in cellular process and pathophysiological state such as hypoxia occurring during ischemia.

Structure function studies helped us to determine that pH sensor in both subunits can act independently. However, it is interesting to consider how the subunits combine their influences on the gating mechanism. Given the opposite effects of extracellular pH (pH_{ext}) on TREK1 and TREK-2, we would have expected that the pH_{ext} would exert a lower effect on the heteromer or that one of the subunit regulation would have overlapped the other. But this study showed the opposite: the two mechanisms complement each other, suggesting that the influence of the subunits on the inner gate is very complex.

We found that TREK1 and TREK2 were able to heteromerize with no preference, and with TRAAK to a lesser extent. TREK channels are able to assemble even at a low level of expression in heterologous system, as it would be the case in nature, and their expression pattern is overlapping in several tissues (Fink et al., 1998; Sandoz et al., 2008). We also have shown that TASK1 and TASK3, which share only about 30% of identity with TREK1, are not able to form dimers with TREK1. We therefore wonder if we could find a rule, based on sequence homology to explain the recognition between subunits leading to their assembly. Thus, we further extend the study of TREK1 interaction to other subunits. And found that TREK1 can co-assemble with TREK2, TRAAK and TRESK with a smaller advantage for TREK2. It can be noticed that we obtained few spots with TWIK2 and KCNK7 which are minors.

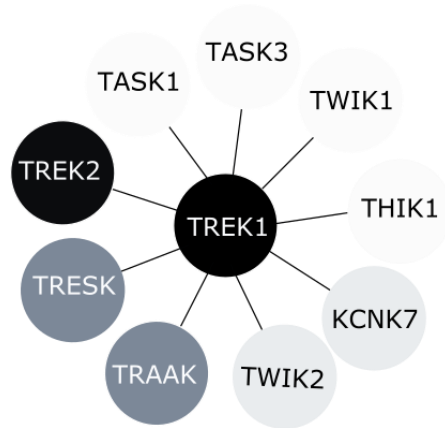


Figure 38: Interacting K_{2P} partners. Subunits interacting with TREK1 are darker, subunits that show no interaction with TREK1 are in light grey circles.

V. Article II

A. Introduction

Given the central place of TREK channels in several paradigms previously described, and having found that K_{2P} channels were able to heteromerize, as it was observed in other potassium channel families, we wonder if their heteromerization could play a role in their mode of regulation involved in pathophysiology.

TREK-TRESK association, how the story started

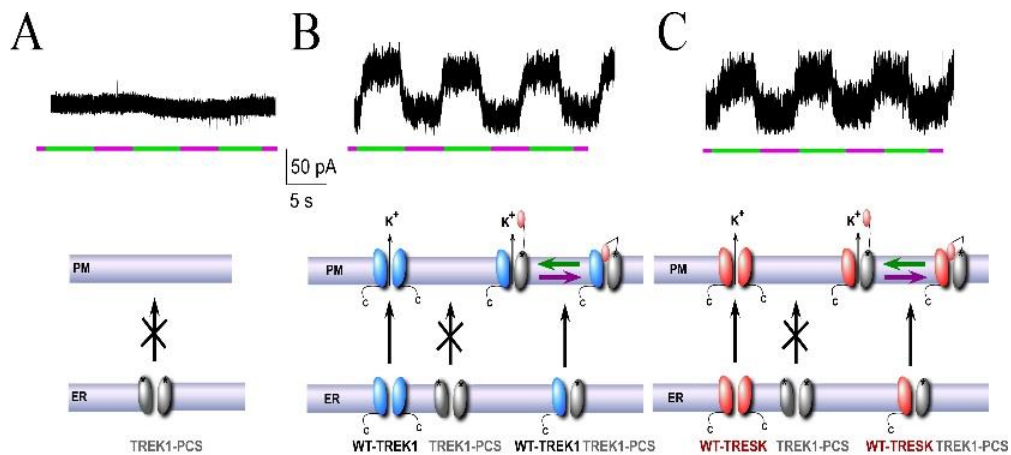


Figure 39: TREK1-PCS for functional heteromerization study. (A) Deletion of the TREK1 carboxy-terminal tail (TREK1-PCS, grey) results in retention of the homomeric mutant channel in the endoplasmic reticulum. Co-expression of TREK1-PCS with WT-TREK1 produces a heteromeric channel that traffics to the membrane and which can be light-gated because of MAQ attachment to the TREK1-PCS. (C) Same as (B) for TRESK.

Merely showing that 2 subunits are able to interact is not sufficient to validate the functionality of a dimer. Up to now, tandems based on using genetic fusion between

subunits to force the heteromerization was the only way to isolate and study the functionality of heteromeric channels. Nevertheless, the possibility to have multimerization between tandems cannot be excluded. Therefore the lab wanted to develop a new approach allowing to functionally validate the heteromer. To test the functionality of the TREK heterodimer, the lab developed a heterodimerization assay based on an engineered “Photoswitchable Conditional Subunit” (TREK1-PCS) of TREK1. The TREK1-PCS is a TREK1 subunit where the C-terminus has been deleted to produce endoplasmic reticulum retention, which can be rescued through co-assembly with a full-length subunit (Sandoz et al., 2012). Following co-assembly and surface targeting, TREK1-PCS can then optically control the channel *via* a tethered photoswitchable blocker (“MAQ”) which attaches to a genetically engineered cysteine. Therefore, gain of photosensitivity of an identified co-expressed TREK interacting subunit allows for the verification of a functional heteromer with TREK1. As expected, expression of TREK1-PCS alone did not generate a photoswitchable current (Figure 38 A) but co-expression with either TREK1 or TREK2 and TRAAK induced a robust photoswitchable current, indicating that the TREK2 and TRAAK subunit are able to co-assemble with TREK1-PCS. Consistent with SiMPull data, no photocurrent was observed when TASK1 or TASK3 were co-expressed with TREK1-PCS. But at the time, they have also tested the channel which share the smaller identity with TREK1, TRESK. Surprisingly, this “negative” control was found to be positive (see Figure 38 C). Co-expression of TRESK with TREK1-PCS induced a robust photoswitchable current which was calcium sensitive, a sensitivity provided by the TRESK moiety. This was the starting point of a long story and my first training in the Sandoz lab in 2013!

B. Article II: Migraine-associated TRESK mutations increase neuronal excitability through alternative translation initiation and inhibition of TREK

Migraine-associated TRESK mutations increase neuronal excitability through alternative translation initiation and inhibition of TREK

Authors:

Perrine Royal^{1,2}, Alba Andres-Bilbe³, Pablo Ávalos Prado^{1,2}, Clément Verkest^{2,4}, Brigitte Wdziekonski^{1,2}, Sébastien Schaub¹, Anne Baron^{2,3}, Florian Lesage^{2,4}, Xavier Gasull³, Joshua Levitz⁵, Guillaume Sandoz^{1,2*}

Affiliations:

¹Université Cote d'Azur, CNRS, INSERM, iBV, France.

²Laboratories of Excellence, Ion Channel Science and Therapeutics Nice, France.

³Neurophysiology Laboratory, Department of Biomedicine, Medical School, Institute of Neurosciences, Universitat de Barcelona, IDIBAPS, Barcelona, Spain.

⁴Université Cote d'Azur, CNRS, INSERM, Institut de Pharmacologie Moléculaire et Cellulaire, France

⁵Department of Biochemistry, Weill Cornell Medicine, New York, NY.

*Correspondence to: sandoz@unice.fr

In brief: Royal et al. demonstrate that migraine-associated frameshift mutations of TRESK, a two-pore-domain K⁺ channel, lead to the production of a second protein fragment, which carries the pathophysiological function by inhibiting TREK1 and 2, due to a mechanism called frameshift mutation-induced Alternative Translation Initiation (fsATI).

Abstract:

Mutations in ion channels contribute to neurological disorders, but determining the basis of their role in pathophysiology is often unclear. In humans, 2 mutations have been found to produce a dominant negative for TRESK, a two-pore-domain K⁺ channel implicated in migraine: TRESK-MT, a 2 bp frameshift mutation (F139WfsX24) and TRESK-C110R, a missense mutation. Despite the fact that both mutants strongly inhibit TRESK, only TRESK-MT leads to an increase in sensory neuron excitability and is associated with a migraine phenotype. Here, we identify a new mechanism, termed frameshift mutation induced Alternative Translation Initiation (fsATI) that explains why TRESK-MT but not TRESK-C110R is associated with migraine disorder. fsATI leads, from the same TRESK-MT mRNA, to two proteins: TRESK-MT1 and TRESK-MT2. We show that by co-assembling with and inhibiting TREK1 and TREK2, another subfamily of K_{2P} channels, TRESK-MT2 increases trigeminal sensory neuron excitability, a key component of migraine induction, leading to a migraine-like phenotype. This finding identifies TREK as a molecular target in migraine pathophysiology and resolves the contradictory lack of effect of TRESK-C110R which targets only TRESK and not TREK. Finally, taking into account the potential for fsATI allowed us to identify a new migraine-related TRESK mutant, Y121LfsX44, which also leads to the production of two TRESK fragments, indicating that this mechanism may be widespread. Together, our results suggest that genetic analysis of disease-related mutations should consider fsATI as a distinct class of mutations.

Key Words: K_{2P} channels, leak current, migraine, alternative translation initiation, frameshift mutation, neuronal excitability, sensory neuron, single molecule fluorescence, pain, KCNK

Introduction

Migraine is a common, disabling neurological disorder with a genetic, environmental and hormonal component with an annual prevalence estimated at ~15%. It is characterized by attacks of severe, usually unilateral and throbbing headache, and can be accompanied by nausea, vomiting and photophobia. Migraine is clinically divided into two main subtypes, migraine with aura (MA) when a migraine is preceded by transient neurological disturbances which are usually visual and migraine without aura (MO). Cortical spreading depression (CSD) underlies the aura, although its precise relationship to headache is unclear. Activation and sensitization of trigeminal neurons (TG) leading to the release of pro-inflammatory peptides is likely a key component in pain initiation and transmission in migraine (Nosedá and Burstein, 2013) (Yan and Dussor, 2014).

Recent evidence points to a pivotal contribution of a variety of two-pore domain potassium (K_{2P}) channels in chronic pain processing. The diverse K_{2P} channel family is made of 15 subtypes which form 6 subfamilies. The activity of these channels drives the membrane potential toward the K⁺ equilibrium potential and therefore reduces cellular excitability. Expression of several K_{2P} channel subunits has been detected in nociceptive dorsal root ganglion and trigeminal neurons (Alloui et al., 2006; Bautista et al., 2008; Blin et al., 2016; Morenilla-Palao et al., 2014; Noël et al., 2009; Yamamoto et al., 2009). One subtype of K_{2P} channels that is highly expressed in sensory neurons, TRESK, has been directly linked to MA via a causally linked 2 bp frameshift mutation (F139WfsX24) identified in the *KCNK18* gene which causes premature truncation of TRESK (“TRESK-MT”) (Lafrenière et al., 2010; Wood, 2010). This mutation segregated perfectly with the MA phenotype in a large pedigree and was shown to produce a non-functional protein that can serve as a dominant-negative that functionally downregulates the wild type (WT) TRESK channel (Lafrenière et al., 2010; Wood, 2010). TRESK-MT has been shown to induce hyper-excitability of TG neurons (Guo et al., 2014; Liu et al., 2013), which likely underscores its role in migraine. However, in subsequent genetic screening studies, another missense TRESK variant, C110R, was identified (Andres-Enguix et al., 2012). TRESK-C110R, similar to TRESK-MT, exerts a dominant negative effect on WT-TRESK in heterologous cells, but expression of this mutant was found to have no effect on TG excitability (Guo

et al., 2014). This absence of effect explains why this mutant was found in both migraine patients and control subjects (Guo et al., 2014). Therefore, despite the fact that both mutations lead to the same apparent effect on TRESK function, only TRESK-MT is able to increase TG excitability and is linked to migraine pathophysiology.

Classically a eukaryotic mRNA is thought to contain one translation start codon which allows the production of a single protein species. However, in some cases, eukaryotic ribosomes can recognize several alternative translation start sites to induce the formation of several different proteins from the same mRNA (Kochetov, 2008). This alternative translation initiation is a means of expanding the proteome (Kochetov, 2008) and has been shown to increase the functional diversity of K_{2P} channels (Thomas et al., 2008), raising the possibility that it plays a role in TRESK-mediated migraine pathophysiology.

In this study, we addressed why TRESK-MT (F139WfsX24), but not TRESK-C110R, is able to increase TG excitability and, potentially, play a role in migraines. Using single molecule fluorescence and chemical optogenetic methods, we found that TRESK is able to heterodimerize with 2 distantly-related K_{2P} channels from another subfamily, TREK1 and TREK2 and that TRESK-MT strongly inhibits TRESK, TREK1, and TREK2 currents. In stark contrast, we show that TRESK-C110R is only able to inhibit TRESK, but not TREK1 or TREK2. Furthermore, we show, using double KO mice for TREK1 and TREK2, that TRESK-MT increases TG neuronal excitability by inhibiting TREK1 and TREK2. Consistent with a role for TREK1 and TREK2 in migraine induction, we found that double KO mice for TREK1 and TREK2 present, at rest, a migraine-like allodynia phenotype. These results resolve the contradictory lack of effect of TRESK-C110R which targets only TRESK and not TREK1 or TREK2. Strikingly, we next find that the 2 bp frameshift mutation of TRESK-MT puts an alternative start codon in frame which leads to the translation of a second TRESK fragment, termed MT2, which specifically co-assembles with TREK1 and TREK2 to downregulate their function leading to the TG excitability increase. Consistent with a role for MT2 in migraine induction, we found that MT2 expression within the trigeminal ganglia induced a migraine-like allodynia phenotype in rat. Finally,

we find that other previously uncharacterized migraine-associated TRESK mutations also produce multiple fragments via alternative translation initiation (ATI) that can have distinct effects on TRESK and TREK channels. Together these findings identify frameshift induced-alternative translation initiation (fsATI) as a mechanism initiated by TRESK mutations which leads to two protein fragments with dominant negative effects on distinct channel targets to, ultimately, increase sensory neuron excitability which may contribute to migraine induction.

Results

TRESK heteromerizes with TREK1 and TREK2

Despite the fact that K_{2P} channels share a similar architecture and global function, they share a low level of sequence identity, even between members of the same subfamily. Surprisingly, this low level of identity does not preclude heteromerization, as we and others recently showed within the TREK subfamily (Blin et al., 2016; Hwang et al., 2014; Lengyel et al., 2016; Levitz et al., 2016). Based on this and the fact that TG neurons express many K_{2P} channels (TREK1, TREK2, TRAAK, TASK1 and TASK3) (Bautista et al., 2008; Yamamoto et al., 2009), we hypothesized that the difference between TRESK mutants is due to their differential ability to modify the function of other K_{2P} channels through heteromerization. To assess the ability of TRESK to heteromerize with other K_{2P} channels which are expressed in TG neurons, we used the single-molecule pull-down (“SiMPull”) assay (Jain et al., 2012) to visualize individual antibody-immobilized protein complexes on polyethylene glycol-passivated glass coverslips (Figure 1A). We co-expressed GFP-TRESK with either HA-TRESK, HA-TREK1, HA-TREK2, HA-TRAAK, HA-TASK1, or HA-TASK3 and assessed their ability to co-immunoprecipitate (Co-IP) GFP-TRESK *via* an anti-HA antibody. HA-TRESK, HA-TREK1, and HA-TREK2, were able to co-IP many fluorescent GFP-TRESK spots (Figure 1B, C), whereas no GFP-TRESK spots were observed for HA-TRAAK, HA-TASK1 or HA-TASK3 (Figure 1C), indicating that TRESK co-assembly with other K_{2P} channels is specific for TREK1 and TREK2. Importantly, controls showed that identical results were observed in two different non-ionic detergents (Figure 1C), that similar expression levels were seen for GFP-TRESK when co-expressed with HA-TREK1 or HA-TRESK (Figure S1A), that all HA-tagged K_{2P} constructs were able to pull down themselves (Figure S1B, C), that pulldown was dependent on the presence of the anti-HA antibody (Figure S1D) and confirm that TREK1, TREK2 and TRESK are coexpressed in the same cultured trigeminal (TG) neurons using immunofluorescence and single cell RT-PCR (Figure S1F).

We next used photobleaching step analysis (Ulbrich and Isacoff, 2007) to determine the stoichiometry of TREK1 and TRESK complexes to test the hypothesis that they form heterodimers. First we confirmed that HA-GFP-TREK1 form homodimers in our assay by observing ~70% 2-step

bleaching for each when expressed and immunoprecipitated alone with anti-HA antibodies (Figure S2A), consistent with the formation of strict dimers with a GFP maturation rate of ~80%. Then, we counted the number of GFP-TRESK subunits within a HA-TREK1/GFP-TRESK complex by observing bleaching steps of GFP-TRESK co-immunoprecipitated with immobilized HA-TREK1 (Figure S2C). The majority of fluorescence intensity trajectories showed one bleaching step (~70%) (Figure S2C). This distribution is similar to the one observed for HA-TREK1/GFP-TREK1 complexes (Figure S2B) and agrees well with a 1:1 stoichiometry showing that TREK1-TRESK is primarily a heterodimer.

To test the functionality of the TREK1-TRESK heterodimer, we developed a heterodimerization assay based on an engineered “Photoswitchable Conditional Subunit” (TREK1-PCS) of TREK1. The TREK1-PCS is a TREK1 subunit where the C-terminus has been deleted to produce endoplasmic reticulum retention, which can be rescued through co-assembly with a full-length subunit (Sandoz et al., 2012). Following co-assembly and surface targeting, TREK1-PCS can then optically control the channel via a tethered photoswitchable blocker (“MAQ”) which attaches to a genetically engineered cysteine. Therefore, gain of photosensitivity of an identified co-expressed TREK interacting subunit allows for the verification of a functional heteromer with TREK1. As expected, expression of TREK1-PCS alone did not generate a photoswitchable current (Figure 1D) but co-expression with either TREK1 or TRESK induced a robust photoswitchable current (Figure 1E, F), indicating that the TRESK subunit is able to co-assemble with TREK1-PCS. Consistent with SiMPull data, no photocurrent was observed when TASK1 (Figure 1G) or TASK3 (Figure S1E) were co-expressed with TREK1-PCS. Furthermore, the bleaching step distribution of GFP-TREK1-PCS spots co-immunoprecipitated with immobilized HA-TREK1 is similar to HA-TREK1/GFP-TREK1, the majority of fluorescence spots showed one bleaching step (~70%) (Figure S2D), supporting the conclusion that the light-gated TREK1-PCS/TRESK current is carried by a TREK1-PCS/TRESK heterodimer with a common pore.

Next, to test the functional properties of the TREK1-TRESK heteromer, we constructed a linked, tandem dimer to have a uniform representation at the surface of the cell of the TREK1-TRESK heteromer (Figure S3). This heteromeric channel displayed properties which are a mix of those from TREK1 and TRESK homodimers. Notably, TRESK is insensitive to arachidonic acid while TREK1 is

sensitive (Figure S3A, B, C) and TRESK-TREK1 tandems show an intermediate sensitivity to arachidonic acid (Figure S3C). Furthermore, similar to TRESK, but not TREK1, TRESK-TREK1 tandems showed sensitivity to intracellular calcium, as tested with ionomycin application (Figure S3D, F). Consistent with this, the light-gated TREK1-PCS/TRESK current is also calcium sensitive (Figure S3E, F), confirming that the light-gated TREK1-PCS/TRESK current is carried by a TRESK1-TRESK heteromer with a common pore.

Having found that TREK can physically and functionally heteromerize with TRESK and that all three channel subtypes are co-expressed in sensory neurons, we next investigated the ability of TRESK mutants to modify TREK1 and TREK2 currents.

TRESK-MT, but not TRESK-C110R, acts as a dominant negative on TREK1 and TREK2 channels

As previously shown (Andres-Enguix et al., 2012), both TRESK-MT and TRESK-C110R exert a dominant-negative effect on whole cell TRESK currents (Figure 2A-C). Since TREK1 can co-assemble with TRESK (Figure 1), we addressed the impact of the MT and C110R variants on TREK1 current. We found that TRESK-C110R co-expression did not modify TREK1 current whereas TRESK-MT co-expression induced a near-complete inhibition of TREK1 current (Figure 2D-F). Similar to TREK1, TRESK-MT, but not TRESK-C110R strongly inhibited, TREK2 current (Figure 2G-I). This dominant negative effect is specific and likely dependent on co-assembly since TASK1, TASK3 and TRAAK, which do not co-IP with TRESK (Figure 1), were not sensitive to TRESK-MT co-expression (Figure S4). To address why TRESK-C110R does not modify TREK1 or TREK2 current, we used the SiMPull assay to test the ability of TRESK-C110R to physically interact with TREK1. We co-expressed HA-TREK1 with either GFP-TRESK or GFP-TRESK-C110R and tested their ability to be co-immunoprecipitated (Co-IP) with HA-TREK1 *via* an anti-HA antibody. Whereas GFP-TRESK was able to be co-immunoprecipitated with HA-TREK1 leading to many fluorescent spots, very few spots were observed for GFP-TRESK-C110R (Figure S5A). This indicates that TREK1 can co-assemble with TRESK and that the C110R mutation leads to a drastic reduction of this association explaining why

TRESK-C110R have no effect on TREK1 current. Together these data show that TRESK-MT can inhibit TRESK, TREK1 and TREK2 whereas TRESK-C110R is only able to inhibit TRESK. Based on the fact that TRESK-MT but not TRESK-C110R is able to induce TG neuron hyperexcitability (Guo et al., 2014; Liu et al., 2013), we hypothesized that TRESK-MT induces sensory neuron hyper-excitability primarily by acting on TREK1 and TREK2, not TRESK.

TRESK-MT increases neuronal excitability through the inhibition of TREK1 and TREK2

To investigate the role of TREK1 and TREK2 in the induction of TG hyperexcitability by TRESK-MT, we tested if overexpression of GFP-TRESK-MT alters the passive and active electrophysiological properties of small-diameter (<25 μm) TG neurons from wild-type or TREK1/TREK2 double knockout (TREK1^{-/-}/TREK2^{-/-}) mice. As previously shown, TRESK-MT expression in WT TG neurons led to a decrease of the lamotrigine current (Figure S6) leading to an increase in excitability (Figure 3C) which included a decrease in the rheobase (74 ± 11 pA vs 47 ± 5 pA, $P < 0.05$ for TG neurons expressing GFP or TRESK-MT, respectively) and an increase in the number of action potentials (APs) evoked by suprathreshold current injections compared to control (Figure 3A, C). As shown in Figure 3B, neurons from TREK1^{-/-}/TREK2^{-/-} mice were more excitable than WT TG neurons. These neurons have a smaller lamotrigine current (Figure S6), smaller rheobase (55 ± 6 pA, $P < 0.05$) and a significant increase in the number of APs evoked by suprathreshold current injections compare to WT TG neurons. Consistent with a role for TREK1 and 2 in mediating the effects of TRESK-MT, TRESK-MT overexpression did not alter the excitability of TREK1^{-/-}/TREK2^{-/-} mice (Figure 3D). TREK1^{-/-}/TREK2^{-/-} TG neurons showed no increase in the number of evoked APs number nor a reduction in rheobase (55 ± 6 pA vs 53 ± 5 pA, for TG neuron expressing GFP or TRESK-MT respectively, $P > 0.5$). Together these data strongly support a major role for TREK1 and TREK2 in the control of TG neuron excitability and support the idea that TRESK-MT differs functionally from TRESK-C110R in its ability to target TREK1 and TREK2 to increase the excitability of TG neurons which is likely a crucial step in the induction of migraines.

TREK1^{-/-}/TREK2^{-/-} mice show a mechanical allodynia which is not increased by NO donors

Having found that expression of the TRESK-MT mutant increases TG excitability through TREK1-TREK2 inhibition, we hypothesized that TREK1^{-/-}/TREK2^{-/-} mice would show an increased susceptibility to a migraine-related phenotype. Migraine is associated with an increase of the sensitivity to all sensory modalities and cutaneous allodynia can be used as a quantifiable marker of migraine disorder (Bates et al., 2010; Pradhan et al., 2014; Verkest et al., 2018). One approach to model acute and chronic migraine is the quantification of this increase in response to known migraine triggers such as nitric oxide (NO) donors (Bates et al., 2010), including isosorbide dinitrate (ISDN) (Verkest et al., 2018). We quantified ISDN-evoked mechanical hyperalgesia in TREK1^{-/-}/TREK2^{-/-} and wild-type controls in acute and chronic conditions. In a first experiment, paw mechanical nociception thresholds were determined with a dynamic von Frey aesthesiometer before and during a 3-hour period after intraperitoneal injection of ISDN (10 mg/kg) (Figure 3E) (Bates et al., 2010; Verkest et al., 2018). In a second experiment, we assessed mechanical nociception thresholds in both TREK1^{-/-}/TREK2^{-/-} and wild-type controls, by intraperitoneally injecting ISDN every day for four days as a model of chronic migraine-associated pain (Figure 3E). We found that, at rest, TREK1^{-/-}/TREK2^{-/-} mice showed a decreased mechanical threshold compared to WT mice ($2.6 \pm 0.1\text{g}$ vs $3.9 \pm 0.1\text{g}$; $P < 0.001$). Notably, the basal mechanical threshold of TREK1^{-/-}/TREK2^{-/-} mice is similar to the threshold observed 1.5 hours after acute ISDN injection in WT mice (Figure 3F, $P = 0.831$). In the acute model experiment, during the first 1.5 hours following ISDN injection, the mechanical thresholds remained significantly lower in TREK1^{-/-}/TREK2^{-/-} mice than in wild-type controls (Figure 3F, $P < 0.001$ after 30 minutes and $P < 0.01$ after 1 hour with a linear mixed-effects model). In the chronic migraine-associated pain assay, the mechanical thresholds remained significantly lower for TREK1^{-/-}/TREK2^{-/-} mice compared to wild-type controls but the difference was strongly reduced (Δ mechanical threshold $0.33 \pm 0.2\text{g}$ vs $1.12 \pm 0.1\text{g}$) (Figure 3G).

Having found that ISDN did not change the mechanical threshold in both acute and chronic migraine-associated pain models in TREK1^{-/-}/TREK2^{-/-} mice, we wondered if a treatment used in prophylaxis in migraine patient, topiramate, could reverse this observed migraine-like phenotype as was observed for both models of NO donor-induced migraine (Pradhan et al., 2014). We assessed the

mechanical nociception threshold in TREK1^{-/-}/TREK2^{-/-} mice before and 2 hours following the intraperitoneal injection of 30 mg/kg of topiramate. Treatment with topiramate reversed the chronic basal hyperalgesia seen in TREK1^{-/-}/TREK2^{-/-} mice (1.2 ± 0.2 g; Figure 3H), as was previously observed for a nitroglycerin-evoked form of hyperalgesia (Pradhan et al., 2014). As a control, we tested non-treated ISDN WT mice and did not observe any significant shift of the mechanical threshold following topiramate treatment (Figure 3H).

These data demonstrate that at rest the TREK1^{-/-}/TREK2^{-/-} mice present a hyperalgesia phenotype which is similar to the phenotype observed in ISDN-treated animals. This is consistent with a role of TREK1/TREK2 in sensory neuron hypersensitivity that is relevant to migraine and this phenotype is partially reversed by topiramate, a drug used in the clinic to treat chronic migraine.

TRESK-MT mutation induces the translation of a second protein, MT2

We next explored how TRESK-MT exerts its effects on TREK channels at the molecular level. The F139WfsX24 frameshift mutation of TRESK-MT results in the premature truncation of the human TRESK protein from 384 amino acids (aa) to 162 aa. The truncated TRESK includes the first 138 aa of wild-type TRESK followed by a 24 aa aberrant sequence. The corresponding mutation has very similar effects on the mouse TRESK gene, generating a truncated protein with the first 149 aa of wild-type TRESK and followed by a 50 aa aberrant sequence at the C terminus (Figure 4B). We fused a GFP tag to the N-terminus of the mouse TRESK-MT and tested its ability to be immobilized by HA-TRESK, HA-TREK1 or HA-TREK2 in the SiMPull assay. Surprisingly, only HA-TRESK was able to co-IP GFP-TRESK-MT via an anti-HA antibody (Figure 4A). This result confirms that TRESK-MT associates with TRESK to induce its dominant negative effect but raises the question of how TRESK-MT is able to inhibit TREK1 and TREK2 without direct association.

It has been hypothesized that alternative translation initiation (ATI) of eukaryotic mRNAs, including those that encode K_{2P} channels (Thomas et al., 2008), may provide a method to expand the proteome (Kochetov, 2008). A close examination of the nucleotide sequence of TRESK-MT revealed that the F139WfsX24 frameshift mutation places two new ATG codons in frame with the reference open reading frame of TRESK (ATGs at position +356 and +407 for the human TRESK cDNA and

+389 and +490 for the mouse cDNA). We hypothesized that one of these codons may serve as an ATI site that can lead to the formation of a second truncated TRESK protein, termed “MT2”, that would include a short (either 2 or 19 aa) N-terminal aberrant sequence followed by the C-terminal part of TM2, including the 2-3 intracellular loop, TM3, P2 loop, TM4 and the C terminal domains (Figure 4B). To test whether MT2 is co-translated with MT1, we introduced an N-terminal mCherry-tag in frame with MT1 and a C-terminal GFP in frame with MT2 within the mouse TRESK-MT cDNA (“mCherry-TRESK-MT-GFP”). Expression of this construct led to HEK 293T cells with both mCherry and GFP fluorescence, showing the co-translation of mCherry-MT1 and MT2-GFP (Figure 4C). This co-translation was observed in other cell lines including MDCK cells (Figure 4C), as well as in primary TG neurons (Figure 4C). Next, we introduced an N-terminal hemagglutinin (HA) tag in frame with MT1 and another one in frame with MT2 within the mouse TRESK-MT cDNA (“HA-TRESK-MT-HA”). Lysate from cells transfected with HA-TRESK-MT-HA was probed in a western blot with anti-HA antibodies and 2 bands, with a similar intensity, corresponding to the expected molecular weights for MT1 (~23 kDa) and MT2 (~29 kDa) were detected (Figure 4D). Together these data clearly show that TRESK-MT leads to the production of two distinct fragments of TRESK.

To probe the function of MT2, we introduced a stop codon into the MT2 ORF of TRESK-MT at the beginning of the 2-3 loop (Figure 4B) inducing the loss of expression of MT2 (Figure S7A). As shown in Figure 5, whereas the introduction of the stop codon in the MT2 ORF did not change the ability of TRESK-MT to inhibit TRESK current (Figure 5B), this stop codon abolished the ability of TRESK-MT to produce a dominant negative functional effect on TREK1 (Figure 5A). We next confirmed the importance of this second ORF by mutating, in TRESK-MT, the putative ATI start codons one by one. Mutation of the first ATG abolished the ability of TRESK-MT to inhibit TREK1 (Figure 5C), but not TRESK (Figure 5D) whereas mutation of the second ATG did not alter the ability of TRESK-MT to inhibit TREK1 current (Figure 5C and Figure S7B). This data indicates that the ATI site is the first internal ATG. As a control, we mutated a third ATG, which is also present in the WT-TRESK sequence, and found that it did not change the ability of TRESK-MT to inhibit both TRESK and TREK1 currents (Figure 5C and Figure S7C). Similar to TREK1, introduction of a stop codon into the MT2 ORF or mutation of the first ATG also abolished the inhibition of TREK2 by TRESK-MT

(Figure 5E, F). To further demonstrate that the first ATG serves as a start codon, we mutated the potential Kozak sequence **GCTATGG** to **CCTATGC** and found that alteration of the Kozak sequence strongly reduced the inhibitory effect of TRESK-MT on TREK1 current (Figure 5C and Figure S7D) without affecting the effect on TRESK (Figure 5D and Figure S7E).

MT2, but not MT1, by acting as a dominant negative on TREK1 and TREK2 channels, increases neuronal excitability of WT small TG neurons leading to facial allodynia

To independently express MT1 and MT2 for functional characterization, we sub-cloned both ORFs into separate mammalian expression vectors. Co-expression of MT2 with TRESK did not modify TRESK current (Figure 6B, E), while MT1 co-expression induced a ~3-fold decrease of the current which was similar to what was observed for the co-expression of the full TRESK-MT construct (Figure 6A, E). On the contrary, co-expression of MT1 did not modify TREK1 current (Figure 6C, E) but co-expression of MT2 induced a ~4-fold decrease of the current, similar to what was observed with co-expression of the full TRESK-MT construct (Figure 6D, E). Similar results were obtained for TREK2 (Figure 6E, Figure S8). Consistent with the functional data, we found that GFP-MT2 is co-immunoprecipitated with HA-TREK1 or HA-TREK2 in the SiMPull assay (Figure 6F).

To validate the physiological role of interaction between TREK1, TREK2 and MT2, we tested the functional effect of MT2 in TG neurons. Whereas MT1 expression did not alter the excitability of WT TG neurons (Figure 7A, B), MT2 increased it significantly (Figure 7A, C). In fact, MT1 did not modify the rheobase (74 ± 11 pA vs 79 ± 5 pA, $P > 0.5$ for TG neurons expressing GFP or MT1, respectively) and did not modify the number of action potentials (APs) evoked by suprathreshold current injections compared to control. Conversely, MT2 expression in WT TG neurons led to an increase in excitability (Figure 7) which included a decrease in the rheobase (74 ± 11 pA vs 55 ± 5 pA, $P < 0.05$ for TG neurons expressing GFP or MT2, respectively, $P < 0.05$) and an increase in the number of action potentials (APs) evoked by suprathreshold current injections compared to control (Figure 7A, C). We confirmed that this effect is linked to TREK1 and TREK2 since MT2 overexpression failed to increase the excitability of TREK1^{-/-}/TREK2^{-/-} TG neurons (Figure 7D).

Having found that MT2, by inhibiting TREK1 and TREK2, is sufficient to increase TG excitability we asked if MT2 expression in TG ganglia would induce a migraine-related phenotype. We conducted behavioral experiments in rats in which MT2 was virally overexpressed within the trigeminal ganglia. Rats allow to test the mechanical pain threshold on the face which is directly linked to TG excitability, constituting a relatively direct, reliable and quantifiable marker of migraine disorder in clinical contexts as well as in NO-induced migraine (Pradhan et al., 2014; Kopruszinski et al., 2017; Harris et al., 2017). As shown in Figure 7F, MT2 expression in TG ganglia (Figure S9) significantly increased the facial mechanical threshold (3.3 ± 0.4 g vs 7.7 ± 0.4 g, $P < 0.001$). Furthermore, as was seen for the TREK1^{-/-}/TREK2^{-/-} mice, the basal mechanical facial threshold of MT2-expressing rats is similar to the threshold observed 1.5, 2 and 3 hours after acute ISDN injection in WT rats. Having found that MT2 overexpression induced allodynia, we quantified ISDN-evoked mechanical hyperalgesia and found that MT2 overexpression prevents the effect of ISDN, similarly to what was observed for TREK1^{-/-}/TREK2^{-/-} mice.

Together these data demonstrate that at rest MT2 leads to an increase in TG excitability and a chronic cutaneous allodynia similar to the one observed following NO-donor injection and in TREK1^{-/-}/TREK2^{-/-} double KO mice.

MT2-producing alternative translation initiation is found in other migraine-associated TRESK mutants

Having found that MT2 is responsible for the migraine-associated increase in TG excitability and induction of a migraine-like phenotype through the inhibition of TREK1 and TREK2, we anticipated that other frameshift mutations may exist which place the ATG at position +356 in-frame with the reference open reading frame of TRESK. Such mutations would lead to the formation of MT2. This mutation could be either a 2 bp deletion or 1 bp insertion in the region between the ATG at position +356 and the TGA at position +427 (Figure S10). We used the Exome Aggregation Consortium (ExAC) database (Lek et al., 2016) and found one variant (Y121LfsX44) with a T duplication (+1 pb, c.361dupT) that places the ATI site in frame with the TRESK ORF (Figure S9). We introduced this insertion into the mCherry-TRESK-GFP (mCherry-TRESK-c.361dupT-GFP) sequence and found,

similar to mCherry-TRESK-MT-GFP (Figure 4C), that this construct led to HEK 293T cells with both mCherry and GFP fluorescence (Figure 8A) due to the co-translation of both MT1 and MT2 proteins. Similar to TRESK-MT, this mutant is able to inhibit both TRESK, TREK1 and TREK2 (Figure 8). As was seen for TRESK-MT (Figure 5), introduction of a stop codon into the MT2 ORF (TRESK c.361dupT_{STOP}) of this mutant abolished its ability to inhibit TREK1 and TREK2 (Figure 8), but not TRESK. Since this Y121LfsX44 mutation leads to the same molecular effects as TRESK-MT on TREK function, we hypothesized that it may be associated with a migraine phenotype. To address this, we looked in the ClinVar database (Landrum et al., 2016) and found that this mutant has been correlated with a migraine phenotype (RCV000490385.1).

Discussion

While initial findings of migraine-associated mutations of TRESK represented a major breakthrough (Lafrenière et al., 2010), a direct relationship between TRESK channel disruption and migraine has been challenged based on the discovery of a TRESK mutation (C110R) which produces a dominant negative form of TRESK but is found in a control cohort population (Andres-Enguix et al., 2012). The presence of this mutation in control individuals indicates that a single non-functional TRESK variant alone may not be sufficient to cause migraines, consistent with the genetic complexity of this disorder. In this study, we have addressed this controversy and found that the migraine-associated mutation of TRESK exerts its effects on sensory neurons by associating and serving as a dominant negative not only for TRESK, but also for TREK1 and TREK2 channels. In stark contrast, TRESK-C110R is not able to regulate TREK channels. Consistent with a function of TREK1 and TREK2 in TRESK-MT-induced migraine, the $TREK1^{-/-}/TREK2^{-/-}$ mice show a migraine-like hypersensitivity to mechanical stimuli. Surprisingly, we find that migraine-associated frameshift mutations of TRESK induce alternative translation initiation which allows the formation of a second product, MT2, which mediates the dominant negative action on TREK1 and TREK2. This dominant negative action on TREK1 and TREK2, ultimately, leads to an increase in TG neuron excitability and a migraine-like hypersensitivity to facial mechanical stimuli. Supporting this phenomenon as a general mechanism, we found another migraine-associated frameshift mutation in TRESK that produces a similar ORF shift which also leads to the formation of MT2. Together these findings support a role of frameshift induced alternative translation initiation (fsATI) and for TREK potassium channels as a key part of sensory neuron excitability and the underlying cellular mechanism of migraine.

We and others (Blin et al., 2016; Hwang et al., 2014; Lengyel et al., 2016; Levitz et al., 2016) have recently shown that K_{2P} channels are able to form both homodimeric and heterodimeric potassium channels. In this study, we show that TREK and TRESK readily assemble as heteromers. We show that this TRESK-TREK heteromer is a functional dimer since one TRESK is able to co-assemble with one TREK subunit to form a heterodimeric channel with a common pore using a photoswitchable conditional TREK1 (Sandoz et al., 2012). This is quite surprising given that TREK1/2 and TRESK are in different K_{2P} channel subfamilies and only show low sequence identity of ~19.7% (Sano et al., 2003).

We previously found that all members of the TREK channel subfamily (TREK1, TREK2, and TRAAK) can co-assemble but that TREK was unable to interact with TASK channels. Similar to the other reported heteromers, TREK1-TRESK heterodimers show unique biophysical behavior that blends the properties of the parent subunits. Notably, TREK1-TRESK is both arachidonic acid- and calcium-sensitive. In this study, we also show that TRESK does not heteromerize with three other K_{2P} channels, one from the TREK subfamily, TRAAK, and two from the TASK subfamily TASK1 and TASK3. Together this indicates that not all pairs of K_{2P} channel subunits are able to interact and that there are indeed rules of interaction that remain to be deciphered. Future work will be needed to determine the molecular mechanisms and structural interfaces that mediate specific K_{2P} heteromer assembly and the associated functional consequences of heteromerization.

TRESK channels are expressed in the dorsal root ganglion (DRG) and show their highest expression levels in trigeminal ganglion (TG). In DRG and TG, TRESK is most abundant in the small and medium-size sensory neurons (Dobler et al., 2007) (Lafrenière et al., 2010). In TG neurons, introduction of TRESK-MT has been shown to reduce the lamotrigine-sensitive K^+ current leading to an increase in excitability (Guo et al., 2014; Liu et al., 2013). This increase of TG excitability cannot be explained by TRESK inhibition since TRESK-C110R, which also strongly inhibits wild-type TRESK, does not inhibit the lamotrigine-sensitive K^+ current and does not increase TG excitability, explaining its lack of involvement in migraine (Guo et al., 2014). TREK1 and TREK2 are also expressed in DRG and show high expression levels in TG (Blin et al., 2016; Yamamoto et al., 2009). Furthermore, TREK1 and TREK2 have recently been shown to also be lamotrigine-sensitive (Walsh et al., 2016 and Figure S6A, B). We found that TRESK-MT inhibits TREK1 and TREK2 to increase TG excitability, showing that TREK1 and TREK2 control TG neuron excitability. To address the impact of this sensory neuron excitability increase, linked to TREK1 and TREK2 inhibition, we tested TREK1^{-/-}/TREK2^{-/-} mice for their susceptibility to a migraine-like phenotype. Migraine is associated with increased sensitivity to all sensory modalities and it appears that cutaneous allodynia can be used as a quantifiable marker of migraine disorder (Bates et al., 2010). Increase of basal mechanical hyperalgesia induced by TREK1 and TREK2 invalidation, to a similar level compared to WT animals after ISDN injection, is in agreement with a KO-induced increase of sensory neuron excitability that is relevant to migraine

(Brennan et al., 2013). Furthermore, trigeminal expression of MT2 in rats also induced a chronic facial allodynia which is directly linked to TG excitability and therefore relevant to migraine (Pradhan et al., 2014) (Kopruszinski et al., 2017) (Harris et al., 2017). Topiramate was previously shown to inhibit NO donor-induced acute or basal chronic hyperalgesia (Pradhan et al., 2014). We found that topiramate was able to partially reverse TREK1-TREK2 invalidation-induced hyperalgesia which is consistent with its action as a prophylactic migraine therapy (Pradhan et al., 2014). Therefore, the dysfunction of TREK1 and TREK2, and not TRESK alone, contributes to the increase of TG excitability which may lead to the altered pain processing associated with migraines. Together these results suggest that TREK1, TREK2 and TREK-TRESK heterodimers should be considered as new targets for migraine treatment.

An important remaining question is: how does TREK1 and TREK2 dysfunction lead to migraine phenotypes? Importantly, the TRESK-MT mutant has been found in migraine with aura phenotype (Lafrenière et al., 2010). Aura has been linked to cortical spreading depression (CSD) which precedes the activation of TG neurons (Noseda and Burstein, 2013). TREK1 and TREK2 channel activity, by reducing TG excitability, may serve as a brake to prevent the pathological activation of TG neurons during the early stages of CSD. In patients expressing TRESK-MT this mechanism may be reduced or eliminated, enhancing the activation of TG neurons, thus leading to migraines. Fitting the model in which an increase in TG excitability is the primary underlying cause of headaches, the TRESK-MT proband described in the original Lafrenière paper (Lafrenière et al., 2010; OMIM #613656) also showed migraine headaches in isolation without a preceding aura.

Most importantly, this study led us to uncover an undescribed mechanism involving alternative translation initiation. We provide evidence that the 2 bp deletion observed for TRESK-MT introduces an in-frame start codon with the reference open reading frame of TRESK, allowing the formation of MT2, the TRESK fragment responsible for the increase in TG excitability. Translation initiation of most eukaryotic mRNAs follows a linear scanning mechanism where the 40S ribosome is recruited to the 5' cap structure of the mRNA followed by downstream movement until an initiation codon is encountered (Kozak, 1999). In these cases, the translation initiation site is the first cap-proximal start codon for methionine (AUG). In most eukaryotic mRNA this first AUG is embedded into the Kozak consensus sequence [A/G]-XX-ATGG (Kozak, 1984a, b) (Jackson et al., 2010). However, if the first AUG is used

inefficiently, some ribosomes read through the site without recognition; this leaky scanning can result in translation initiation at a downstream position (Thomas et al., 2008). This has been observed for TREK1, where the second strong ATI site allows the physiological formation of a TREK1 channel with a shorter N-terminus which leads to altered TREK1 ion selectivity (Thomas et al., 2008). Similar to what was seen with TREK1, the TRESK ATG at position +356 is embedded into the Kozak consensus sequence (GCTATGG), which may explain why this ATG can serve as an ATI. To further determine why the ATG at position +356 is able to serve as an ATI, we submitted the TRESK-MT sequence to TIS Miner and the ATGpr algorithms (Nishikawa et al., 2000) and both algorithms predicted that the ATG at position +356 is a strong start codon and it is the second possible start codon after ATG at position +1. Furthermore, we found that Kozak sequence mutation significantly reduced the TRESK-MT effect on TREK1 current. This indicates that leaky scanning may explain the generation of TRESK-MT2.

At the physiological level, ATI is thought to increase protein functional diversity as is also the case with RNA splicing. For example, it was recently shown in Osteogenesis Imperfecta (OI) disease, that a causative missense mutation of c.-14C>T of the cDNA encoding IFITM5 creates an upstream ATG (ACG at position -15 was mutated to give ATG) in the 5' UTR in frame with IFITM5 which can serve as an ATI site, resulting in addition of an N-terminal 15 AA sequence (Lazarus et al., 2014). Here, we find that an ATG embedded by a strong Kozak sequence, downstream of the ATG at position +1, can be put in frame by a frameshift mutation to induce the translation of a second truncated protein. In the present work, this second product was found to target TREK1 and TREK2 to increase TG neuron excitability and to produce mechanical allodynia, linking this mutant to migraine. This represents the first example where a frameshift mutation downstream of an ATG start codon at position +1 creates a new ORF allowing the production of a second product which is at the origin of a physiological disturbance. To see if this “frameshift mutation-induced Alternative Translation Initiation” (fsATI) is a general phenomenon in TRESK, we predicted that any mutations before the stop codon TGA at position +427 that put the ATG at position +356 in frame would induce the formation of an MT2 that would lead to disease. Indeed, we demonstrate that another frameshift mutation, c.361dupT (Y121LfsX44), also leads to the formation of MT2 and is correlated to migraine (Clinvar, RCV000490385.1). It's not

possible to make any causal statements from this observation, but it is worth noting that this is the only other TRESK mutation which has been linked to a migraine phenotype. Together, this work shows that different frameshift mutations downstream of the first start codon can lead to ATI to produce a second protein which can carry the physiological function, suggesting that this mechanism may be widespread in nature and therefore needs to be considered when analyzing frameshift mutations linked to human disorders.

Materials and Methods

Molecular Biology, Cell Culture and Gene Expression

Channel DNA was used in the pIRES2eGFP, pcDNA3.1 and pCMV-HA vectors. HEK293T cells were maintained in DMEM with 5% FBS on poly-L-lysine-coated glass coverslips in 12 well plates. Cells were transiently co-transfected using Lipofectamine 2000 (Invitrogen) with a total of 1-1.6 µg of DNA total per 35 mm dish. When two genes were co expressed, a ratio of 1:1 DNA was used.

Primary cultures of mouse TG neurons

All mouse experiments were conducted according to national and international guidelines and have been approved by the local ethical committee (CIEPAL NCE). The C57BL/6J breeders were maintained on a 12 h light/dark cycle with constant temperature (23–24°C), humidity (45–50%), and food and water ad libitum at the animal facility of Valrose. TG tissues were collected from postnatal day 8 mice of either sex and treated with 2 mg/ml collagenase type II (Worthington) for ~2 hours, followed by 2.5 mg/ml trypsin for 15 min. Neurons were dissociated by triturating with fire-polished glass pipettes and seeded on polylysine/laminin coated coverslips. The DMEM-based culture medium contained 10% fetal bovine serum and 2mM GlutaMAX (Invitrogen). Neurons were transfected at 1 d *in vitro* (DIV) using Lipofectamine 2000 (Invitrogen). Transfected neurons were identified by the green fluorescence and patch clamp recordings were performed between DIV 3 and 5.

Knock-out mice

Mice lacking TREK1 and TREK2 were generated as described (Guyon et al., 2009). Null mutations were backcrossed against the C57BL/6J inbred strain for 10+ generations prior to establishing the breeding cages to generate subjects for this study. Age- and sex-matched C57BL/6J WT mice, aged 9-12 weeks, were obtained from Charles River Laboratories (Wilmington, MA).

Vector preparation

Adenovirus vector (DJ) encoding an IRES2EGFP or MT2-IRES2EGFP were used. Following linearization, this vector was recombined with the mouse version of the MT2 protein. The recombinant was amplified with PCR, and DNA sequencing was performed to verify the DNA sequence. Viral vectors were packaged and harvested by transfection of HEK 293T cells, followed by quantification of the viral titer through quantitative PCR. In addition, as a control, an adenovirus vector containing only the IRES2EGFP sequence was used.

Behavioral experiments

Animals

Experiments were performed on male Sprague Dawley rats (Janvier Labs) weighing 250 to 400 g (mean weight: 337 ± 16 g, 6 to 9 weeks old), and on male knock-out mice for TREK1 and TREK2 (weighting 20-25 g 7- to 13-weeks-old). Animals were housed in a 12 hour light-dark cycle with food and water available ad libitum. Animal procedures were approved by the Institutional Local Ethical Committee and authorized by the French Ministry of Research and the Spanish Ministry of Research according to the European Union regulations and the Directive 2010/63/EU (Agreements C061525 and 01550.03). Animals were sacrificed at experimental end points by CO₂ euthanasia.

Drug administration and virus injection

For the topiramate experiment, mice were injected intraperitoneally with topiramate once at a dose of 30 mg/kg and mechanical nociception thresholds were assessed every 30 minutes for two hours after the injection.

The procedures of virus trigeminal injections are described by Long *et al.* (Long et al., 2017). Briefly, following general anesthesia with a cocktail of ketamine and xylazine (100 mg/kg and 10 mg/kg respectively in i.p), rats were shaved on the right side, which is the injected side, and placed on a warmed surgical plate. The site of injection was determined using a notch between the condylar process and the ipsilateral angular process. The depth of injection was 9 mm. Antibiotics were used 5 days following injections. Viral vector suspension (10 μ L, 10^{11} transduction unit) containing 6 μ g/mL of Polybrene was injected slowly over 1 min. Rats in the experimental group (n=14) received 10 μ L of viral vector

containing the MT2 protein sequence, while those in the control group (n=14) received the same amount of EGFP viral vector. Epifluorescence imaging and qPCR were performed to verify successful transduction of trigeminal ganglia by viral vector.

Mechanical sensitivity measurements

The face mechanical sensitivity was measured using calibrated von Frey filaments (Bioseb, France). Unrestrained rats placed in individual plastic boxes on top of a wire surface were trained over one week to stimulation on the periorbital area, following a progressive protocol, starting with non-noxious filaments during the first 3 days of training. The face withdrawal force threshold (g) was determined by the filament evoking at least three responses over five trials, starting with lower force filaments. Basal values were determined 2 days before experiments.

The hindpaw mechanical sensitivity was evaluated with a dynamic plantar aesthesiometer (Ugo Basile, Italy). Unrestrained mice were placed in 10 individual plastic boxes on top of a wire surface. The mouse hindpaw was submitted to a force ramp up to 7.5 g during 10 s, the paw withdrawal force threshold (g) was assessed in three consecutive trials with at least 3–5 min between the trials and averaged to select animals. Basal values were determined 2 days before experiments.

Migraine rodent models

The rodent model of NO-induced migraine was induced by intraperitoneal (i.p.) injection of ISDN (Risordan®, Sanofi) at 10mg/kg, a long-lasting NO donor. The vehicle control used in these experiments was 0.9% saline. The acute mechanical allodynia induced by a single ISDN injection was followed on the hindpaw for mice and on the face for rats before (basal value) and for 3 hours after injection, every 30 minutes. Chronic mechanical allodynia was induced by a single daily injection of ISDN during 4 days. The hindpaw extra-cephalic mechanical sensitivity was measured each day before the ISDN i.p. injection for mice. Topiramate was tested on chronic mechanical allodynia on the 5th day and effects were followed every 30 min during 2 hours after injection in mice.

Electrophysiology

HEK 293T cell electrophysiology was performed 24-72 h after Lipofectamine transfection in solution containing (in mM): 145 mM NaCl, 4 mM KCl, 1 mM MgCl₂, 2 mM CaCl₂ and 10 mM HEPES. For co-expression of K2P channels and mutant channels, a DNA ratio of 1:1 was used. Glass pipettes of resistance between 3 and 6 MΩ were filled with intracellular solution containing (in mM): 140 KCl, 10 Hepes, 5 EGTA, 3 MgCl₂, pH 7.4. Cells were patch clamped using an Axopatch 200A (Molecular Devices) amplifier in the whole cell mode. Currents were elicited by voltage-ramps (from -100 to 100 mV, 1 s in duration) and the current density was calculated at 0 mV.

Oocyte two-electrode voltage clamp electrophysiology was performed in a 0.3-mL perfusion chamber; a single oocyte was impaled with two standard microelectrodes (1–2.5 MΩ resistance) filled with 3 M KCl, and maintained under voltage clamp using a Dagan TEV 200 amplifier in standard ND96 solution [96 mM NaCl, 2 mM KCl, 1.8 mM CaCl₂, 2 mM MgCl₂, 5 mM Hepes pH 7.4 with NaOH]. For the high K solution contained 80 mM K⁺, 78 mM NaCl was replaced by KCl. Stimulation of the preparation, data acquisition, and analysis were performed using pClamp software (Molecular Devices).

Neuronal excitability was studied in small-diameter TG neurons transfected with 1 μg of the pIRES2EGFP vector containing the X insert in which there is no N-terminal tag on the insert and EGFP is co-translated as a transfection marker or the pIRES2EGFP control plasmid with Lipofectamine 2000. Extracellular solution contained (in mM): 135 NaCl, 5 KCl, 2 CaCl₂, 1 MgCl₂, 5 HEPES, 10 glucose, pH 7.4 with NaOH, 310 mOsm. The pipette solution contained the following (in mM): 140 K-gluconate, 10 NaCl, 2 MgCl₂, 5 EGTA, 10 HEPES, 2 ATP-Mg, 0.3 GTP-Na, 1 CaCl₂ pH 7.3 with KOH, 290 mOsm. Recording pipettes had < 4.5 MΩ resistance. Series resistance (<20 MΩ) was not compensated. Signals were filtered at 10 kHz and digitized at 20 kHz. After establishing whole-cell access, membrane capacitance was determined with amplifier circuitry. The amplifier was then switched to current-clamp mode to measure resting membrane potential (V_{rest}). Neurons were excluded from analysis if the V_{rest} was higher than -40 mV or if the input resistance was smaller than 200 MΩ. To test neuronal excitability, neurons were held at V_{rest} and injected with 1 s depolarizing currents in 25 pA incremental steps until at least 1 action potential (AP) was elicited.

Trigeminal neurons RNA extraction and reverse transcription

Total RNA was isolated from trigeminal neurons in suspension using a Nucleospin RNA Plus XS kit (from MACHEREY-NAGEL GmbH & Co. KG) according to the manufacturer's protocols and 1 µg of RNA was reverse transcribed (with 10 nM random hexamers for 5 min at 65°C, then with 10 mM DTT, 0.5 mM each dNTP, 100 U SuperScript II (Invitrogen) 42°C for 50 min). Subsequently, the cDNA was quantified by qPCR with PowerUp SYBR Green Master Mix (Thermo Fisher).

Single cell reverse transcription

The procedures of single cell RT-PCR are adapted from Johansen *et al.* (Johansen *et al.*, 1995). The content of each cell was aspirated into the patch pipette by applying negative pressure. The flow of the cytosol in the pipette as well as the aspiration of the nucleus was controlled under the microscope. Only cell samples which included the nucleus were investigated in the present study.

The pipette was then released from the holder and mounted on a syringe to expel its content into a test tube. To the ~6.5 µL of the pipette-content expelled into the test tube was added 3.5 µL of a solution containing random hexamers (Invitrogen, 5 µM final concentration), dithiothreitol (DTT, final concentration 10 mM), the four deoxyribonucleotide triphosphates (dNTP, Thermo Fisher, final 0.5 mM each), 20 U ribonuclease inhibitor (Promega), and 100 U Moloney murine leukemia virus reverse transcriptase (Invitrogen).

The total 10 µL reaction was incubated for 1h at 35°C for synthesis of single stranded cDNA, and then kept on ice until PCR.

PCR amplification and quantification

Semi-quantitative PCR were performed to determine the relative levels of TREK1, TREK2, and TRESK after RNA extraction and reverse transcription using primers described below. qPCR (10 µL) was performed using the aforementioned reverse-transcribed cDNA (4 µL) and the primers for TREK1 (forward: catcttcatctgtttgctg, reverse : atcatgctcagaacagctgc, 240 pb), TREK2 (forward : aacagtgttgccatcttcg, reverse: ccagcaagaagaaggcact, 276 pb), TRESK (forward : ctgcttctttgctgctg, reverse : aagaagagagcgtcaggaa, 256 pb) and GAPDH (forward : cctggagaaacctgccaagtatga, reverse :

tgctgtgaagtcgcaggaga) as a reference. After initial denaturation at 95°C for 15 seconds, 40 cycles of amplification (95°C for 15 seconds and 60°C for 1 minute) were performed.

Quantitative PCR were performed to determine the levels of GFP after inoculation of adenovirus vectors containing GFP MT2 sequences into trigeminal ganglia using the same protocol with specific primers for the GFP (forward : aagctgaccctgaagttcatctgc, reverse : cttgtagttgccgtcgtccttgaa).

Analysis were made using the GAPDH as the housekeeping gene along with the $2^{-\Delta\Delta Ct}$ Calculation Method.

Western blot analysis

24 to 48 hours after transfection using 1µg DNA with Lipofectamine 2000, HEK 293T cells were homogenized in PBS containing saponin (0.5% w/v), Triton X-100 (0.5% w/v) and protease inhibitors (Roche Diagnostics, Basel, Switzerland). Lysates were clarified by centrifugation at 20 000 g for 30 min. Proteins were separated on 10% SDS polyacrylamide gel and blotted onto nitrocellulose membrane (Hybond-C extra, Amersham Biosciences, Freiburg, Germany). Detection was carried out using mouse monoclonal antibody clone HA-7 against the HA epitope (Sigma).

Immunocytochemistry

Transfected neurons on coverslips were fixed with PBS containing 4% paraformaldehyde for 15 minutes at room temperature (RT), then permeabilized with PBS and 0,1% Triton X-100 (PBST) and blocked for 1h with 5% horse serum (HS) in PBST. Primary and secondary antibodies were diluted in PBST and 5% HS and incubated for 1h at RT. Three 5-min washes with PBST were carried out between each incubation step and at the end of the procedure. Coverslips were mounted in Dako Fluorescent Mounting medium (Dako Corporation, Carpinteria, CA, USA). The following antibodies were used: rabbit anti-TREK1 and TREK2 (Blin et al., 2016), anti-TRESK (ab96868, abcam) conjugated with Cy3 (ab146452, abcam), Cy5 (ab146454, abcam) and Atto 488 (Sigma) respectively. Microscopy analysis and data acquisition were carried out with an Axioplan 2 Imaging Microscope (Zeiss®).

Single Molecule Pulldown

For SiMPull experiments, a DNA ratio of 1:1 was used. 24 hours after transfection, HEK 239T cells were harvested from coverslips by incubating with Ca^{2+} -free PBS buffer for 20-30 minutes followed by gentle pipetting. Cells were lysed in buffer containing (in mM): 150 NaCl, 10 Tris pH 7.5, 1 EDTA, protease inhibitor cocktail (Thermo Scientific) and 1.5% IGEPAL (Sigma) or 1% DDM (Sigma). After 30-60 minute incubation at 4°, lysate was centrifuged for 20 minutes at 12,500 g and the supernatant was collected. Coverslips passivated with PEG (~99%)/ biotin-PEG (~1%) and treated with NeutrAvidin (Pierce) were prepared as described (Jain et al., 2012). 15 nM biotinylated anti-HA antibody (clone 16B12, BioLegend) was applied for 20 minutes and then washed out. Antibody dilutions and washes were done in T50 buffer with BSA containing (in mM): 50 NaCl, 10 Tris pH 7.5, and 0.1 mg/mL BSA. Lysate, diluted in lysis buffer containing 0.04% IGEPAL, was then applied to the chamber and washed away following brief incubation (~2 minutes). Single molecules were imaged using a 488 nm Argon laser on a total internal reflection fluorescence microscope with a 60x objective (Olympus). We recorded the emission light after an additional 3x magnification and passage through a double dichroic mirror and an emission filter (525/50 for GFP) with a back-illuminated EMCCD camera (Andor iXon DV-897 BV). Movies of 250-500 frames were acquired at frame rates of 10–30 Hz. The imaged area was 13 x 13 μm^2 . At least 5 movies were recorded for each condition and data was analyzed using custom software. Multiple independent experiments were performed for each condition. Representative data sets are presented to quantitatively compare conditions tested on the same day.

Acknowledgments

We thank Rainer Waldman, Bernard Mari, Kevin Le Brigand, Eric Lingueglia, Michel Lanteri-Minet, Emile Piquet and Maximilian Furthauer for helpful discussion. The work was supported by a grant to GS by the ATIP-AVENIR funds and the Fondation pour la Recherche Medicale (Equipe labellisée FRM 2017, FRM DEQ20170336753) as well as grants to GS and FL from the Agence Nationale de la Recherche (Laboratory of Excellence “Ion Channel Science and Therapeutics“, grant ANR-11-LABX-0015-01 and ANR Dynaselect, Grant ANR-14-CE13-0010). We thank A. Monteil and C. Lemmers from the Vectorology facility, PVM, Biocampus Montpellier, CNRS UMS3426 for virus production. The microscopy was done in the Prism facility, “Plateforme PRISM – IBV- CNRS UMR 7277-INSERM U1091-UNS». Magali Mondin is acknowledged. Histopathological analyses were performed on the Experimental Histopathology Platform of iBV, CNRS UMR7277-INSERM U1091-UNS». The help of Samah REKIMA is acknowledged.

References:

- Alloui, A., Zimmermann, K., Mamet, J., Duprat, F., Noël, J., Chemin, J., Guy, N., Blondeau, N., Voilley, N., Rubat-Coudert, C., *et al.* (2006). TREK1, a K⁺ channel involved in polymodal pain perception. *EMBO J* 25, 2368-2376.
- Andres-Enguix, I., Shang, L., Stansfeld, P.J., Morahan, J.M., Sansom, M.S., Lafrenière, R.G., Roy, B., Griffiths, L.R., Rouleau, G.A., Ebers, G.C., *et al.* (2012). Functional analysis of missense variants in the TRESK (KCNK18) K channel. *Sci Rep* 2, 237.
- Bates, E.A., Nikai, T., Brennan, K.C., Fu, Y.H., Charles, A.C., Basbaum, A.I., Ptáček, L.J., and Ahn, A.H. (2010). Sumatriptan alleviates nitroglycerin-induced mechanical and thermal allodynia in mice. *Cephalalgia* 30, 170-178.
- Bautista, D.M., Sigal, Y.M., Milstein, A.D., Garrison, J.L., Zorn, J.A., Tsuruda, P.R., Nicoll, R.A., and Julius, D. (2008). Pungent agents from Szechuan peppers excite sensory neurons by inhibiting two-pore potassium channels. *Nat Neurosci* 11, 772-779.
- Blin, S., Ben Soussia, I., Kim, E.J., Brau, F., Kang, D., Lesage, F., and Bichet, D. (2016). Mixing and matching TREK/TRAAK subunits generate heterodimeric K²P channels with unique properties. *Proc Natl Acad Sci U S A* 113, 4200-4205.
- Brennan, K.C., Bates, E.A., Shapiro, R.E., Zyuzin, J., Hallows, W.C., Huang, Y., Lee, H.Y., Jones, C.R., Fu, Y.H., Charles, A.C., and Ptáček, L.J. (2013). Casein kinase Iδ mutations in familial migraine and advanced sleep phase. *Sci Transl Med* 5, 183ra156, 181-111.
- Dobler, T., Springauf, A., Tovornik, S., Weber, M., Schmitt, A., Sedlmeier, R., Wischmeyer, E., and Döring, F. (2007). TRESK two-pore-domain K⁺ channels constitute a significant component of background potassium currents in murine dorsal root ganglion neurones. *J Physiol* 585, 867-879.
- Guo, Z., Liu, P., Ren, F., and Cao, Y.Q. (2014). Nonmigraine-associated TRESK K⁺ channel variant C110R does not increase the excitability of trigeminal ganglion neurons. *J Neurophysiol* 112, 568-579.
- Guyon, A., Tardy, M.P., Rovère, C., Nahon, J.L., Barhanin, J., and Lesage, F. (2009). Glucose inhibition persists in hypothalamic neurons lacking tandem-pore K⁺ channels. *J Neurosci* 29, 2528-2533.
- Harris, H.M., Carpenter, J.M., Black, J.R., Smitherman, T.A., and Sufka, K.J. (2017). The effects of repeated nitroglycerin administrations in rats; modeling migraine-related endpoints and chronification. *J Neurosci Methods* 284, 63-70.
- Hwang, E.M., Kim, E., Yarishkin, O., Woo, D.H., Han, K.S., Park, N., Bae, Y., Woo, J., Kim, D., Park, M., *et al.* (2014). A disulphide-linked heterodimer of TWIK-1 and TREK1 mediates passive conductance in astrocytes. *Nat Commun* 5, 3227.
- Jackson, R.J., Hellen, C.U., and Pestova, T.V. (2010). The mechanism of eukaryotic translation initiation and principles of its regulation. *Nat Rev Mol Cell Biol* 11, 113-127.
- Jain, A., Liu, R., Xiang, Y.K., and Ha, T. (2012). Single-molecule pull-down for studying protein interactions. *Nat Protoc* 7, 445-452.
- Johansen, F.F., Lambolez, B., Audinat, E., Bochet, P., and Rossier, J. (1995). Single cell RT-PCR proceeds without the risk of genomic DNA amplification. *Neurochem Int* 26, 239-243.
- Kochetov, A.V. (2008). Alternative translation start sites and hidden coding potential of eukaryotic mRNAs. *Bioessays* 30, 683-691.
- Kopruszinski, C.M., Xie, J.Y., Eyde, N.M., Remeniuk, B., Walter, S., Stratton, J., Bigal, M., Chichorro, J.G., Dodick, D., and Porreca, F. (2017). Prevention of stress- or nitric oxide donor-induced medication overuse headache by a calcitonin gene-related peptide antibody in rodents. *Cephalalgia* 37, 560-570.

- Kozak, M. (1984a). Compilation and analysis of sequences upstream from the translational start site in eukaryotic mRNAs. *Nucleic Acids Res* 12, 857-872.
- Kozak, M. (1984b). Point mutations close to the AUG initiator codon affect the efficiency of translation of rat preproinsulin *in vivo*. *Nature* 308, 241-246.
- Kozak, M. (1999). Initiation of translation in prokaryotes and eukaryotes. *Gene* 234, 187-208.
- Lafrenière, R.G., Cader, M.Z., Poulin, J.F., Andres-Enguix, I., Simoneau, M., Gupta, N., Boisvert, K., Lafrenière, F., McLaughlan, S., Dubé, M.P., *et al.* (2010). A dominant-negative mutation in the TRESK potassium channel is linked to familial migraine with aura. *Nat Med* 16, 1157-1160.
- Landrum, M.J., Lee, J.M., Benson, M., Brown, G., Chao, C., Chitipiralla, S., Gu, B., Hart, J., Hoffman, D., Hoover, J., *et al.* (2016). ClinVar: public archive of interpretations of clinically relevant variants. *Nucleic Acids Res* 44, D862-868.
- Lazarus, S., McInerney-Leo, A.M., McKenzie, F.A., Baynam, G., Broley, S., Cavan, B.V., Munns, C.F., Pruijs, J.E., Sillence, D., Terhal, P.A., *et al.* (2014). The IFITM5 mutation c.-14C > T results in an elongated transcript expressed in human bone; and causes varying phenotypic severity of osteogenesis imperfecta type V. *BMC Musculoskelet Disord* 15, 107.
- Lek, M., Karczewski, K.J., Minikel, E.V., Samocha, K.E., Banks, E., Fennell, T., O'Donnell-Luria, A.H., Ware, J.S., Hill, A.J., Cummings, B.B., *et al.* (2016). Analysis of protein-coding genetic variation in 60,706 humans. *Nature* 536, 285-291.
- Lengyel, M., Czirják, G., and Enyedi, P. (2016). Formation of Functional Heterodimers by TREK1 and TREK-2 Two-pore Domain Potassium Channel Subunits. *J Biol Chem* 291, 13649-13661.
- Levitz, J., Royal, P., Comoglio, Y., Wdziekonski, B., Schaub, S., Clemens, D.M., Isacoff, E.Y., and Sandoz, G. (2016). Heterodimerization within the TREK channel subfamily produces a diverse family of highly regulated potassium channels. *Proc Natl Acad Sci U S A* 113, 4194-4199.
- Liu, P., Xiao, Z., Ren, F., Guo, Z., Chen, Z., Zhao, H., and Cao, Y.Q. (2013). Functional analysis of a migraine-associated TRESK K⁺ channel mutation. *J Neurosci* 33, 12810-12824.
- Long, H., Liao, L., Zhou, Y., Shan, D., Gao, M., Huang, R., Yang, X., and Lai, W. (2017). A novel technique of delivering viral vectors to trigeminal ganglia in rats. *Eur J Oral Sci* 125, 1-7.
- Morenilla-Palao, C., Luis, E., Fernández-Peña, C., Quintero, E., Weaver, J.L., Bayliss, D.A., and Viana, F. (2014). Ion channel profile of TRPM8 cold receptors reveals a role of TASK-3 potassium channels in thermosensation. *Cell Rep* 8, 1571-1582.
- Nishikawa, T., Ota, T., and Isogai, T. (2000). Prediction whether a human cDNA sequence contains initiation codon by combining statistical information and similarity with protein sequences. *Bioinformatics* 16, 960-967.
- Nosedá, R., and Burstein, R. (2013). Migraine pathophysiology: anatomy of the trigeminovascular pathway and associated neurological symptoms, CSD, sensitization and modulation of pain. *Pain* 154 Suppl 1.
- Noël, J., Zimmermann, K., Busserolles, J., Deval, E., Alloui, A., Diochot, S., Guy, N., Borsotto, M., Reeh, P., Eschalier, A., and Lazdunski, M. (2009). The mechano-activated K⁺ channels TRAAK and TREK1 control both warm and cold perception. *EMBO J* 28, 1308-1318.
- Pradhan, A.A., Smith, M.L., McGuire, B., Tarash, I., Evans, C.J., and Charles, A. (2014). Characterization of a novel model of chronic migraine. *Pain* 155, 269-274.
- Sandoz, G., Levitz, J., Kramer, R.H., and Isacoff, E.Y. (2012). Optical control of endogenous proteins with a photoswitchable conditional subunit reveals a role for TREK1 in GABA(B) signaling. *Neuron* 74, 1005-1014.

Sano, Y., Inamura, K., Miyake, A., Mochizuki, S., Kitada, C., Yokoi, H., Nozawa, K., Okada, H., Matsushime, H., and Furuichi, K. (2003). A novel two-pore domain K⁺ channel, TRESK, is localized in the spinal cord. *J Biol Chem* 278, 27406-27412.

Thomas, D., Plant, L.D., Wilkens, C.M., McCrossan, Z.A., and Goldstein, S.A. (2008). Alternative translation initiation in rat brain yields K2P2.1 potassium channels permeable to sodium. *Neuron* 58, 859-870.

Ulbrich, M.H., and Isacoff, E.Y. (2007). Subunit counting in membrane-bound proteins. *Nat Methods* 4, 319-321.

Verkest, C., Piquet, E., Diochot, S., Dauvois, M., Lanteri-Minet, M., Lingueglia, E., and Baron, A. (2018). Effects of systemic inhibitors of acid-sensing ion channels 1 (ASIC1) against acute and chronic mechanical allodynia in a rodent model of migraine. *Br J Pharmacol*.

Walsh, Y., Leach, M J, Veale, E., and Mathie, A. (2016). Identified regions of TREK and TRESK two pore domain potassium channels critical for inhibition by sipatragine and lamotrigine. In *Proceedings of The Physiological Society*, T.P. Socitey, ed. (Dublin, **Proc Physiol Soc**).

Wood, H. (2010). Migraine: Familial migraine with aura is associated with a mutation in the TRESK potassium channel. *Nat Rev Neurol* 6, 643.

Yamamoto, Y., Hatakeyama, T., and Taniguchi, K. (2009). Immunohistochemical colocalization of TREK1, TREK-2 and TRAAK with TRP channels in the trigeminal ganglion cells. *Neurosci Lett* 454, 129-133.

Yan, J., and Dussor, G. (2014). Ion channels and migraine. *Headache* 54, 619-639.

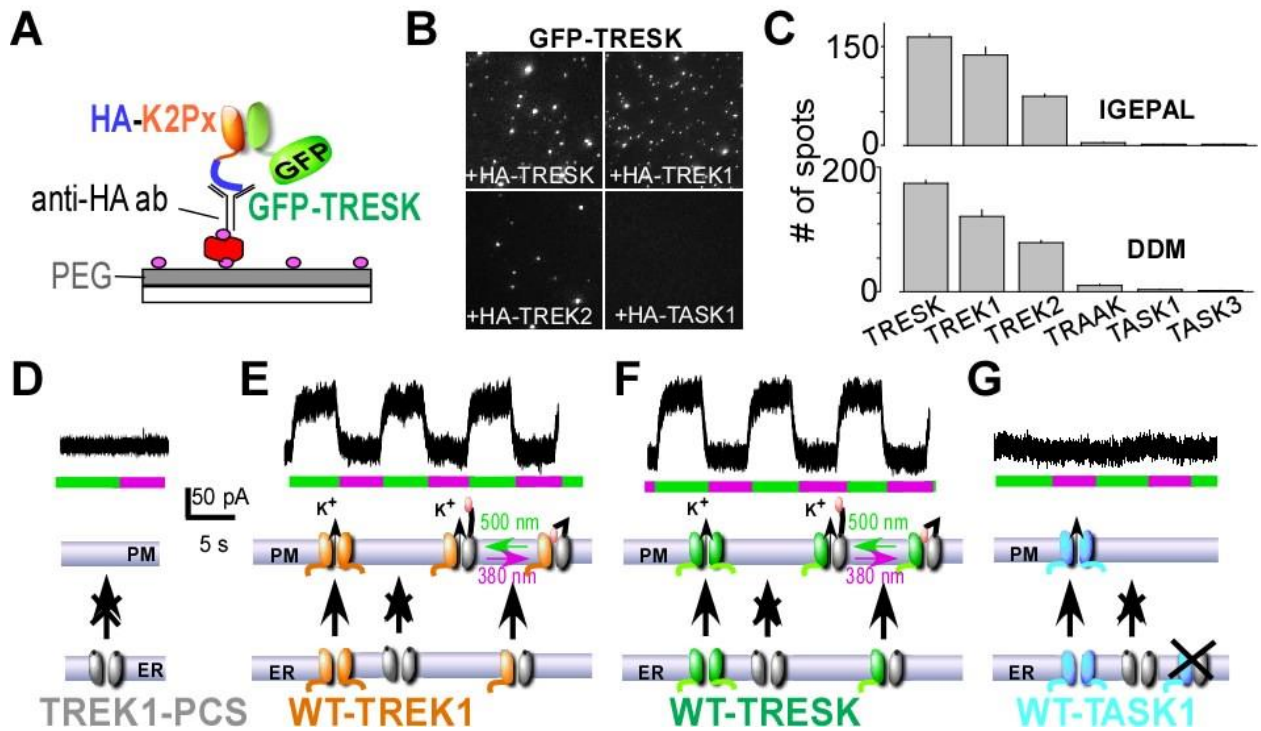


Figure 1: TRESK heteromerizes physically and functionally with TREK1 and TREK2. (A) Schematic of single molecule pulldown (SiMPull) of GFP-TRESK. HEK 293T cells expressing GFP-TRESK and an HA-tagged K2P channel (“HA-K2Px”) were lysed and then immobilized on a PEG-passivated coverslip conjugated to a biotinylated anti-HA antibody. (B-C) Representative images (IGEPAL) and summary bar graphs with 2 different detergents, IGEPAL and DDM, showing pulldown of GFP-TRESK by HA-TRESK, HA-TREK1 or HA-TREK2, but not by HA-TASK1, HA-TASK3, or HA-TRAAK. (D-G) Co-expression of TREK1-PCS with WT-TREK1 produces a heteromeric channel that traffics from the endoplasmic reticulum (ER) to the plasma membrane (PM) and which can be light-gated due to attachment of a photoswitchable blocker to the TREK1-PCS. TREK1-PCS expression alone does not produce any photoswitchable current (D), but co-expression of TREK1 (E) or TRESK (F), but not TASK1 (G) leads to a photoswitchable current indicating that TREK1-TRESK form functional heteromers but there is no functional assembly of TREK1 and TASK1.

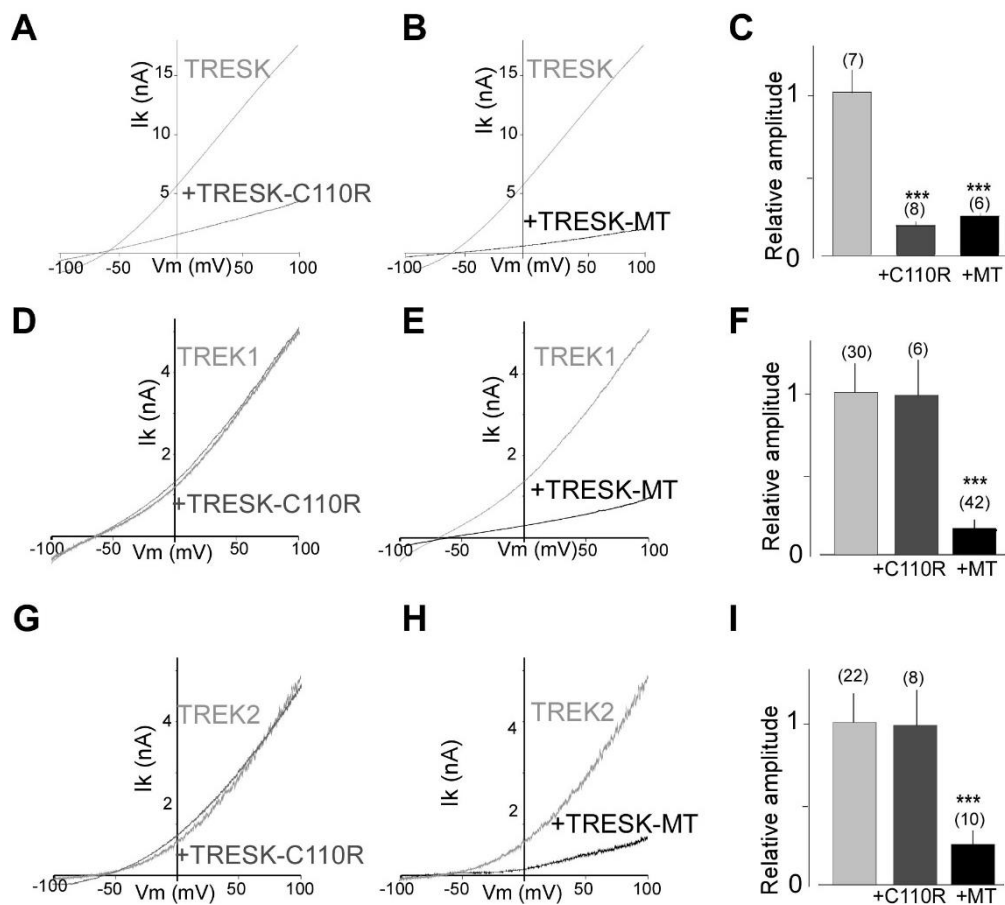


Figure 2. TRESK-MT, but not TRESK-C110R, acts as a dominant negative on TREK1 and TREK2 channels. (A, B) Representative traces showing the effect of TRESK-C110R (A) and TRESK-MT (B) co-expression on TRESK current in HEK 293T cells. Currents were elicited by voltage-ramps (from -100 to 100 mV, 1s duration). (C) Bar graph summarizing the relative TRESK current amplitude at 0 mV for TRESK when TRESK-C110R and TRESK-MT are or not coexpressed. (D-F) Same as (A-C) for TREK1. (G-I) same as (A-C) for TREK2. The numbers of cells tested are indicated in parentheses. Student's *t* test (***) $P < 0.001$.

TG neurons from WT and TREK1^{-/-}/TREK2^{-/-} double KO mice. **(C, D)** TRESK-MT acts as a dominant negative on TREK1 and TREK2 channels to increase excitability of TG neurons. Input-output plots of the spike frequency in response to 1s depolarizing current injection in transfected small TG neurons from WT **(C)** and TREK1^{-/-}/TREK2^{-/-} double KO mice **(D)**, show that an increase in excitability elicited by TRESK-MT is observed in WT, but not T1^{-/-}/T2^{-/-} neurons. The numbers of tested cells are indicated in parentheses. Student's *t* test (**P* < 0.05, ***P* < 0.01, ****P* < 0.001). **(E-H)** TREK1^{-/-}/TREK2^{-/-} double knockout animals present a migraine-like hypersensitivity to mechanical stimuli. **(E)** Schematic of experimental behavioral paradigms. Green arrows represent the injection of ISDN, a known migraine trigger. Blue arrows represent the measurement of mechanical sensitivity. **(F)** Paw withdrawal mechanical threshold, assessed after the first ISDN injection, were significantly decreased in double knockout animals and remained less than WT for the first 1.5 hrs following ISDN injection. **(G)** Mechanical responses, assessed prior to and after chronic ISDN injections, were significantly decreased in double knockout animals. **(H)** Comparison of the Paw withdrawal mechanical threshold before and after topiramate injection. Mechanical responses were assessed before and 2 hours after topiramate injection from WT and TREK1^{-/-}/TREK2^{-/-} double knockout ISDN-non treated mice. Numbers of mice tested are indicated in parentheses, Student's *t* test to compare WT vs TREK1^{-/-}/TREK2^{-/-} mice (**P* < 0.05, ***P* < 0.01, ****P* < 0.001).

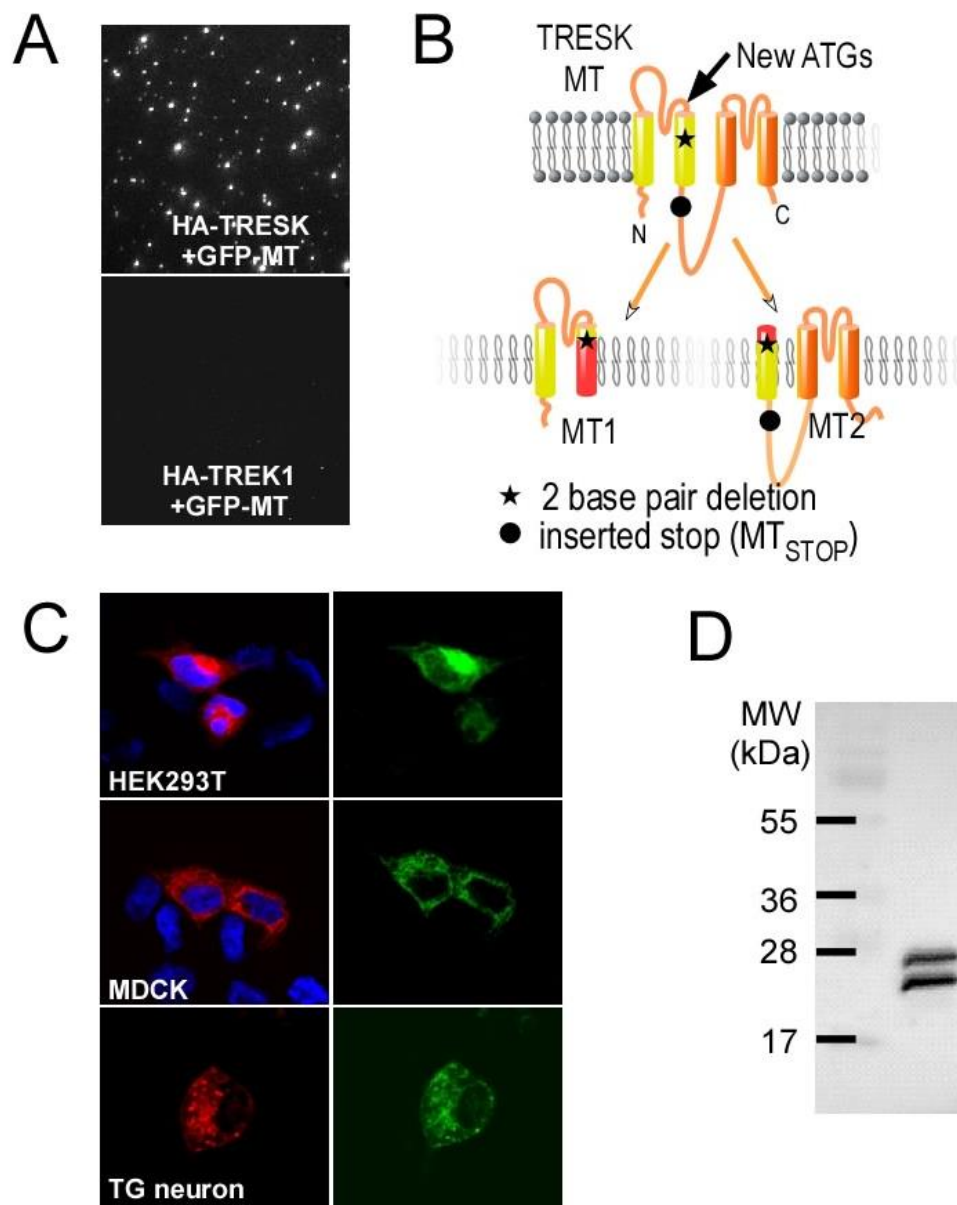


Figure 4. TRESK-MT induces the translation of a second protein, MT2. (A) Representative images from SiMPull experiments showing that GFP-TRESK-MT can be pulled down by HA-TRESK but not by HA-TREK1. (B) Cartoon showing the membrane topology of TRESK and the expected products induced by ATI in the TRESK-MT mutation. The region corresponding to aberrant sequences are shown in red. (C) Co-synthesis of mCherry-MT1 and MT2-GFP products from the mCherry-TRESK-MT-GFP cDNA in HEK 293T cells (top), MDCK (middle) and TG neurons (bottom). DAPI nuclear stain is shown in blue. (D) Western blot against HA-TRESK-MT-HA probed with anti-HA antibodies from HEK 293T cells lysate.

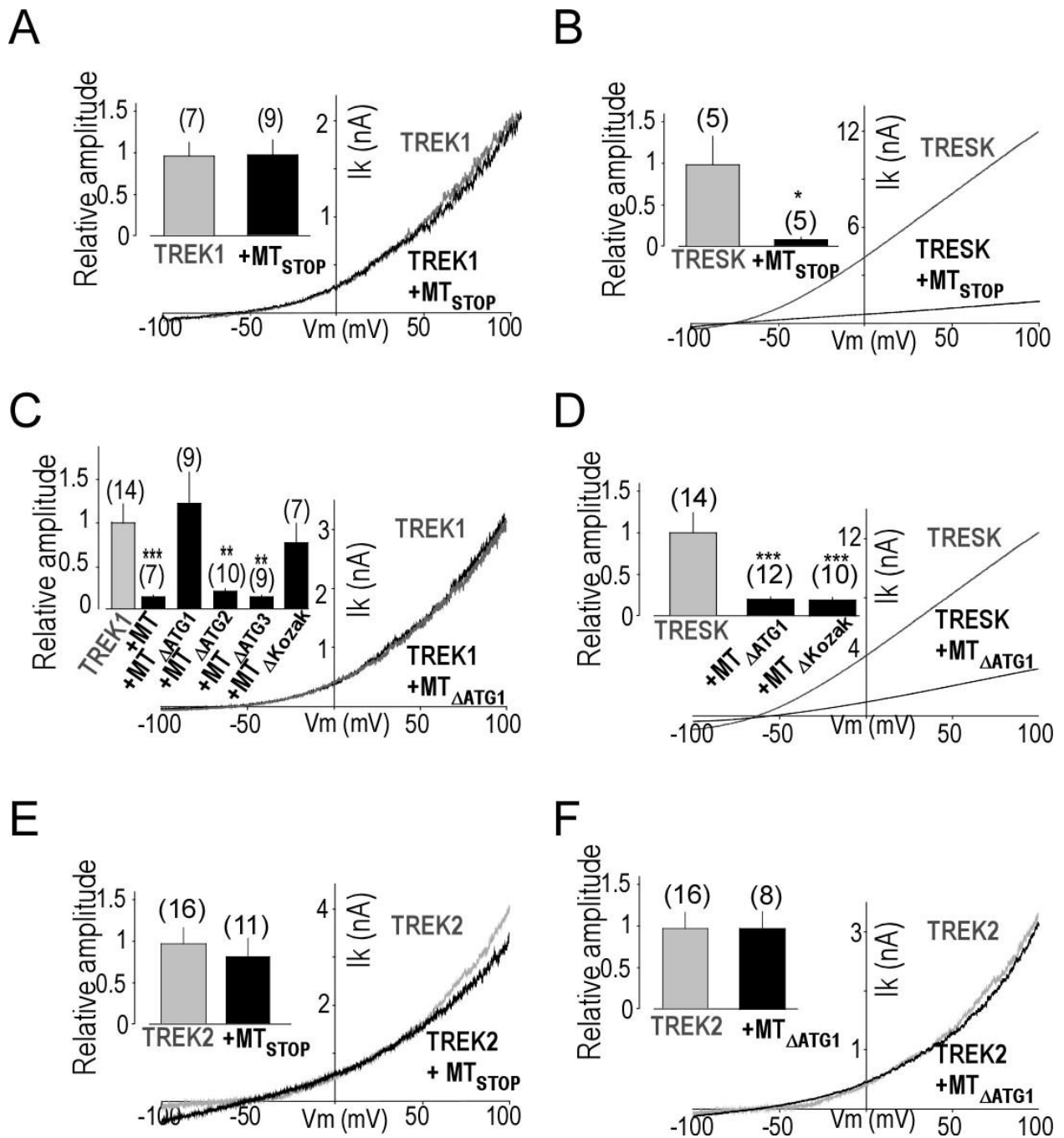


Figure 5. MT2 mediates TREK1 inhibition. (A) Representative traces showing the effect of introduction of a STOP codon at the beginning of the MT2 ORF within the 2-3 loop (TRESK-MT_{STOP}) on TREK1 current in HEK 293T cells. Inset shows a summary of TREK1 relative current densities when TRESK-MT_{STOP} is coexpressed. (B) Representative traces showing the effect of TRESK-MT_{STOP} on TRESK current. Insets, TRESK relative current densities when TRESK-MT_{STOP} is coexpressed. (C) Representative traces showing the effect of introduction of a mutation of ATG at position +356 (ΔATG1) on TREK1 current and summary bar graph showing the effect of mutation of candidate

alternative start codons (Δ ATG1, Δ ATG2, or Δ ATG3) and mutation of the Kozak sequence surrounding ATG1 (Δ Kozac) in TRESK-MT. Currents were elicited by voltage-ramps (from -100 to 100 mV, 1s duration). **(D)** Representative traces showing the effect of TRESK-MT $_{\Delta$ ATG1 on TRESK current. Insets, TRESK relative current densities when TRESK-MT $_{\Delta$ ATG1 is coexpressed. **(E, F)** same as (A, C) for TREK2. The numbers of cells tested are indicated in parentheses. Student's *t* test (**P* < 0.05, ***P* < 0.01, ****P* < 0.001) shows the difference between TREK1 or TRESK or TREK2 and TREK1 or TRESK or TREK2 when co-expressed with different TRESK-MT constructs.

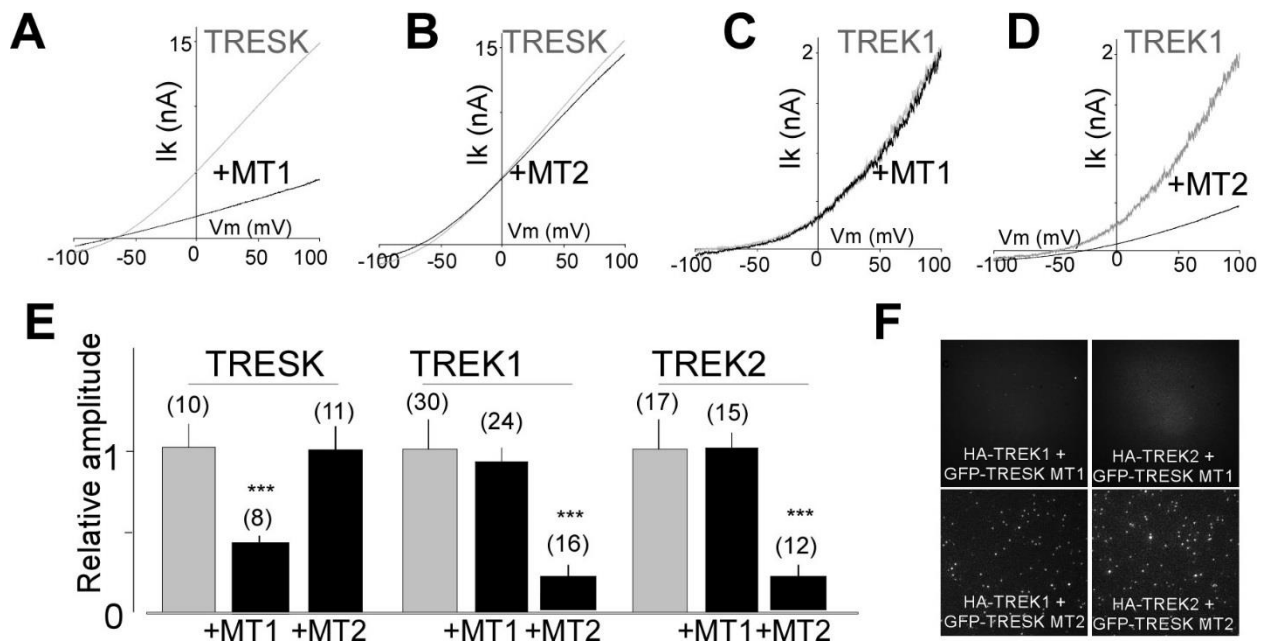


Figure 6. MT1 acts as dominant negative on TRESK whereas MT2 acts as a dominant negative on TREK1 and TREK2 channels. (A-D) Representative traces showing the effect of TRESK-MT1 (A and C) or TRESK-MT2 (B and D) co-expression on TRESK (A and B) or TREK1 (C and D) currents in HEK 293T cells. Currents were elicited by voltage-ramps (from -100 to 100 mV, 1s duration). (E) Bar graph summarizing the relative TRESK, TREK1 and TREK2 current amplitudes at 0 mV when MT1 or MT2 are co-expressed. Student's *t* test (***) $P < 0.001$). (F) Representative images showing that GFP-MT2, but not GFP-MT1, can be pulled down by HA-TREK1 and HA-TREK2 via an anti-HA antibody in the SiMPull assay with HEK 293T cells.

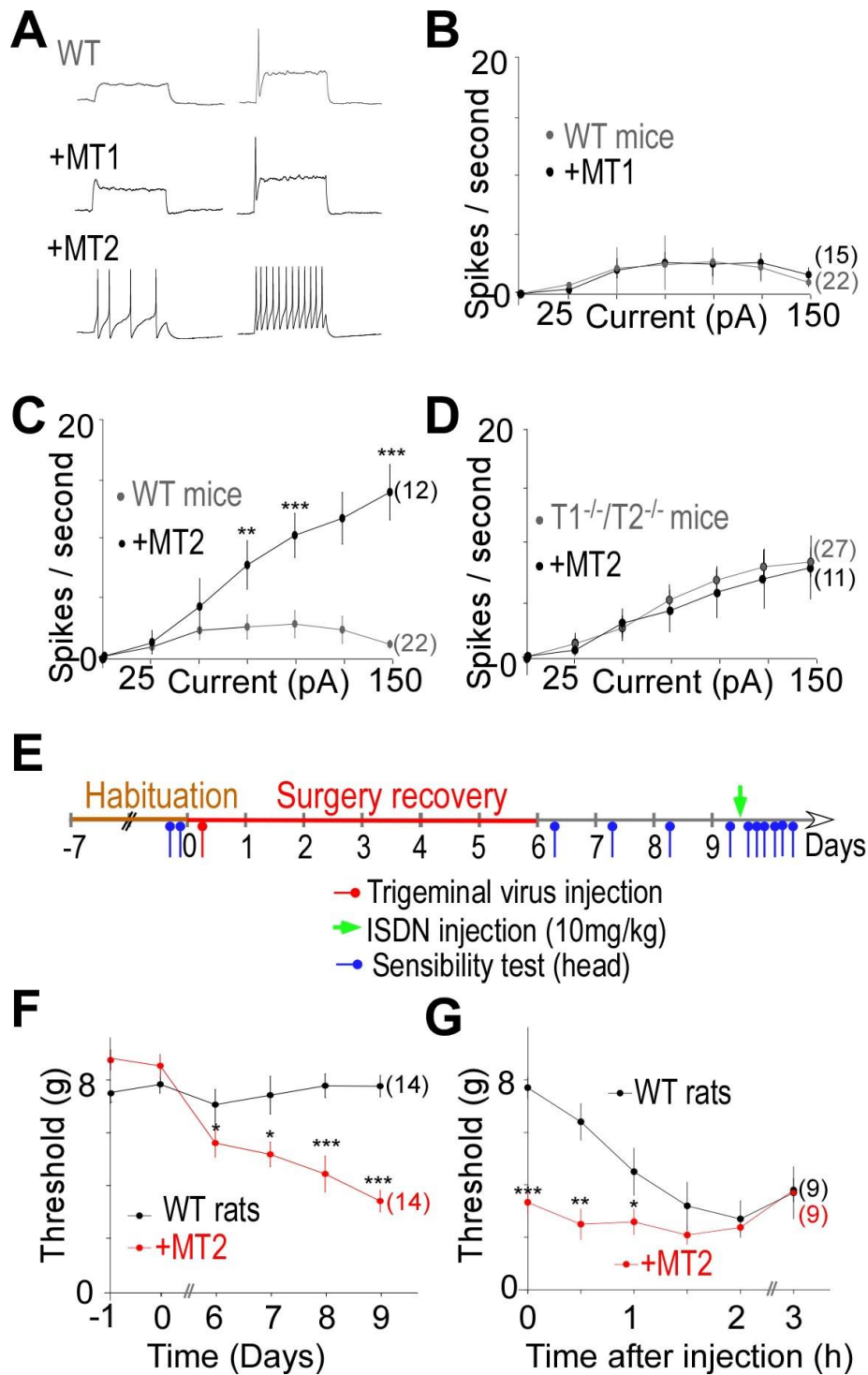


Figure 7. MT2, but not MT1, increases neuronal excitability of WT small TG neurons through TREK1 and TREK2 inhibition. (A) Representative traces showing spikes generated by incremental depolarizing current injections (+50 pA and +100 pA) in small-diameter TG neurons. (B and C) Input-output plots of spike frequency in response to 1s depolarizing current injections in WT small-diameter TG neurons transfected with either GFP ("WT"), the GFP-tagged MT1 subunit ("MT1") (B) or the GFP-tagged MT2 subunit ("MT2") (C). (D) Input-output plots of spike frequency show a lack of

effect of GFP-MT2 expression on TG neurons from TREK1/TREK2 double KO mice (T1^{-/-}/T2^{-/-}). **(E-G)** MT2 expression in TG leads to facial mechanical allodynia in rats. **(E)** Schematic of experimental behavioral paradigms. After a week of habituation rat were injected with 10 μ l of AAV2 encoding for either MT2 + GFP or GFP. **(F)** Face withdrawal mechanical threshold assessed after trigeminal virus infection encoding either GFP (WT rat condition) or MT2. **(G)** Face withdrawal mechanical threshold, assessed after the first ISDN injection. The threshold for MT2 expressing rats were significantly decreased before the injection and remained less than WT for the first 1.5 hrs following ISDN injection. The numbers of tested cells and rats are indicated in parentheses. Student's *t* test (**P* < 0.05, ***P* < 0.01, ****P* < 0.001).

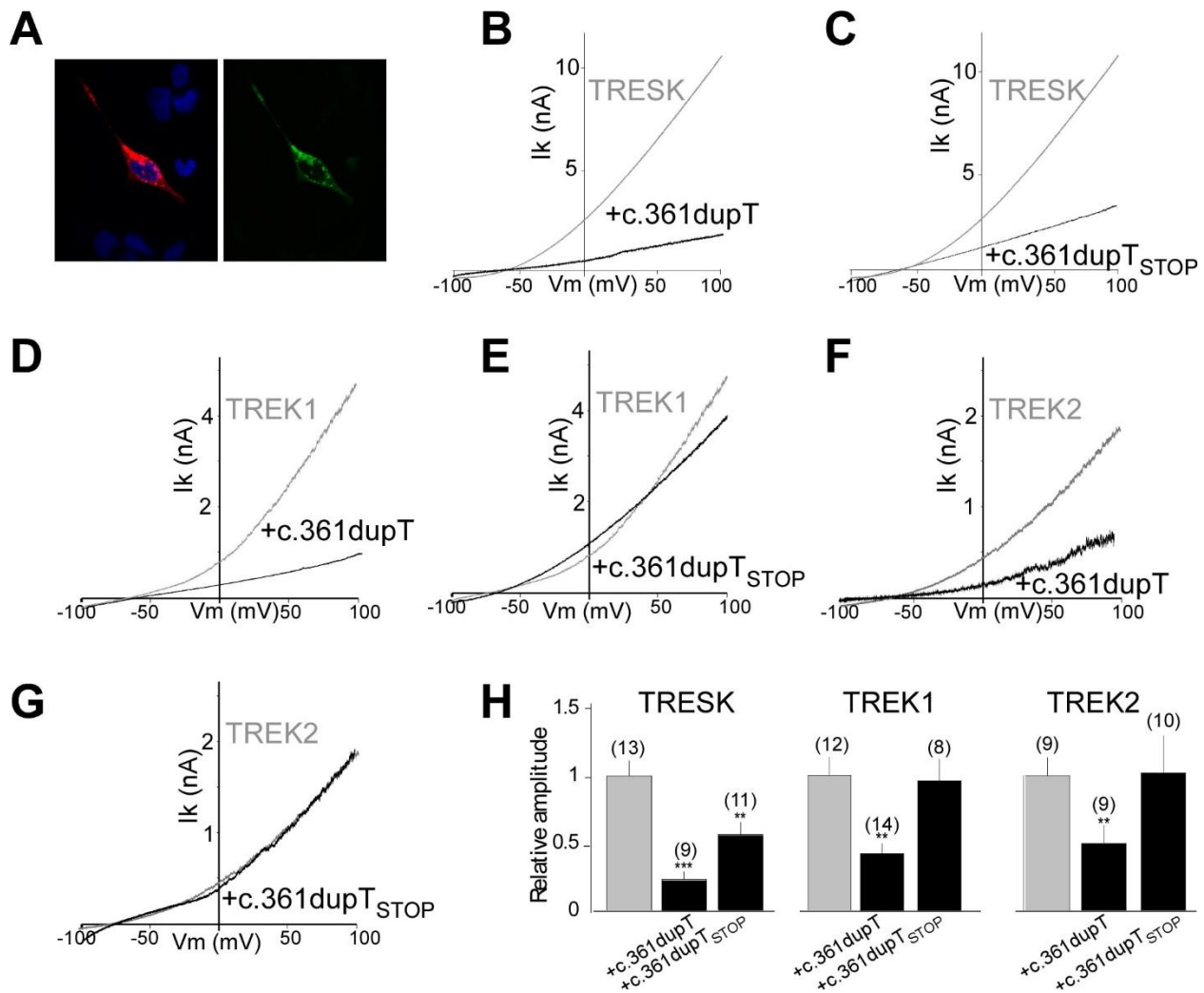


Figure 8. TRESK-c.361dupT (Y121LfsX44) acts as a dominant negative to reduce both TRESK and TREK1 current. (A) Co-synthesis of mCherry-MT1 and MT2-GFP products from the mCherry-TRESK- c.361dupT-GFP cDNA in HEK 293T cells. (B, C) Representative traces showing the effect of TRESK c.361dupT (B) and TRESK c.361dupT_{STOP} (C) co-expression on TRESK current. Currents were elicited by voltage-ramps (from -100 to 100 mV, 1s duration). (D, E) Same as (B, C) for TREK1. (F, G) same as (A, B) for TREK2. (H) Bar graph summarizing the relative TRESK, TREK1 and TREK2 current amplitudes at 0 mV for TRESK, TREK1 and TREK2 when TRESK c.361dupT and TRESK c.361dupT_{STOP} are coexpressed. Student's *t* test (**P<0.01 and ***P< 0.001).

Supplementary Materials for

Migraine-associated TRESK mutations increase neuronal excitability through alternative translation initiation and inhibition of TREK

Perrine Royal, Alba Andres-Bilbe, Pablo Ávalos Prado, Clément Verkest, Brigitte Wdziekonski, Sébastien Schaub, Anne Baron, Florian Lesage, Xavier Gasull, Joshua Levitz, Guillaume Sandoz*

Correspondence to: sandoz@unice.fr

This file includes:

Figs. S1 to S11

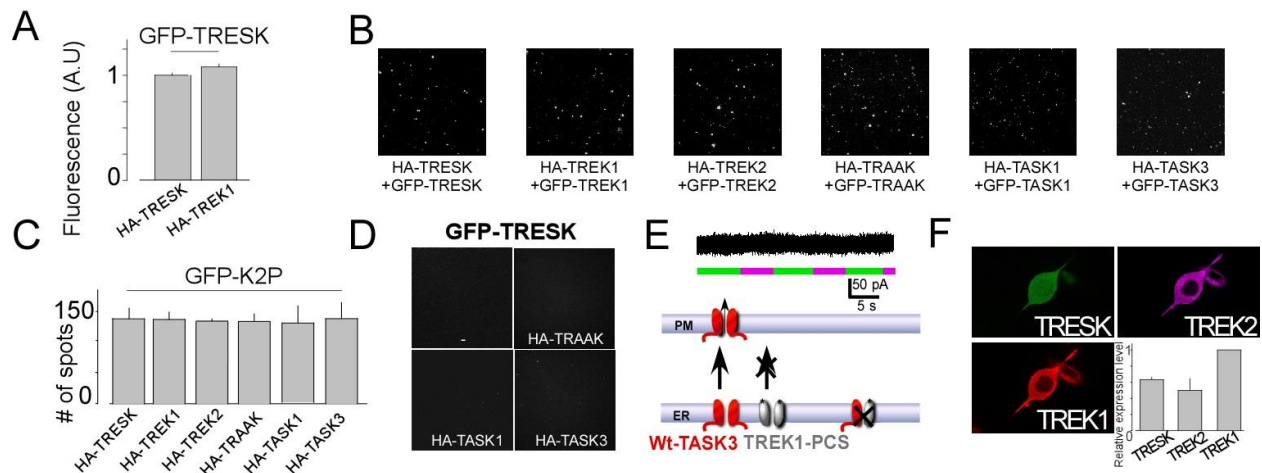


Figure S1. SiMPull assay controls. (A) GFP-fluorescence intensity of lysates from cells expressing HA-TRESK + GFP-TRESK or HA-TREK1 + GFP-TRESK. (B-C) Representative images and summary bar graph showing that HA-TREK1 pulldown GFP-TREK1, HA-TREK2 pulldown GFP-TREK2, HA-TRESK pulldown GFP-TRESK, HA-TRAAK pulldown GFP-TRAAK, HA-TASK1 pulldown GFP-TASK1 and HA-TASK3 pulldown GFP-TASK3. (D) Representative images showing that HA-TRAAK or HA-TASK1 or HA-TASK3 are not able to pull down GFP-TRESK and the control (-) showing that there are no fluorescent spots in the absence of antibody. (E) TREK1-PCS expression with TASK3 does not lead to photocurrent, indicating that TREK1 and TASK3 do not physically or functionally interact. (F) TREK1, TREK2 and TRESK are co-expressed in TG neurons. Immunodetection of TREK1, TREK2 and TRESK. Inset, bar graph representing the average relative mRNA expression of TREK1, TREK2, TRESK obtained from 4 single cell semi-quantitative RT-PCR.

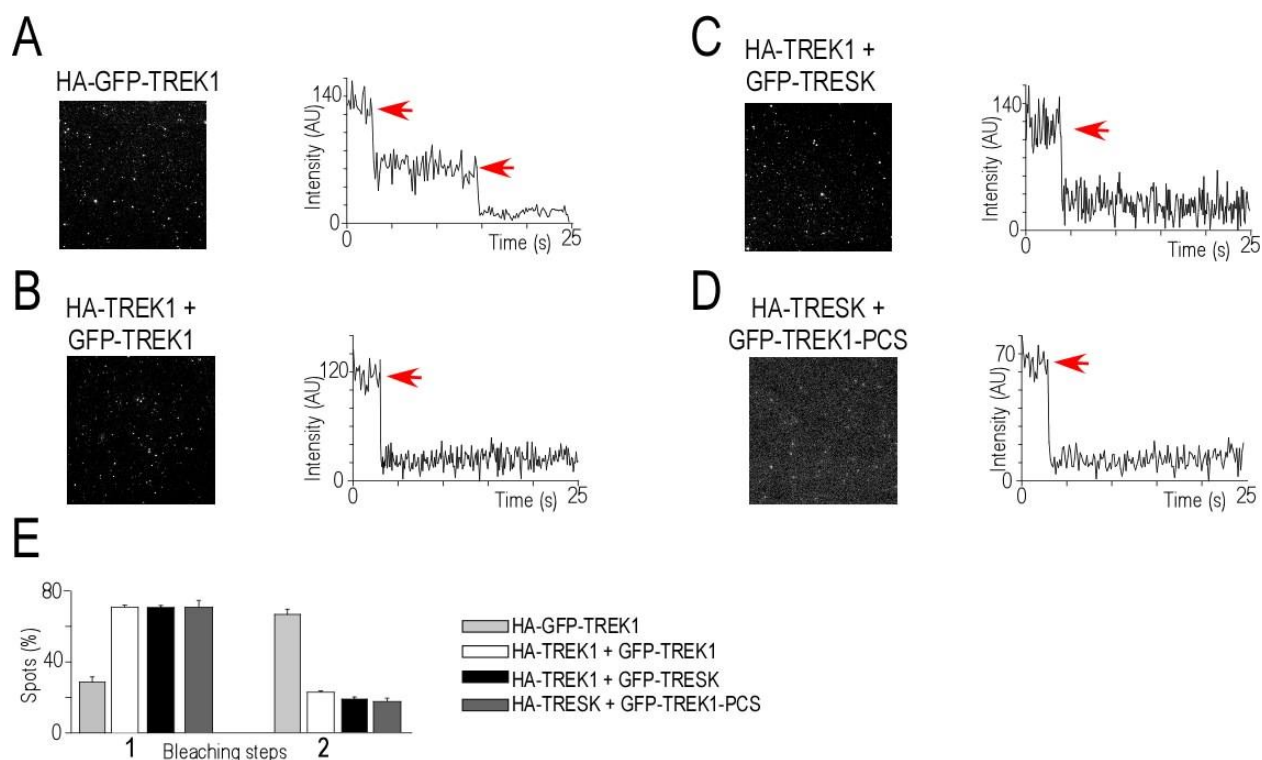


Figure S2: TRESK-TREK1 forms a dimer. (A) SiMPull assay for dimer control, left, TIRF images of HA-GFP-TREK1 single molecules, right, representative trace showing two-step photobleaching of HA-GFP-TREK1. (B) Same as in (A) for monomer control, HA-TREK1 pulldown of GFP-TREK1. (C) Same as in (A) for HA-TREK1 pulldown of GFP-TRESK. (D) Same as in (A) for HA-TRESK pulldown of GFP-TREK1-PCS. (E) Summary of photobleaching step distribution for HA-GFP-TREK1, HA-TREK1 pulldown of GFP-TREK1 and HA-TREK1 pulldown of GFP-TRESK and HA-TRESK pulldown of GFP-TREK1-PCS. AU, Arbitrary Unit.

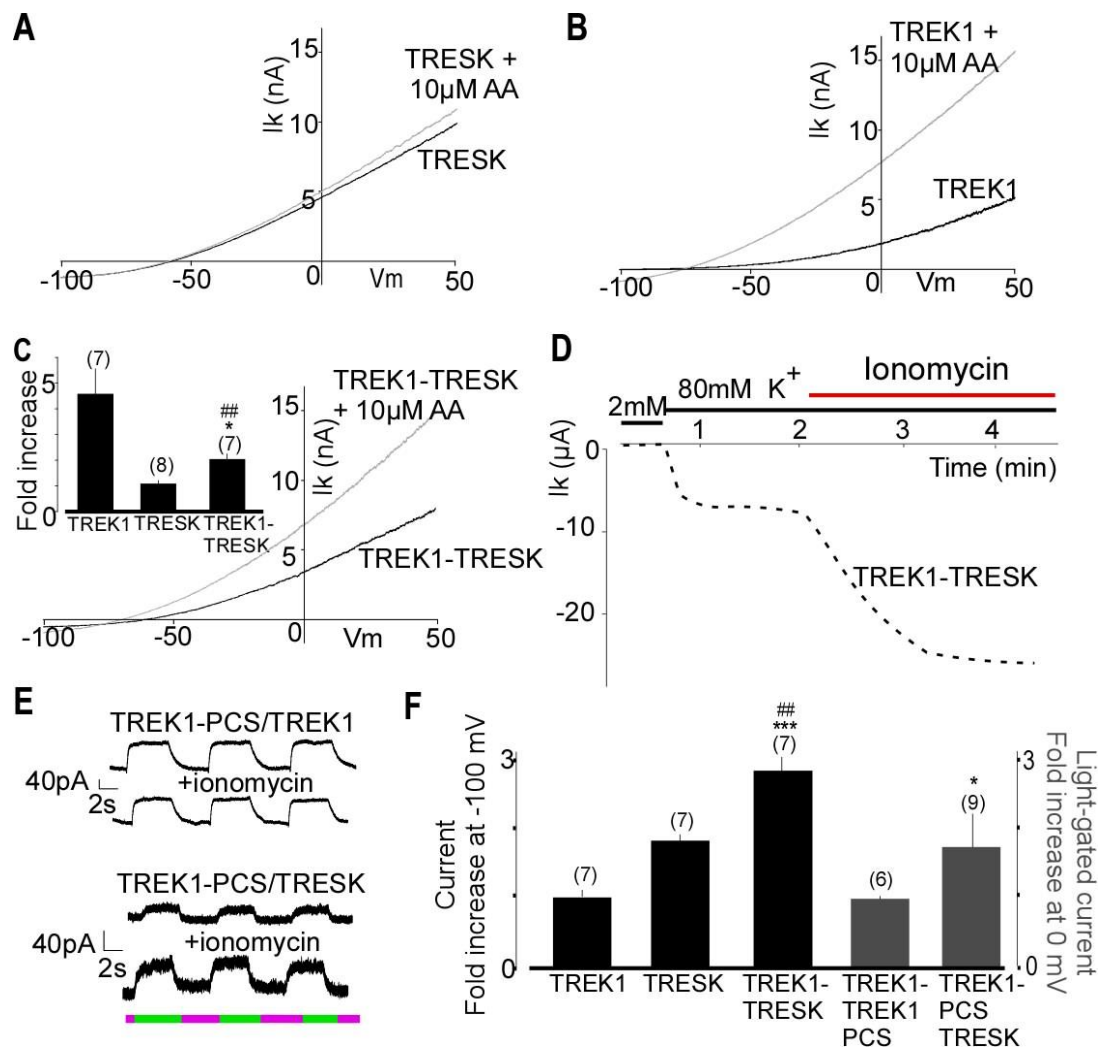


Figure S3. Functional characterization of TREK1-TRESK heterodimers. (A-C) Representative traces of TRESK (A) and TREK1 (B) and TREK1-TRESK (C) currents showing the effect of 10µM arachidonic acid application. Inset, summary of relative current amplitudes in HEK293T cells. (D) Representative TREK1-TRESK current amplitude modification induced by application of 0.5µM ionomycin, in *Xenopus* oocytes (E) Representative example of the effect of ionomycin on the light-gated currents of TREK1/TREK1PCS and TREK1-PCS/TRESK. Alternating illumination at 500 nm (green) and 380 nm (magenta) reversibly blocks and unblocks, respectively, the constant outward current, both with or without ionomycin, but the amplitude of the photomodulation for TRESK/TREK1PCS is bigger in the presence of ionomycin, in HEK293T cells.. (F) Summary of relative current amplitudes and their response to ionomycin. Student's *t* test (**P* < 0.05, ***P* < 0.01, ****P* < 0.001 for TREK1-TRESK vs TREK1 and ##*P* < 0.01 for TREK1-TRESK vs TRESK).

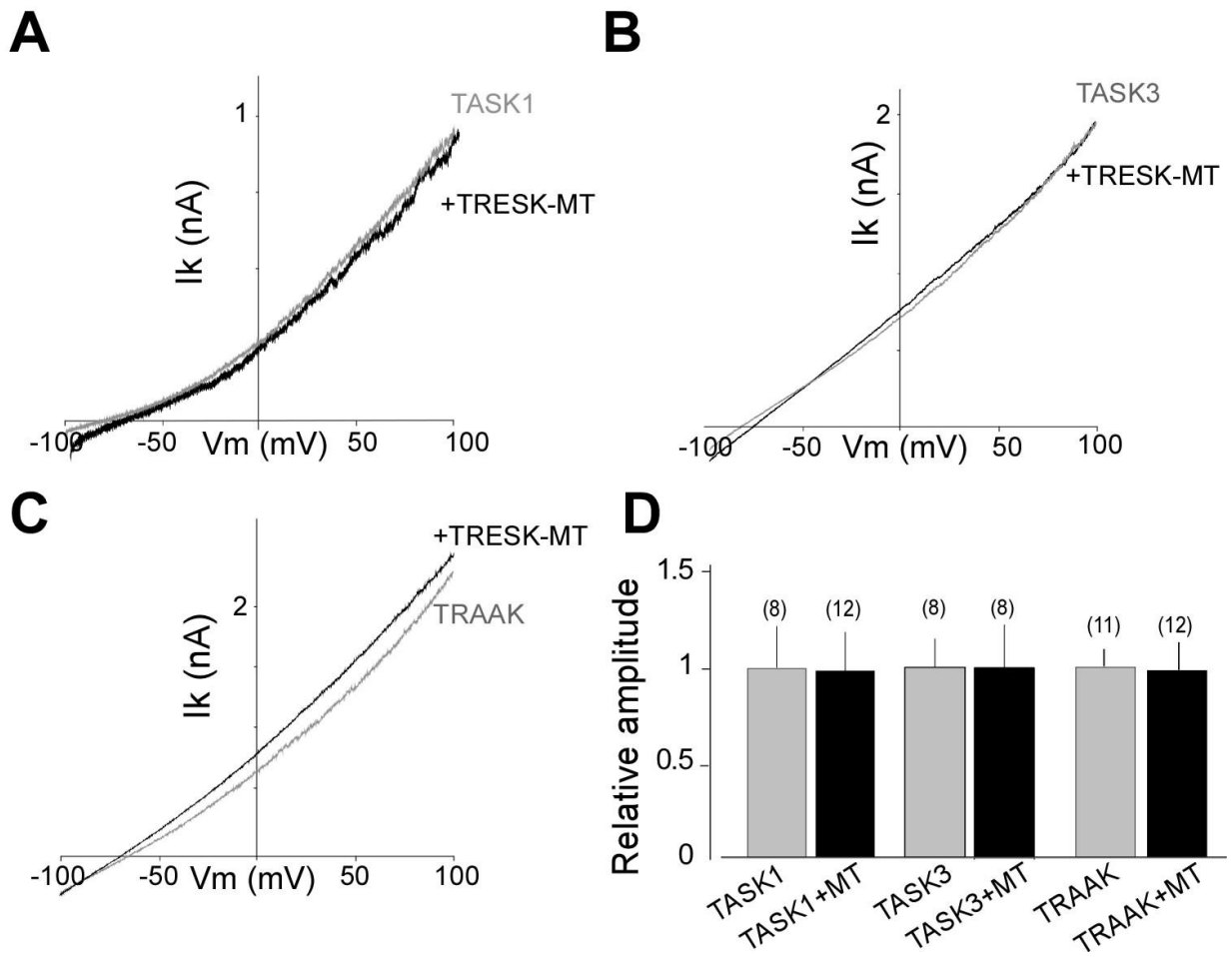


Figure S4. TRESK-MT does not inhibit TRAAK, TASK1 or TASK3. (A to C) Representative traces showing the effect of TRESK-MT co-expression TASK1 (A), TASK3 (B) or TRAAK (C) currents. Currents were elicited by voltage-ramps (from -100 to 100 mV, 1s duration). (D) Bar graph summarizing the relative TASK1, TASK3, or TRAAK current amplitudes at 0 mV with or without TRESK-MT co-expression.

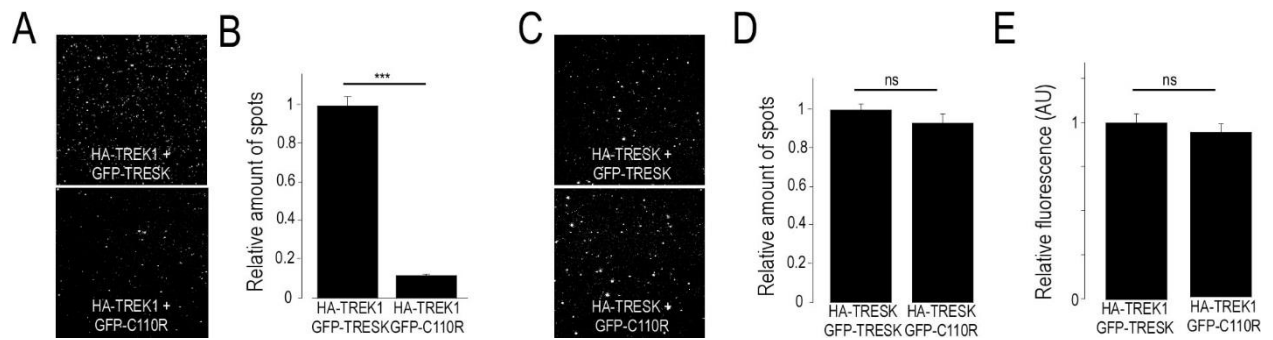


Figure S5. TRESK-C110R mutation inhibits TRESK-TREK1 association. Representative images showing HA-TREK1 pull down of GFP-TRESK and GFP-TRESK-C110R via an anti-HA antibody. **(B)** Bar graph showing the relative pulldown of GFP-TRESK and GFP-TRESK-C110R by HA-TREK1. Both conditions were done on the same day at the same dilution. **(C and D)** Same as (A and B) for HA-TRESK pull down of GFP-TRESK and GFP-TRESK-C110R. Student's *t* test (***) $P < 0.001$. **(E)** GFP-fluorescence intensity of lysate from HA-TREK1 + GFP-TRESK and HA-TREK1 + GFP-TRESK-C110R cells showing that GFP-TRESK and GFP-TRESK-C110R are expressed at similar levels in HEK 293T cells.

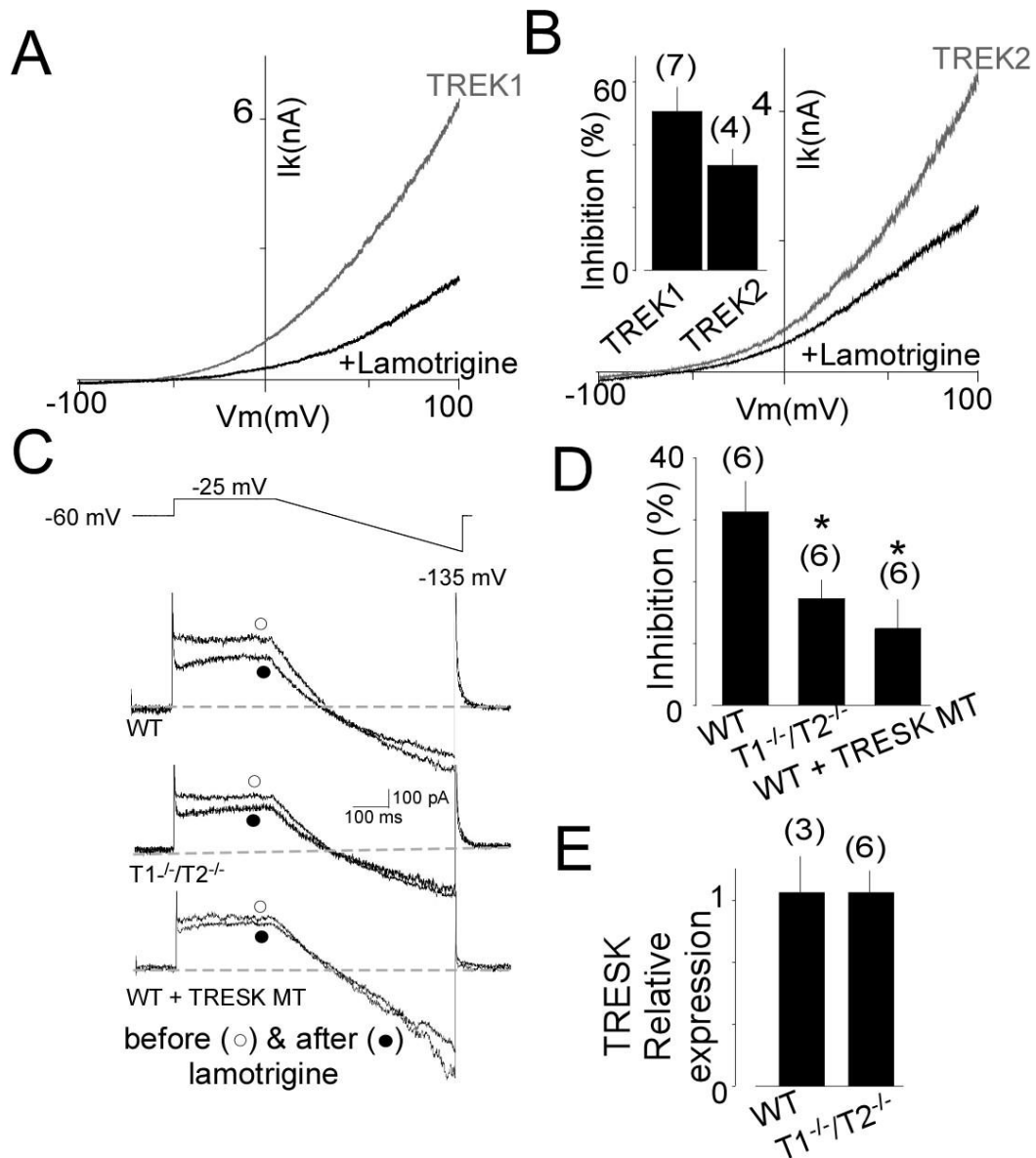


Figure S6. The lamotrigine sensitive leak current is reduced in TG neuron from TREK1^{-/-}/TREK2^{-/-} KO mice. (A) Representative traces of TREK1 (A) and TREK2 (B) showing the effect of 30 μ M lamotrigine application in HEK293T cells. Inset, summary of inhibition induced by lamotrigine application. (C) Representative current traces from WT TG neurons expressing GFP (WT) or TRESK-MT (WT + TRESK-MT) and from TREK1^{-/-}/TREK2^{-/-} (T1^{-/-}/T2^{-/-}) TG neuron expressing GFP (T1^{-/-}/T2^{-/-}). (D) Percentage of outward current (measured at the end of the depolarizing step) inhibited by lamotrigine. (E) Relative TRESK expression. TREK1 and 2 invalidation did not change the expression of TRESK. The numbers of tested cells or tissues are indicated in parentheses.

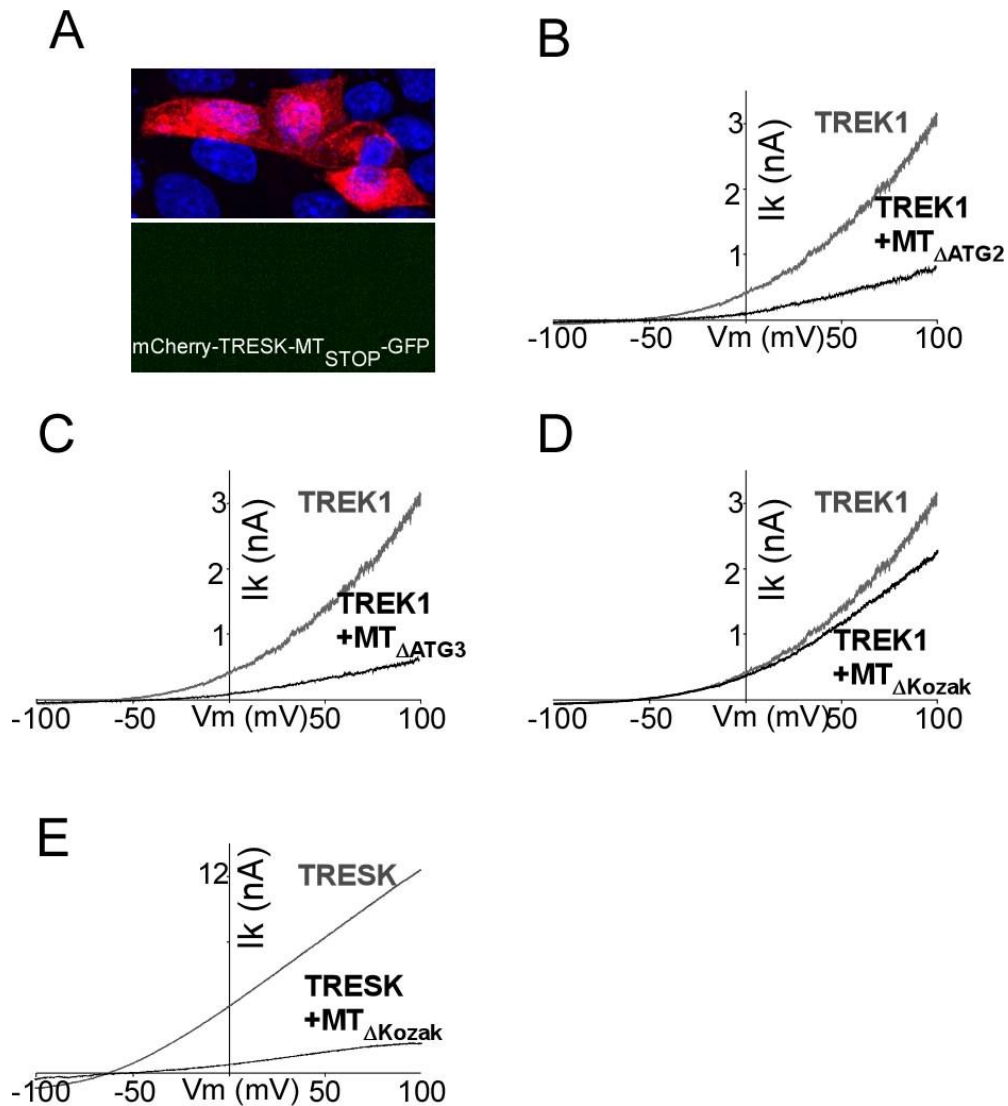


Figure S7. MT2 is cotranslated with MT1 and mediates TREK1 inhibition. (A) Introduction of a stop codon into the MT2 ORF of mCherry-TRESK-MT-GFP (mCherry-TRESK-MT_{STOP}-GFP) induces a loss of the GFP fluorescence in HEK 293T cells (B-D) Representative traces showing the effect of introduction of a mutation of ATG2 (MT_{ΔATG2}) (B), ATG3 (MT_{ΔATG3}) (C) and ΔKozak (MT_{ΔKozak}) (D) on TRESK-MT on TREK1 current in HEK 293 T cells. (E) Representative traces showing the effect of TRESK-MT_{ΔKozak} on TRESK current.

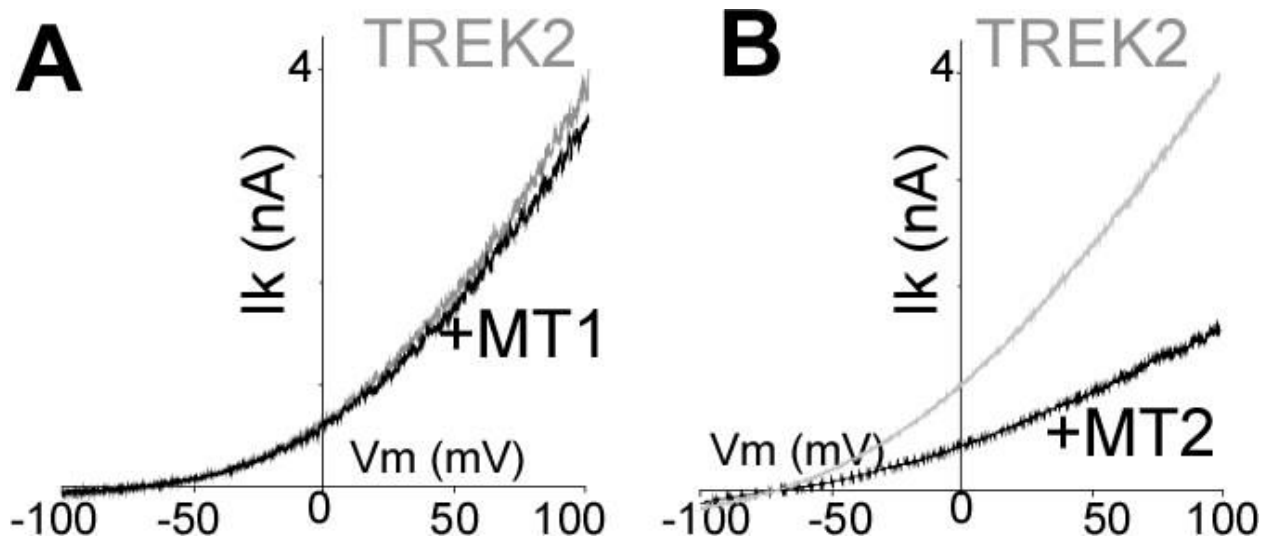


Figure S8. MT2, but not MT1, acts as a dominant negative on TREK2 channels. (A and B) Representative traces showing the effect of TRESK-MT1 (A) or TRESK-MT2 (B) co-expression on TREK2 current.

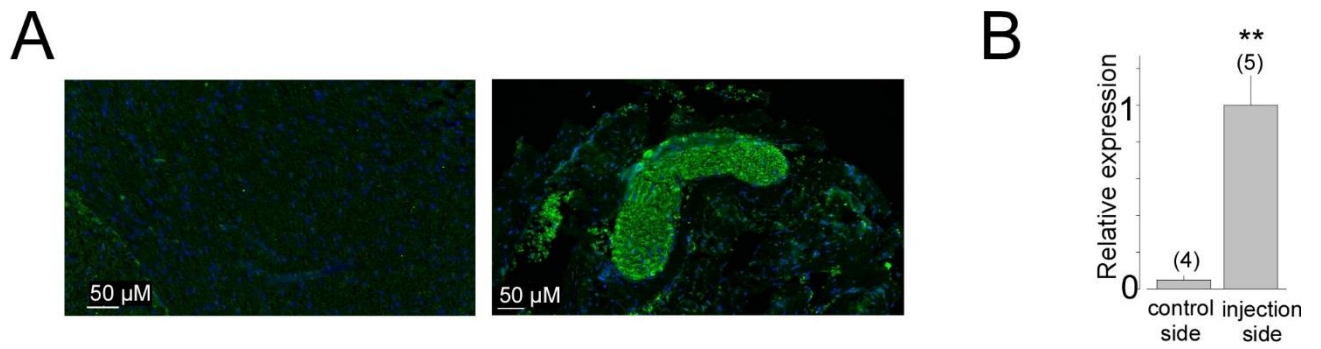


Figure S9. Viral expression of TRESK-MT2 pIRES 2 EGFP into trigeminal neurons. (A) The viral expression into trigeminal ganglia marked by the coexpressed-EGFP protein labelled in green (right). (B) Quantification of the viral infection through quantitative PCR 9 days post injection.

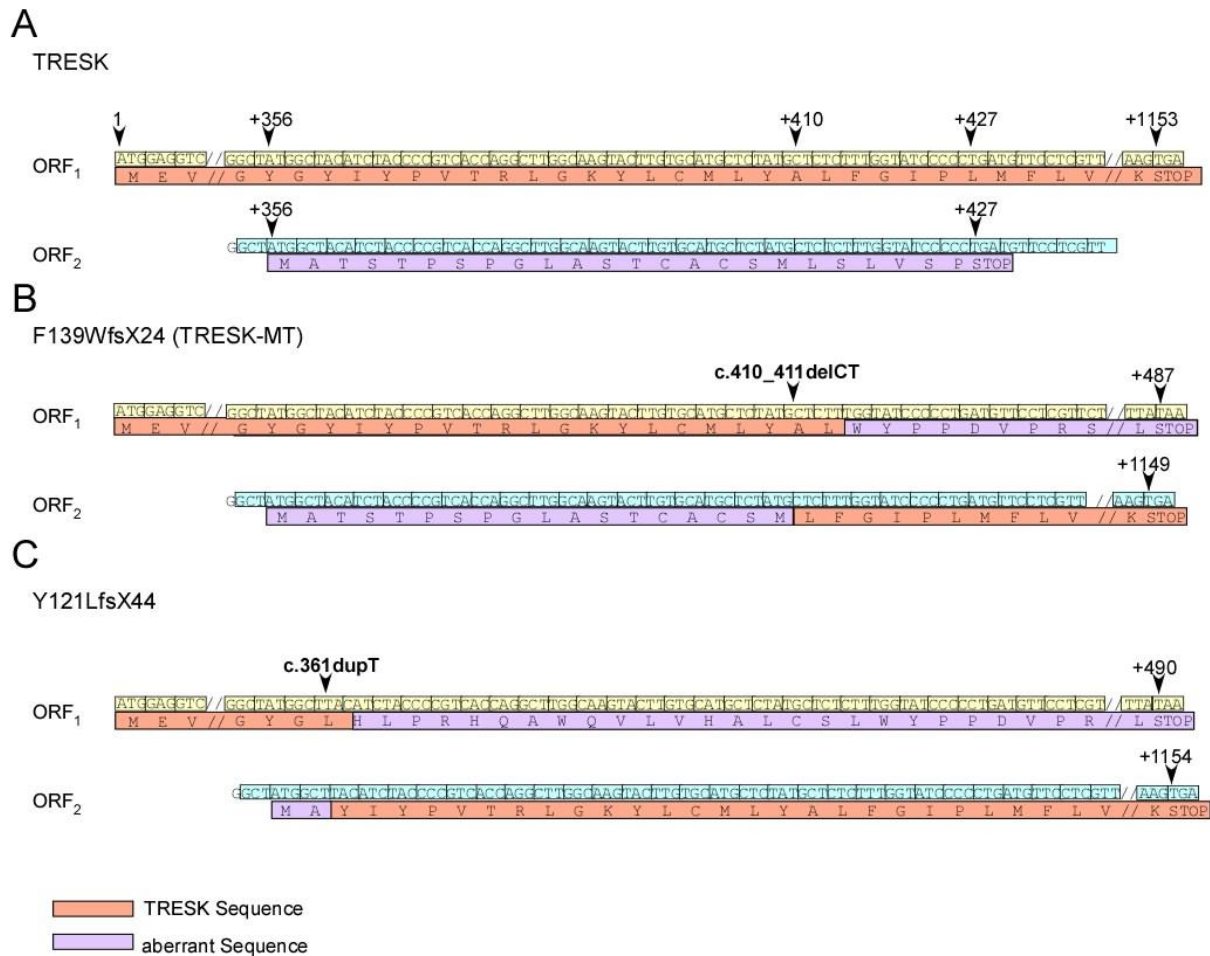


Figure S10. Sequence organization of TRESK, TRESK-F139WfsX24 and TRESK-Y121LfsX44.

(A) cDNA sequence of TRESK and deduced amino acid sequence for ORF1 and ORF2, (B) 2 pb deletion c.410_411delCT resulting in the change of reading frame leading to a premature stop codon in ORF1 at position +427 (MT1) and putting the ATG +356 in frame with the reference open reading frame of TRESK inducing the production of MT2. (C) 1 pb insertion c.361dupT resulting, as c.410_411delCT, in the change of reading frame leading to a premature stop codon in ORF1 at position +490 (MT1) and putting the ATG +356 in frame with the reference open reading frame of TRESK inducing the production of MT2.

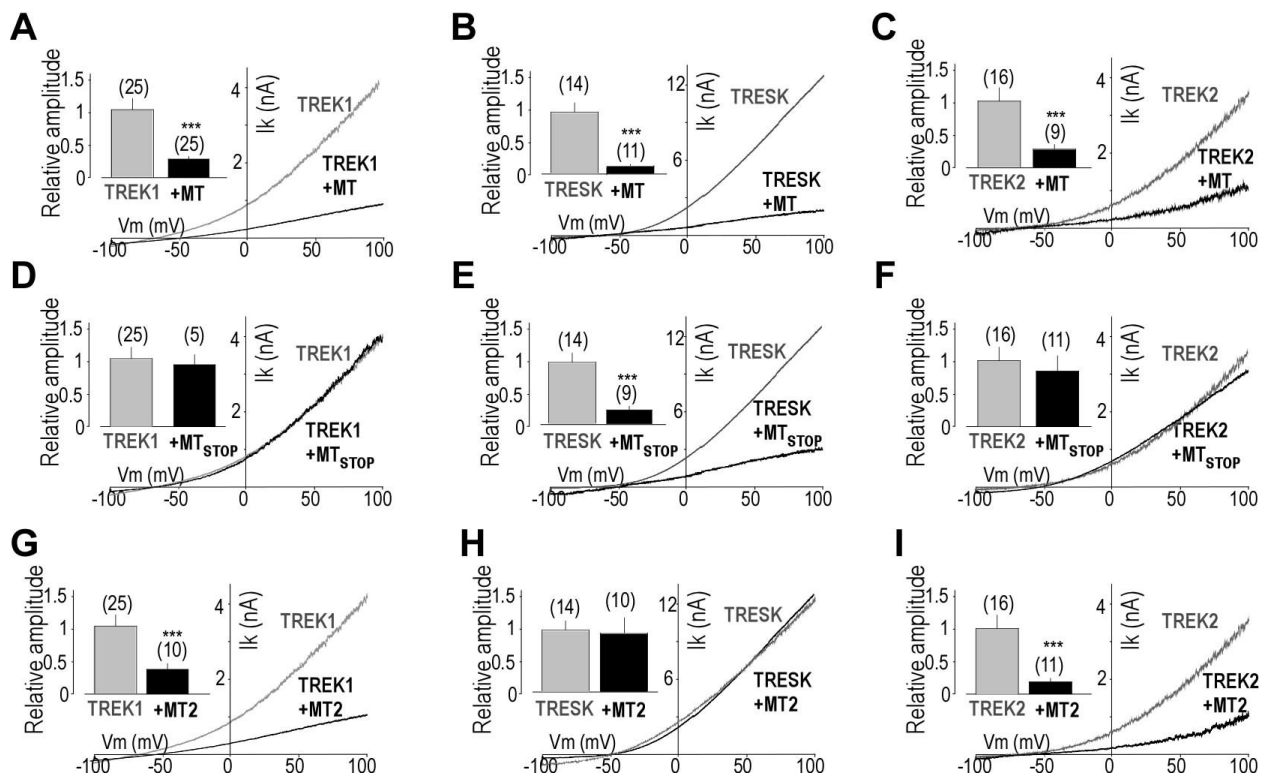


Figure S11. Regulation of the hTRESK, hTREK1 and hTREK2 by hTRESK-MT, hTRESK-MT_{STOP} and hMT2. (A-C) Representative traces and insets showing the effect of co-expression of hTRESK-MT on hTREK1 (A) hTRESK (B) and hTREK2 (C) currents HEK 293T cells. (D-F) Representative traces and insets showing the effect of hTRESK-MT_{STOP} on hTREK1 (D), hTRESK (E), and hTREK2 (F) currents. (G-I) Representative traces and insets showing the effect of hTRESK-MT2 co-expression on hTREK1 (G), hTRESK (H), and hTREK2 (I) currents in HEK293T cells. Currents were elicited by voltage-ramps (from -100 to 100 mV, 1s duration. The numbers of cells tested are indicated in parentheses. Student's *t* test (**P* < 0.05, ***P* < 0.01, ****P* < 0.001) shows the difference between hTREK1 or hTRESK or hTREK2 and hTREK1 or TRESK or TREK2 when co-expressed with different TRESK-MT constructs.

E. Discussion and conclusions

Having found the association between TRESK and TREK1 using SiMPull, we characterized the regulations of the TRESK-TREK1 heteromeric channels by several stimuli. The heteromer was activated by calcium, and had a lower regulation by arachidonic acid compare to the WT-TREK1 homomer. We then tried to pull-down TRESK-MT using TREK1. It was an astonishment to see that they were not able to interact.

If this inhibition is not coming from TRESK-MT1, it has to come from another protein. Normally one mRNA gives one protein, but in some cases this rule is not followed (Kozak, 1999). We took a deeper look into TRESK-MT DNA sequence and found an ATG embedded by a Kozak sequence which was, due to the deletion, in frame with WT-TRESK's open reading frame. We hypothesized that it could serve as a new initiation site allowing the formation of second truncated TRESK protein made of the 2-3 loop, MT3 and MT4 of TRESK (called TRESK-MT2). We therefore used series of experiments to demonstrate the existence of this second transcript. We found that we were able to see spots when co-expressing TRESK-MT-GFP (the MT2 ORF fused to GFP) with HA-TREK1 and 2, proving the interaction of TRESK-MT2, with TREK1.

These first data suggested that the interaction between the two subunits was a very complex mechanism, and the residues involved in this structure still need to be characterized. The second raised point was the following: how TRESK-MT C-terminus domain can be translated in addition to TRESK-MT1, the expected N-terminal truncated version of TRESK (Liu et al., 2013)?

We described for the first time a mechanism, called frameshift mutation induced alternative translation initiation –that leads to the production of two different proteins from one mRNA. Moreover, we proved that the N-terminus side TRESK-MT1 (previously termed TRESK-MT) is involved in the dominant negative effect on TRESK, while the protein resulting from the new initiation site TRESK-MT2 inhibits TREK1 and TREK2 in a dominant negative manner.

Not only we proved the existence of this process *in vitro*, but also we assessed this regulation *in vivo* in two animal models of migraine. They led us to conclude that TRESK-MT, thanks to the second translated protein, was downregulating both TREK1

and TREK2 current, and this phenomenon was at the origin of the hyperexcitability of TG neuron, leading to migraine phenotype.

VI. Discussion

A. Pathologies linked to K_{2P} heteromerization

1. About the formation of heteromers

Heteromerization is a process used in nature to increase the functional diversity of protein complexes, without changing the number of genes. This diversity is even more increased by alternative splicing, and alternative translation initiation. In this manuscript, we show how heteromerization mechanism that first increases K_{2P} diversity, is involved in the apparition of a migraine like phenotype via a newly translated mutant protein.

Heteromerization and trafficking. The localization of the assembly process, thought to be endoplasmic reticulum and Golgi apparatus, has never been shown. We now know that K_{2P} channels possess a C-terminus signal that facilitates the targeting of the channel to the plasma membrane. The channel being maintained in the endoplasmic reticulum in absence of this peptide. It has been shown that only one subunit carrying this peptide is sufficient for membrane localization (Blin et al., 2014; Sandoz et al., 2012). Heteromerization is thus a way for silent channels retained in the ER to be expressed at the plasma membrane.

Heteromerization and dominant negative effect. Nevertheless, this heteromerization process can also be a damaging mechanism. For instance in TREK1, it has been shown that an alternative splice variant of TREK1 reduces TREK1 current in a dominant negative fashion (Veale et al., 2010). It seems that TREK1 is able to interact with the variant, this last is not able to traffic to the plasma membrane by itself. Unfortunately in that case, TREK1 remains maintained in an intracellular compartment instead of acting as a chaperone.

If the creation of a new heteromer gives the cell a way to finely tune the resting membrane potential and the numerous functions in which the channels are involved, it can also lead to non-functional channel, by exerting a dominant negative effect on other subunits (as seen in Andersen's disease).

Domains involved in heteromerization. We have shown that TREK1 is able to interact with MT2, the second moiety of TRESK channel, but not with MT1, the N-terminus moiety. TM1 and P1 may be involved in the heteromerization with TRESK, whereas TM3, P2 and TM4 may be involved in the recognition between TREK1/2 and TRESK. The mutation of the cysteine to arginine in the TRESK-C110R mutant may induce a change of conformation that would avoid the recognition between the mutant and TREK1/2.

Isoforms of TREK1 lacking the C-terminus are still able to heteromerize with wild-type TREK1, meaning that C-terminus may not be mandatory for the heteromerization process (Veale et al., 2010). Blin and collaborators have shown that heteromerization does not depend on the isoforms. Thus, the ability of the different isoforms of TREK2 to form heteromers with isoforms of TREK1 increases complexity but also diversity of properties between the different TREK1/TREK2 heteromers (Blin et al., 2016).

Gain of function linked to heteromerization. TREK1 and TRESK have a comparable role in maintaining the resting potential. However, many differences in their regulations appear. The formation of heteromers therefore presents itself an alternative regulatory, from two subunits, three types of different channels are formed. In addition, at the level of the regulation of global currents, the heteromers, activated or inhibited more subtly than the monomer TREK1, could play a "buffer" role by avoiding too abrupt regulations by these stimuli. This would bring more control in the regulation of background currents, and the physiological functions associated with them. Finally, with the characteristics that are their own, these heteromers could also intervene preferentially in certain physiological processes for which they would have a more suitable profile; as has been postulated for TWIK1/TREK1 in passive conductance in the astrocyte (Hwang et al., 2014, and see chapter Heteromerization p.92).

TWIK/TREK interaction found by Hwang and collaborators, in our hands, using the single molecule pull down, together with the TREK1-PCS subunit experiments, have never been demonstrated. This phenomenon could be due to the lack of affinity between these two subunits, under the limit of the detection range by SiMPull. Indeed, the lysis process could break the interaction between these subunits. Furthermore, maybe that the engineered cysteine in the light gated TREK1 could avoid the formation of a disulfide bound between TWIK1 and TREK1. Finally this interaction could simply

just not be existing. Further characterizations need to be made to understand these different results.

2. Pathophysiological involvement of the heteromers

The existence of TREK1/TREK2 heterodimers has been recently revealed in DRG neurons using the differential sensitivity of TREK1 and TREK2 to spadinine and ruthenium red (Lengyel et al., 2016). In these neurons, they are at the origin of a conductance that differs from the homomers. We can imagine that it can play a role in the transmission of the action potential from nociceptors to second order neurons.

Blin and collaborators assessed the regulation by PKA and PKC of the heterodimer TREK1/TRAAK and demonstrated a differential regulation compare to the homomeric version of these two channels. We also assessed the sensitivity of TREK1/TRAAK heterodimer to PLD2. This difference in regulation is a dynamic adaptive response to stimuli. For instance, if there is a co-expression of TREK1 and TRAAK, TREK1 being mostly associated with TRAAK, it will allow a potentiation of the current by PLD2, a response that would not exist if only TRAAK was expressed. We can describe the same adaptive mechanism with PKA and PKC. In a neuron expressing both TREK1 and TRAAK a regulation by G_q protein will have a lesser effect than in a neuron only expressing TREK1, leading to an absence of depolarization, and any further response. The ratio of homo versus heterodimers present on the cell surface is a way to tune its response to stimuli.

The presence of the heteromer TREK1/TREK2 would have an effect during ischemia or other pathophysiological processes. For instance, ischemia exerts on the environment an extracellular acidification (Lesage and Barhanin, 2011). This last would exert an activation of the TREK1/TREK2 heteromer and TREK2, leading to an increase of potassium current and thus a decrease of excitability, protecting the neuron against death.

It is interesting to note that the regulation of TREK1-TRESK by the acidification of the intracellular pH leads to a higher current increase than the one found in TREK1. This increase in TREK1 current by intracellular acidification has been demonstrated to be involved in cerebral neuroprotection during ischemia (Heurteaux et al., 2004). The

heteromer being more sensitive than TREK1, we can imagine a primordial role of this one in this neuroprotective process.

B. Physiological implications of TRESK and TREKs as background K⁺ channels

1. Functional expression of TRESK and TREK1/TREK2 in TG neurons

We validated in three ways the expression of these channels in TG neurons. First we did qPCR on whole trigeminal ganglia, then single cell RT-PCR, from patched neurons, to know the differential expression in each tested cell. And finally using antibodies. This last experiment can be controversial, due to the lack of specificity of the antibodies targeting TREK1 and TREK2. In the single-cell PCR study we obtained reproducible results for three K_{2P} channels: TREK1, TREK2, and TRESK. The single-cell PCR study did not reveal significant differences in distribution for TREK or TRESK channels. Therefore we can definitely imagine a possibility for these channels to interact and form heteromers in these cells.

2. TREKs and TRESK involvement in pain sensation

Concerning the temperature sensitivity, it has been well characterized that TREK1, TRAAK and TREK2 are the ones involved in noxious and non-noxious detection of temperature (Alloui et al., 2006; Noël et al., 2009; Pereira et al., 2014). Recently, using combined techniques of immunoreactivity and electrophysiology, TREK1, TREK2 and TRAAK expression have been verified in rat DRG neurons (Viatchenko-Karpinski et al., 2018), suggesting their role in the temperature sensitivity of these fibers. There, TRP channels are considered to be major cellular sensors of such stimuli since they are sensitive to temperature as well as cell volume. TRP channels activated by these stimuli lead to an influx of cations, leading to depolarization and thus increase excitability of the cell. TREKs channel could counterbalance these excitability by tuning the potassium efflux.

The presence of TRESK in the capsaicin-sensitive small trigeminal neurons reduced the spike frequency, decreasing the resting membrane potential, thus excitability in

contrast of the effect of the capsaicin-sensitive TRPV1 channel, a non-selective cation channel.

This indicates a major role for TREKs and TRESK channels in DRG and TG neurons to regulate cell excitability in response to different stimuli. By their presence in these fibers, and their several modes of activation, TREKs and TRESK could also have a major role in the transmission of sensory information: we have shown here that, by dominant negative effect of TRESK mutant, a disease can occur, the migraine. Inhibition of these channels, by neurotransmitters, or genetic defection, leads to an increase of excitability.

To have shown that TREK1/2 and TRESK are able to interact and form functional heterodimers which properties that differ from homomers, we can wonder how heteromers would behave *in vivo*. TREK1 being inhibited by neurotransmitters that act on G_q protein pathway, and TRESK being activated by the intracellular increased concentration of calcium induced by such pathway, it seems interesting to study these mechanisms in native TG neurons and compare between WT and TREK1/TREK2 KO mice. To test it, we could also use the new StarTREK mice model in which we can remote control the activity of TREK using the light.

C. TREK channels to treat migraine

Recent investigations in structure and function of TREK and TRESK channels give rise to the development of potent and selective TREKs and TRESK channel openers as potential analgesics. Trigeminal and dorsal root ganglia lying outside the blood-brain bilayer, it provides a selected way to modulate TREK and TRESK in primary afferent neurons, without touching the channels expressed in the CNS and therefore allowing specifically action on pain.

An idea to treat the alternative translation: hide the Kozac consensus site with a microRNA (miRNA), so ribosome would not fix the second Kozac sequence. This methodology has been used recently in the disease discussed earlier in the manuscript, the spinocerebellar ataxia type 6 (SCA6). To completely remove the CACNA1A gene expression being lethal, they used a miRNA embedded in a virus approach to downregulated the translation of the poison peptides by targeting the IRES sequence at the origin of its translation (Pastor et al., 2018).

VII. Perspectives

A. Frameshift induced alternative translation initiation as a new mechanism for genetic diseases

1. Database analysis of frameshift mutants

Thanks of a collaboration with Arnaud Droit in Quebec, we have been able to start a project on frameshift mutations. Using the database Exac, our collaborators look forward the different insertion/deletion that would that would lead to fsATI allowing the translation of a second protein fragment. This insertion/deletion was supposed to put in frame of the sequence of the protein after the occurring mutation.

We helped these bioinformatics to create filters, indicating what they had to investigate in the database, and then compute the data together in a table. Our criteria were the following:

- Mutation of the gene must have not been a multiple of 3 nucleotides, either insertion or deletion, otherwise the frameshift would never have occurred
- Potential new ATGs had to be before the mutation, 5' upstream
- ATGs need to be embedded by a kozak sequence and need to be predicted to be a strong START initiation site
- Calculate the proportion of the size of the truncated protein compare to the wild type form of the protein
- The similarity between the new protein and the wild type is expected to be the same, excepted for the N-terminus. The new protein needs to be able to interact with the wild-type form, thus we need a protein sequence with a sufficient size
- Found the Clinvar association disease to know if the disease has been reported
- The expected product is expected to have a dominant negative effect on the wild-type version of the complexed subunit.

Starting from this database, the idea was then to characterize the functional effect of this mutation by generating the mutant using molecular biology techniques (see example KCNQ1 below p.182). Using electrophysiological properties for instance or Single Molecule Pull down, we would investigate their ability to interact. Cell imaging

will help us determine rather there was a co-synthesis of a peptide tagged in N-terminus and C-terminus with two different colors.

2. KCNQ1

Via analysis of databases, we have been able to select one potassium channel of interest, involved in a disease. This channel was selected because it reunited all the criteria depicted above.

As observed for TRESK, a mutation in KCNQ1 sequence led to a dominant negative form of KCNQ1, that completely inhibit the WT current formed by association between KCNQ1 and KCNE1. This mutation termed KCNQ1del572-576 was found to lead, as it was the case in TRESK-MT, to a second translated protein, using an alternative translation initiation, that has been put in phase with the ORF of the wild type subunit thank to the 4 base pair deletion leading theoretically to an N-terminus truncated channel. In fact, expression of this mutant, in which mCherry was in frame with the first ORF and GFP with the second ORF, leads to cells expressing both mCherry and GFP.

mCherry-KCNQ1del572-576-GFP

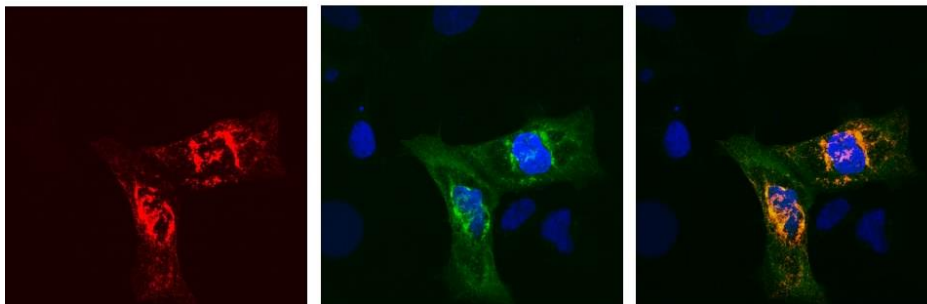


Figure 40: MDCK cells expressing mCherry-KCNQ1del572-576-GFP, the supposed to be truncated version of KCNQ1. mCherry-KCNQ1del572-576-GFP expression leads to cell which are red and green showing the coexpression of 2 proteins.

In order to see if this second translated protein could be involved in the inhibition of this channel, we inserted a stop using molecular biology, just after the mutation (KCNQ1del572-576STOP). The existing alternative start codon, if used as so, would no longer lead to expression of the mutant (see Figure 40).

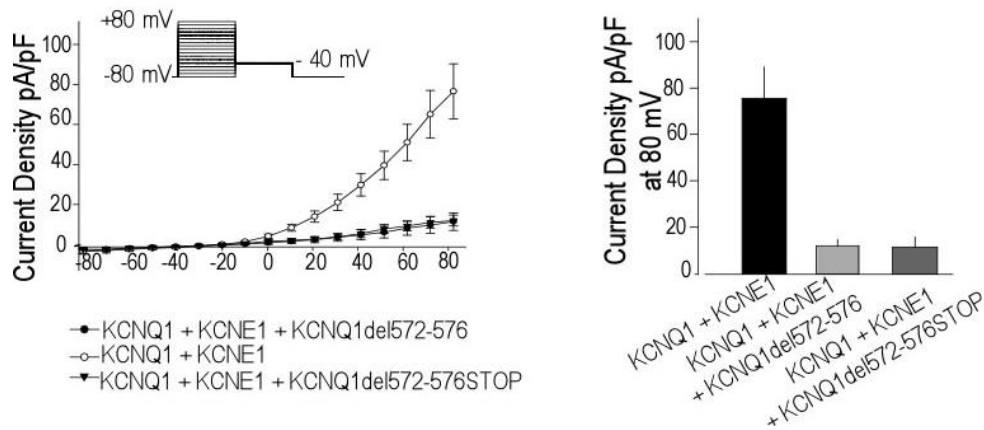


Figure 41: Translation of a second protein is not at the origin of a dominant negative effect on KCNQ1. Co-expression of KCNQ1del572-576 is at the origin of a dominant negative effect on KCNQ1. The insertion of a STOP codon after the mutation does not restore KCNQ1 current, even with different ratio (data not shown).

As shown in Figure 41, this stop-codon did not abolish the ability of the mutant to inhibit KCNQ current. Therefore, in this case, the second transcript is not involved in the inhibition.

B. SiMPull: toward an automatization

Single molecule pull down is more efficient than conventional immunoprecipitation assays. It allows to:

- test the ability of two different partners to interact,
- reveal the stoichiometry of protein complexes,
- decipher different treatments affecting the complexes,
- directly visualize cellular protein complexes in a fast and efficient way.

All the above in SiMPull assay is furthermore easy to assess, due to the shortness preparation conditions, and improved use of total internal reflection fluorescence microscopy (TIRFM).

Nowadays, the use of high-throughput techniques to assess an increased number of conditions at once, would worth it in SiMPull assay. Using microfluidics together with beads coated with several antibodies for instance, it sounds possible to flow the lysate and determine different interactions in a high-throughput manner. Leading this technique to be a useful tool to highlight unknown partners of a bait of interest.

1. Advantages of TIRF microscopy

Several events occur in cellular surface in mammalian cells and have already been studied using old fashion microscope techniques combined with fluorescence. For instance the binding of cells by hormones, the secretion of neurotransmitters, or even the membrane dynamics. The main issue of these microscope techniques used to study membrane trafficking is the background fluorescence that we cannot get rid of. Indeed, the fluorophores that are not bound to the specimen surface remain in the medium environment of the sampled image, and create a signal often higher than the one detected from the fluorophores of interest. Total internal reflection fluorescence microscopy (TIRFM) allows for selective excitation of the surface-bound fluorophores, while non-bound molecules are not excited and do not fluoresce. Due to the fact of sub-micron surface selectivity, TIRFM has become a method of choice for single molecule detection.

Also, the objective possesses a high numerical aperture that can produce high contrast images even with weak fluorescent signal. The evanescent wave resulting from this objective is just on the edge of the sample, with a very small penetration depth.

To observe a membrane trafficking or an internalization of protein from the plasma membrane, we could use TIRF microscopy in living cells, and mark them with SNAP-tags. We could observe across the time, the de novo formation of protein at the plasma membrane, or the disappearance of protein pool from the membrane.

2. Transition from coverslips to beads

Beads can be well adapted for high-throughput when using microfluidic. During my PhD, I attempted to pass from the coated coverslips to 1 mm diameter coated beads to work with single molecule. To do so would have been more convenient for several reasons, the first one being the time spend to only have 8 passivated and coated slides, each of them allowing 5 samples. The main advantages of beads compare to use passivated and coated slides is that we could use beads to target one bait in several samples or several beads, each targeting one bait, in one sample (see Figure 43).

Beads would have been passivated by hundreds at a time, and each of these beads would have been used for one sample. This schematic sums up the idea of the single molecule pull down on beads (SiMBeads).

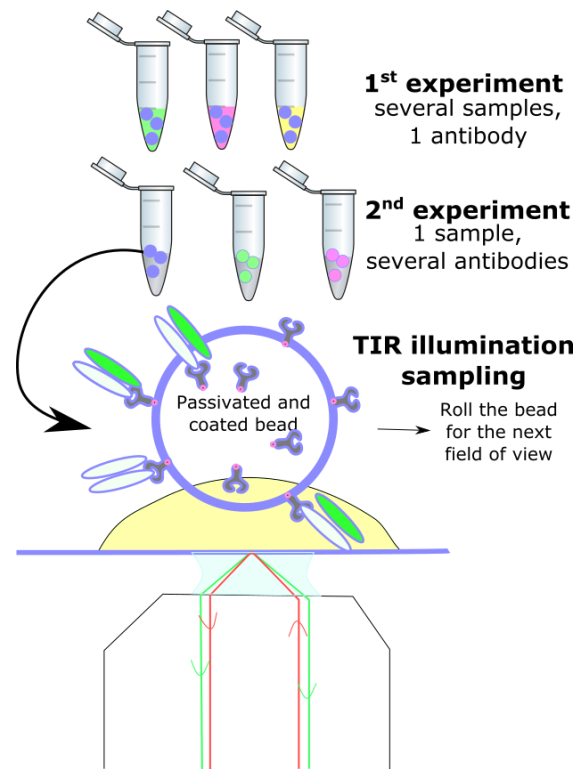


Figure 42: Schematic representation of the SiMBeads. 2 different sets of experiment can be assessed:

- antibodies against one bait, but different lysates samples,
- different beads, each one carrying antibodies targeted against one prey, in the same lysate sample.

The blue ellipse represents the bait, the green one is the prey, tagged with a green fluorescent protein, or revealed with a specific antibody, and a secondary carrying a fluorescent protein.

The constraints for the beads are the following :

Passivation: Beads must resist several treatments, such as sonication, aminosilation using acetic acid, and very concentrated KOH solutions to then be frozen. Silicate beads have been found to perfectly fit.

Drying: The second problem was to dry the beads. Indeed, these very small beads of 1 mm diameter fly away when the air is approached to dry them, but they must not be touched, otherwise the passivation and coating is spoiled. Cell strainers were used to dry them in an enclosed space.

Having been able to prepare these beads, we have now to work on an automatic microfluidic system that would allow to present beads in high-throughput manner to a TIRFM system.

VIII. Conclusions

In the present study, we gave new examples of heteromers formed among K₂P family, and suggested some of their potential roles *in vivo*, due to their regulations.

We provided the first evidence that an alternative translation initiation induced by a frameshift mutation is at the origin of a migraine phenotype, linked to trigeminal neuron excitability. This way, we shed light on a controversial statement, in which two mutations of TRESK, both leading to a complete loss of function of TRESK and a dominant negative effect on WT-TRESK, were not both associated to a migraine phenotype.

The composition of K₂P channels might be controlled by the level of affinity between the different subunits. However, this composition can also be randomized and relies on the level of transcription of each subunit. The mechanisms of assembly, composition and identification of the regions involved in the assembly of the K₂P channels still remain to be identified.

Ci-VSP stoichiometry and assembling

In the introduction, we have seen that phosphatidylinositol phosphates (PIPs) were important regulators of K_{2P} channels. These lipids can either act directly on K_{2P} channel activities, or as second messengers in transduction pathway. Voltage sensing phosphatases (VSPs) are all-in-one proteins, which directly couple the voltage sensing and the enzyme catalysis. They combine an N-terminal voltage-sensing domain (VSD) resembling that of ion channels and a C-terminal phosphatase domain (PD) homologous to PTEN (phosphatase and tensin homologue deleted on chromosome 10). PD dephosphorylate 3- and 5-phosphate from PIPs after activation by VSD. Not much is known about the pathophysiological process that involves direct coupling between voltage and PIPs concentrations.

Our collaborator Susy Kohout and its team previously published that the Ci-VSP functions as monomer (Kohout et al., 2008). Recent studies showing that the well-known tumor suppressor and homologue of VSP, PTEN, dimerizes made them reconsider their model. Interestingly, an inactivating mutation in one subunit of the dimer has a dominant-negative effect on function (Heinrich et al., 2015; Papa et al., 2014).

Using voltage clamp fluorometry assay, FRET experiments and SiMPull, we have been able to show that, Ci-VSP form dimers in a concentration dependent manner. This fact has already been reported for the formation of up to a 4:4 ratio depending on the concentration of KCNE1/KCNQ1 (Nakajo et al., 2010). We also have been able to show that the formation of dimers is driven by the voltage sensing domain (VSD) subunit, not the phosphatase domain (PD). The Ci-VSP monomer is a 5-phosphatase, whereas the dimer is both a 5- and a 3-phosphatase. This functional impact of dimerization on enzymatic activity could indicate that Ci-VSP signaling is regulated by expression and may ultimately play a role in its physiological function (Rayaprolu et al., 2018).

RESEARCH ARTICLE

Dimerization of the voltage-sensing phosphatase controls its voltage-sensing and catalytic activity

Vamseedhar Rayaprolu¹, Perrine Royal^{2,3}, Karen Stengel¹, Guillaume Sandoz^{2,3}, and Susy C. Kohout¹

Multimerization is a key characteristic of most voltage-sensing proteins. The main exception was thought to be the *Ciona intestinalis* voltage-sensing phosphatase (Ci-VSP). In this study, we show that multimerization is also critical for Ci-VSP function. Using coimmunoprecipitation and single-molecule pull-down, we find that Ci-VSP stoichiometry is flexible. It exists as both monomers and dimers, with dimers favored at higher concentrations. We show strong dimerization via the voltage-sensing domain (VSD) and weak dimerization via the phosphatase domain. Using voltage-clamp fluorometry, we also find that VSDs cooperate to lower the voltage dependence of activation, thus favoring the activation of Ci-VSP. Finally, using activity assays, we find that dimerization alters Ci-VSP substrate specificity such that only dimeric Ci-VSP is able to dephosphorylate the 3-phosphate from PI(3,4,5)P₃ or PI(3,4)P₂. Our results indicate that dimerization plays a significant role in Ci-VSP function.

Introduction

The discovery of voltage-sensing phosphatases (VSPs) changed how we think about the regulation of phosphatidylinositol phosphates (PIPs). PIPs are crucial lipid second messengers, responsible for regulating many basic cellular functions including cell proliferation, migration, development, synaptic regulation, and ion channel modulation (Di Paolo and De Camilli, 2006; Balla et al., 2009; Logothetis et al., 2010; Koch and Claesson-Welsh, 2012). VSPs link voltage sensing and enzyme catalysis in a unique way. They combine an N-terminal voltage-sensing domain (VSD) resembling that of ion channels and a C-terminal phosphatase domain (PD) homologous to PTEN (phosphatase and tensin homologue deleted on chromosome 10). The VSD responds to changes in membrane potential and then activates the PD to dephosphorylate both the 3- and 5-position phosphates from PIPs (Murata et al., 2005; Iwasaki et al., 2008; Halaszovich et al., 2009; Kohout et al., 2010; Kurokawa et al., 2012; Castle et al., 2015; Grimm and Isacoff, 2016). The VSP from *Ciona intestinalis* was the first to be well characterized (Murata et al., 2005), but VSPs are conserved across many species, including zebrafish (Hossain et al., 2008), mice (Wu et al., 2001; Rosasco et al., 2015), and humans (Walker et al., 2001). Until the discovery of these VSPs, the connection between voltage sensing and PIP signaling was thought to be indirect. We now know that VSPs are a direct link between the electrical and chemical signaling cascades in the cell. Interestingly, the cellular processes requiring voltage regulation of PIP concentrations are still unknown. Thus,

understanding how VSPs function will shed light on two critical signaling cascades and their cellular processes.

An important characteristic for any protein function is whether it multimerizes. Proteins form multimers for many reasons, including to enable, enhance, and regulate function. Some proteins, like the serotonin transporter SERT, form multimers in a dynamic and concentration-dependent manner (Anderluh et al., 2017). GABA_B receptors heterodimerize to function (Jones et al., 1998; Kaupmann et al., 1998; White et al., 1998) while also forming dynamic tetramers (Calebiro et al., 2013) and heteromultimers with auxiliary proteins (Schwenk et al., 2010). Metabotropic glutamate receptors function as either homo- or heterodimers (Kunishima et al., 2000; Doumazane et al., 2011). Other proteins are less variable. Receptor tyrosine kinases, like the epidermal growth factor receptor, dimerize upon ligand binding (Yarden, 2001; Schlessinger, 2014). Voltage-gated potassium channels are obligate or strict tetramers where the pore domains from four subunits assemble to form a central pore (Liman et al., 1992; Perozo et al., 1993; Doyle et al., 1998). Interestingly, the voltage-gated proton channel, Hv, functions as a dimer, but because the pore is located within each subunit, it also conducts protons as a monomer when the dimer interface is disrupted (Tombola et al., 2010). In addition, the Hv subunits are allosterically coupled in their dimer state, creating a positive cooperativity between the subunits (Tombola et al., 2010). These differences in multimerization are important for understanding

¹Department of Cell Biology and Neuroscience, Montana State University, Bozeman, MT; ²Centre National de la Recherche Scientifique, Institut National de la Santé et de la Recherche Médicale, iBV, Université Côte d'Azur, Valbonne, France; ³Laboratory of Excellence, Ion Channel Science and Therapeutics, Nice, France.

Correspondence to Susy C. Kohout: skohout@montana.edu.

© 2018 Rayaprolu et al. This article is distributed under the terms of an Attribution-Noncommercial-Share Alike-No Mirror Sites license for the first six months after the publication date (see <http://www.rupress.org/terms/>). After six months it is available under a Creative Commons License (Attribution-Noncommercial-Share Alike 4.0 International license, as described at <https://creativecommons.org/licenses/by-nc-sa/4.0/>).

how any protein functions on a molecular level and in its physiological context.

The same is true for *C. intestinalis* VSP (Ci-VSP), where knowing whether the VSDs and/or the PDs cooperate with each other is important for understanding how the protein will respond to cellular signals. Although one study suggested Ci-VSP may cluster into domains (Villalba-Galea et al., 2013), most researchers have not considered multimerization when analyzing Ci-VSP function, because our previous study concluded that Ci-VSP functions as a monomer (Kohout et al., 2008). The N and C termini of Ci-VSP were even used in an Hv/VSP chimera to monomerize the Hv channel (Tombola et al., 2010). However, new research sparked a reevaluation of our model. Specifically, recent studies show that the well-known tumor suppressor and homologue of VSP, PTEN, dimerizes, and an inactivating mutation in one subunit of the dimer has a dominant-negative effect on function (Papa et al., 2014; Heinrich et al., 2015). Other studies have shown that the Hv proton channel VSDs directly interact with each other, forming a functional dimer, independent of a separate pore domain (Koch et al., 2008; Tombola et al., 2010). In addition, the crystal structure of the WT VSP VSD found four subunits in the asymmetric unit organized as two dimers (Li et al., 2014). Collectively, these results suggest both the VSP VSD and PD could interact and function as more than just a monomer.

In this study, we find that VSP subunits interact with each other under high-concentration conditions, forming stable dimers. We also find that these dimers are functionally relevant. One subunit of the dimer is able to influence the VSD motions of the other subunit and the enzymatic activity changes when the dimer is favored at high-protein concentrations. We propose a model for VSP dimerization where the orientation of each subunit is important for catalysis.

Materials and methods

Molecular biology

The Ci-VSP in pSD64TF vector was provided by Y. Okamura (Osaka University, Osaka, Japan) and subcloned into pNice for the HEK293T experiments. PLC-PH-based Förster resonance energy transfer (FRET) sensor (fPLC) and TAPP-PH-based FRET sensor (fTAPP) were both provided by E.Y. Isacoff (University of California, Berkeley, Berkeley, CA). ASIC1A was provided by E. Lingueglia (Université Côte d'Azur, Valbonne, France). All mutations and N-terminal epitope tags were added using Pfu Turbo polymerase (Agilent). All DNA was confirmed by sequencing. Complementary RNA (cRNA) was transcribed using SP6 mMessage mMachine (Ambion) kits. The HEK293T cell line was verified by DNA fingerprinting by the Leibniz-Institut, Germany, and was confirmed to be a pure human cell culture with no detectable contamination of mitochondrial sequences from mouse, rat, or Chinese and Syrian hamster cells.

Voltage-clamp fluorometry (VCF)

VCF was performed as described previously (Castle et al., 2015). In brief, surgically removed *Xenopus laevis* oocytes were injected with 50 nl of 0.8–2.0 $\mu\text{g}/\mu\text{l}$ cRNA. The concentrations varied based on the type of experiment and the construct being injected.

Cells were incubated in ND-96 (96 mM NaCl, 2 mM KCl, 1.8 mM CaCl_2 , 1 mM MgCl_2 , 50 mg/ml gentamicin, 2.5 mM sodium pyruvate, and 10 mM HEPES, pH 7.6) at 18°C for 24–36 h.

A Leica DM IRBE inverted microscope with a Leica HC PL APO 20 \times /0.7 fluorescence objective was used with a Dagan CA-1B amplifier and illuminated with a Lumen Dynamics X-Cite XLED1 light source. Intensity was measured with a Thorlabs photomultiplier tube (PMT). The amplifier and light-emitting diode were controlled by a Digidata-1440A board and pClamp10.7 software package (Axon Instruments). For tetramethylrhodamine maleimide (TMRM) experiments, light was filtered through an HQ531/40 excitation filter, an HQ593/40 emission filter, and a Q562LP dichroic (Semrock). Fluorescence signals were low-pass filtered at 2 kHz through an eight-pole Bessel filter (Frequency Devices) for VCF and at 500 Hz for FRET.

On the day of the experiment, oocytes were transferred to a high-potassium solution (92 mM KCl, 0.75 mM CaCl_2 , 1 mM MgCl_2 , and 10 mM HEPES, pH 7.5). TMRM (Invitrogen) was added at a final concentration of 25 μM , and the cells were left in the dark on ice for 30 min. Labeled oocytes were then extensively washed and stored in ND-96' (ND-96 without gentamicin or pyruvate) at 12–18°C until the end of the experiment. The VCF voltage protocol consisted of 10-mV steps starting at –150 mV and ending at 200 mV with a holding potential of –80 mV. The measured fluorescence was then plotted against the applied voltage to generate the fluorescence–voltage relationship.

Fluorescence measurement of activity

FRET-based PIP sensors (Grimm and Isacoff, 2016) were used to measure either $\text{PI}(4,5)\text{P}_2$ (phosphatidylinositol-4,5-bisphosphate) or $\text{PI}(3,4)_2$ (phosphatidylinositol-3,4-bisphosphate). Specifically, we used the pleckstrin homology (PH) domain from PLC for $\text{PI}(4,5)\text{P}_2$ and the PH domain from the tandem PH domain containing protein 1 (TAPP) for $\text{PI}(3,4)_2$. The FRET sensors were designed with an N-terminal CFP and a C-terminal YFP and were called fPLC and fTAPP, respectively. fPLC cRNA was injected at 0.8 $\mu\text{g}/\mu\text{l}$, and fTAPP was injected at 0.4 $\mu\text{g}/\mu\text{l}$. For testing the N-terminal tagged Ci-VSPs, 0.8 $\mu\text{g}/\mu\text{l}$ of tagged VSP cRNA was mixed with either the fTAPP or fPLC cRNA and injected. For the concentration-dependence activity assay, cRNA concentrations ranging from 0.02 to 1.6 $\mu\text{g}/\mu\text{l}$ encoding His-tagged Ci-VSP (His-VSP) were mixed with fTAPP cRNA and injected. For the mixture of active and inactive VSP, His-VSP and the catalytically dead C363S mutant with a FLAG tag (FLAG-CS) were mixed at a ratio of 1:10 (0.1:1.0 $\mu\text{g}/\mu\text{l}$ or 0.2:2.0 $\mu\text{g}/\mu\text{l}$) along with the fTAPP cRNA. In all experiments, 50 nl of the mixtures was injected into oocytes and then incubated in ND-96 for no less than 36 h.

On the day of the experiments, cells were labeled with TMRM as listed above. After incubation, oocytes were washed with ND-96' and stored in ND-96' containing 8 μM insulin to promote PI3 kinase activity and up-regulate $\text{PI}(3,4,5)\text{P}_3$ levels. Ci-VSP expression was confirmed in each oocyte by VCF as described above. For PH domain experiments, light was filtered through a HQ436/20 excitation filter and directed to the objective with a 455LP dichroic (Chroma). The microscope cube did not contain an emission filter, because the Thorlabs PMT module contains its own cube. Thus, the emitted light was filtered before the PMTs

with a 510-nm dichroic, an HQ480/40 emission filter for CFP, and an HQ535/30 emission filter for YFP (Chroma). The voltage protocol consisted of steps from -100 to 160 mV in irregular increments. Rest periods of 1 min between voltage steps were used to allow the cell to recover depleted PIP concentrations before the next voltage step. The resulting fluorescence was then plotted versus the voltage to generate the fluorescence versus voltage relationship.

Abs and Ab beads

6x-His epitope tag Ab (His.H8) was purchased from Invitrogen. Talon Cobalt affinity resin (635501) was purchased from Takara Bio Inc. c-Myc (9E10) Ab was purchased from Developmental Studies Hybridoma Bank. Monoclonal FLAG M2 Ab (F1804-50UG), anti-FLAG M2 affinity gel (A2220-1ML), and anti-c-Myc agarose conjugate (A7470) were purchased from Sigma-Aldrich. Biotinylated anti-HA (human influenza hemagglutinin) Ab (ab26228) was purchased from Abcam. Secondary anti-mouse conjugated to horseradish peroxidase was purchased from GE Healthcare (NA931-100UL).

Coimmunoprecipitation

Oocytes were injected with 50 nl of 0.4–0.8 $\mu\text{g}/\mu\text{l}$ cRNA for each construct. For a mixture of constructs, injection concentrations for each construct were kept the same as the unmixed construct. Oocytes were incubated for 24–36 h in ND-96 at 18–21°C. Protein expression was confirmed using VCF as described above. After expression, four oocytes per construct were lysed in 200 μl lysis buffer (150 mM NaCl, 0.1% IGEPAL, and 20 mM Tris-base, pH 7.6, with protease inhibitors added [25 $\mu\text{l}/\text{ml}$, Pierce Protease inhibitor tablets without EDTA]). The lysate was centrifuged at 21,100 g for 15 min at 4°C. 180 μl of the supernatant was transferred into a fresh tube and centrifuged again for 5 min. 160 μl of the supernatant was split into three parts (two aliquots of 65 μl and one aliquot of 30 μl). Cobalt beads were added to one of the 65- μl aliquots, and anti-FLAG or anti-Myc beads were added to the other aliquot depending on which epitope tag was used. These samples were left to mix overnight at 4°C. The 30- μl aliquot was stored at -20°C and used as an input control. The samples with the beads were then centrifuged at 2,400 g for 5 min at 4°C to precipitate the beads. The supernatant was discarded, and the beads were washed with lysis buffer twice. After the last wash, 50 μl of 4 \times sample buffer was added directly to the beads and boiled for 3 min at 95°C. The samples were then centrifuged at 2,400 g for 5 min at room temperature. The supernatants were collected, and 6 μl of 1 M dithiothreitol was added to each. To the input control, 10 μl of 4 \times sample buffer and 5 μl of 1 M DTT were added. All samples were again boiled for 7 min at 95°C. The samples were then electrophoresed at 200 mV for 55 min on a 10% SDS-polyacrylamide gel.

Western blotting

The samples were transferred from the polyacrylamide gel onto a nitrocellulose membrane at 350 mA for 70 min using a sodium borate buffer system. After transfer, the membranes were incubated in blocking buffer (5% milk in 1 \times TBS-T) for 15–30 min. Blocking buffer was then replaced with the corresponding

primary Ab solutions (1:2,000 dilution prepared in blocking buffer) and incubated overnight at 4°C with shaking. Membranes were then washed three times with 1 \times TBS-T (5–10 min). Secondary Ab solutions prepared in blocking buffer (1:4,000 dilution) were added to the membranes and incubated for 1 h at room temperature. Washes with 1 \times TBS-T were repeated three times (5–10 min each). Membranes were developed using WesternBright ECL reagents (Advansta).

SiMPull

For SiMPull experiments, 24 h after transfection using Lipofectamine 2000 (Invitrogen), HEK239T cells were harvested from 35-mm Petri dishes by incubating with Ca^{2+} -free PBS buffer for 20–30 min, followed by gentle pipetting. Cells were pelleted and lysed in buffer containing 50 mM Tris-HCl, 150 mM NaCl, 1 mM EDTA, protease inhibitor mixture (Thermo Scientific), and 1.5% (vol/vol) IGEPAL (Sigma). After a 30–60-min incubation at 4°C, lysate was centrifuged for 20 min at 15,000 g, and the supernatant was collected. Coverslips passivated with polyethylene glycol (PEG) (~99%)/biotin-PEG (~1%) and treated with Neutravidin (Thermo Scientific) were prepared as described previously (Jain et al., 2011). Biotinylated anti-HA (15 nM) was applied for 20 min and then washed out. Anti-HA dilutions and washes were done in T50 buffer containing 50 mM NaCl and 10 mM Tris, pH 7.5. Lysate, diluted at 1:10 in T50 with BSA, was then applied to the chamber and washed away after a brief incubation (~2 min). Single molecules were imaged using a 488-nm argon laser on a total internal reflection fluorescence (TIRF) microscope with a 100 \times objective (Nikon). We recorded the emission light after an additional 3 \times magnification and passage through a double-dichroic mirror and an emission filter (525/50 for GFP) with a front-illuminated CMOS camera (Zyla 4.2 PLUS sCMOS; Andor). Movies of 250 frames were acquired at frame rates of 10–20 Hz. The imaged area was 13 \times 13 μm^2 . Representative datasets are presented to compare conditions tested on the same day quantitatively.

Data analysis

Fluorescence traces were analyzed using Clampfit 10.7 (Molecular Devices), IGOR Pro (WaveMetrics), and Excel (Microsoft). Steady-state voltage-dependent traces were fit with either single or double Boltzmann equations. TMRM data were normalized to the maximum amplitude of the Boltzmann fits, whereas the PH domain data are shown as $\Delta\text{F}/\text{F}$. Error bars indicate SEM. No explicit power analysis was used to predetermine the sample size for any experiments in the article, but the sample sizes used were comparable to those in previous publications. Fluorescence experiments were repeated on three different days using at least three different batches of oocytes (biological replicates) until a minimum n of 10 was reached (technical replicates). A batch of oocytes is defined as coming from a single frog. Coimmunoprecipitation experiments (from expression to Westerns) were repeated on three different days using at least three different batches of oocytes until a minimum n of 4 was reached.

Photobleaching data were analyzed using ImageJ (National Institutes of Health). Only single and diffraction-limited spots were included for analysis, and the number of spots per movie (768 \times 768 pixels ~100 μm^2) was determined manually using

ImageJ software. For each condition, we used at least four independent movies derived from at least four different HEK293T transfections (biological replicate). Then, the number of bleaching steps was manually determined using ImageJ software from at least three independent movies (~50 spots per movie were quantified, technical replicate). Regions of clustered or not fully diffraction limited spots were excluded, as well as spots that moved, showed extreme intensity fluctuations, or unequal bleaching steps. The bleaching step histograms present pooled data, taken from at least three different movies. For both, the error bars give the statistical uncertainty for a counting experiment, which is \sqrt{n} , for n being the number of counts (Reiner et al., 2012). For statistical analysis, when the distribution was normal and the variances of the two populations are assumed to be equal, we used the Student's t test to determine significance.

Online supplemental material

Table S1 summarizes the voltage dependence of VSD motions. Fig. S1 shows that the catalytically inactive VSP (C363S) mutant does not alter PIP concentrations in oocytes. Fig. S2 shows the uncropped Western blots shown in Fig. 2. Fig. S3 shows Western blots from oocytes injected with increasing cRNA concentrations. The higher concentrations of cRNA led to higher protein expression, validating the protein concentrations used in Fig. 7 b. Fig. S4 shows Western blots from oocytes injected with a 1:10 ratio of WT and C363S, validating the relative protein concentration used in Fig. 7 d.

Results

N-terminal tags do not alter Ci-VSP function

To differentiate the potential subunits within a Ci-VSP complex, we attached N-terminal epitope tags: a 6xHis tag, a FLAG tag, a Myc tag, and an HA tag. This allowed us to use validated Abs in our pull-downs and Westerns. We tested both the VSD motions and the catalytic activity of each tagged VSP to ensure the tags did not interfere with normal VSP function. First, the VSD motions were tested using VCF, a technique that uses environmentally sensitive fluorophores to track protein conformations in a voltage-dependent manner (Mannuzzu et al., 1996). In brief, each protein was engineered with an external cysteine in the S3-S4 loop, G214C, for labeling with TMRM (labeled proteins denoted with an asterisks). The kinetics of the VSD motions (Fig. 1 a) and the voltage dependence of those motions (Fig. 1 b and Table S1) were similar between WT Ci-VSP (WT*), His-VSP*, FLAG-VSP*, Myc-VSP*, and HA-VSP*. The N-terminal tags do not change how the VSD from Ci-VSP responds to voltage.

Second, we tested the catalytic activity of the tagged VSPs. Ci-VSP functions as both a 3- and 5-phosphatase, catalyzing four different reactions (Fig. 1, c and d; Murata et al., 2005; Iwasaki et al., 2008; Halaszovich et al., 2009; Kohout et al., 2010; Kurokawa et al., 2012; Castle et al., 2015; Grimm and Isacoff, 2016). To monitor all Ci-VSP reactions, PH domains that bind specific PIPs were used (Stauffer et al., 1998; Halaszovich et al., 2009; Castle et al., 2015; Grimm and Isacoff, 2016). In particular, we used a FRET-based PH domain assay where CFP and YFP are fused to a PH domain anchored to the membrane through a prenylation site at the C terminus (Fig. 1 e; Sato et al., 2003; Grimm and Isacoff,

2016). As the PH domains from these sensors bind to their respective PIPs, a conformational change is induced, which results in an increased FRET signal between the CFP and YFP proteins (Fig. 1 e). As the appropriate PIP is depleted, the PH domain unbinds and the FRET signal decreases. We chose the PH domains from PLC and TAPP because they bind specifically to PI(4,5)P₂ and PI(3,4)P₂, respectively. Both fPLC and fTAPP change their FRET signals with changing concentrations of their respective PIPs (Grimm and Isacoff, 2016). For fPLC and WT*, the expected increase in fPLC FRET, after the 3-phosphatase activity, was too small to accurately analyze (<0.1% $\Delta F/F$); however, we observed a robust decrease in fPLC FRET after the 5-phosphatase activity (Fig. 1 f). When testing the N-terminal tagged proteins (His-VSP*, FLAG-VSP*, Myc-VSP*, and HA-VSP*) using fPLC, we found the catalytic activity indistinguishable from WT* (Fig. 1 e). For fTAPP and WT*, the expected increase and decrease in fTAPP FRET, after the known 5- and 3-phosphatase activities, was observed (Fig. 1 f). When using fTAPP with the tagged VSPs, minor shifts in voltage dependence were seen between the tagged VSP*s and WT* (Fig. 1 g). To control for the endogenous VSP present in *X. laevis* oocytes, we tested both sensors with catalytically dead Ci-VSP, C363S (CS*), and found minimal changes in FRET, even at the highest voltages tested (Fig. S1). Overall, the N-terminal tags do not adversely influence either the VSD motions or catalytic activity of Ci-VSP, allowing us to use them in various assays to probe for Ci-VSP multimerization.

Coimmunoprecipitation indicates higher-order multimers in Ci-VSP

We next performed coimmunoprecipitations with the N-terminal tagged Ci-VSPs to determine whether VSP multimers are present. The cRNA for both His-VSP and FLAG-VSP or His-VSP and Myc-VSP were coinjected into *X. laevis* oocytes, and protein expression was confirmed by VCF 24–36 h later. Cells injected with His-VSP alone, FLAG-VSP alone, or Myc-VSP alone were tested as positive controls and to ensure no cross-reactivity existed between the N-terminal tags. Untagged Ci-VSP (WT) was also tested as a negative control. Expressing cells were lysed and tagged proteins pulled down with Co²⁺ beads or immunoprecipitated with anti-FLAG-coated beads or anti-Myc-coated beads to be tested by Western blot. The Co²⁺, anti-FLAG-, and anti-Myc-coated beads all pulled down a protein band corresponding to the expected molecular weight for monomeric Ci-VSP, ~66 kD (Fig. 2, a and c, lanes 6 and 8; Fig. 2 b, lanes 11 and 12; Fig. 2 d, lanes 11 and 12). No nonspecific interactions were observed with any of the pull-down controls; for example, no His-VSP* was observed in the His-VSP*-only sample when pulled down with anti-FLAG beads (Fig. 2 a, lane 10). When the mixtures were pulled down using Co²⁺ beads, the FLAG-VSP* from the His/FLAG mixture (Fig. 2 b, lane 8) and the Myc-VSP* from the His/Myc mixture (Fig. 2 d, lane 8) showed consistent bands at ~66 kD, indicating they interact with the His-VSP*. The reverse was also observed where the anti-FLAG-coated beads coimmunoprecipitated the His-VSP* from the His/FLAG mixture (Fig. 2 a, lane 12), and the anti-Myc-coated beads coimmunoprecipitated the His-VSP* from the His/Myc mixture (Fig. 2 c, lane 12). These results show that at least two Ci-VSP subunits interact with each other, suggesting Ci-VSP exists as multimers.

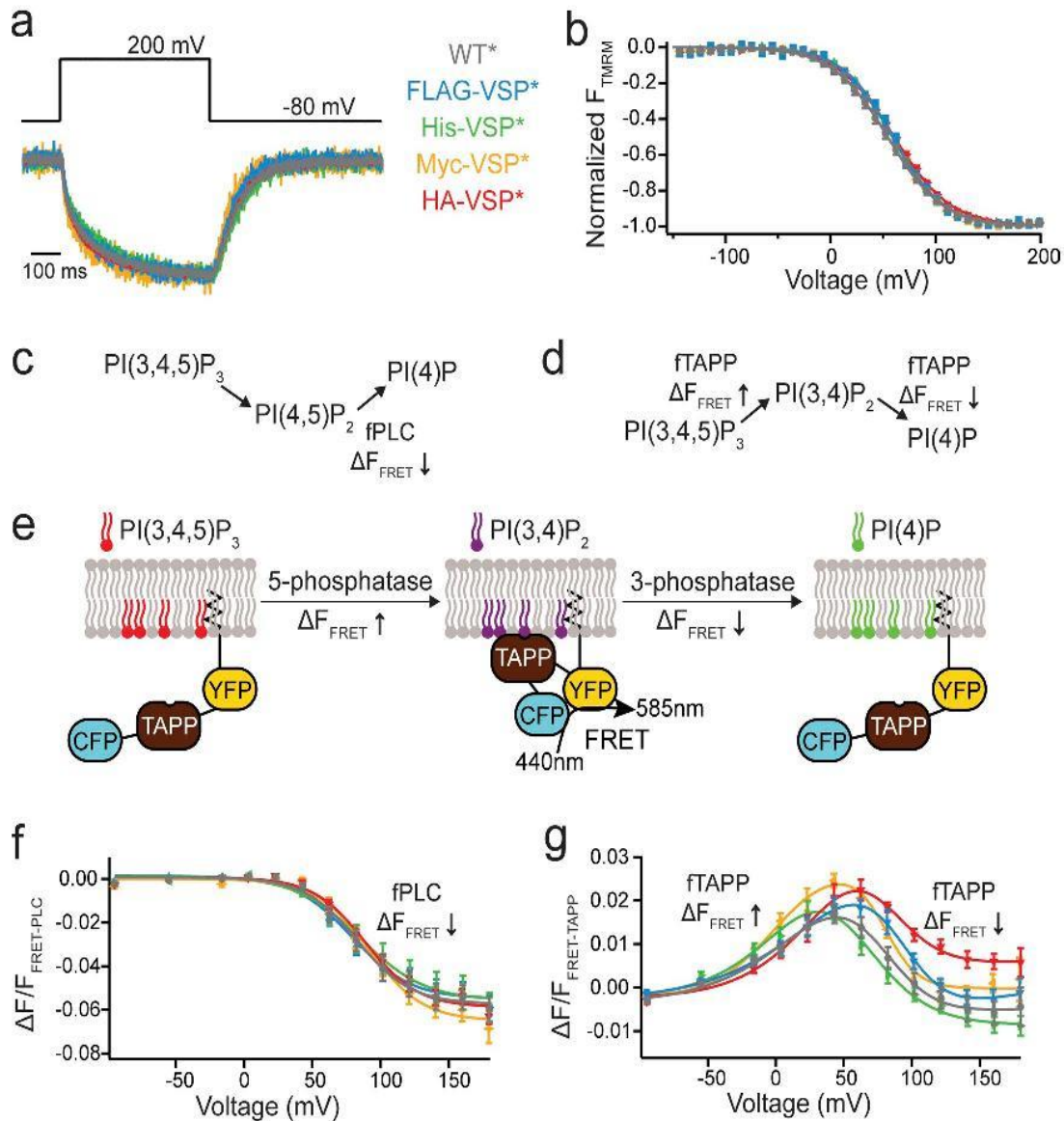


Figure 1. N-terminal tags do not alter Ci-VSP function. (a) Representative TMRM fluorescence traces during a step from a holding potential of -80 to 200 mV for WT*, FLAG-VSP*, His-VSP*, Myc-VSP*, and HA-VSP* (where the * indicates TMRM labeling). Traces are normalized to the maximal fluorescence change. The voltage trace shows the actual voltage recorded during acquisition. (b) Normalized TMRM fluorescence versus voltage relationship. Data fit to single Boltzmann equations. None of the N-terminal tags alter the kinetics or the voltage dependence of the VSD motions, indicating they are not influencing VSP function. $n \geq 11$. Some error bars are smaller than the size of the symbols. (c and d) Schematics of the VSP reactions where the fPLC monitors the PI(4,5)P₂ reactions and the ftAPP monitors the PI(3,4)P₂ reactions. (e) Cartoon representation of ftAPP binding and release with increasing and decreasing PI(3,4)P₂ concentrations. The binding of ftAPP to PI(3,4)P₂ results in a conformational change that increases the FRET signal. Similarly, a reduction of PI(3,4)P₂ results in a decrease in the FRET signal. (f) $\Delta F/F$ fPLC FRET ratio versus voltage relationship shows a fluorescence decrease (net 5-phosphatase reaction). $n \geq 9$. Data fit with a single Boltzmann equation. (g) $\Delta F/F$ ftAPP FRET ratio versus voltage relationship with the fluorescence increase (net 5-phosphatase reaction) predominating at lower voltages and the fluorescence decrease (net 3-phosphatase reaction) predominating at higher voltages. $n \geq 11$. Data fit with a double Boltzmann equation. Error bars are \pm SEM.

SiMPull indicates two subunits in VSP complex

If Ci-VSP subunits are capable of interacting with each other, then a single molecule pull-down (SiMPull) assay will determine the exact number of subunits within a Ci-VSP complex. SiMPull is a recently developed technique that maintains high plasma membrane expression levels of Ci-VSP and then dilutes the lysates to count single molecules via TIRF (Fig. 3 a; Jain et al., 2011; Levitz et al., 2016). We first counted the number of subunits in a Ci-VSP complex using an N-terminal HA and C-terminal GFP tag on the same protein (HA-VSP-GFP). Neither the HA tag (Fig. 1) nor the GFP tag (Kohout et al., 2008; Ratzan et al., 2011) alters

Ci-VSP function. HEK293T cells were transfected with HA-VSP-GFP, and after 24 h of expression, dilute cell lysates were flowed over coverslips previously passivated and coated with anti-HA at very low concentrations (Fig. 3 a). Because of the lysate dilution, the final concentration of bound HA-VSP-GFP at the surface of the coverslip is low enough for single-molecule subunit counting, whereas the formation of the complex was under typical, high-expression conditions. To count the subunits in the complex, the GFP fluorescence was bleached, and the resulting fluorescence intensity drops were recorded over time (see Materials and methods). The majority of HA-VSP-GFP spots bleached in

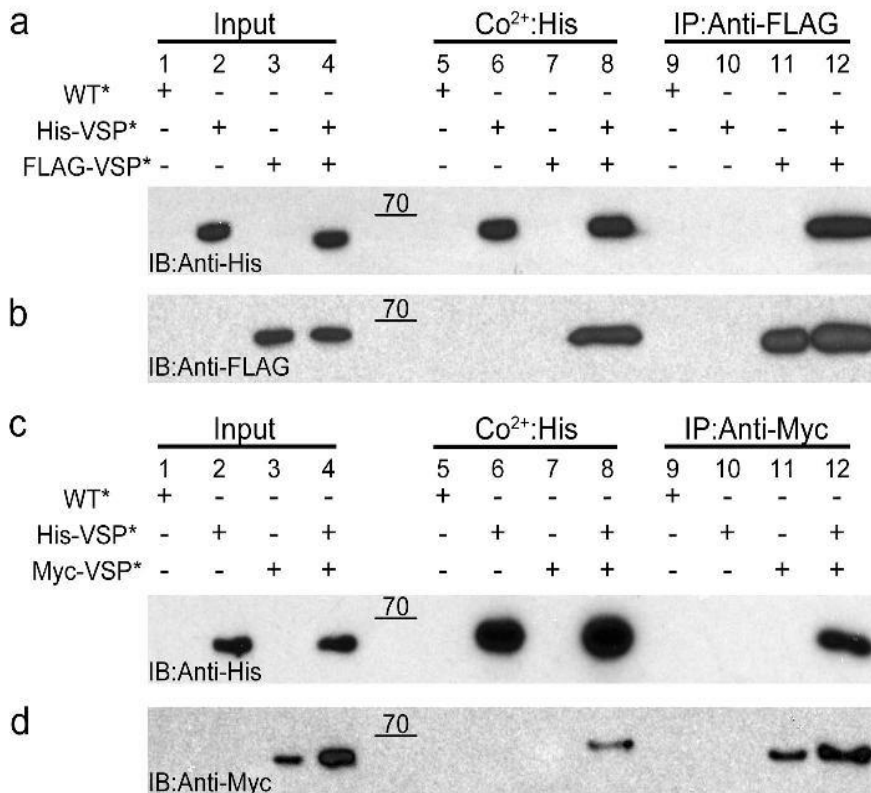


Figure 2. Ci-VSP subunits interact with each other. (a and b) Oocytes expressing WT*, His-VSP*, FLAG-VSP*, or a His-VSP*/FLAG-VSP* mixture were processed and pulled down with Co²⁺ beads or coimmunoprecipitated with anti-FLAG beads. Subsequent Western blots were stained with anti-His (a) and anti-FLAG (b). The His blot shows His-VSP* coimmunoprecipitated from the His/FLAG mixture using anti-FLAG beads (lane 12), whereas the FLAG blot shows FLAG-VSP* pulled down from the His/FLAG mixture using Co²⁺ beads (lane 8). (c and d) Oocytes expressing WT*, His-VSP*, Myc-VSP*, or a His-VSP*/Myc-VSP* mixture were processed and pulled down with Co²⁺ beads or coimmunoprecipitated with anti-Myc beads. Western blots were stained with anti-His (c) and anti-Myc (d). The His blot shows His-VSP* coimmunoprecipitated from the His/Myc mixture using anti-Myc beads (lane 12), whereas the Myc blot shows Myc-VSP* pulled down from the His/Myc mixture using Co²⁺ beads (lane 8). These pull-downs indicate that the individual Ci-VSP subunits interact with each other and form multimers on the membrane. Blots are representative of *n* = 4 experiments. Raw data for the Western blots are shown in Fig. S2. IB, immunoblotting; IP, immunoprecipitation.

two steps, indicating dimers (52%), whereas the remaining spots bleached in single steps (40%) or in three steps (8%; Fig. 3 b). In parallel with the HA-VSP-GFP, we also tagged control proteins with HA and GFP to quantitate known multimerization states: ASIC1A channels with the GFP on all subunits (trimers), TREK1 channels with the GFP on all subunits (dimers), and TREK1 channels with the GFP on only one subunit (monomer). For ASIC1A channel spots, 44% bleached in three steps, 30% bleached in two steps, and 26% bleached in a single step (Fig. 3 c). For TREK1 channel spots with the GFP on all the subunits, 69% bleached in two steps, 24% bleached in single steps, and 7% bleached in three steps (Fig. 3 d). For TREK1 channel spots with the GFP on only one subunit, 80% bleached in single steps, and 20% bleached in two steps (Fig. 3 e). This distribution of bleaching in our controls indicates a GFP maturation probability of ~80%, which follows a binomial distribution. Ci-VSP more closely resembles the distribution seen for TREK1 channels, indicating that Ci-VSP does form dimeric complexes on the membrane. However, Ci-VSP does not follow the distribution for an obligate dimer. The larger number of VSP monomers suggests that Ci-VSP is in a dynamic equilibrium between the dimer and monomer states.

To further investigate the nature of this Ci-VSP dimer, we split the tags between two different subunits: an N-terminal HA-tagged Ci-VSP (HA-VSP) and a C-terminal GFP-tagged Ci-VSP (VSP-GFP). HA-VSP and VSP-GFP were transfected individually or mixed together in HEK293T cells (Fig. 4 a). Under these conditions, the HA-VSP will bind to the passivated coverslip and VSP-GFP will not. As expected, when each construct is expressed alone, no visible fluorescence is observed for either protein (Fig. 4 b, left and middle). When coexpressing HA-VSP with VSP-GFP, we observed fluorescent spots on the coverslips, indicating that the VSP-GFP interacts with the HA-VSP (Fig. 4 b,

right). These spots were also bleached and counted (Fig. 4 c). The majority of spots (65%) were monomers (Fig. 4 d) resembling the distribution of spots for the single tagged TREK1 (Fig. 3 e, right). These results further support our conclusion that Ci-VSP subunits form dimers when present under normal cell conditions.

Multimerization mediated mainly by the VSD

Both the VSD and the PD are known to fold and function as independent domains (Liu et al., 2012; Li et al., 2014). To determine whether one or both domains were responsible for mediating the observed Ci-VSP subunit interactions, Ci-VSP was split into the VSD and the PD. Specifically, we tested the VSD-only protein (VSDo) and the phosphatase-only protein (PDo) using SIMPull to pull down full-length VSP-GFP. The HA-VSDo pulled down about half of the VSP-GFP (Fig. 5, a [middle] and b) compared with full-length HA-VSP (Fig. 5, a [left] and b), whereas only a small but significant fraction (*P* < 0.001) of VSP-GFP was pulled down by the HA-PDo (Fig. 5, a [right] and b). These results indicate that the VSD may be the main driving force behind dimer formation. Next, the ability of each domain to pull each other or a copy of itself down was tested (VSD-PD, VSD-VSD, and PD-PD). When HA-PDo is coexpressed with VSDo-GFP (Fig. 5, c [left] and d) or when HA-VSDo is coexpressed with GFP-PDo (Fig. 5 c [right] and d), no spots were detected, showing that VSD and PD are not interacting. When the HA-VSDo was coexpressed with VSDo-GFP, the GFP is clearly pulled down, giving $1,121 \pm 29$ spots with 65% bleaching in a single step (Fig. 5, d and e). When HA-PDo is coexpressed with PDo-GFP, we also observed spots but fewer in number (368 ± 8), and 80% bleach in a single step (Fig. 5, d and f). In both cases, the VSDo pull down and the PDo pull down, reinforcing the dimer organization on a domain level. To further characterize the domain interactions, we determined

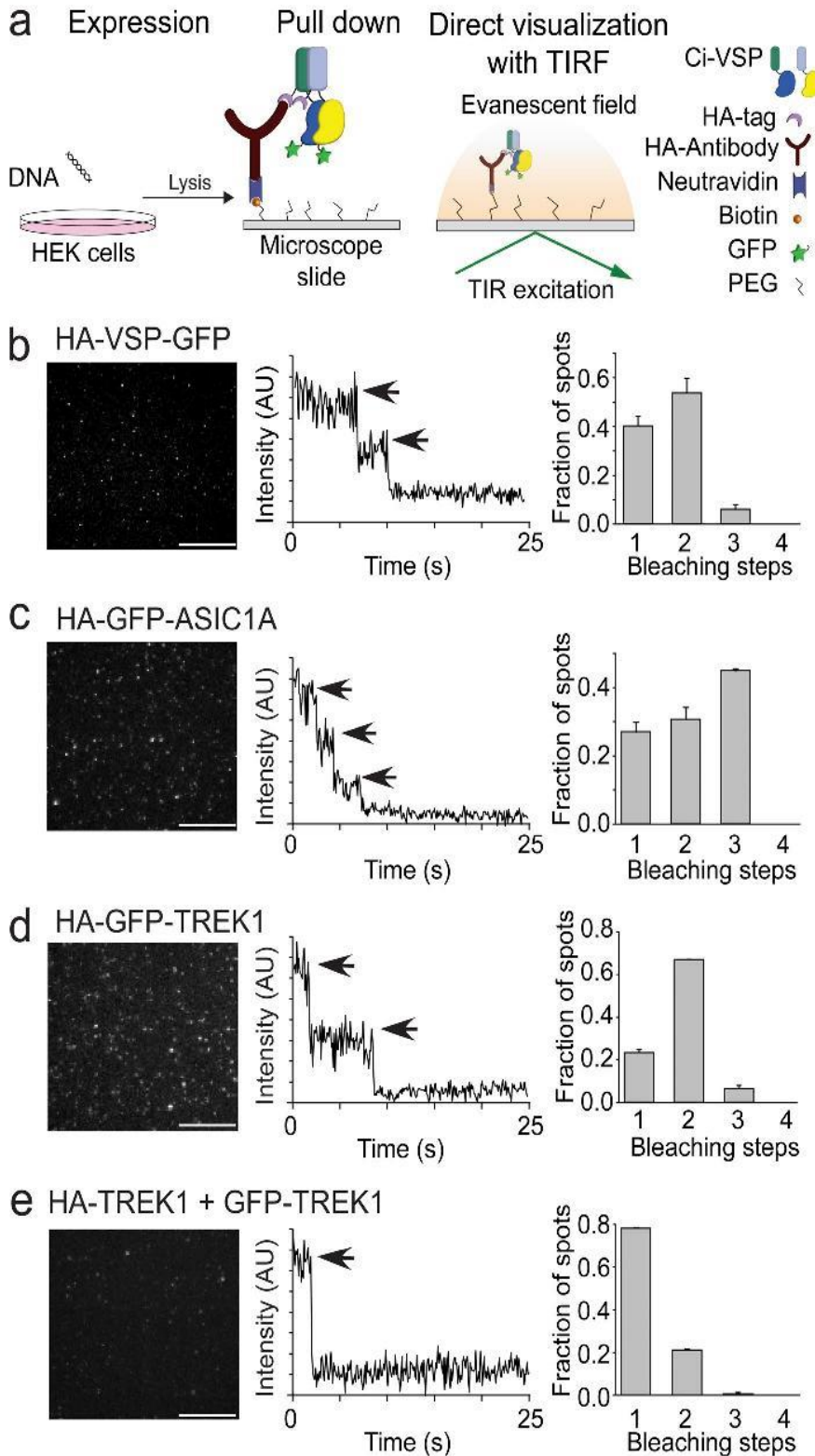


Figure 3. Ci-VSP forms dimers. (a) Schematic of the SiMPull subunit counting assay depicting the HA-VSP-GFP expression in HEK293 cells followed by pull down of the HA tag with anti-HA on coverslips and recording of the GFP fluorescence using TIRF. TIR, total internal reflection. (b) Left: TIRF images of HA-VSP-GFP single molecules. Middle: Representative trace showing two-step photobleaching of HA-VSP-GFP. AU, arbitrary units. Right: Summary of photobleaching step distribution for HA-VSP-GFP. Two-step bleaching events indicate VSP forms dimers on the membrane. (c) SiMPull data for trimer control, HA-GFP-ASIC1A. Left: TIRF images. Middle: Representative trace showing three-step photobleaching. Right: Summary of photobleaching step distribution. (d) SiMPull data for dimer control, HA-GFP-TREK1. Left: TIRF images. Middle: Representative trace showing two-step photobleaching. Right: Summary of photobleaching step distribution. (e) SiMPull data for monomer control, HA-TREK1 pull down of TREK1-GFP. Left: TIRF images. Middle: Representative trace showing single-step photobleaching. Right: Summary of photobleaching step distribution. Error bars are \pm SEM. Bars, 2 μ m.

the number of subunits in HA-VSDo-GFP and HA-PDo-GFP. The HA-VSDo-GFP bleached in a combination of two steps (55%) and one step (37%), mimicking the distribution observed for full-length VSP (Fig. 5 g). The HA-PDo-GFP also bleached in one and two steps, but the distribution favored single steps (57% for single, 34% for double; Fig. 5 h). From our results, we suggest that the VSD is the main driving force behind Ci-VSP dimerization. The PDs may contribute, but that contribution is likely much weaker than the interaction between VSDs.

Is the dimerization of VSP important for function?

Voltage sensing

We tested this question by investigating the VSD motions. Because the VSDs help mediate the dimer interaction, each VSD within the dimer is expected to cooperate with its neighboring VSD as seen in the Hv channel (Tombola et al., 2010). VSD cooperativity was investigated with a previously characterized mutation, D331A, that significantly altered VSD kinetics and voltage dependence when compared with WT (Fig. 6 and Table

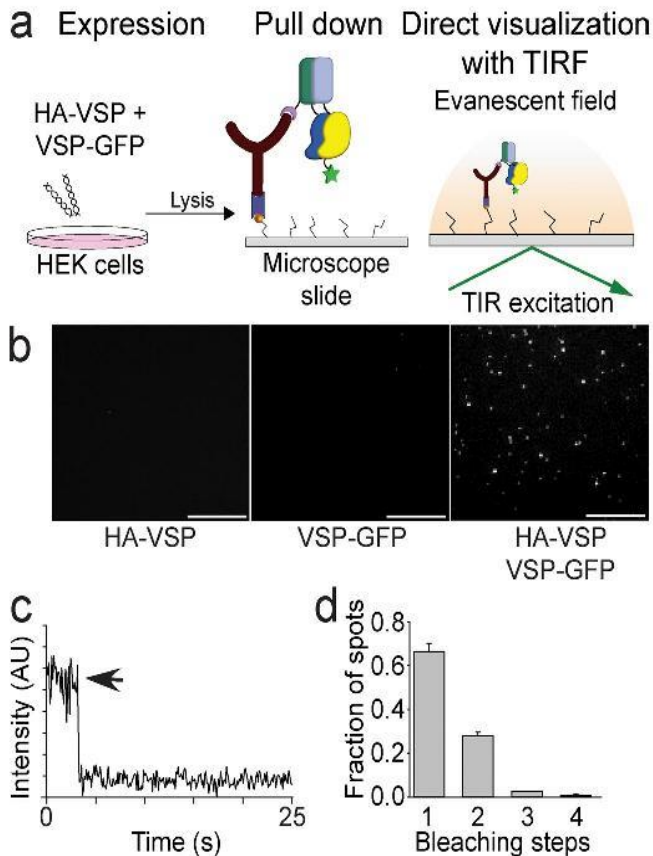


Figure 4. Ci-VSP subunits pull each other down consistent with a dimer complex. (a) Schematic of the SiMPull assay where HA-VSP is coexpressed with VSP-GFP in HEK293 cells followed by pull down of the HA-VSP with anti-HA on coverslips. Any HA-VSP dimers that will not be visible, and VSP-GFP dimers do not interact and are washed away, leaving the HA-VSP with VSP-GFP dimer as the only visible fluorescent spot using TIRF. TIR, total internal reflection. (b) SiMPull TIRF images of the HA-VSP alone (left), VSP-GFP alone (middle), and HA-VSP/VSP-GFP mixture (right). Fluorescent spots are only visible in the HA-VSP/VSP-GFP sample. Bars, 2 μm . (c) Representative trace showing single-step photobleaching of the HA-VSP/VSP-GFP spots in b. AU, arbitrary units. (d) Summary of the photobleaching step distribution of the HA-VSP/VSP-GFP spots in b. As expected, monomers predominate the mixture, indicating that a HA-VSP subunit pulls down a VSP-GFP subunit, forming a dimer complex. Error bars are \pm SEM.

S1; Kohout et al., 2010). In particular, we mixed WT* (where the * indicates TMRM labeling) with D331A (DA*) or WT (unlabeled) with DA* and tested whether the VSD motions were influenced by the mixtures. In both cases, the deactivation kinetics of the mixtures were closer to that of WT than of DA, indicating that the VSD from the WT subunit (either WT* or WT) accelerates the VSD repolarization of the DA* subunit (Fig. 6 a). Interestingly, the voltage dependences of the mixtures were shifted to lower voltages, closer to DA* than to WT* alone, suggesting that the DA subunit lowers the energy needed to move the WT subunit VSD (Figs. 6 b and S1).

Enzymatic activity

If Ci-VSP subunit interactions change the VSD cooperativity, then catalytic activity is also expected to change as a result of dimer formation. Because the Ci-VSP dimers may not be obligate as suggested by the SiMPull results, we hypothesized that

the dimers are concentration dependent. To test this hypothesis, we used the fTAPP activity assay (Fig. 7 a) under two different conditions: decreasing concentrations of active Ci-VSP alone, and mixtures between active and inactive Ci-VSPs. If the dimers are concentration dependent, the monomer should be favored at lower concentrations. For the first set of conditions, oocytes were injected with several concentrations of active His-VSP cRNA (0.02, 0.05, 0.1, 0.2, 0.8, and 1.6 $\mu\text{g}/\mu\text{l}$) mixed with fTAPP cRNA. As expected, after 36 h expression, all cells expressed His-VSP though in lower amounts when injected with lower cRNA concentrations (Fig. S3). For the higher His-VSP cRNA concentrations (0.2, 0.8, and 1.6 $\mu\text{g}/\mu\text{l}$), the fTAPP FRET assay showed the characteristic 5- and 3-phosphatase activities that have been previously reported (Murata et al., 2005; Iwasaki et al., 2008; Halaszovich et al., 2009; Kohout et al., 2010; Kurokawa et al., 2012; Castle et al., 2015; Grimm and Isacoff, 2016; Fig. 7 b, top three). At the next concentration (0.1 $\mu\text{g}/\mu\text{l}$), the 3-phosphatase activity was more variable, with about half the tested cells showing 3-phosphatase activity ($n = 10$) and half showing no 3-phosphatase activity ($n = 11$; Fig. 7 b, two yellow traces). The 5-phosphatase activity stayed robust regardless of concentration. At the lowest concentrations tested (0.02 and 0.05 $\mu\text{g}/\mu\text{l}$), only 5-phosphatase activity was observed (Fig. 7 b, bottom two). Based on these strong results, we propose that the 3-phosphatase activity is dependent on dimerization, whereas the 5-phosphatase activity is inherent in the monomer. The voltage dependence of the 5-phosphatase activity also shifted to higher voltages when Ci-VSP was at lower concentrations, suggesting a cooperative interaction between the PDs (Fig. 7 c). Under our second set of conditions, we included the inactivating mutant, Ci-VSP-C363S (CS), where we mixed active His-VSP* and inactive FLAG-CS* at a 1:10 ratio. By using a 1:10 ratio, the majority of the dimers should contain, at maximum, one His-VSP* active subunit. The N-terminal tags allowed us to confirm the mixtures were strongly biased toward the inactive FLAG-CS protein (Fig. S4). Repeating the fTAPP FRET assay with His-VSP:FLAG-CS (0.1:1.0 or 0.2:2.0 $\mu\text{g}/\mu\text{l}$), we detected only 5-phosphatase activity (Fig. 7 d), even though the His-VSP alone at 0.2 $\mu\text{g}/\mu\text{l}$ showed both 3- and 5-phosphatase activity (Fig. 7 b, brown trace) and at 0.1 $\mu\text{g}/\mu\text{l}$ showed a mix between both 3- and 5-phosphatase activity and 5-phosphatase only (Fig. 7 b, yellow traces). This result suggests the mixed active/inactive dimer either is not functional (dominant negative) and only the monomeric His-VSP is functional or two active subunits are required for the 3-phosphatase activity and the mixed active/inactive dimers are only capable of 5-phosphatase activity.

Discussion

Ci-VSP allows the cell to convert an electrical signal into a chemical signal because of its unique architecture, combining a VSD with a PD. We set out to determine whether Ci-VSP exists only as a monomer or whether Ci-VSP multimerizes into a higher-order complex. We demonstrated that Ci-VSP does form dimers. The next question we addressed was whether the dimerization is functionally important. We found that the dimers influence the VSD motions and

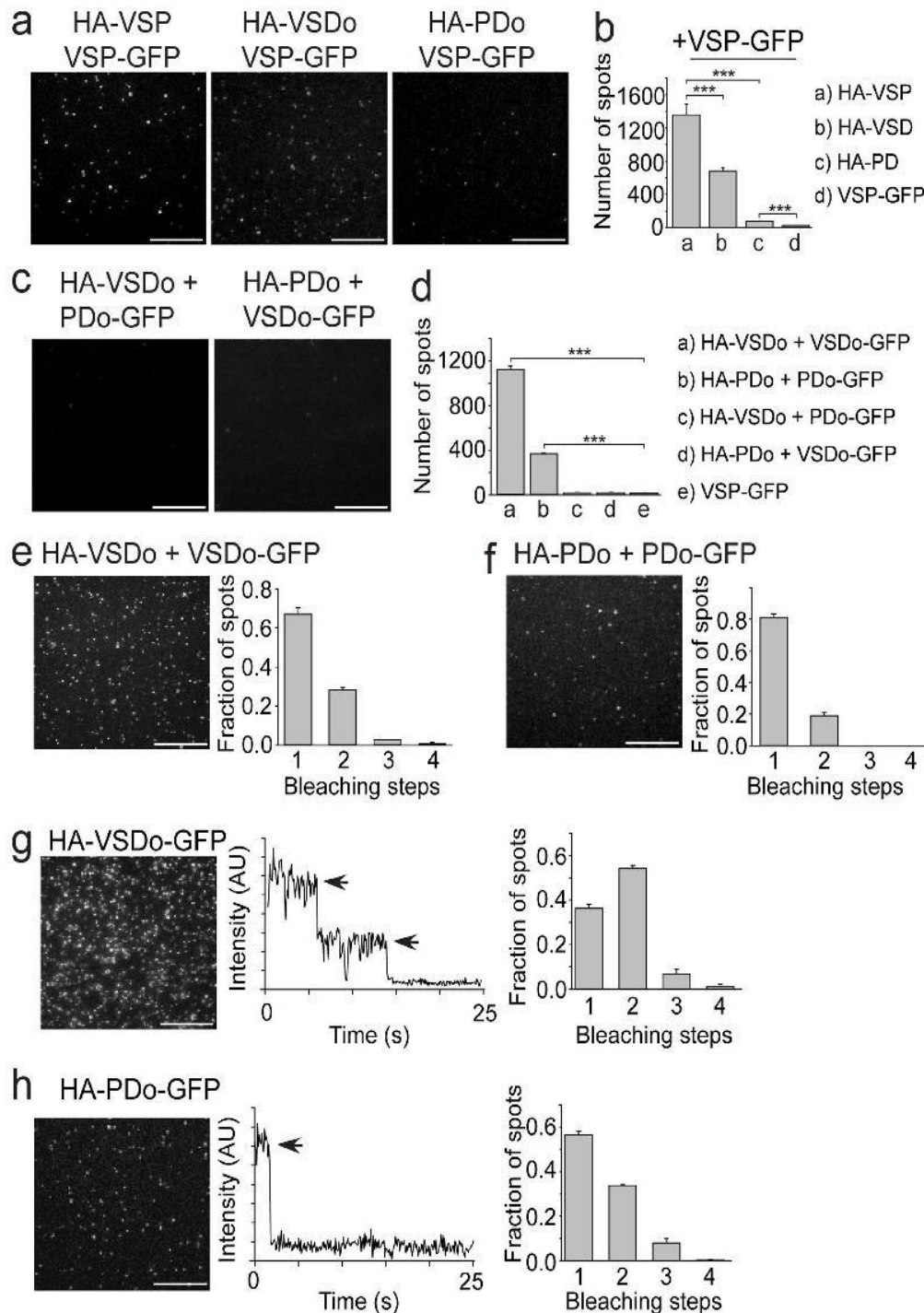


Figure 5. Ci-VSP dimerization mediated mainly by VSD. (a) TIRF images of a VSP-GFP pull-down using either HA-VSP (full length, left, reused from Fig. 4 b, right), HA-VSDo (middle), or HA-PDo (right). (b) Summary of the number of single-molecule spots for each pull-down condition. The HA-VSDo was able to pull down almost half of the number of VSP-GFPs compared with full-length HA-VSP. VSP-GFP pull down with HA-PDo was significantly higher than pull down with VSP-GFP alone. Student's *t* tests, ***, $P < 0.001$. (c) TIRF images of HA-VSDo pull-down of PDo-GFP (left) and HA-PDo pull-down of VSDo-GFP (right). No spots were detected in either experiment as expected. (d) Summary of the number of single-molecule spots for each pull-down condition shown in c, e, and f. Student's *t* tests, ***, $P < 0.001$. (e) HA-VSDo pull-down of VSDo-GFP. TIRF single-molecule image is shown on the left, and a summary of the photobleaching step distribution is shown on the right. Spots bleached in mostly single steps, indicating that a VSD is able to pull down another. (f) HA-PDo pull-down of PDo-GFP. TIRF single-molecule image is shown on the left, and a summary of the photobleaching step distribution is shown on the right. Spots bleached in mostly single steps, indicating that a PD is able to pull down another. (g) SIMPull data for HA-VSDo-GFP. Left: TIRF image of single molecules. Middle: Representative trace showing two-step photobleaching. Right: Summary of photobleaching step distribution. Two-step bleaching events indicate VSD-VSDs form dimers on the membrane. (h) SIMPull data for HA-PDo-GFP. Left: TIRF image of single molecules. Middle: Representative trace showing single-step photobleaching. Right: Summary of photobleaching step distribution. PD-PD dimers are weaker than the VSD-VSD dimers. Error bars are \pm SEM. Bars, 2 μ m.

appear to be responsible for Ci-VSP's 3-phosphatase activity. Specifically, at low concentrations, Ci-VSP only displayed 5-phosphatase

activity, whereas at higher concentrations, favoring dimerization, it showed both 3- and 5-phosphatase activity. From our activity data,

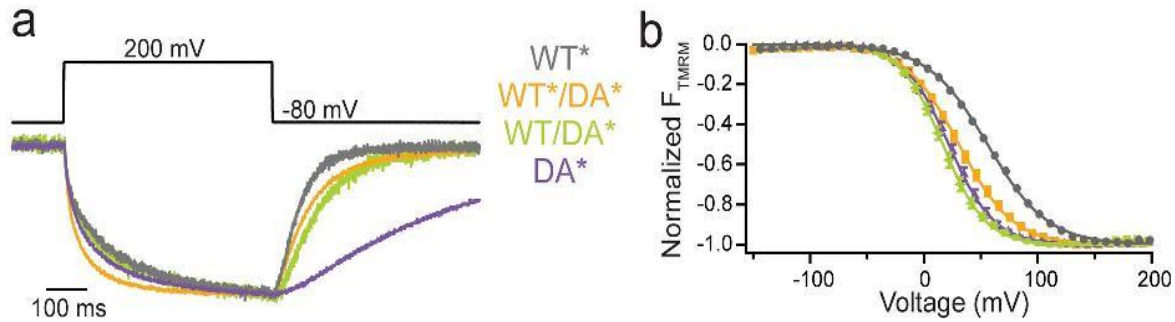


Figure 6. Ci-VSP VSD motions influence each other across the multimer complex. (a) Representative TMRM fluorescence traces during a step from a holding potential of -80 to 200 mV for WT* (G214C), DA* (G214C D331A), WT*/DA*, and WT/DA*. Traces are normalized to the maximal fluorescence change. The deactivation kinetics of the mixtures more closely resemble the WT* alone than the DA* alone, indicating that the WT* VSD influences the VSD kinetics from the DA* subunit. (b) Normalized TMRM fluorescence versus voltage relationship. Data fit to single Boltzmann equations. The voltage dependence of the mixtures more closely resembles the DA* alone than the WT* alone, suggesting that the DA* VSD more strongly influences the VSD voltage dependence. Error bars represent \pm SEM; $n \geq 12$. Some errors bars are smaller than the size of the symbols.

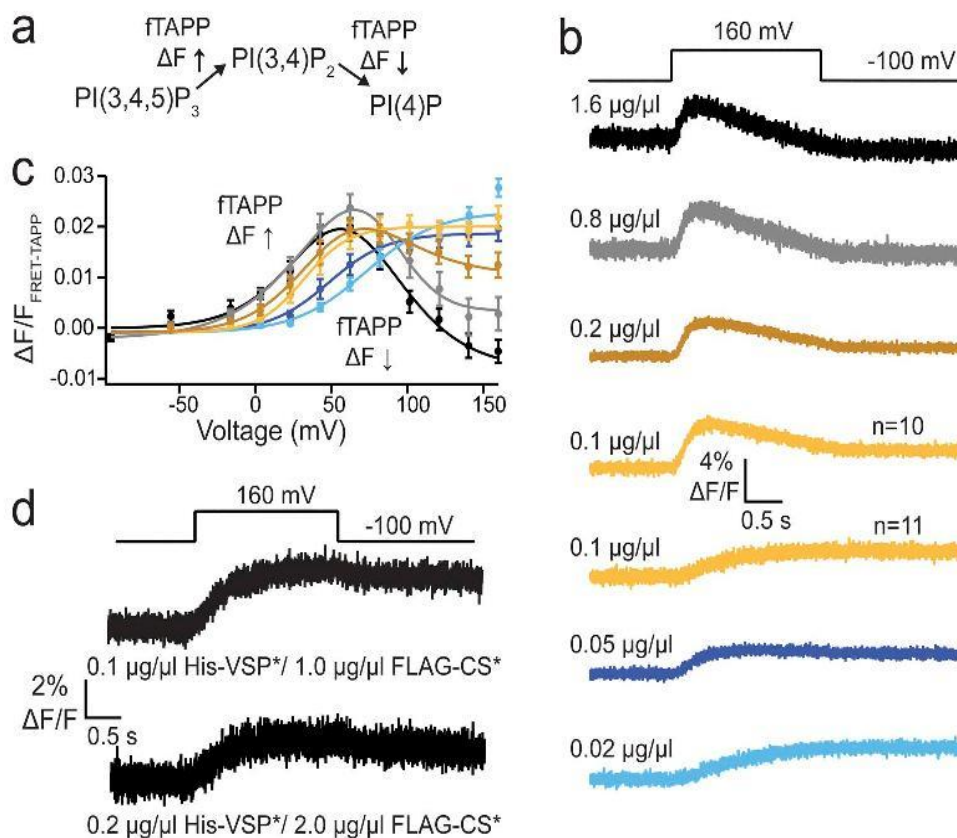


Figure 7. Ci-VSP dimerization responsible for 3-phosphatase activity. (a) Schematic of ftAPP assay where the ftAPP FRET sensor increases FRET when PI(3,4)P₂ is produced and decreases FRET when PI(3,4)P₂ is depleted. (b) Averaged ftAPP FRET traces over time during a voltage step from a holding potential of -100 to 160 mV for ftAPP coexpressed with varying amounts of His-VSP cRNA: 1.6, 0.8, 0.2, 0.1, 0.05, and 0.02 $\mu\text{g}/\mu\text{l}$. Higher His-VSP* concentrations display both 5- and 3-phosphatase activity, whereas the lower concentrations only show 5-phosphatase activity. The 0.1 $\mu\text{g}/\mu\text{l}$ samples were evenly split with half the cells showing both activities and half the cells showing only one. $n \geq 11$. (c) $\Delta F/F$ ftAPP FRET ratio versus voltage relationships for all six cRNA concentrations. As the concentration of His-VSP* decreases, the voltage dependence of the FRET increase shifts to higher voltages whereas the FRET signal decrease disappears. Error bars represent \pm SEM; $n \geq 11$. Data fit with a double or single Boltzmann equation. (d) Averaged ftAPP FRET traces over time for ftAPP coexpressed with 1:10 mixtures of active and inactive VSP: 0.1:1.0 $\mu\text{g}/\mu\text{l}$, His-VSP*:FLAG-CS* and 0.2:2.0 $\mu\text{g}/\mu\text{l}$, His-VSP*:FLAG-CS*. In both cases, only a FRET increase is observed, even though the 0.2 $\mu\text{g}/\mu\text{l}$ concentration alone in b always show both an increase and a decrease, and the 0.1 $\mu\text{g}/\mu\text{l}$ concentration alone in b was evenly split. $n \geq 10$.

not only are dimers responsible for part of Ci-VSP's activity, but dimer formation is also driven by concentration, making Ci-VSP dimerization important for its enzymatic activity.

Multiple complementary approaches were used to address the question of Ci-VSP multimerization. Initially, we tested for

interactions between Ci-VSP subunits using coimmunoprecipitation. Regardless of which epitope tag we used to differentiate Ci-VSP subunits, we found one Ci-VSP subunit could pull down another Ci-VSP subunit (Fig. 2), indicating that at a minimum, Ci-VSP could form dimers if not higher-order complexes. Our

SiMPull results further indicate interactions between Ci-VSP subunits (Fig. 4) and show that the complex is a dimer (Fig. 3). On the surface, our current results appear to contradict our previous study, which suggested that Ci-VSP functions as a monomer (Kohout et al., 2008). In that work, the monomer interpretation was based on TIRF experiments where the Ci-VSP was kept at single-molecule concentrations in live oocytes. Subunit counting at high concentrations was not tested at that time because TIRF subunit counting in living cells is limited to low concentrations. This limitation is not important when testing proteins that are obligate multimers, like channels, because they will multimerize during protein processing in the ER before trafficking to the plasma membrane. However, not all proteins are obligate multimers in this way. Some proteins form multimers in a concentration- or ligand-dependent way (Yarden, 2001; Schwenk et al., 2010; Calebiro et al., 2013; Anderluh et al., 2017). As a result, the TIRF concentration restrictions limit the interpretation of the original subunit counting experiment. Here, we turned to SiMPull, giving us the advantage of exogenous concentrations of Ci-VSP on the plasma membrane followed by a diluted lysate to lower the concentration enough to count individual complexes. Under these conditions, Ci-VSP forms a mixture of monomers and dimers. In fact, the number of bleaching steps observed does not follow the same ratio of one and two bleaching steps as a protein known to only exist on the plasma membrane as a strict dimer, TREK1 (Levitz et al., 2016). Because TREK1 is an obligate dimer, we suggest that Ci-VSP is not an obligate dimer; instead, it exists on the plasma membrane as a mixture of monomers and dimers. Given that the main difference between our current results and our previous results is concentration, we propose that Ci-VSP forms dimers in a concentration-dependent manner.

To test our concentration hypothesis as well as to determine whether the dimerization was functionally relevant, we used an activity assay and manipulated the relative Ci-VSP concentrations from low to high by injecting six different concentrations of cRNA into oocytes (Fig. S3). At low concentrations, only 5-phosphatase activity was observed, whereas at high concentrations, both 3- and 5-phosphatase activities were present, as has been reported previously (Murata et al., 2005; Iwasaki et al., 2008; Halaszovich et al., 2009; Kohout et al., 2010; Kurokawa et al., 2012; Castle et al., 2015; Grimm and Isacoff, 2016; Fig. 7). This functional difference between low and high concentrations of Ci-VSP supports our hypothesis that Ci-VSP dimer formation is driven by its concentration in the membrane. It also indicates that Ci-VSP dimerization is functionally relevant. By manipulating the concentration of Ci-VSP, the enzymatic activity and any cellular signaling driven by Ci-VSP will be altered. This suggests that Ci-VSP function in a cell is controlled by expression. The physiological function of Ci-VSP remains elusive and concentration dependence could lead to a better understanding of how it contributes to cellular signaling.

Other factors may also contribute to dimerization. Previous studies have suggested Ci-VSP is regulated by $PI(4,5)P_2$ binding to the linker between the VSD and the PD (Villalba-Galea et al., 2009; Kohout et al., 2010). How $PI(4,5)P_2$ concentrations may impact dimerization or selectivity remain to be determined. Another factor stems from *X. laevis* oocyte expression of small

amounts of an endogenous VSP (Xl-VSP1 and 2). Although we cannot rule out heterodimerization between Ci-VSP and Xl-VSP1 or Xl-VSP2, the overexpressed Ci-VSP is expected to overwhelm the Xl-VSP1 and 2 proteins, minimizing any contribution from theoretical heterodimers. HEK293 cells do not express an endogenous VSP (Mavrantoni et al., 2015). Further experiments are needed to explore lipid and heterodimerization influences.

We next separated Ci-VSP into its component domains, the VSD and the PD, to determine whether one or both are responsible for the dimerization. Our SiMPull results show that the VSDo can efficiently pull down full-length Ci-VSP when compared with the PDo (Fig. 5, a and b). We also found that HA-VSDo can pull down VSDo-GFP (Fig. 5 c) and that HA-VSDo-GFP forms dimers (Fig. 5 e), though not strict dimers like TREK. These data strongly support the VSD-VSD interactions being the main driving force behind Ci-VSP dimer organization. Functionally, this interaction seems to facilitate the activation of Ci-VSP because the voltage dependence of the 5-phosphatase activity is shifted to lower voltages when Ci-VSP is dimeric (Fig. 7 c). In addition, it suggests the motions of both VSDs are coordinated within the dimer in response to depolarization. This result is confirmed by the fact that the D331A mutant VSD shifts the voltage dependence of the WT VSD toward hyperpolarized values similar to those observed for the D331A alone (Fig. 6 b).

Interestingly, we found that HA-PDo pulled down PDo-GFP (Fig. 5 d) and HA-PDo-GFP formed dimers (Fig. 5 f) even though HA-PDo was not able to efficiently pull down full-length Ci-VSP (Fig. 5 b). This apparent discrepancy between the ability of the PD to pull down another PD (Fig. 5 f) and its inability to pull down the full-length Ci-VSP may stem from the PD-PD interaction being inherently weaker than the VSD-VSD interaction. However, if the PD-PD interaction is weaker, then a similar number of spots should be visible (compare Fig. 5 a, right, to Fig. 5 f). Instead, more spots are observed when just the PD pulls down another PD. Although the VSD and PD do fold independently, there is a tight coupling between the VSD and PD in full-length Ci-VSP (Villalba-Galea et al., 2009; Kohout et al., 2010). Thus, it is possible that in full-length Ci-VSP, the PD is in a resting conformation not adopted by the PDo. This is consistent with activity data because full-length Ci-VSP is off at resting potentials, whereas the Ci-VSP PDo is constitutively active. This conformational difference could reduce the affinity of the soluble PD for the PD in full-length Ci-VSP. However, this does not mean that the PDs are not interacting within the Ci-VSP dimer. Our functional data support the PDs interacting with each other within the full-length Ci-VSP dimer because only 5-phosphatase activity is observed at low concentrations, where monomers are favored, compared with 3- and 5-phosphatase activity at high concentrations, where dimers are favored. This change in activity indicates that the PDs are likely interacting and influencing the substrate specificity of their immediate neighbor.

Based on our results, we suggest a model for how the individual subunits within a Ci-VSP dimer may be organized. Because we see a strong contribution of the VSD, a PD-only organization can be ruled out (Fig. 8 a). A VSD-only organization is also unlikely (Fig. 8 b) because we see PD-PD pull-down and a dimerization-dependent substrate selectivity different than that of the monomer.

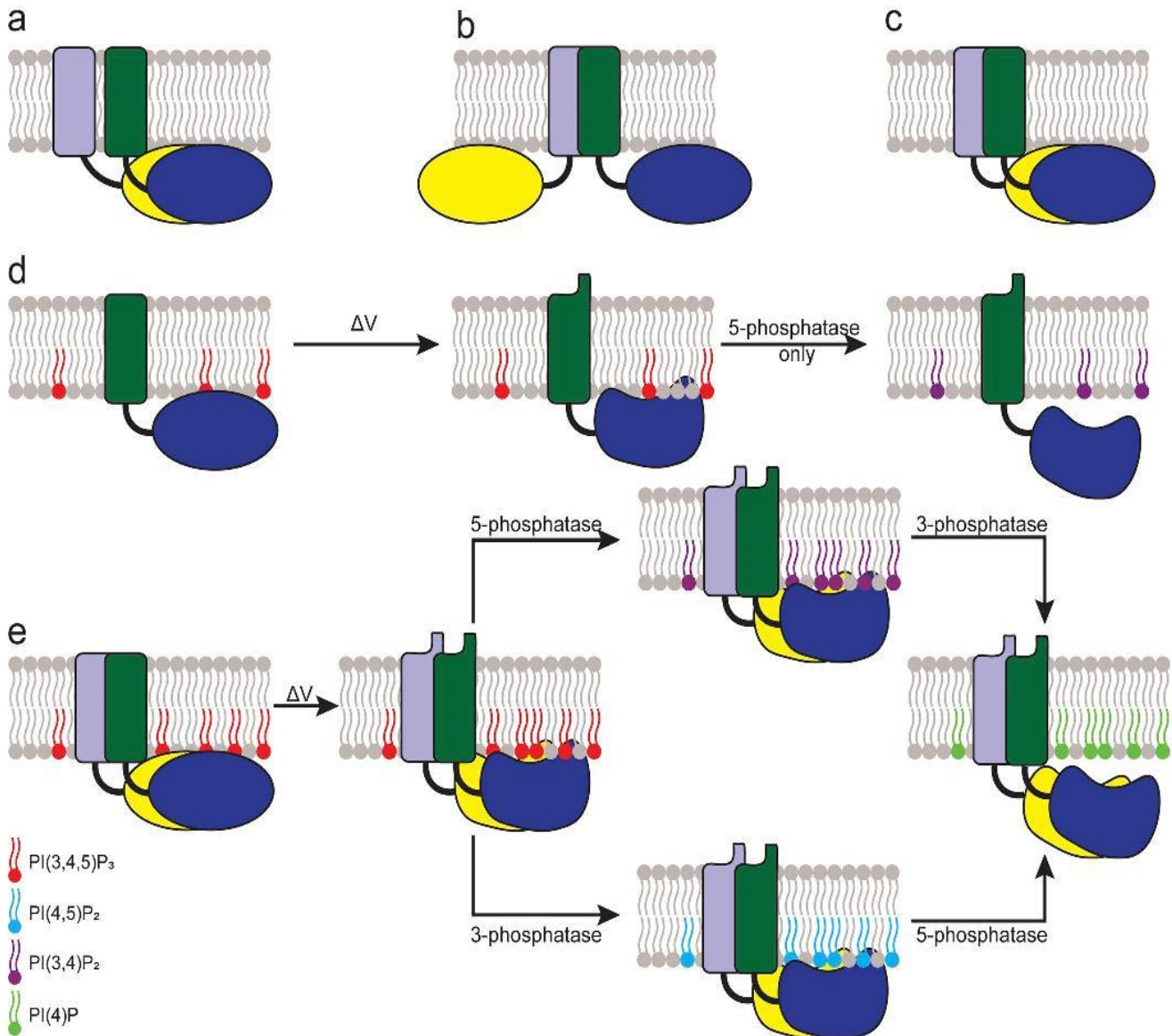


Figure 8. Cartoon schematics presenting possible Ci-VSP dimer organizations. (a) PD-based dimer. (b) VSD-based dimer. (c) Both VSD and PD contribute to dimer interactions. The side-by-side organization most closely agrees with our data. (d) Model for the 5-phosphatase reaction catalyzed by VSP monomer. (e) Model for the 5- and 3-phosphatase reactions catalyzed by VSP dimer.

We cannot rule out extensive allosteric conformational changes caused by the VSD dimers leading to changes in the individual PDs. However, it is more likely that Ci-VSP subunits organize in a side-by-side fashion (Fig. 8 c). In this model, the VSD induces the dimerization of Ci-VSP in a concentration-dependent manner. This dimerization alters the PD conformations, allowing their interaction. The VSDs in the dimer cooperate, causing a coordinated motion after a membrane depolarization. The PD dimer interaction then changes the active site in each PD, allowing the 3-phosphatase activity in addition to the 5-phosphatase activity (Fig. 8, d and e).

Although the organization of Ci-VSP is important for understanding its function, it is also important for its use as a tool. Specifically, VSPs are used to manipulate PIP concentrations when studying PIP-dependent processes. By changing VSP concentrations, PIP concentrations can now be more finely tuned, targeting only 5-phosphates instead of both 3- and 5-phosphate. In addition, VSP domains have been used to generate biosensors

to noninvasively track biologically relevant signaling processes within live cells (Dimitrov et al., 2007; Lundby et al., 2008; Jung et al., 2017; Lee et al., 2017). For many years, making a sensor to track membrane voltage was stymied because the sensors were not properly trafficked to the plasma membrane. When Ci-VSP was discovered, the field exploded because the Ci-VSP VSD overcame those expression issues. When the monomer result was published, this also simplified the interpretation of the voltage sensor results, because any fluorescence signal was the result of a single sensor. However, with our dimer results, we now know that the voltage biosensors using the Ci-VSP VSD form dimers in a concentration-dependent manner. This possibility will have significant implications on biosensor design and needs to be considered when interpreting the biosensor fluorescence signals.

In conclusion, we have shown that Ci-VSP dimerizes in a concentration-dependent manner. The Ci-VSP monomer is a 5-phosphatase, whereas the dimer is both a 5- and

3-phosphatase. This functional impact of dimerization on enzymatic activity could indicate that Ci-VSP signaling is regulated by expression and may ultimately play a role in its physiological function.

Acknowledgments

We thank Y. Okamura for providing the Ci-VSP cDNA, E.Y. Isacoff for the fPLC and fTAPP, and E. Lingueglia for ASIC1A.

This work was supported by start-up funds from the Vice President for Research, Creativity and Technology Transfer at Montana State University (S.C. Kohout); National Institute of General Medical Science of the National Institutes of Health grants R01GM111685 (S.C. Kohout) and P20GM103474 (K. Stengel); Fondation pour la Recherche Médicale Equipe FRM grant DEQ20170336753 (G. Sandoz); ATIP-AVENIR grants (G. Sandoz); and Fondation NRJ-Institut de France and Agence Nationale de la Recherche (Laboratory of Excellence “Ion Channel Science and Therapeutics” grant ANR-11LABX-0015-01).

The authors declare no competing financial interests.

Author contributions: G. Sandoz and S.C. Kohout conceived the experiments. V. Rayaprolu, K. Stengel, G. Sandoz, and S.C. Kohout designed experiments. V. Rayaprolu, K. Stengel, P. Royal, and S.C. Kohout collected and analyzed data. S.C. Kohout, G. Sandoz, and V. Rayaprolu interpreted data and drafted and revised the manuscript. All authors approved the final version of the manuscript.

Sharona E. Gordon served as editor.

Submitted: 9 March 2018

Accepted: 28 March 2018

References

- Anderluh, A., T. Hofmaier, E. Klotzsch, O. Kudlacek, T. Stockner, H.H. Sitte, and G.J. Schütz. 2017. Direct PIP₂ binding mediates stable oligomer formation of the serotonin transporter. *Nat. Commun.* 8:14089. <https://doi.org/10.1038/ncomms14089>
- Balla, T., Z. Szentpetery, and Y.J. Kim. 2009. Phosphoinositide signaling: new tools and insights. *Physiology (Bethesda)*. 24:231-244. <https://doi.org/10.1152/physiol.00014.2009>
- Calebiro, D., F. Rieken, J. Wagner, T. Sungkaworn, U. Zabel, A. Borzi, E. Cocucci, A. Zürn, and M.J. Lohse. 2013. Single-molecule analysis of fluorescently labeled G-protein-coupled receptors reveals complexes with distinct dynamics and organization. *Proc. Natl. Acad. Sci. USA*. 110:743-748. <https://doi.org/10.1073/pnas.1205798110>
- Castle, P.M., K.D. Zolman, and S.C. Kohout. 2015. Voltage-sensing phosphatase modulation by a C2 domain. *Front. Pharmacol.* 6:63. <https://doi.org/10.3389/fphar.2015.00063>
- Dimitrov, D., Y. He, H. Mutoh, B.J. Baker, L. Cohen, W. Akemann, and T. Knöpfel. 2007. Engineering and characterization of an enhanced fluorescent protein voltage sensor. *PLoS One*. 2:e440. <https://doi.org/10.1371/journal.pone.0000440>
- Di Paolo, G., and P. De Camilli. 2006. Phosphoinositides in cell regulation and membrane dynamics. *Nature*. 443:651-657. <https://doi.org/10.1038/nature05185>
- Doumazane, E., P. Scholler, J.M. Zwier, E. Trinquet, P. Rondard, and J.-P. Pin. 2011. A new approach to analyze cell surface protein complexes reveals specific heterodimeric metabotropic glutamate receptors. *FASEB J*. 25:66-77. <https://doi.org/10.1096/fj.10-163147>
- Doyle, D.A., J. Morais Cabral, R.A. Pfuetzner, A. Kuo, J.M. Gulbis, S.L. Cohen, B.T. Chait, and R. MacKinnon. 1998. The structure of the potassium channel: molecular basis of K⁺ conduction and selectivity. *Science*. 280:69-77. <https://doi.org/10.1126/science.280.5360.69>
- Grimm, S.S., and E.Y. Isacoff. 2016. Allosteric substrate switching in a voltage-sensing lipid phosphatase. *Nat. Chem. Biol.* 12:261-267. <https://doi.org/10.1038/nchembio.2022>
- Halaszovich, C.R., D.N. Schreiber, and D. Oliver. 2009. Ci-VSP is a depolarization-activated phosphatidylinositol-4,5-bisphosphate and phosphatidylinositol-3,4,5-trisphosphate 5'-phosphatase. *J. Biol. Chem.* 284:2106-2113. <https://doi.org/10.1074/jbc.M803543200>
- Heinrich, F., S. Chakravarthy, H. Nanda, A. Papa, P.P. Pandolfi, A.H. Ross, R.K. Harishchandra, A. Gericke, M. Lösche, and M. Lö Sche. 2015. The PTEN Tumor Suppressor Forms Homodimers in Solution. *Structure*. 23:1952-1957. <https://doi.org/10.1016/j.str.2015.07.012>
- Hossain, M.I., H. Iwasaki, Y. Okochi, M. Chahine, S. Higashijima, K. Nagayama, and Y. Okamura. 2008. Enzyme domain affects the movement of the voltage sensor in ascidian and zebrafish voltage-sensing phosphatases. *J. Biol. Chem.* 283:18248-18259. <https://doi.org/10.1074/jbc.M706184200>
- Iwasaki, H., Y. Murata, Y. Kim, M.I. Hossain, C.A. Worby, J.E. Dixon, T. McCormack, T. Sasaki, and Y. Okamura. 2008. A voltage-sensing phosphatase, Ci-VSP, which shares sequence identity with PTEN, dephosphorylates phosphatidylinositol 4,5-bisphosphate. *Proc. Natl. Acad. Sci. USA*. 105:7970-7975. <https://doi.org/10.1073/pnas.0803936105>
- Jain, A., R. Liu, B. Ramani, E. Arauz, Y. Ishitsuka, K. Ragunathan, J. Park, J. Chen, Y.K. Xiang, and T. Ha. 2011. Probing cellular protein complexes using single-molecule pull-down. *Nature*. 473:484-488. <https://doi.org/10.1038/nature10016>
- Jones, K.A., B. Borowsky, J.A. Tamm, D.A. Craig, M.M. Durkin, M. Dai, W.J. Yao, M. Johnson, C. Gunwaldsen, L.Y. Huang, et al. 1998. GABA(B) receptors function as a heteromeric assembly of the subunits GABA(B)R1 and GABA(B)R2. *Nature*. 396:674-679. <https://doi.org/10.1038/25348>
- Jung, A., D. Rajakumar, B.-J. Yoon, and B.J. Baker. 2017. Modulating the Voltage-sensitivity of a Genetically Encoded Voltage Indicator. *Exp. Neurobiol.* 26:241-251. <https://doi.org/10.5607/en.2017.26.5.241>
- Kaupmann, K., B. Malitschek, V. Schuler, J. Heid, W. Froestl, P. Beck, J. Mosbacher, S. Bischoff, A. Kulik, R. Shigemoto, et al. 1998. GABA(B)-receptor subtypes assemble into functional heteromeric complexes. *Nature*. 396:683-687. <https://doi.org/10.1038/25360>
- Koch, S., and L. Claesson-Welsh. 2012. Signal transduction by vascular endothelial growth factor receptors. *Cold Spring Harb. Perspect. Med.* 2:a006502. <https://doi.org/10.1101/cshperspect.a006502>
- Koch, H.P., T. Kurokawa, Y. Okochi, M. Sasaki, Y. Okamura, and H.P. Larson. 2008. Multimeric nature of voltage-gated proton channels. *Proc. Natl. Acad. Sci. USA*. 105:9111-9116. <https://doi.org/10.1073/pnas.0801553105>
- Kohout, S.C., M.H. Ulbrich, S.C. Bell, and E.Y. Isacoff. 2008. Subunit organization and functional transitions in Ci-VSP. *Nat. Struct. Mol. Biol.* 15:106-108. <https://doi.org/10.1038/nsmb1320>
- Kohout, S.C., S.C. Bell, L. Liu, Q. Xu, D.L. Minor Jr., and E.Y. Isacoff. 2010. Electrochemical coupling in the voltage-dependent phosphatase Ci-VSP. *Nat. Chem. Biol.* 6:369-375. <https://doi.org/10.1038/nchembio.349>
- Kunishima, N., Y. Shimada, Y. Tsuji, T. Sato, M. Yamamoto, T. Kumasaka, S. Nakanishi, H. Jingami, and K. Morikawa. 2000. Structural basis of glutamate recognition by a dimeric metabotropic glutamate receptor. *Nature*. 407:971-977. <https://doi.org/10.1038/35039564>
- Kurokawa, T., S. Takasuga, S. Sakata, S. Yamaguchi, S. Horie, K.J. Homma, T. Sasaki, and Y. Okamura. 2012. 3' Phosphatase activity toward phosphatidylinositol 3,4-bisphosphate [PI(3,4)P₂] by voltage-sensing phosphatase (VSP). *Proc. Natl. Acad. Sci. USA*. 109:10089-10094. <https://doi.org/10.1073/pnas.1203799109>
- Lee, S., T. Geiller, A. Jung, R. Nakajima, Y.-K. Song, and B.J. Baker. 2017. Improving a genetically encoded voltage indicator by modifying the cytoplasmic charge composition. *Sci. Rep.* 7:8286. <https://doi.org/10.1038/s41598-017-08731-2>
- Levitz, J., P. Royal, Y. Comoglio, B. Wdziekonski, S. Schaub, D.M. Clemens, E.Y. Isacoff, and G. Sandoz. 2016. Heterodimerization within the TREK channel subfamily produces a diverse family of highly regulated potassium channels. *Proc. Natl. Acad. Sci. USA*. 113:4194-4199. <https://doi.org/10.1073/pnas.1522459113>
- Li, Q., S. Wanderling, M. Paduch, D. Medovoy, A. Singharoy, R. McGreevy, C.A. Villalba-Galea, R.E. Hulse, B. Roux, K. Schulten, et al. 2014. Structural mechanism of voltage-dependent gating in an isolated voltage-sensing domain. *Nat. Struct. Mol. Biol.* 21:244-252. <https://doi.org/10.1038/nsmb.2768>

- Liman, E.R., J. Tytgat, and P. Hess. 1992. Subunit stoichiometry of a mammalian K⁺ channel determined by construction of multimeric cDNAs. *Neuron*. 9:861–871. [https://doi.org/10.1016/0896-6273\(92\)90239-A](https://doi.org/10.1016/0896-6273(92)90239-A)
- Liu, L., S.C. Kohout, Q. Xu, S. Müller, C.R. Kimberlin, E.Y. Isacoff, D.L. Minor Jr., S. Müller, C.R. Kimberlin, E.Y. Isacoff, and D.L. Minor. 2012. A glutamate switch controls voltage-sensitive phosphatase function. *Nat. Struct. Mol. Biol.* 19:633–641. <https://doi.org/10.1038/nsmb.2289>
- Logothetis, D.E., V.I. Petrou, S.K. Adney, and R. Mahajan. 2010. Channelopathies linked to plasma membrane phosphoinositides. *Pflügers Arch.* 460:321–341. <https://doi.org/10.1007/s00424-010-0828-y>
- Lundby, A., H. Mutoh, D. Dimitrov, W. Akemann, and T. Knöpfel. 2008. Engineering of a genetically encodable fluorescent voltage sensor exploiting fast Ca²⁺-VSP voltage-sensing movements. *PLoS One*. 3:e2514. <https://doi.org/10.1371/journal.pone.0002514>
- Mannuzzo, L.M., M.M. Moronne, and E.Y. Isacoff. 1996. Direct physical measure of conformational rearrangement underlying potassium channel gating. *Science*. 271:213–216. <https://doi.org/10.1126/science.271.5246.213>
- Mavrantoni, A., V. Thallmair, M.G. Leitner, D.N. Schreiber, D. Oliver, and C.R. Halaszovich. 2015. A method to control phosphoinositides and to analyze PTEN function in living cells using voltage sensitive phosphatases. *Front. Pharmacol.* 6:68. <https://doi.org/10.3389/fphar.2015.00068>
- Murata, Y., H. Iwasaki, M. Sasaki, K. Inaba, and Y. Okamura. 2005. Phosphoinositide phosphatase activity coupled to an intrinsic voltage sensor. *Nature*. 435:1239–1243. <https://doi.org/10.1038/nature03650>
- Papa, A., L. Wan, M. Bonora, L. Salmena, M.S. Song, R.M. Hobbs, A. Lunardi, K. Webster, C. Ng, R.H. Newton, et al. 2014. Cancer-associated PTEN mutants act in a dominant-negative manner to suppress PTEN protein function. *Cell*. 157:595–610. <https://doi.org/10.1016/j.cell.2014.03.027>
- Perozo, E., R. MacKinnon, F. Bezanilla, and E. Stefani. 1993. Gating currents from a nonconducting mutant reveal open-closed conformations in Shaker K⁺ channels. *Neuron*. 11:353–358. [https://doi.org/10.1016/0896-6273\(93\)90190-3](https://doi.org/10.1016/0896-6273(93)90190-3)
- Ratzan, W.J., A.V. Evsikov, Y. Okamura, and L.A. Jaffe. 2011. Voltage sensitive phosphoinositide phosphatases of *Xenopus*: their tissue distribution and voltage dependence. *J. Cell. Physiol.* 226:2740–2746. <https://doi.org/10.1002/jcp.22854>
- Reiner, A., R.J. Arant, and E.Y. Isacoff. 2012. Assembly stoichiometry of the GluK2/GluK5 kainate receptor complex. *Cell Reports*. 1:234–240. <https://doi.org/10.1016/j.celrep.2012.01.003>
- Rosasco, M.G., S.E. Gordon, and S.M. Bajjalieh. 2015. Characterization of the Functional Domains of a Mammalian Voltage-Sensitive Phosphatase. *Biophys. J.* 109:2480–2491. <https://doi.org/10.1016/j.bpj.2015.11.004>
- Sato, M., Y. Ueda, T. Takagi, and Y. Umezawa. 2003. Production of PtdInsP₃ at endomembranes is triggered by receptor endocytosis. *Nat. Cell Biol.* 5:1016–1022. <https://doi.org/10.1038/ncb1054>
- Schlessinger, J. 2014. Receptor tyrosine kinases: legacy of the first two decades. *Cold Spring Harb. Perspect. Biol.* 6:1–13. <https://doi.org/10.1101/cshperspect.a008912>
- Schwenk, J., M. Metz, G. Zolles, R. Turecek, T. Fritzius, W. Bildl, E. Tarusawa, A. Kulik, A. Unger, K. Ivankova, et al. 2010. Native GABA(B) receptors are heteromultimers with a family of auxiliary subunits. *Nature*. 465:231–235. <https://doi.org/10.1038/nature08964>
- Stauffer, T.P., S. Ahn, and T. Meyer. 1998. Receptor-induced transient reduction in plasma membrane PtdIns(4,5)P₂ concentration monitored in living cells. *Curr. Biol.* 8:343–346. [https://doi.org/10.1016/S0960-9822\(98\)70135-6](https://doi.org/10.1016/S0960-9822(98)70135-6)
- Tombola, F., M.H. Ulbrich, S.C. Kohout, and E.Y. Isacoff. 2010. The opening of the two pores of the Hv1 voltage-gated proton channel is tuned by cooperativity. *Nat. Struct. Mol. Biol.* 17:44–50. <https://doi.org/10.1038/nsmb.1738>
- Villalba-Galea, C.A., F. Miceli, M. Tagliatalata, and F. Bezanilla. 2009. Coupling between the voltage-sensing and phosphatase domains of Ca²⁺-VSP. *J. Gen. Physiol.* 134:5–14. <https://doi.org/10.1085/jgp.200910215>
- Villalba-Galea, C.A., L. Frezza, W. Sandtner, and F. Bezanilla. 2013. Sensing charges of the *Ciona intestinalis* voltage-sensing phosphatase. *J. Gen. Physiol.* 142:543–555. <https://doi.org/10.1085/jgp.201310993>
- Walker, S.M., C.P. Downes, and N.R. Leslie. 2001. TPIP: a novel phosphoinositide 3-phosphatase. *Biochem. J.* 360:277–283. <https://doi.org/10.1042/bj3600277>
- White, J.H., A. Wise, M.J. Main, A. Green, N.J. Fraser, G.H. Disney, A.A. Barnes, P. Emson, S.M. Foord, and F.H. Marshall. 1998. Heterodimerization is required for the formation of a functional GABA(B) receptor. *Nature*. 396:679–682. <https://doi.org/10.1038/25354>
- Wu, Y., D. Dowbenko, M.T. Pisabarro, L. Dillard-Telm, H. Koeppen, and L.A. Lasky. 2001. PTEN 2, a Golgi-associated testis-specific homologue of the PTEN tumor suppressor lipid phosphatase. *J. Biol. Chem.* 276:21745–21753. <https://doi.org/10.1074/jbc.M101480200>
- Yarden, Y. 2001. The EGFR family and its ligands in human cancer: signaling mechanisms and therapeutic opportunities. *Eur. J. Cancer*. 37(Suppl 4):S3–S8. [https://doi.org/10.1016/S0959-8049\(01\)00230-1](https://doi.org/10.1016/S0959-8049(01)00230-1)

B. Annex 2: Patent

Acknowledgement of receipt

We hereby acknowledge receipt of your request for the processing of an international application according to the Patent Cooperation Treaty as follows:

Submission number	6470854	
PCT application number	PCT/EP2018/067581	
Date of receipt	29 June 2018	
Receiving Office	European Patent Office, The Hague	
Your reference	SANDOZ17200MS	
Applicant	INSERM (INSTITUT NATIONAL DE LA SANTÉ ET DE LA RECHERCHE MÉDICALE)	
Number of applicants	3	
Country	FR	
Title	METHODS AND COMPOSITIONS FOR TREATING MIGRAINE	
Documents submitted	package-data.xml application-body.xml validation-log.xml abst.txt	request.xml fee-sheet.xml eolf-appb-P000001.pdf (13 p.) eolf-othd-000001.pdf (24 p.)
Submitted by	CN=secure.epoline.org,OU=PDIS,O=European Patent Office,C=NL	
Method of submission	Online	
Date and time receipt generated	29 June 2018, 11:33 (CEST)	

Message Digest

37:27:97:32:75:9D:A2:A3:CC:8D:FB:5A:93:7B:ED:40:19:4E:4B:B2

Correction by the EPO of errors in debit instructions filed by eOLF

Errors in debit instructions filed by eOLF that are caused by the editing of Form 1038E entries or the continued use of outdated software (all forms) may be corrected automatically by the EPO, leaving the payment date unchanged (see decision T 152/82, OJ EPO 1984, 301 and point 6.3 ff ADA, Supplement to OJ EPO 10/2007).

/European Patent Office/

METHODS AND COMPOSITIONS FOR TREATING MIGRAINE

FIELD OF THE INVENTION:

5 The invention is in the field of neurology more particularly, the invention relates to methods and composition for treating migraine.

BACKGROUND OF THE INVENTION:

Worldwide, migraines affect nearly 15% or approximately one billion people. According to International Headache Society's ICHD-3 classification system, there are seven
10 types of Migraine, but the two major types of migraine are: migraine without Aura (formerly called Common Migraine) and migraine with Aura (formerly called Classic or Complicated Migraine). Migraine without Aura is the most frequent type of migraine. Symptoms include moderate to severe pulsating headache pain that occurs without warning and is usually felt on one side of the head. It comes along with nausea, confusion, blurred vision, mood changes,
15 fatigue, and increased sensitivity to light, sound, or smells. Migraine with Aura is a type of migraine includes visual disturbances and other neurological symptoms that appear about 10 to 60 minutes before the actual headache and usually last no more than an hour.

Currently, there is not any medication to treat the migraine, there is only the medication to prevent migraine or reduce the frequency of migraine. Accordingly, there is a need to
20 understand the mechanism of the migraine and identify new targets to treat migraine.

Activation and sensitization of primary afferent neurons within the trigeminal (TG) sensory system is likely a key step in the initiation of migraine headache attacks (1). It has been proposed that the underlying pathophysiology of migraine is in part due to ion channel dysfunction (2), including most recently the linking of TRESK, a two-pore-domains K⁺ (K2P)
25 channel, to inherited migraine with aura (MA) (3, 4) . In humans, 2 types of TRESK channel mutations have been found to produce a dominant negative for TRESK: TRESK-MT, a 2 bp frameshift mutation (F139WfsX24) identified in the KCNK18 gene which causes premature truncation of TRESK(3), and TRESK-C110R (5), a missense variant. Despite the fact that both mutants are able to strongly inhibit TRESK current, only TRESK-MT produces an increase in
30 TG neuron excitability and is associated with an MA phenotype (6, 7) . Thus, there is a need to study the molecular mechanisms which link TRESK-MT.

SUMMARY OF THE INVENTION:

The invention relates to a method for treating migraine in a subject in need thereof comprising a step of administering the subject with a therapeutically effective amount of

agonists of: TREK1, TREK2, or agonists of heteromers TRESK-TREK1, TRESK-TREK2 or TREK1-TREK2. In particular, the invention is defined by claims.

DETAILED DESCRIPTION OF THE INVENTION:

Inventors have found that the MT mutation puts an alternative start codon in frame which leads to the translation of a second TRESK fragment. Surprisingly, the 2 gene products, termed MT1 and MT2, have differential dominant negative effects: MT1 targets TRESK while MT2 targets TREK1 and TREK2, members of another subfamily of K2P channels. Furthermore, they have shown that by co-assembling with and inhibiting TREK1 and TREK2, MT2 increases TG excitability. This resolves the contradictory lack of effects of TRESK-C110R which targets only TRESK and not TREK1 or TREK2. Together their results demonstrate that alternative translation initiation is a mechanism initiated by the TRESK-MT mutation which leads to two protein fragments with dominant negative effects on distinct channel targets. This work supports a role for regulation of leak potassium channels as a key part of the underlying cellular mechanism of MA and identifies TREK1, TREK2 and TREK1-TREK2, TREK-TRESK heteromers as novel potential targets for treatment of this disorder. Inventors have also identified a new migraine-related TRESK mutant, Y121LfsX44, which also leads to the production of two TRESK fragments.

Accordingly, the invention relates to a method for treating migraine in a subject in need thereof comprising a step of administering the subject with a therapeutically effective amount of agonists of TREK1, TREK2, or agonists of heteromers TRESK-TREK1, TRESK-TREK2 or TREK1-TREK2.

As used herein, the terms "treating" or "treatment" refer to both prophylactic or preventive treatment as well as curative or disease modifying treatment, including treatment of subject at risk of contracting the disease or suspected to have contracted the disease as well as subject who are ill or have been diagnosed as suffering from a disease or medical condition, and includes suppression of clinical relapse. The treatment may be administered to a subject having a medical disorder or who ultimately may acquire the disorder, in order to prevent, cure, delay the onset of, reduce the severity of, or ameliorate one or more symptoms of a disorder or recurring disorder, or in order to prolong the survival of a subject beyond that expected in the absence of such treatment. By "therapeutic regimen" is meant the pattern of treatment of an illness, e.g., the pattern of dosing used during therapy. A therapeutic regimen may include an induction regimen and a maintenance regimen. The phrase "induction regimen" or "induction period" refers to a therapeutic regimen (or the portion of a therapeutic regimen) that is used for the initial treatment of a disease. The general goal of an induction regimen is to provide a high

level of drug to a subject during the initial period of a treatment regimen. An induction regimen may employ (in part or in whole) a "loading regimen", which may include administering a greater dose of the drug than a physician would employ during a maintenance regimen, administering a drug more frequently than a physician would administer the drug during a
5 maintenance regimen, or both. The phrase "maintenance regimen" or "maintenance period" refers to a therapeutic regimen (or the portion of a therapeutic regimen) that is used for the maintenance of a subject during treatment of an illness, e.g., to keep the subject in remission for long periods of time (months or years). A maintenance regimen may employ continuous therapy (e.g., administering a drug at a regular intervals, e.g., weekly, monthly, yearly, etc.) or
10 intermittent therapy (e.g., interrupted treatment, intermittent treatment, treatment at relapse, or treatment upon achievement of a particular predetermined criteria [e.g., pain, disease manifestation, etc.]).

As used herein, the term "migraine" refers to a disabling neurological disorder with an annual prevalence estimated at ~20 which is characterized by attacks of severe, throbbing
15 headaches. According to the International Headache Society's ICHD-3 classification system, there are seven types of Migraine: 1) Migraine without Aura (formerly called Common Migraine). This is the most frequent type of Migraine. Symptoms include moderate to severe pulsating headache pain that occurs without warning and is usually felt on one side of the head. It comes along with nausea, confusion, blurred vision, mood changes, fatigue, and increased
20 sensitivity to light, sound, or smells; 2) Migraine with Aura (formerly called Classic or Complicated Migraine). This type of Migraine includes visual disturbances and other neurological symptoms that appear about 10 to 60 minutes before the actual headache and usually last no more than an hour; 3) Migraine without Headache is characterized by visual problems or other aura symptoms, nausea, vomiting, and constipation, but without head pain.
25 Technically, this is known as Typical Aura without Headache; 4) Migraine with Brainstem Aura (formerly called Basilar-Type Migraine) mainly affects children and adolescents, this includes Migraine with Aura symptoms that originate from the brainstem, but without motor weakness. It occurs most often in teenage girls and may be associated with their menstrual cycles. Symptoms include partial or total loss of vision or double vision, dizziness and loss of
30 balance (vertigo), poor muscle coordination, slurred speech, a ringing in the ears (tinnitus), and fainting; 5) hemiplegic Migraine (a sub-type of Migraine with Aura) is a rare but severe form of Migraine that causes temporary paralysis, sometimes lasting several days, on one side of the body prior to or during a headache. Symptoms such as vertigo, a pricking or stabbing sensation, and problems seeing, speaking, or swallowing may begin prior to the headache pain and usually

stop shortly thereafter; 6) Retinal Migraine is a very rare type of Migraine characterized by attacks of visual loss or disturbances in one eye; 7) Chronic Migraine is characterized by headaches occurring on 15 or more days per month for more than 3 months, which have the features of Migraine headache on at least 8 days per month. They can be with or without aura, they usually require preventative medications and behaviours to control, and they are often disabling. The two major types of migraine are: migraine without Aura and migraine with Aura. In a particular embodiment, the method according to the invention, wherein the migraine is migraine without Aura. In another particular embodiment, the method according to the invention, wherein the migraine is Migraine with Aura.

As used herein, the term “subject” refers to any mammals, such as a rodent, a feline, a canine, and a primate. Particularly, in the present invention, the subject is a human afflicted with or susceptible to be afflicted with at least one of migraine as described above. In a particular embodiment, the subject is afflicted with or susceptible to be afflicted with Migraine with Aura (MA). In a particular embodiment, the subject has or is susceptible to have a mutation affecting TREK1 or TREK2. In another embodiment, the subject has or is susceptible to have a mutation which induce the production of MT2. In a particular embodiment, the subject has or is susceptible to have Y121LfsX44 mutation (TRESK c.361dupT_{STOP}) in TRESK.

As used herein, the term “TREK1”, also known as potassium channel subfamily K member 2 (KCNK2) refers to Twik-related K⁺ channel 2. It is a protein that in humans is encoded by the KCNK2 gene. TREK-1 is part of the subfamily of mechano-gated potassium channels that are present in mammalian neurons. TREK-1 channels are important in physiological, pathophysiological, and pharmacological processes, including having a role in electrogenesis, ischemia, and anesthesia. The naturally occurring human TREK1 gene has a nucleotide sequence as shown in Genbank Accession numbers: NM_001017424.2, NM_001017425.2 and NM_014217.3. The naturally occurring human TREK1 protein has an aminoacid sequence as shown in Genbank Accession numbers: NP_001017424.1, NP_001017425.2 and NP_055032.1. In a particular embodiment, TREK1 is affected by mutation.

As used herein, the term “TREK2”, also known as potassium two pore domain channel subfamily K member 10 (KCNK10) refers Twik-related K⁺ channel 2. It is a protein encoded by KCNK10 gene belongs to the family of potassium channel proteins containing two pore-forming P domains. This channel is an open rectifier which primarily passes outward current under physiological K⁺ concentrations, and is stimulated strongly by arachidonic acid and to a lesser degree by membrane stretching, intracellular acidification, and general anaesthetics. The

naturally occurring human TREK2 gene has a nucleotide sequence as shown in Genbank Accession numbers: NM_021161.4, NM_138317.2 and NM_138318.2. The naturally occurring human TREK2 protein has an aminoacid sequence as shown in Genbank Accession numbers: NP_066984.1, NP_612190.1 and NP_612191.1. In a particular embodiment, TREK2 is affected by mutation.

As used herein, the term “TRESK”, also known as Potassium channel subfamily K member 18 (KCNK18) or K2P18.1 refers to TWIK-related spinal cord potassium channel. It is a protein that in humans is encoded by the KCNK18 gene. This potassium channel contains two pore-forming P domains. The naturally occurring human TRESK gene has a nucleotide sequence as shown in Genbank Accession number NM_181840.1 and the naturally occurring human TRESK protein has an aminoacid sequence as shown in Genbank Accession numbers NP_862823.1. In a particular embodiment, TRESK has at least one mutation: F139WfsX24 or Y121LfsX44. As used herein, the term “homodimer” refers to a dimer consisting of two structurally similar monomers joined by bonds that can be either strong or weak, covalent or intermolecular. In the context of the invention, the term “heterodimer” is used when two molecules different structurally and linked together. In the context of the invention, heteromerization of subunits is a widespread mechanism for increasing diversity in voltage-gated (Kv) and inwardly-rectifying (Kir) K⁺ channel subfamilies. The resulting heteromers are typically characterized by different biophysical and regulatory properties from the homomers of the parent subunits. In particular, the method according to the invention is suitable to treat migraine by administering agonists of heteromers TRESK/TREK1, TRESK/TREK2 or TREK1/TREK2.

As used herein, the term “TRESK-TREK1” refers to a heterodimer. Typically, TRESK and TREK1 are joined each other by bonds that can be either strong or weak, covalent or intermolecular.

As used herein, the term “TRESK-TREK2” refers to a heterodimer. Typically, TRESK and TREK2 are joined each other by strong or weak, covalent or intermolecular.

As used herein, the term “TREK1-TREK2” refers to a heterodimer. Typically, TREK1 and TREK2 are joined each other by strong or weak, covalent or intermolecular.

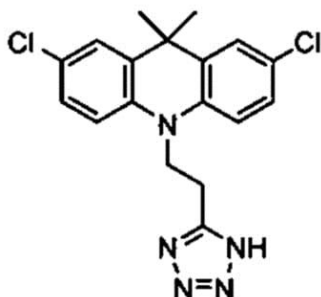
As used herein, the term “agonist” refers to a compound that binds specifically to TREK1, TREK2 or to the heteromers TRESK/TREK1, TRESK/TREK2 or TREK1/TREK2. Thus, the compound stimulates or promotes the expression and/or the biological activity of TREK1, TREK2 or heteromers TRESK/TREK1, TRESK/TREK2 or TREK1/TREK2. The agonist used according to the invention may be any substance, derived from natural sources or

from synthesis by chemical and/or genetic engineering methods. Agonists typically include but are not limited to small organic molecule, peptides, polypeptides, antibodies, nucleic acids or aptamers.

Agonistic activities of a test compound toward TREK1, TREK2, TRESK/TREK1, TRESK/TREK2 or TREK1/TREK2 may be determined by any well-known method in the art. For example, since the agonist of the present invention can promote the function of the TREK1, TREK2, the agonist can be screened using the natural agonist of TREK1, TREK2 and those which activate their associated receptors. For example, the G protein-coupled receptors (GPCRs) coupled to Gi proteins which lead to the activation of TREK1.

Typically, the agonist of the present invention can be obtained using the method screening the substance promoting the function of the TREK1, TREK2, TRESK/TREK1, TRESK/TREK2 or TREK1/TREK2 which comprises direct or indirect agonist. As used herein, a "direct agonist" refers to a compound that has a direct activity on TREK channels, particularly TREK1 and/or TREK2 homodimers, and TREK1-TREK2, TREK1-TRESK and TREK2-TRESK heterodimers that do not have an activity on a second protein upstream. As used herein, a "indirect agonist" refers to a compound that has an activity on TREK channels through a second protein (receptor) upstream. For example, activation of Gi protein-coupled receptors such as GABAB receptor or mGluR2 by their respective agonists can lead to TREK channel activation. Example of activators of GABAB receptors are well known in the art (Pin et al 2007) typically, they are selected from the group consisting of: Baclofen, gamma-Hydroxybutyrate (GHB), Phenibut, Isovaline, 3-Aminopropylphosphinic acid, Lesogaberan, SKF-97541, CGP-44532, CGP-7930, CGP-7930, BHFF, Fendiline, Fasoracetam, BHF-177, BSPP or GS-39783. Example of activators of mGluR2 are well known in the art (Lin Li et al 2015; WO2010130424) typically they are selected from the group consisting of: JNJ-46356479, JNJ-40411813, GSK-1331258, Imidazo[1,2-a]pyridines, 3-Aryl-5-phenoxyethyl-1,3-oxazolidin-2-ones, 3-(Imidazolyl methyl)-3-aza-bicyclo[3.1.0]hexan-6-yl)methyl ethers, BINA, LY-487,379.

In one embodiment, the agonist is a small organic molecule. The term "small organic molecule" refers to a molecule of a size comparable to those organic molecules generally used in pharmaceuticals. The term excludes biological macromolecules (e.g., proteins, nucleic acids, etc.). Preferred small organic molecules range in size up to about 5000 Da, more preferably up to 2000 Da, and most preferably up to about 1000 Da. In a particular embodiment, the small molecule is ML67 and its derivate. More particularly, the ML67's derivate is ML67-33 which has the following formula and structure in the art C18H17Cl2N5 (Sviatoslav N. et al 2013):



5

10 In another embodiment the agonist is an aptamer. Aptamers are a class of molecules that represents an alternative to antibodies in term of molecular recognition. Aptamers are oligonucleotide sequences with the capacity to recognize virtually any class of target molecules with high affinity and specificity.

15 In another embodiment the agonist is a polypeptide. The term “polypeptide” refers both short peptides with a length of at least two amino acid residues and at most 10 amino acid residues, oligopeptides (11-100 amino acid residues), and longer peptides (the usual interpretation of "polypeptide", i.e. more than 100 amino acid residues in length) as well as proteins (the functional entity comprising at least one peptide, oligopeptide, or polypeptide which may be chemically modified by being glycosylated, by being lipidated, or by comprising prosthetic groups).

20 In some embodiments, the agonist is an antibody. As used herein, the term “antibody” is used in the broadest sense and specifically covers monoclonal antibodies, polyclonal antibodies, multispecific antibodies (e.g. bispecific antibodies) formed from at least two intact antibodies, and antibody fragments so long as they exhibit the desired biological activity. The term includes antibody fragments that comprise an antigen binding domain such as Fab', Fab, 25 F(ab')₂, single domain antibodies (DABs), TandAbs dimer, Fv, scFv (single chain Fv), dsFv, ds-scFv, Fd, linear antibodies, minibodies, diabodies, bispecific antibody fragments, bibody, tribody (scFv-Fab fusions, bispecific or trispecific, respectively); sc-diabody; kappa(lamda) bodies (scFv-CL fusions); BiTE (Bispecific T-cell Engager, scFv-scFv tandems to attract T cells); DVD-Ig (dual variable domain antibody, bispecific format); SIP (small immunoprotein, a kind of minibody); SMIP ("small modular immunopharmaceutical" scFv-Fc dimer; DART 30 (ds-stabilized diabody "Dual Affinity ReTargeting"); small antibody mimetics comprising one or more CDRs and the like. The techniques for preparing and using various antibody-based constructs and fragments are well known in the art (see Kabat et al., 1991, specifically incorporated herein by reference). Diabodies, in particular, are further described in EP 404, 097

and WO 93/1 1 161; whereas linear antibodies are further described in Zapata et al. (1995). Antibodies can be fragmented using conventional techniques. For example, F(ab')₂ fragments can be generated by treating the antibody with pepsin. The resulting F(ab')₂ fragment can be treated to reduce disulfide bridges to produce Fab' fragments. Papain digestion can lead to the formation of Fab fragments. Fab, Fab' and F(ab')₂, scFv, Fv, dsFv, Fd, dAbs, TandAbs, ds-scFv, dimers, minibodies, diabodies, bispecific antibody fragments and other fragments can also be synthesized by recombinant techniques or can be chemically synthesized. Techniques for producing antibody fragments are well known and described in the art. For example, each of Beckman et al., 2006; Holliger & Hudson, 2005; Le Gall et al., 2004; Reff & Heard, 2001 ; Reiter et al., 1996; and Young et al., 1995 further describe and enable the production of effective antibody fragments. In some embodiments, the antibody is a "chimeric" antibody as described in U.S. Pat. No. 4,816,567. In some embodiments, the antibody is a humanized antibody, such as described U.S. Pat. Nos. 6,982,321 and 7,087,409. In some embodiments, the antibody is a human antibody. A "human antibody" such as described in US 6,075,181 and 6,150,584. In some embodiments, the antibody is a single domain antibody such as described in EP 0 368 684, WO 06/030220 and WO 06/003388. In a particular embodiment, the inhibitor is a monoclonal antibody. Monoclonal antibodies can be prepared and isolated using any technique that provides for the production of antibody molecules by continuous cell lines in culture. Techniques for production and isolation include but are not limited to the hybridoma technique, the human B-cell hybridoma technique and the EBV-hybridoma technique.

As used herein the terms "administering" or "administration" refer to the act of injecting or otherwise physically delivering a substance as it exists outside the body (e.g., an agonist of TREK1, TREK2, TRESK/TREK1; TRESK/TREK2; TREK1/TREK2) into the subject, such as by mucosal, intradermal, intravenous, subcutaneous, intramuscular delivery and/or any other method of physical delivery described herein or known in the art. When a disease, or a symptom thereof, is being treated, administration of the substance typically occurs after the onset of the disease or symptoms thereof. When a disease or symptoms thereof, are being prevented, administration of the substance typically occurs before the onset of the disease or symptoms thereof.

A "therapeutically effective amount" is intended for a minimal amount of active agent which is necessary to impart therapeutic benefit to a subject. For example, a "therapeutically effective amount" to a subject is such an amount which induces, ameliorates or otherwise causes an improvement in the pathological symptoms, disease progression or physiological conditions associated with or resistance to succumbing to a disorder. It will be understood that the total

daily usage of the compounds of the present invention will be decided by the attending physician within the scope of sound medical judgment. The specific therapeutically effective dose level for any particular subject will depend upon a variety of factors including the disorder being treated and the severity of the disorder; activity of the specific compound employed; the specific composition employed, the age, body weight, general health, sex and diet of the subject; the time of administration, route of administration, and rate of excretion of the specific compound employed; the duration of the treatment; drugs used in combination or coincidental with the specific compound employed; and like factors well known in the medical arts. For example, it is well within the skill of the art to start doses of the compound at levels lower than those required to achieve the desired therapeutic effect and to gradually increase the dosage until the desired effect is achieved. However, the daily dosage of the products may be varied over a wide range from 0.01 to 1,000 mg per adult per day. Typically, the compositions contain 0.01, 0.05, 0.1, 0.5, 1.0, 2.5, 5.0, 10.0, 15.0, 25.0, 50.0, 100, 250 and 500 mg of the active ingredient for the symptomatic adjustment of the dosage to the subject to be treated. A medicament typically contains from about 0.01 mg to about 500 mg of the active ingredient, preferably from 1 mg to about 100 mg of the active ingredient. An effective amount of the drug is ordinarily supplied at a dosage level from 0.0002 mg/kg to about 20 mg/kg of body weight per day, especially from about 0.001 mg/kg to 7 mg/kg of body weight per day.

The agonists as described above may be combined with pharmaceutically acceptable excipients, and optionally sustained-release matrices, such as biodegradable polymers, to form pharmaceutical compositions. "Pharmaceutically" or "pharmaceutically acceptable" refer to molecular entities and compositions that do not produce an adverse, allergic or other untoward reaction when administered to a mammal, especially a human, as appropriate. A pharmaceutically acceptable carrier or excipient refers to a non-toxic solid, semi-solid or liquid filler, diluent, encapsulating material or formulation auxiliary of any type. The pharmaceutical compositions of the present invention for oral, sublingual, subcutaneous, intramuscular, intravenous, transdermal, local or rectal administration, the active principle, alone or in combination with another active principle, can be administered in a unit administration form, as a mixture with conventional pharmaceutical supports, to animals and human beings. Suitable unit administration forms comprise oral-route forms such as tablets, gel capsules, powders, granules and oral suspensions or solutions, sublingual and buccal administration forms, aerosols, implants, subcutaneous, transdermal, topical, intraperitoneal, intramuscular, intravenous, subdermal, transdermal, intrathecal and intranasal administration forms and rectal administration forms. Typically, the pharmaceutical compositions contain vehicles which are

pharmaceutically acceptable for a formulation capable of being injected. These may be in particular isotonic, sterile, saline solutions (monosodium or disodium phosphate, sodium, potassium, calcium or magnesium chloride and the like or mixtures of such salts), or dry, especially freeze-dried compositions which upon addition, depending on the case, of sterilized water or physiological saline, permit the constitution of injectable solutions. The pharmaceutical forms suitable for injectable use include sterile aqueous solutions or dispersions; formulations including sesame oil, peanut oil or aqueous propylene glycol; and sterile powders for the extemporaneous preparation of sterile injectable solutions or dispersions. In all cases, the form must be sterile and must be fluid to the extent that easy syringability exists. It must be stable under the conditions of manufacture and storage and must be preserved against the contaminating action of microorganisms, such as bacteria and fungi. Solutions comprising compounds of the invention as free base or pharmacologically acceptable salts can be prepared in water suitably mixed with a surfactant, such as hydroxypropylcellulose. Dispersions can also be prepared in glycerol, liquid polyethylene glycols, and mixtures thereof and in oils. Under ordinary conditions of storage and use, these preparations contain a preservative to prevent the growth of microorganisms. The polypeptide (or nucleic acid encoding thereof) can be formulated into a composition in a neutral or salt form. Pharmaceutically acceptable salts include the acid addition salts (formed with the free amino groups of the protein) and which are formed with inorganic acids such as, for example, hydrochloric or phosphoric acids, or such organic acids as acetic, oxalic, tartaric, mandelic, and the like. Salts formed with the free carboxyl groups can also be derived from inorganic bases such as, for example, sodium, potassium, ammonium, calcium, or ferric hydroxides, and such organic bases as isopropylamine, trimethylamine, histidine, procaine and the like. The carrier can also be a solvent or dispersion medium containing, for example, water, ethanol, polyol (for example, glycerol, propylene glycol, and liquid polyethylene glycol, and the like), suitable mixtures thereof, and vegetable oils. The proper fluidity can be maintained, for example, by the use of a coating, such as lecithin, by the maintenance of the required particle size in the case of dispersion and by the use of surfactants. The prevention of the action of microorganisms can be brought about by various antibacterial and antifungal agents, for example, parabens, chlorobutanol, phenol, sorbic acid, thimerosal, and the like. In many cases, it will be preferable to include isotonic agents, for example, sugars or sodium chloride. Prolonged absorption of the injectable compositions can be brought about by the use in the compositions of agents delaying absorption, for example, aluminium monostearate and gelatin. Sterile injectable solutions are prepared by incorporating the active polypeptides in the required amount in the appropriate

solvent with several of the other ingredients enumerated above, as required, followed by filtered sterilization. Generally, dispersions are prepared by incorporating the various sterilized active ingredients into a sterile vehicle which contains the basic dispersion medium and the required other ingredients from those enumerated above. In the case of sterile powders for the preparation of sterile injectable solutions, the preferred methods of preparation are vacuum-drying and freeze-drying techniques which yield a powder of the active ingredient plus any additional desired ingredient from a previously sterile-filtered solution thereof. Upon formulation, solutions will be administered in a manner compatible with the dosage formulation and in such amount as is therapeutically effective. The formulations are easily administered in a variety of dosage forms, such as the type of injectable solutions described above, but drug release capsules and the like can also be employed. For parenteral administration in an aqueous solution, for example, the solution should be suitably buffered if necessary and the liquid diluent first rendered isotonic with sufficient saline or glucose. These particular aqueous solutions are especially suitable for intravenous, intramuscular, subcutaneous and intraperitoneal administration. In this connection, sterile aqueous media which can be employed will be known to those of skill in the art in light of the present disclosure. For example, one dosage could be dissolved in 1 ml of isotonic NaCl solution and either added to 1000 ml of hypodermoclysis fluid or injected at the proposed site of infusion. Some variation in dosage will necessarily occur depending on the condition of the subject being treated. The person responsible for administration will, in any event, determine the appropriate dose for the individual subject.

The invention will be further illustrated by the following figures and examples. However, these examples and figures should not be interpreted in any way as limiting the scope of the present invention.

FIGURES:

Figure 1. TRESK heteromerizes physically and functionally with TREK1 and TREK2. Summary bar graph showing pulldown of GFP-TRESK by HA-TRESK, HA-TREK1 or HA-TREK2, but not by HA-TASK1, HA-TASK3, or HA-TRAAK.

Figure 2. TRESK-MT, but not TRESK-C110R, acts as a dominant negative on TREK1 and TREK2 channels to increase excitability of TG neurons. (A and B) Representative traces showing the effect of TRESK-C110R and TRESK-MT co-expression on TRESK (A) or TREK1 (B) on currents elicited by voltage-ramps (from -100 to 100 mV, 1s duration). (C) Bar graph summarizing the relative current amplitude at 0 mV for TRESK, TREK1, and TREK2 with or without co-expression of TRESK-C110R or TRESK-MT. (D and E) Input-output plots of the spike frequency in response to 1s depolarizing current injection in

transfected small TG neurons show that an increase in excitability elicited by TRESK-MT is observed in WT, but not T1-/-/T2-/- neurons. The numbers of tested cells are indicated in parentheses. Student's t test (*P< 0.05, **P< 0.01, ***P< 0.001).

Figure 3. TRESK-MT induces the translation of a second protein, MT2, which mediates TREK1 inhibition. (A) Representative traces showing the effect of introduction of a STOP codon at the beginning of the MT2 ORF within the 2-3 loop (TRESK-MTSTOP) on TREK1 current. Inset shows a summary of TREK1 relative current densities when TRESK-MTSTOP is coexpressed. (B) Representative traces and summary bar graph showing the effect of mutation of candidate alternative start codons (Δ ATG1, Δ ATG2, or Δ ATG3) in TRESK-MT. Currents were elicited by voltage-ramps (from -100 to 100 mV, 1s duration). The numbers of cells tested are indicated in parentheses. Student's t test (**P< 0.01, ***P< 0.001) shows the difference between TREK1 and TREK1 co-expressed with different TRESK-MT constructs.

Figure 4. MT2, but not MT1, by acting as a dominant negative on TREK1 and TREK2 channels, increases neuronal excitability of WT small TG neurons. (A and B) Representative traces showing the effect of TRESK-MT1 or TRESK-MT2 co-expression on TRESK (A) or TREK1 (B) currents. Currents were elicited by voltage-ramps (from -100 to 100 mV, 1s duration). (C) Bar graph summarizing the relative TRESK, TREK1 and TREK2 current amplitudes at 0 mV when MT1 or MT2 are co-expressed. Student's t test (***P< 0.001). (D and E) Representative traces and input-output plots of spikes generated by incremental depolarizing current injections in WT small-diameter TG neurons transfected with either GFP ("WT"), the GFP-tagged MT1 subunit ("MT1") or the GFP-tagged MT2 subunit ("MT2"). (F) Input-output plots of spike frequency show a lack of effect of GFP-MT2 expression on TG neurons from TREK1/TREK2 double KO mice (T1-/-/T2-/-). The numbers of cells tested are indicated in parentheses. Student's t test (**P< 0.01, ***P< 0.001).

Figure 5: TREK1-/-/TREK2-/- double knockout animals present a migraine-like hypersensitivity to mechanical stimuli. (a, b) Schematic of experimental behavioral paradigms. Green arrows represent the injection of ISDN, a known migraine trigger. Blue arrows represent the measurement of mechanical sensitivity. (c) Basal mechanical responses, assessed after the first ISDN injection, were significantly decreased in double knockout animals and remained less than WT for the first 1.5 hrs following ISBN injection. (d) Mechanical responses, assessed prior to and after chronic ISDN injections, were significantly decreased in double knockout animals (c, d) Student's t test to compare WT vs TREK1-/-/TREK2-/- mice (*P< 0.05, **P< 0.01, ***P< 0.001). (e) Comparison of the mechanical threshold before and after chronic treatment with ISDN. Topiramate treatment were assessed before and 2 hours after

topiramate injection. Numbers of mice tested are indicated in parentheses, Student's t test to compare WT vs TREK1-/-/TREK2-/- mice (*P< 0.05, **P< 0.01, ***P< 0.001).

Figure 6: TRESK-c.361dupT (Y121LfsX44) acts as a dominant negative to reduce both TRESK and TREK1 current. Co-synthesis of mCherry-MT1 and MT2-GFP products from the mCherry-TRESK- c.361dupT-GFP cDNA in HEK293T cells. (A) Representative traces showing the effect of TRESK c.361dupT (A) and TRESK c.361dupTSTOP (A) co-expression on TRESK current. Currents were elicited by voltage-ramps (from -100 to 100 mV, 1s duration). (B) Same as (A) for TREK1. (C) same as (A) for TREK2. (D) Bar graph summarizing the relative TRESK, TREK1 and TREK2 current amplitudes at 0 mV for TRESK, TREK1 and TREK2 when TRESK c.361dupT and TRESK c.361dupTSTOP are coexpressed. Student's t test (**P<0.01 and ***P< 0.001).

EXAMPLE:

Material & Methods

Molecular Biology, Cell Culture and Gene Expression

Channel DNA was used in the pIRES2eGFP, pcDNA3.1 and pCMV-HA vectors. HEK293 cells were maintained in DMEM with 5% FBS on poly-L-lysine-coated glass coverslips in 12 well plates. Cells were transiently co-transfected using Lipofectamine 2000 (Invitrogen) with a total of 1-1.6 µg of DNA total per 18 mm diameter cover slip.

Primary cultures of mouse TG neurons

All mouse experiments were conducted according to national and international guidelines and have been approved by the local ethical committee (CIEPAL NCE). The C57BL/6 breeders were maintained on a 12 h light/dark cycle with constant temperature (23–24°C), humidity (45–50%), and food and water ad libitum at the animal facility of Valrose. TG tissues were collected from postnatal day 8 mice of either sex and treated with 2 mg/ml collagenase type II (Worthington) for ~2 hours, followed by 2.5 mg/ml trypsin for 15 min. Neurons were dissociated by triturating with fire-polished glass pipettes and seeded on polylysine/laminin coated coverslips. The DMEM-based culture medium contained 10% fetal bovine serum and 2mM GlutaMAX (Invitrogen). Neurons were transfected at 1 d in vitro (DIV) using Lipofectamine 2000 (Invitrogen). Transfected neurons were identified by the green fluorescence and patch clamp recordings were performed between DIV 3 and 5.

Knock-out mice

Mice lacking *Trek1* and *Trek2* were generated as described (19). Null mutations were backcrossed against the C57BL/6J inbred strain for 10+ generations prior to establishing the

breeding cages to generate subjects for this study. Age- and sex-matched C57bl/J6 WT mice, aged 9-12 weeks, were obtained from Charles River Laboratories (Wilmington, MA).

Electrophysiology

HEK293 cell electrophysiology was performed 24-72 h after transfection in solution containing (in mM): 145 mM NaCl, 4 mM KCl, 1 mM MgCl₂, 2 mM CaCl₂ and 10 mM HEPES. Glass pipettes of resistance between 3 and 6 M Ω were filled with intracellular solution containing (in mM): 140 KCl, 10 HEPES, 5 EGTA, 3 MgCl₂, pH 7.4. Cells were patch clamped using an Axopatch 200A (Molecular Devices) amplifier in the whole cell mode. Currents were elicited by voltage-ramps (from -100 to 100 mV, 1s in duration) and the current density was calculated at 0 mV.

Neuronal excitability was studied in small-diameter TG neurons transfected with the pCMV-HA-GFP-X constructs (X is in frame with GFP) or the pCMV-HA-GFP control plasmid. Both plasmids derive from pCMV-HA in which we have subcloned the GFP sequence in frame. Extracellular solution contained (in mM): 135 NaCl, 5 KCl, 2 CaCl₂, 1 MgCl₂, 5 HEPES, 10 glucose, pH 7.4 with NaOH, 310 mOsm. The pipette solution contained the following (in mM): 140 K-gluconate, 10 NaCl, 2 MgCl₂, 5 EGTA, 10 HEPES, 2 ATP-Mg, 0.3 GTP-Na, 1CaCl₂ pH 7.3 with KOH, 290 mOsm. Recording pipettes had < 4.5 M Ω resistance. Series resistance (<20 M Ω) was not compensated. Signals were filtered at 10 kHz and digitized at 20 kHz. After establishing whole-cell access, membrane capacitance was determined with amplifier circuitry. The amplifier was then switched to current-clamp mode to measure resting membrane potential (V_{rest}). Neurons were excluded from analysis if the V_{rest} was higher than -40 mV or if the input resistance was smaller than 200 M Ω . To test neuronal excitability, neurons were held at V_{rest} and injected with 1 s depolarizing currents in 25 pA incremental steps until at least 1 action potential (AP) was elicited.

Western blot analysis

HEK293T cells were homogenized in PBS containing saponin (0.5% w/v), Triton X - 100 (0.5% w/v) and protease inhibitors (Roche Diagnostics, Basel, Switzerland). Lysates were clarified by centrifugation at 20 000 g for 30 min. Proteins were separated on 10% SDS polyacrylamide gel and blotted onto nitrocellulose membrane (Hybond - C extra, Amersham Biosciences, Freiburg, Germany). Detection was carried out using mouse monoclonal antibody clone HA-7 against the HA epitope (Sigma).

Single Molecule Pulldown

For SimPull experiments, HEK 239T cells were harvested from coverslips by incubating with Ca²⁺-free PBS buffer for 20-30 minutes followed by gentle pipetting. Cells were lysed in buffer containing (in mM): 150 NaCl, 1 EDTA, protease inhibitor cocktail (Thermo Scientific) and 1.5% IGEPAL (Sigma). After 30-60 minute incubation at 4°, lysate was centrifuged for 20 minutes at 16,000 g and the supernatant was collected. Coverslips passivated with PEG (~99%)/ biotin-PEG(~1%) and treated with neutravidin were prepared as described(2). 15 nM biotinylated anti-HA antibody (abcam, #ab26228) was applied for 20 minutes and then washed out. Antibody dilutions and washes were done in T50 buffer containing (in mM): 50 NaCl, 10 Tris, pH 7.5. Lysate, diluted in standard patch clamp electrophysiology extracellular recording solutions (see Electrophysiology), was then applied to the chamber and washed away following brief incubation (~2 minutes). Single molecules were imaged using a 488 nm Argon laser on a total internal reflection fluorescence microscope with a 60x objective (Olympus). We recorded the emission light after an additional 3x magnification and passage through a double dichroic mirror and an emission filter (525/50 for GFP) with a back-illuminated EMCCD camera (Andor iXon DV-897 BV). Movies of 500-800 frames were acquired at frame rates of 10–30 Hz. The imaged area was 13 x 13 μm². At least 5 movies were recorded for each condition and data was analyzed using custom software. Multiple independent experiments were performed for each condition. Representative data sets are presented to quantitatively compare conditions tested on the same day.

Results

In this invention, inventors addressed the following question: why is TRESK-MT, but not TRESK-C110R, able to increase TG excitability and, subsequently, induce migraine despite sharing the same dominant-negative functional effect? Despite the fact that K2P channels share a similar architecture and global function, they share a low level of sequence identity, even between members of the same subfamily. Surprisingly, this low level of identity does not preclude heteromerization, as we and others recently showed within the TREK subfamily (8-10). Based on this and the fact that TG neurons express many K2P channels (TREK1, TREK2, TRAAK, TASK1 and TASK3) (11, 12), inventors hypothesized that the difference between TRESK mutants is due to their differential ability to modify the function of other K2P channels through heteromerization. To assess the ability of TRESK to heteromerize with other K2P channels which are expressed in TG neurons, we used the recently-developed single-molecule pull-down (“SiMPull”) assay (13, 14) to visualize individual antibody-immobilized protein complexes on polyethylene glycol-passivated glass coverslips. We co-expressed GFP-TRESK

with either HA-TRESK, HA-TREK1, HA-TREK2, HA-TRAAK, HA-TASK1, or HA-TASK3 and assessed their ability to co-immunoprecipitate (Co-IP) GFP-TRESK via an anti-HA antibody. HA-TRESK, HA-TREK1, and HA-TREK2, were able to co-IP many fluorescent GFP-TRESK spots (Fig. 1 A whereas no GFP-TRESK spots were observed for HA- TRAAK, HA-TASK1 or HA-TASK3 (Fig. 1A) indicating that TRESK co-assembly with other K2P channels is specific for TREK1 and TREK2.

Next, to test the ability of TREK1 and TRESK to form a functional complex we developed a TREK functional heterodimerization assay based on an engineered “Photoswitchable Conditional Subunit” (TREK1-PCS) of TREK1. The TREK1-PCS is a TREK1 subunit where the C-terminus has been deleted to produce ER retention, which can be rescued through co-assembly with a full-length subunit (15). Following co-assembly and surface targeting, TREK1-PCS can then optically control the channel via a tethered photoswitchable blocker which attaches to a genetically engineered cysteine. Therefore, gain of photosensitivity of an identified co-expressed TREK interacting subunit allows for the verification of a functional heteromer with TREK1. As expected, expression of TREK1-PCS alone did not generate a photoswitchable current (data not shown) but co-expression with either TREK1 or TRESK induced a robust photoswitchable current (data not shown), indicating that the TRESK subunit is able to co-assemble with TREK1-PCS to form a heteromeric channel with a common pore. Consistent with SiMPull data (data not shown), no photocurrent was observed when TASK3 was co-expressed with TREK1-PCS. Having found that TREK1 and TREK2 can heteromerize with TRESK, we next investigated the ability of TRESK mutants to modify TREK1 and TREK2 currents.

As previously shown (7), both TRESK-MT and TRESK-C110R exert a dominant-negative effect on whole cell TRESK currents (Fig. 2A, C). Since TREK1 can co-assemble with TRESK (Fig. 1), we addressed the impact of the MT and C110R variants on TREK1 current. We found that TRESK-C110R co-expression did not modify TREK1 current whereas TRESK-MT co-expression induced a near-complete inhibition of TREK1 current (Fig. 2B, C). Similar to TREK1, TRESK-MT but not TRESK-C110R strongly inhibited TREK2 current (Fig. 2C). This dominant negative effect is likely dependent on co-assembly since TASK1, TASK3 and TRAAK, which do not co-IP with TRESK (Fig. 1), were not sensitive to TRESK-MT co-expression (data not shown). Together these data show that TRESK-MT can inhibit TRESK, TREK1 and TREK2 whereas TRESK-C110R is only able to inhibit TRESK. Based on the fact that TRESK-MT but not TRESK-C110R is able to induce TG neuron hyperexcitability (5, 6),

we hypothesized that TRESK-MT induces sensory neuron hyper-excitability primarily by acting on TREK1 and TREK2, not TRESK.

To investigate the role of TREK1 and TREK2 in the induction of TG hyperexcitability by TRESK-MT, we tested if overexpression of GFP-TRESK-MT alters the passive and active electrophysiological properties of small-diameter (<25 μ m) TG neurons from wild-type or TREK1/TREK2 double knockout (TREK1^{-/-}/TREK2^{-/-}) mice. As previously shown, TRESK-MT expression in WT TG neurons led to an increase in excitability (Fig. 2) which included a decrease in the rheobase (74 ± 11 pA vs 47 ± 5 pA, $P < 0.05$ for TG neurons expressing GFP or TRESK-MT, respectively) and an increase in the number of action potentials (APs) evoked by suprathreshold current injections compared to control (Fig. 2D). Notably, neurons from TREK1^{-/-}/TREK2^{-/-} mice were more excitable than WT TG neurons (data not shown). These neurons present a smaller rheobase (55 ± 6 pA, $P < 0.05$) and a significant increase in the number of APs evoked by suprathreshold current injections compare to WT-TG. Consistent with a role for TREK1 and 2 in mediating the effects of TRESK-MT, TRESK-MT overexpression did not alter the excitability or rheobase (55 ± 6 pA vs 53 ± 6 pA, for TG neuron expressing GFP or TRESK-MT respectively) of TREK1^{-/-}/TREK2^{-/-} neurons (Fig. 2D). Together these data strongly support the idea that TRESK-MT differs from TRESK- C110R by its ability to target TREK1 and TREK2 to increase the excitability of TG neurons, likely a crucial step in the induction of migraines.

We next explored how TRESK-MT exerts its effects on TREK channels at the molecular level. The F139WfsX24 frameshift mutation of TRESK-MT results in the premature truncation of human TRESK protein from 384 to 162 aa. The corresponding mutation has very similar effects on the mouse TRESK gene, generating a truncated protein with the first 149 aa of wild-type TRESK and a 50 aa aberrant sequence at the C terminus. We fused a GFP tag to the N-terminus of the MT subunit and tested its ability to be immobilized by HA-TRESK, HA-TREK1 or HA-TREK2 in the SiMPull assay. Surprisingly, only HA-TRESK was able to co-IP GFP-TRESK-MT via an anti-HA antibody (data not shown). This result confirms that TRESK-MT associates with TRESK to induce its dominant negative effect but raises the question of how TRESK-MT is able to inhibit TREK1 and TREK2 without direct association.

It has been hypothesized that alternative translation initiation (ATI) of eukaryotic mRNAs, including those that encode K2P channels (16), may be a method to expand the proteome (17). A close examination of the nucleotide sequence of TRESK-MT revealed that the F139WfsX24 frame shift mutation puts two new ATG codons in frame. We hypothesized that one of these codons may serve as an ATI site that can lead to the formation of a second

truncated TRESK protein (“MT2”) of ~28 kDa that would include short (either 2 or 19 aa) N-terminal aberrant sequence followed by the C-terminal part of TM2, the 2-3 intracellular loop, TM3, P2 loop, TM4 and the C terminal domains. To test whether MT2 is co-expressed with MT1, we introduced an N-terminal mCherry-tag in frame with MT1 and a C-terminal GFP in frame with MT2 within the mouse TRESK-MT cDNA (“mCherry-TRESK-MT-GFP”; Fig. 3C). Expression of this construct leads to cells with both mCherry and GFP fluorescence. Next, we introduced an N-terminal hemagglutinin (HA) tag in frame with MT1 and another one in frame with MT2 within the mouse TRESK-MT cDNA (“HA-TRESK-MT-HA”). Lysate from cells transfected with HA-TRESK-MT-HA was probed in a western blot with anti-HA antibodies and 2 bands, with a similar intensity, corresponding to the expected molecular weight for MT1 (~23 kDa) and MT2 (~28 kDa) were detected (data not shown). Together these data show that TRESK-MT leads to the production of two distinct fragments of TRESK that may produce distinct functional effects.

To probe the function of MT2, we introduced a stop codon into the MT2 ORF of TRESK-MT at the beginning of the 2-3 loop. The introduction of the stop codon in MT2 ORF did not change the ability of TRESK-MT to inhibit TRESK current (data not shown), this stop codon abolished the ability of TRESK-MT to produce a dominant negative functional effect on TREK1 (Fig. 3A). We next confirmed the importance of this second ORF by mutating, in TRESK-MT, the putative ATI one by one. Mutation of the first ATG abolished the ability of TRESK-MT to inhibit TREK1 but not TRESK (Fig. 3B) whereas mutation of the second ATG did not alter the ability of TRESK-MT to inhibit TREK1 current (Fig. 3B). This data indicates that the ATI site is the first internal ATG. As a control, we mutated a third ATG, which is also present in the WT-TRESK sequence, and found that it did not change the ability of TRESK-MT to inhibit both TRESK and TREK1 currents (Fig. 3B)

To independently express MT1 and MT2 for functional characterization, we subcloned both ORFs into separate mammalian expression vectors. Co-expression of MT2 with TRESK did not modify TRESK current (Fig. 4A, C), while MT1 co-expression induced a ~3-fold decrease of the current which was similar to what was observed for the co-expression of the full TRESK-MT construct (Fig. 4A, C). On the contrary, co-expression of MT1 did not modify TREK1 current (Fig. 4B, C) but co-expression of MT2 induced a ~4-fold decrease of the current, similar to what was observed with co-expression of the full TRESK-MT construct (Fig. 4B, C). Similar results were obtained for TREK2 (Fig. 4C). Consistent with the functional data, we found that GFP-MT2 is co-immunoprecipitated with TREK1 and TREK2 (data not shown).

Finally, to validate the physiological role of interaction between TREK1, TREK2 and MT2, we tested the functional effect of MT2 in TG neurons. Whereas MT1 expression did not alter the excitability of TG neurons (Fig. 4D), MT2 increased it significantly (Fig. 4D,E). We confirmed that this effect is linked to TREK1 and TREK2 since MT2 overexpression failed to increase the excitability of TREK1^{-/-}/TREK2^{-/-} TG neurons (Fig. 4F).

An increase in TG neuron excitability is a crucial step in the induction of migraines. Having found that expression of the TRESK-MT mutant increases TG excitability through TREK1-TREK2 inhibition, we hypothesized that TREK1-TREK2 KO mice would show an increased susceptibility to a migraine-related phenotype. Migraine is associated with increased sensitivity to all sensory modalities and it appears that cutaneous allodynia can be used as a quantifiable marker of migraine disorder¹. One approach to model acute and chronic migraine is the quantification of this increase in response to known migraine triggers such as Isosorbide Dinitrate (ISDN). We quantified ISDN-evoked mechanical hyperalgesia in TREK1^{-/-}/TREK2^{-/-} and wild-type controls in acute and chronic conditions. In a first experiment mechanical nociception thresholds were determined with a dynamic von Frey aesthesiometer before and during a 3-hour period after intraperitoneal injection of ISDN (10 mg/kg) (Fig. 5a). In a second experiment, we assessed mechanical nociception thresholds in both TREK1^{-/-}/TREK2^{-/-} and wild-type littermate controls, by intraperitoneally injecting ISDN every day for four days as a model of chronic migraine-associated pain (Fig. 5b)². We found that, at rest, TREK1^{-/-}/TREK2^{-/-} mice showed a decreased mechanical threshold compared to WT mice ($2.6 \pm 0.1\text{g}$ vs $3.9 \pm 0.1\text{g}$; $P < 0.001$). Notably, the basal threshold of TREK1^{-/-}/TREK2^{-/-} mice is similar to both the threshold observed 1.5 hours after acute ISDN injection ($P = 0.831$) (Fig. 5c) and after 4 days of chronic injection (Fig. 5c) in WT mice. In the acute model experiment, during the first 1.5-hour following ISDN injection, the mechanical thresholds remained significantly lower in TREK1^{-/-}/TREK2^{-/-} mice than in wild-type controls ($P < 0.001$ after 30 minutes and $P < 0.01$ after 1 hour with a linear mixed-effects model). In the chronic migraine-associated pain assay, the mechanical thresholds remained significantly lower for TREK1^{-/-}/TREK2^{-/-} mice compared to wild-type controls over the four day period despite a strong reduction in the threshold for WT mice over the course of treatment.

Having found that ISDN did not change the mechanical threshold in both acute and chronic migraine-associated pain models in TREK1^{-/-}/TREK2^{-/-} mice, we wondered if a treatment used in prophylaxis in migraine patient, topiramate, could reverse this observed migraine-like phenotype. We assessed the mechanical nociception threshold in TREK1^{-/-}/TREK2^{-/-} mice before and 2 hours following the intraperitoneal injection of 30 mg/kg of

topiramate. Treatment with topiramate inhibited the chronic basal hyperalgesia seen in TREK1-
-/-/TREK2-/- mice ($1.2 \pm 0.2g$; Fig. 1e), as was previously observed for a nitroglycerin-evoked
form of hyperalgesia². As a control, we tested WT mice and did not observe any significant
shift of the mechanical threshold following topiramate treatment (Fig. 5e).

5 MT2-producing alternative translation initiation is found in other migraine-associated
TRESK mutants. Having found that MT2 is responsible for the migraine-associated increase
in TG excitability through the inhibition of TREK1 and TREK2, we anticipated that other
frameshift mutations may exist which place the ATG at position +356 in-frame with the
reference open reading frame of TRESK. Such mutations would lead to the formation of MT2.
10 This mutation could be either a 2 bp deletion or 1 bp insertion in the region between the ATG
at position +356 and the TGA at position +427 (data not shown). We used the Exome
Aggregation Consortium (ExAC) database (Lek et al., 2016) and found one variant
(Y121LfsX44) with a T duplication (+1 pb, c.361dupT) that places the ATI site in frame with
the TRESK ORF (data not shown). We introduced this insertion into the mCherry-TRESK-
15 GFP (mCherry-TRESK-c.361dupT-GFP) sequence and found, similar to mCherry-TRESK-
MT-GFP (data not shown), that this construct led to HEK293T cells with both mCherry and
GFP fluorescence (data not shown) showing the co-translation of both MT1 and MT2 proteins.
Similar to TRESK-MT, this mutant is able to inhibit both TRESK, TREK1 and TREK2 (Figure
6). As was seen for TRESK-MT (data not shown), introduction of a stop codon into the MT2
20 ORF (TRESK c.361dupTSTOP) of this mutant abolished its ability to inhibit TREK1 and
TREK2 (Figure 6), but not TRESK. Since this Y121LfsX44 mutation leads to the same
molecular effects as TRESK-MT on TREK function, we hypothesized that it may be associated
with a migraine phenotype. To address this, we looked in the ClinVar database (Landrum et al.,
2016) and found that this mutant has been correlated with a migraine phenotype
25 (RCV000490385.1).

Together these results show that, unexpectedly, the strongly MA-associated TRESK
mutations F139WfsX2 and Y121LfsX44 lead to the production of two protein fragments that
can either target wild-type TRESK or wild-type TREK1 and TREK2 potassium channels. This
resolves the contradictory lack of effects of TRESK-C110R which also serves as a dominant
30 negative of TRESK but, as we show here, has no effect on TREK1 nor TREK2. These findings
suggest that ATI may be a more prevalent phenomenon than previously thought which can lead
to unexpected effects in a protein's function, regulation and role in disease. Future work will
be needed to elucidate the molecular, cellular, and circuit mechanisms of heteromeric K2P
channel modulation in MA to gain a deeper understanding of the underlying pathophysiology

and to devise a means of targeting this complex for treatment. The results with using ISDN show that TREK1-/-/TREK2-/- mice present a phenotype at rest which is similar to the phenotype observed in ISDN-treated animals in which migraine have been induced and this phenotype is partially reversed by topiramate, a drug used in the clinic to treat chronic migraine.

5 **REFERENCES:**

Throughout this application, various references describe the state of the art to which this invention pertains. The disclosures of these references are hereby incorporated by reference into the present disclosure.

10 1 Nosedá, R. & Burstein, R. Migraine pathophysiology: anatomy of the trigeminovascular pathway and associated neurological symptoms, CSD, sensitization and modulation of pain. *Pain* 154 Suppl 1, doi:10.1016/j.pain.2013.07.021 (2013).

 2 Yan, J. & Dussor, G. Ion channels and migraine. *Headache* 54, 619-639, doi:10.1111/head.12323 (2014).

15 3 Lafrenière, R. G. et al. A dominant-negative mutation in the TRESK potassium channel is linked to familial migraine with aura. *Nat Med* 16, 1157-1160, doi:10.1038/nm.2216 (2010).

 4 Wood, H. Migraine: Familial migraine with aura is associated with a mutation in the TRESK potassium channel. *Nat Rev Neurol* 6, 643, doi:10.1038/nrneurol.2010.166 (2010).

20 5 Andres-Enguix, I. et al. Functional analysis of missense variants in the TRESK (KCNK18) K channel. *Sci Rep* 2, 237, doi:10.1038/srep00237 (2012).

 6 Liu, P. et al. Functional analysis of a migraine-associated TRESK K⁺ channel mutation. *J Neurosci* 33, 12810-12824, doi:10.1523/JNEUROSCI.1237-13.2013 (2013).

25 7 Guo, Z., Liu, P., Ren, F. & Cao, Y. Q. Nonmigraine-associated TRESK K⁺ channel variant C110R does not increase the excitability of trigeminal ganglion neurons. *J Neurophysiol* 112, 568-579, doi:10.1152/jn.00267.2014 (2014).

 8 Talley, E. M., Solorzano, G., Lei, Q., Kim, D. & Bayliss, D. A. Cns distribution of members of the two-pore-domain (KCNK) potassium channel family. *J Neurosci* 21, 7491-7505 (2001).

30 9 Levitz, J. et al. Heterodimerization within the TREK channel subfamily produces a diverse family of highly regulated potassium channels. *Proc Natl Acad Sci U S A* 113, 4194-4199, doi:10.1073/pnas.1522459113 (2016).

 10 Hwang, E. M. et al. A disulphide-linked heterodimer of TWIK-1 and TREK-1 mediates passive conductance in astrocytes. *Nat Commun* 5, 3227, doi:10.1038/ncomms4227 (2014).

11 Blin, S. et al. Mixing and matching TREK/TRAAK subunits generate heterodimeric K2P channels with unique properties. *Proc Natl Acad Sci U S A* 113, 4200-4205, doi:10.1073/pnas.1522748113 (2016).

12 Bautista, D. M. et al. Pungent agents from Szechuan peppers excite sensory neurons
5 by inhibiting two-pore potassium channels. *Nat Neurosci* 11, 772-779, doi:10.1038/nn.2143 (2008).

13 Yamamoto, Y., Hatakeyama, T. & Taniguchi, K. Immunohistochemical colocalization of TREK-1, TREK-2 and TRAAK with TRP channels in the trigeminal ganglion cells. *Neurosci Lett* 454, 129-133, doi:10.1016/j.neulet.2009.02.069 (2009).

10 14 Jain, A., Liu, R., Xiang, Y. K. & Ha, T. Single-molecule pull-down for studying protein interactions. *Nat Protoc* 7, 445-452, doi:10.1038/nprot.2011.452 (2012).

15 Jain, A. et al. Probing cellular protein complexes using single-molecule pull-down. *Nature* 473, 484-488, doi:10.1038/nature10016 (2011).

16 Sandoz, G., Levitz, J., Kramer, R. H. & Isacoff, E. Y. Optical control of endogenous
15 proteins with a photoswitchable conditional subunit reveals a role for TREK1 in GABA(B) signaling. *Neuron* 74, 1005-1014, doi:10.1016/j.neuron.2012.04.026 (2012).

17 Thomas, D., Plant, L. D., Wilkens, C. M., McCrossan, Z. A. & Goldstein, S. A. Alternative translation initiation in rat brain yields K2P2.1 potassium channels permeable to sodium. *Neuron* 58, 859-870, doi:10.1016/j.neuron.2008.04.016 (2008).

20 18 Kochetov, A. V. Alternative translation start sites and hidden coding potential of eukaryotic mRNAs. *Bioessays* 30, 683-691, doi:10.1002/bies.20771 (2008).

19 Guyon, A. et al. Glucose inhibition persists in hypothalamic neurons lacking tandem-pore K⁺ channels. *J Neurosci* 29, 2528-2533, doi:10.1523/JNEUROSCI.5764-08.2009 (2009).

CLAIMS:

- 5 1. A method for treating migraine in a subject in need thereof comprising a step of administering the subject with a therapeutically effective amount of agonists of TREK1, TREK2, or agonists of heteromers TRESK-TREK1, TRESK-TREK2 or TREK1-TREK2.
2. The method according to claim 1, wherein, the agonist is an antibody.
3. The method according to claim 1, wherein, the agonist is a small molecule.
- 10 4. The method according to claims 1 and 3, wherein the small molecule is ML67-33.
5. The method according to claims 1 and 3, wherein the subject has or is susceptible to have a mutation affecting TREK1 or TREK2.
6. The method according to claims 1 and 3, wherein, the subject has or is susceptible to have a mutation which induce the production of MT2.

ABSTRACT OF THE INVENTION

METHODS AND COMPOSITIONS FOR TREATING MIGRAINE

5

Inventors have found that the MT mutation puts an alternative start codon in frame which leads to the translation of a second TRESK fragment. Surprisingly, the 2 gene products, termed MT1 and MT2, have differential dominant negative effects: MT1 targets TRESK while MT2 targets TREK1 and TREK2, members of another subfamily of K2P channels. Furthermore, they have shown that by co-assembling with and inhibiting TREK1 and TREK2, MT2 increases TG excitability. This resolves the contradictory lack of effects of TRESK-C110R which targets only TRESK and not TREK1 or TREK2. Together their results demonstrate that alternative translation initiation is a mechanism initiated by the TRESK-MT mutation which leads to two protein fragments with dominant negative effects on distinct channel targets. The present invention relates to a method for treating migraine in a subject in need thereof comprising a step of administering the subject with a therapeutically effective amount of agonists of: TREK1, TREK2, TRESK-TREK1, TRESK-TREK2 or TREK1-TREK2.

10

15

20

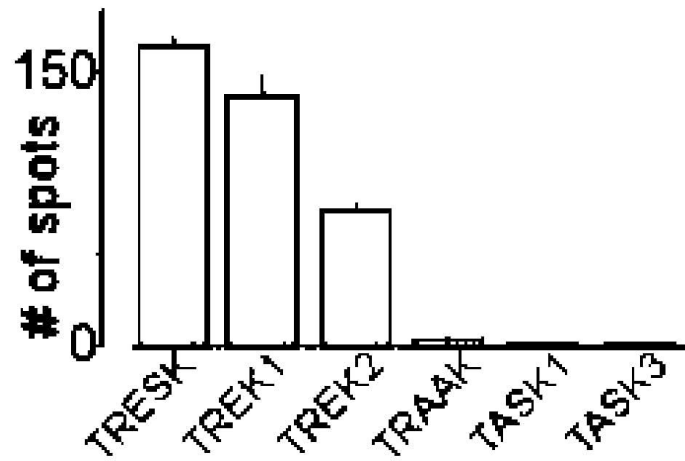


Figure 1

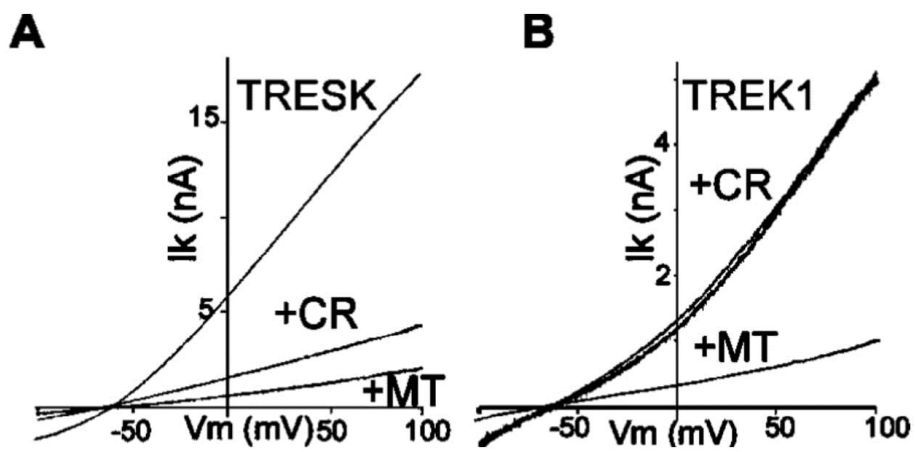


Figure 2 A-B

C

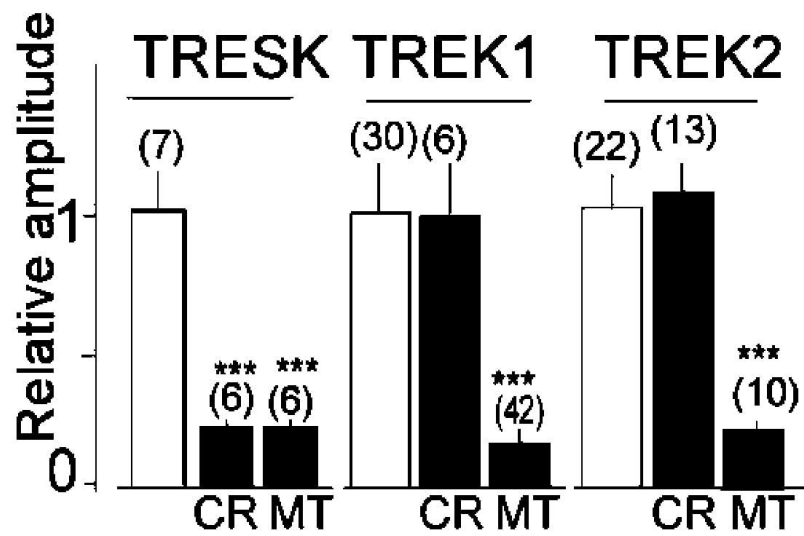


Figure 2C

D

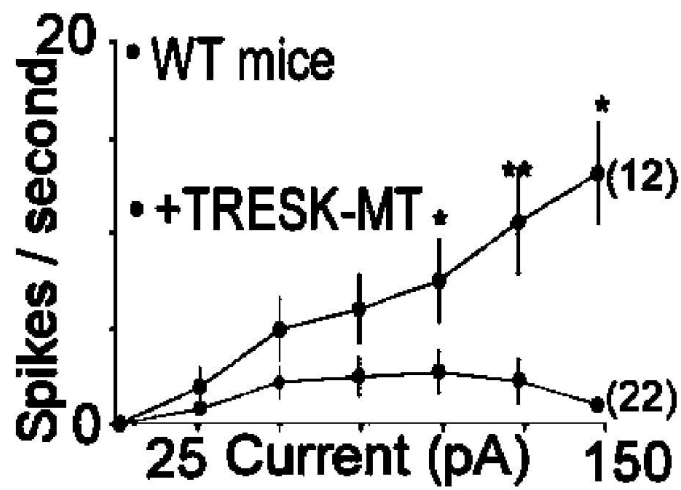


Figure 2D

E

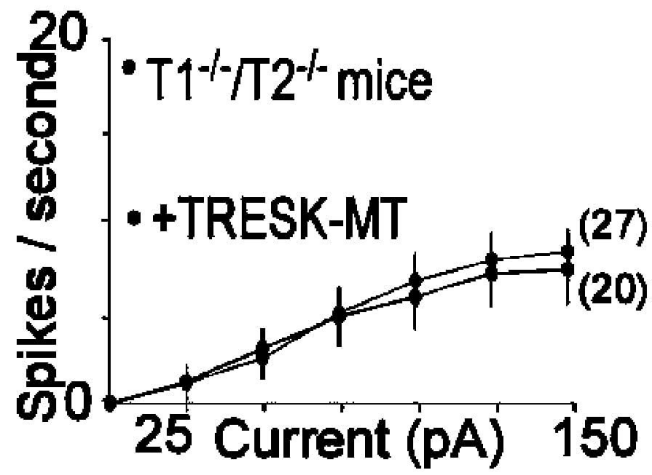


Figure 2E

A

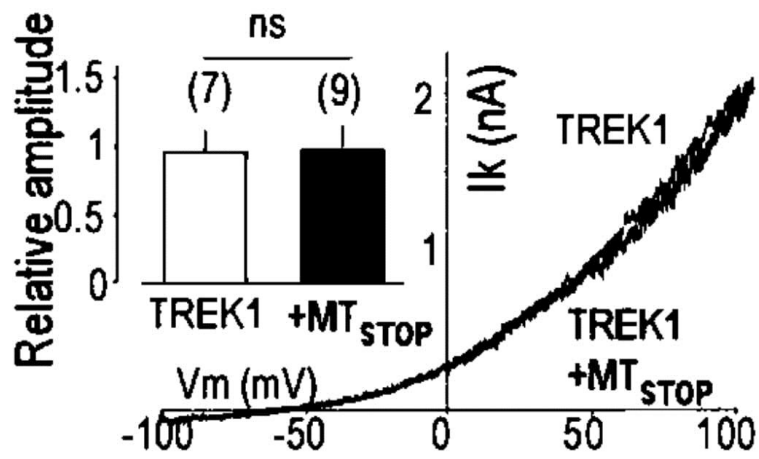


Figure 3A

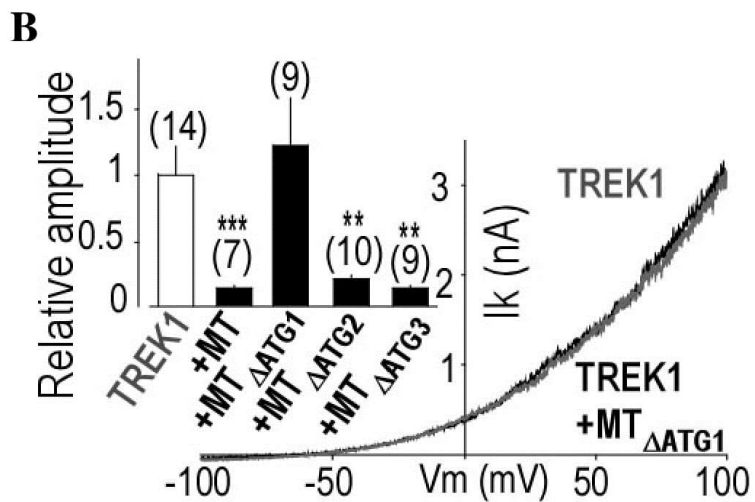


Figure 3B

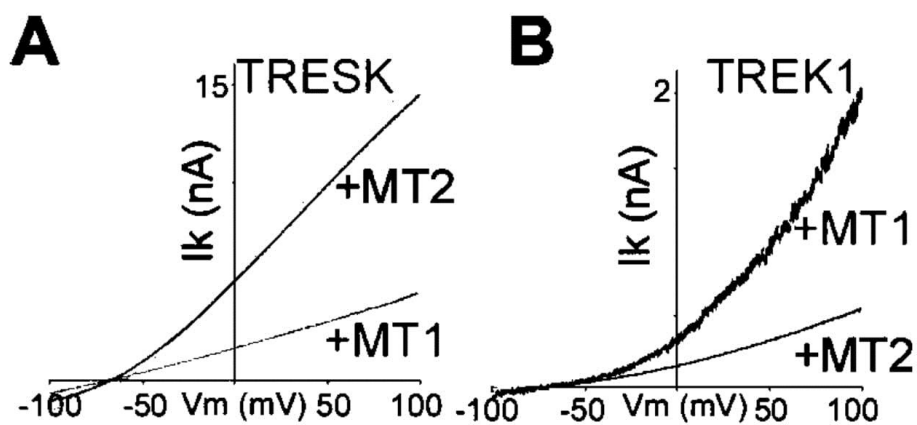


Figure 4A-B

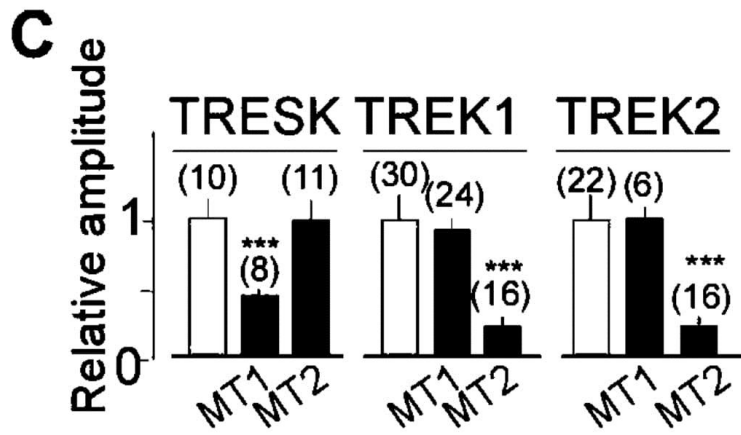


Figure 4C

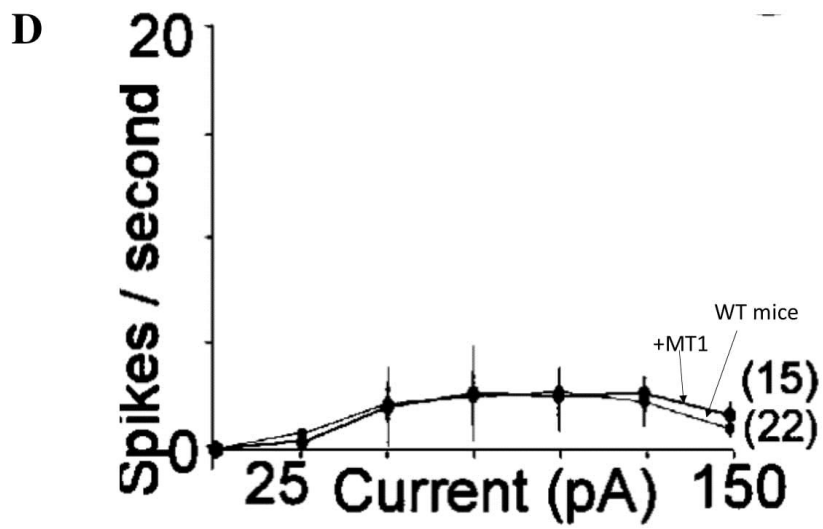


Figure 4D

E

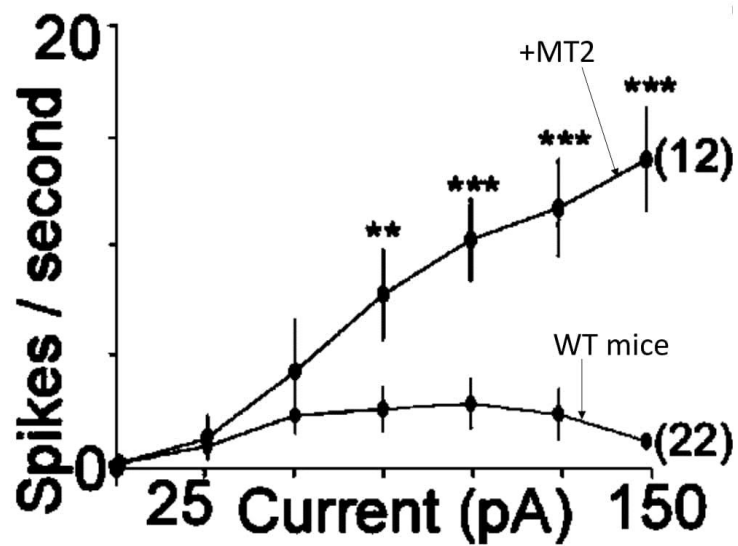


Figure 4E

F

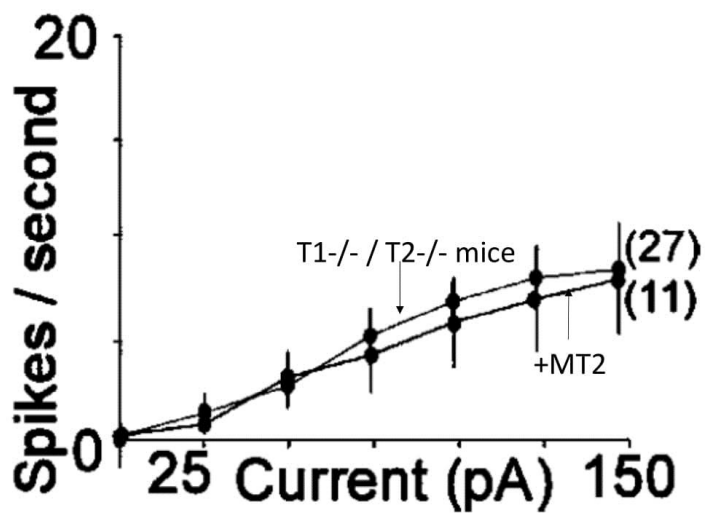


Figure 4F

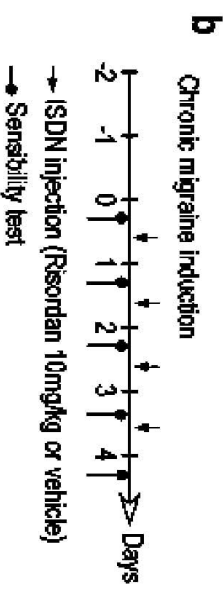
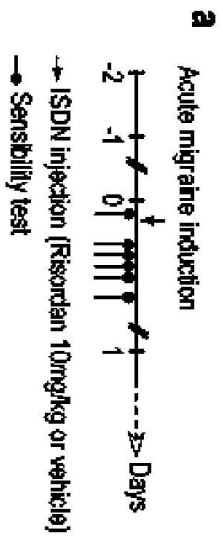


Figure 5A-B

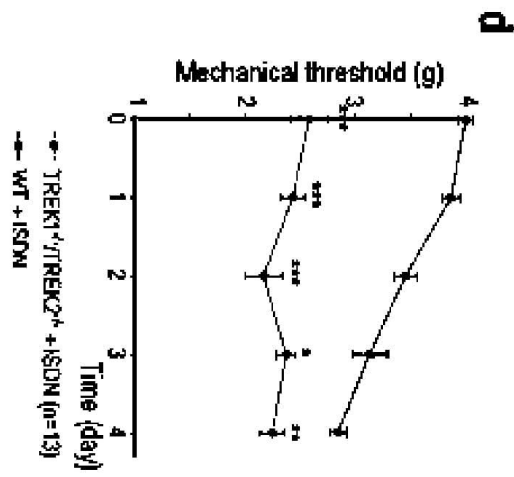
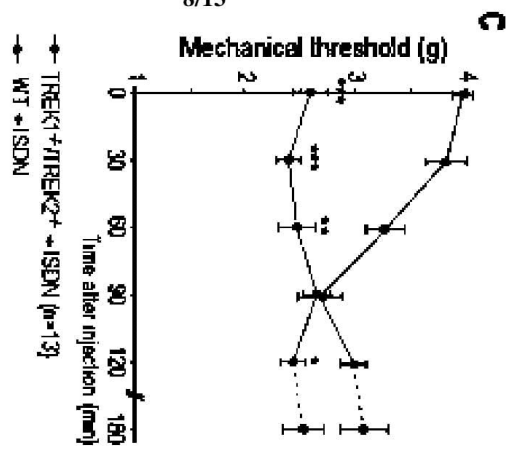


Figure 5C-D

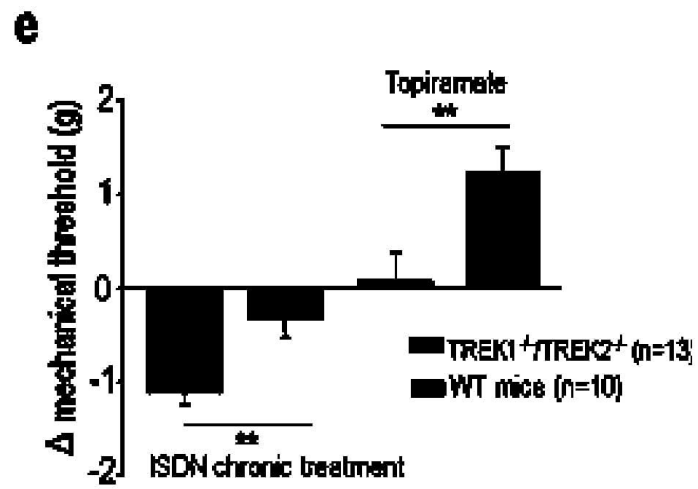


Figure 5E

A

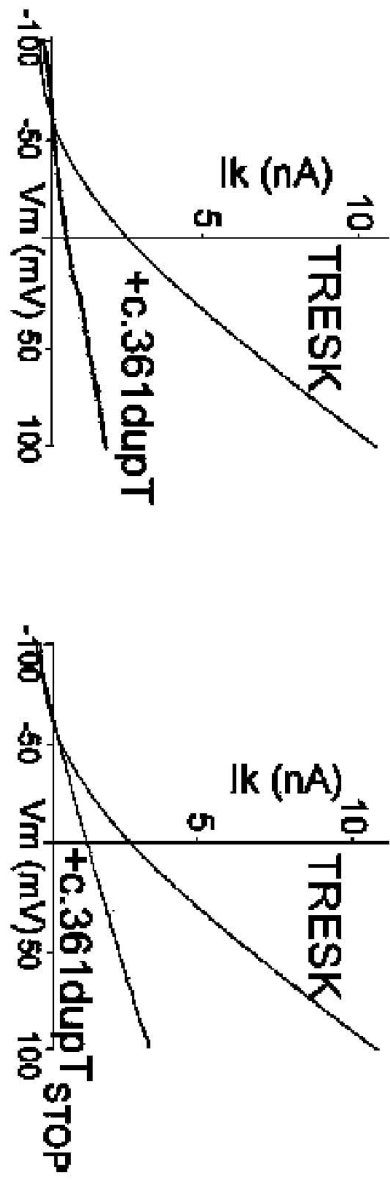


Figure 6A

B

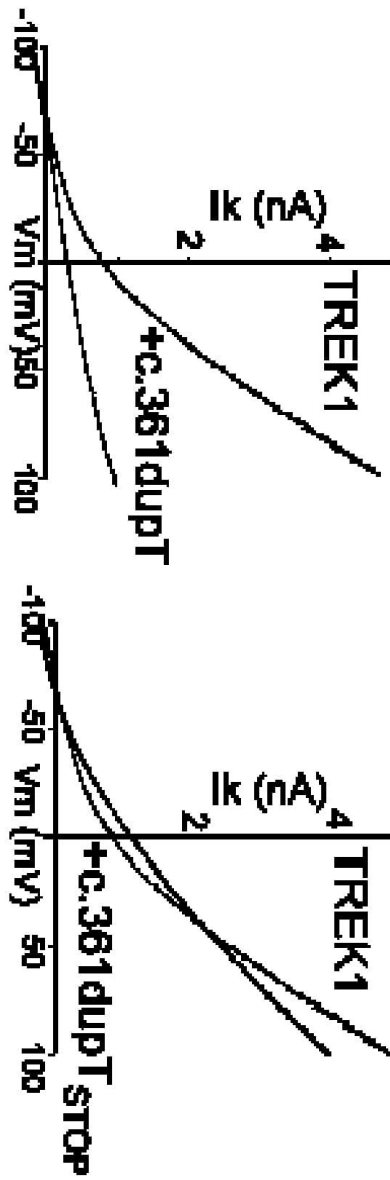


Figure 6B

C

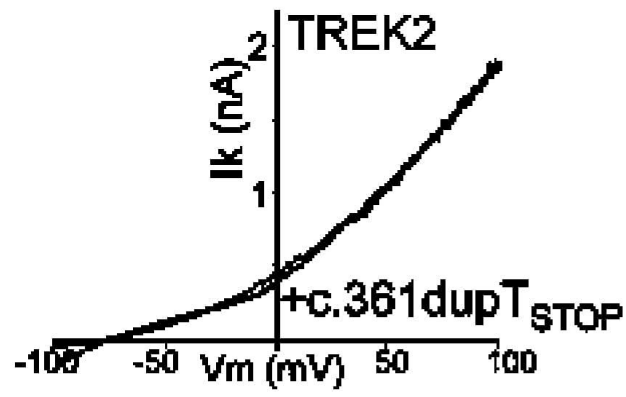


Figure 6C

D

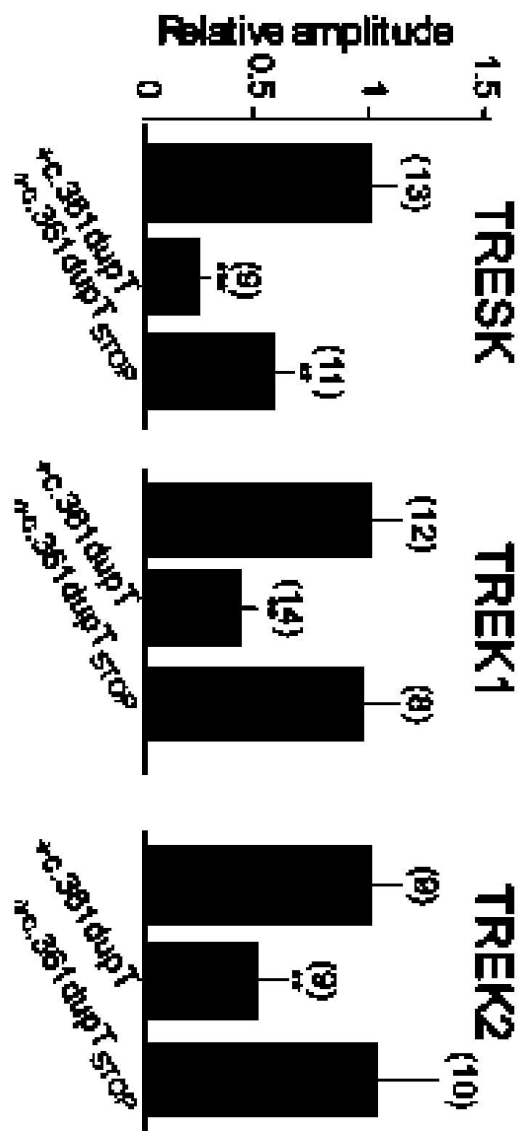


Figure 6D

Screening of protein-protein interaction's modulators

A lot of interest has been given to discover new drugs that will modulate protein-protein interaction. Here, using SiMPull, we provide a very good tool to distinguish the effect of small compounds on the protein interaction.

By acting as stabilizer of the interaction, or as inhibitor or “disruptor”, these new molecules could have an impact on the stability of the complex *in vitro*. This modulation of the interaction between two proteins or two subunits could be directly observed using SiMPull.

Here I provide a cartoon explaining the eventual experiments to set to assess the effect of a molecule on the assembly of a protein complex.

Associated with the FRET technique, we could for instance distinguish within a complex, if a drug could have an impact on the rearrangement of protein subunits. It would further help to understand gating mechanism upon modulator activation. Using SNAP- or CLIP-tags, we could specifically target domains thought to be involved in the gating mechanism. Of course, we have to keep in mind that the tag by itself can play a role in the function of the channel, this would need to be checked.

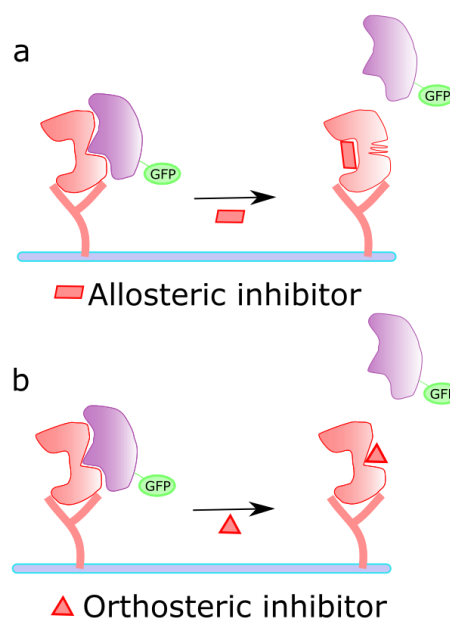


Figure 43: Interaction with inhibitors can make a loss of fluorescent spots observed in SiMPull. a) The addition of an allosteric inhibitor in incubation with cells may make the interaction to be lost, by a change of conformation of the bait protein. b) Addition of an orthosteric inhibitor will lead to a steric clutter, dissociating the complex.

X. Bibliography

- Acosta, C., Djouhri, L., Watkins, R., Berry, C., Bromage, K., and Lawson, S.N. (2014). TREK2 Expressed Selectively in IB4-Binding C-Fiber Nociceptors Hyperpolarizes Their Membrane Potentials and Limits Spontaneous Pain. *J. Neurosci.* **34**, 1494–1509.
- Albury, C.L., Stuart, S., Haupt, L.M., and Griffiths, L.R. (2017). Ion channelopathies and migraine pathogenesis. *Mol. Genet. Genomics* MGG.
- Alloui, A., Zimmermann, K., Mamet, J., Duprat, F., Noël, J., Chemin, J., Guy, N., Blondeau, N., Voilley, N., Rubat-Coudert, C., et al. (2006). TREK-1, a K⁺ channel involved in polymodal pain perception. *EMBO J.* **25**, 2368–2376.
- Aly, S., Emery, C., Fagnani, F., Gourmelen, J., Mahieu, N., Leiba, G., Bashar, B.A., Chouette, I., Levy, P., and Donnet, A. (2018). Fardeau et coût de la migraine en France : une analyse de la base de l'échantillon généraliste des bénéficiaires (EGB). *Rev. D'Épidémiologie Santé Publique* **66**, S206–S207.
- Andres-Enguix, I., Shang, L., Stansfeld, P.J., Morahan, J.M., Sansom, M.S.P., Lafrenière, R.G., Roy, B., Griffiths, L.R., Rouleau, G.A., Ebers, G.C., et al. (2012). Functional analysis of missense variants in the TRESK (KCNK18) K channel. *Sci. Rep.* **2**, 237.
- Arrighi, I., Lesage, F., Scimeca, J.-C., Carle, G.F., and Barhanin, J. (1998). Structure, chromosome localization, and tissue distribution of the mouse *twik* K⁺ channel gene. *FEBS Lett.* **425**, 310–316.
- Aryal, P., Abd-Wahab, F., Bucci, G., Sansom, M.S.P., and Tucker, S.J. (2014). A hydrophobic barrier deep within the inner pore of the TWIK-1 K^{2P} potassium channel. *Nat. Commun.* **5**, 4377.
- Ashcroft, F.M., and Rorsman, P. (1989). Electrophysiology of the pancreatic beta-cell. *Prog. Biophys. Mol. Biol.* **54**, 87–143.
- Bagriantsev, S.N., Peyronnet, R., Clark, K.A., Honoré, E., and Minor, D.L. (2011). Multiple modalities converge on a common gate to control K^{2P} channel function. *EMBO J.* **30**, 3594–3606.
- Bagriantsev, S.N., Clark, K.A., and Minor, D.L. (2012). Metabolic and thermal stimuli control K^{2P2.1} (TREK-1) through modular sensory and gating domains. *EMBO J.* **31**, 3297–3308.
- Bang, H., Kim, Y., and Kim, D. (2000). TREK-2, a new member of the mechanosensitive tandem-pore K⁺ channel family. *J. Biol. Chem.* **275**, 17412–17419.
- Ben-Abu, Y., Zhou, Y., Zilberberg, N., and Yifrach, O. (2009). Inverse coupling in leak and voltage-activated K⁺ channel gates underlies distinct roles in electrical signaling. *Nat. Struct. Mol. Biol.* **16**, 71–79.

- Berg, A.P., Talley, E.M., Manger, J.P., and Bayliss, D.A. (2004). Motoneurons express heteromeric TWIK-related acid-sensitive K⁺ (TASK) channels containing TASK-1 (KCNK3) and TASK-3 (KCNK9) subunits. *J. Neurosci. Off. J. Soc. Neurosci.* *24*, 6693–6702.
- Bernèche, S., and Roux, B. (2001). Energetics of ion conduction through the K⁺ channel. *Nature* *414*, 73–77.
- Berrier, C., Pozza, A., de Lacroix de Lavalette, A., Chardonnet, S., Mesneau, A., Jaxel, C., le Maire, M., and Ghazi, A. (2013). The Purified Mechanosensitive Channel TREK-1 Is Directly Sensitive to Membrane Tension. *J. Biol. Chem.* *288*, 27307–27314.
- Bichet, D., Blin, S., Feliciangeli, S., Chatelain, F.C., Bobak, N., and Lesage, F. (2015). Silent but not dumb: how cellular trafficking and pore gating modulate expression of TWIK1 and THIK2. *Pflugers Arch.* *467*, 1121–1131.
- Blin, S., Chatelain, F.C., Feliciangeli, S., Kang, D., Lesage, F., and Bichet, D. (2014). Tandem pore domain halothane-inhibited K⁺ channel subunits THIK1 and THIK2 assemble and form active channels. *J. Biol. Chem.* *289*, 28202–28212.
- Blin, S., Ben Soussia, I., Kim, E.-J., Brau, F., Kang, D., Lesage, F., and Bichet, D. (2016). Mixing and matching TREK/TRAAK subunits generate heterodimeric K₂P channels with unique properties. *Proc. Natl. Acad. Sci. U. S. A.* *113*, 4200–4205.
- Blunck, R., Cordero-Morales, J.F., Cuello, L.G., Perozo, E., and Bezanilla, F. (2006). Detection of the opening of the bundle crossing in KcsA with fluorescence lifetime spectroscopy reveals the existence of two gates for ion conduction. *J. Gen. Physiol.* *128*, 569–581.
- Bolay, H., Reuter, U., Dunn, A.K., Huang, Z., Boas, D.A., and Moskowitz, M.A. (2002). Intrinsic brain activity triggers trigeminal meningeal afferents in a migraine model. *Nat. Med.* *8*, 136–142.
- Borgdorff, P. (2018). Arguments against the role of cortical spreading depression in migraine. *Neurol. Res.* *40*, 173–181.
- Brohawn, S.G. (2015). How ion channels sense mechanical force: insights from mechanosensitive K₂P channels TRAAK, TREK1, and TREK2. *Ann. N. Y. Acad. Sci.* *1352*, 20–32.
- Brohawn, S.G., del Mármol, J., and MacKinnon, R. (2012). Crystal structure of the human K₂P TRAAK, a lipid- and mechano-sensitive K⁺ ion channel. *Science* *335*, 436–441.
- Brohawn, S.G., Campbell, E.B., and MacKinnon, R. (2014). Physical mechanism for gating and mechanosensitivity of the human TRAAK K⁺ channel. *Nature* *516*, 126–130.
- Browne, D.L., Gancher, S.T., Nutt, J.G., Brunt, E.R., Smith, E.A., Kramer, P., and Litt, M. (1994). Episodic ataxia/myokymia syndrome is associated with point mutations in the human potassium channel gene, KCNA1. *Nat. Genet.* *8*, 136–140.

- Cabanos, C., Wang, M., Han, X., and Hansen, S.B. (2017). A Soluble Fluorescent Binding Assay Reveals PIP2 Antagonism of TREK-1 Channels. *Cell Rep.* 20, 1287–1294.
- Callejo, G., Giblin, J.P., and Gasull, X. (2013). Modulation of TRESK background K⁺ channel by membrane stretch. *PLoS One* 8, e64471.
- Chae, Y.J., Zhang, J., Au, P., Sabbadini, M., Xie, G.-X., and Yost, C.S. (2010). Discrete change in volatile anesthetic sensitivity in mice with inactivated tandem pore potassium ion channel TRESK. *Anesthesiology* 113, 1326–1337.
- Charles, A., and Brennan, K. (2009). Cortical spreading depression—new insights and persistent questions. *Cephalalgia Int. J. Headache* 29, 1115–1124.
- Chatelain, F.C., Bichet, D., Douguet, D., Feliciangeli, S., Bendahhou, S., Reichold, M., Warth, R., Barhanin, J., and Lesage, F. (2012). TWIK1, a unique background channel with variable ion selectivity. *Proc. Natl. Acad. Sci.* 109, 5499–5504.
- Chemin, J., Girard, C., Duprat, F., Lesage, F., Romey, G., and Lazdunski, M. (2003). Mechanisms underlying excitatory effects of group I metabotropic glutamate receptors via inhibition of 2P domain K⁺ channels. *EMBO J.* 22, 5403–5411.
- Chemin, J., Patel, A., Duprat, F., Zanzouri, M., Lazdunski, M., and Honoré, E. (2005). Lysophosphatidic acid-operated K⁺ channels. *J. Biol. Chem.* 280, 4415–4421.
- Chemin, J., Patel, A.J., Duprat, F., Sachs, F., Lazdunski, M., and Honore, E. (2007). Up- and down-regulation of the mechano-gated K(2P) channel TREK-1 by PIP (2) and other membrane phospholipids. *Pflugers Arch.* 455, 97–103.
- Chen, X., Talley, E.M., Patel, N., Gomis, A., McIntire, W.E., Dong, B., Viana, F., Garrison, J.C., and Bayliss, D.A. (2006). Inhibition of a background potassium channel by Gq protein alpha-subunits. *Proc. Natl. Acad. Sci. U. S. A.* 103, 3422–3427.
- Cho, C.-H., Hwang, E.M., and Park, J.-Y. (2017). Emerging Roles of TWIK-1 Heterodimerization in the Brain. *Int. J. Mol. Sci.* 19.
- Choi, J.-H., Wang, W., Park, D., Kim, S.-H., Kim, K.-T., and Min, K.-T. (2018). IRES-mediated translation of cofilin regulates axonal growth cone extension and turning. *EMBO J.* 37, e95266.
- Cohen, A., Ben-Abu, Y., Hen, S., and Zilberberg, N. (2008). A novel mechanism for human K2P2.1 channel gating. Facilitation of C-type gating by protonation of extracellular histidine residues. *J. Biol. Chem.* 283, 19448–19455.
- Collado-Vázquez, S., and Carrillo, J.M. Cranial trepanation in The Egyptian. *Neurol. Engl. Ed.* 433–440.
- Comoglio, Y., Levitz, J., Kienzler, M.A., Lesage, F., Isacoff, E.Y., and Sandoz, G. (2014). Phospholipase D2 specifically regulates TREK potassium channels via direct interaction and local production of phosphatidic acid. *Proc. Natl. Acad. Sci. U. S. A.* 111, 13547–13552.

Czirják, G., and Enyedi, P. (2002). Formation of functional heterodimers between the TASK-1 and TASK-3 two-pore domain potassium channel subunits. *J. Biol. Chem.* *277*, 5426–5432.

Dadi, P.K., Vierra, N.C., Days, E., Dickerson, M.T., Vinson, P.N., Weaver, C.D., and Jacobson, D.A. (2017). Selective Small Molecule Activators of TREK-2 Channels Stimulate Dorsal Root Ganglion c-Fiber Nociceptor Two-Pore-Domain Potassium Channel Currents and Limit Calcium Influx. *ACS Chem. Neurosci.* *8*, 558–568.

Dalkara, T., Nozari, A., and Moskowitz, M.A. (2010). Migraine aura pathophysiology: the role of blood vessels and microembolisation. *Lancet Neurol.* *9*, 309–317.

Dallel, R., Descheemaeker, A., and Luccarini, P. (2018). Recurrent administration of the nitric oxide donor, isosorbide dinitrate, induces a persistent cephalic cutaneous hypersensitivity: A model for migraine progression. *Cephalalgia Int. J. Headache* *38*, 776–785.

Decher, N., Maier, M., Dittrich, W., Gassenhuber, J., Brüggemann, A., Busch, A.E., and Steinmeyer, K. (2001). Characterization of TASK-4, a novel member of the pH-sensitive, two-pore domain potassium channel family. *FEBS Lett.* *492*, 84–89.

Decher, N., Kiper, A.K., and Rinné, S. (2017a). Stretch-activated potassium currents in the heart: Focus on TREK-1 and arrhythmias. *Prog. Biophys. Mol. Biol.* *130*, 223–232.

Decher, N., Ortiz-Bonin, B., Friedrich, C., Schewe, M., Kiper, A.K., Rinné, S., Seemann, G., Peyronnet, R., Zumhagen, S., Bustos, D., et al. (2017b). Sodium permeable and “hypersensitive” TREK-1 channels cause ventricular tachycardia. *EMBO Mol. Med.* *9*, 403–414.

Dedman, A., Sharif-Naeini, R., Folgering, J.H.A., Duprat, F., Patel, A., and Honoré, E. (2009). The mechano-gated K(2P) channel TREK-1. *Eur. Biophys. J. EBJ* *38*, 293–303.

Deng, P.-Y., Xiao, Z., Yang, C., Rojanathammanee, L., Grisanti, L., Watt, J., Geiger, J.D., Liu, R., Porter, J.E., and Lei, S. (2009). GABAB Receptor Activation Inhibits Neuronal Excitability and Spatial Learning in the Entorhinal Cortex by Activating TREK-2 K⁺ Channels. *Neuron* *63*, 230–243.

Descoeur, J., Pereira, V., Pizzoccaro, A., Francois, A., Ling, B., Maffre, V., Couette, B., Busserolles, J., Courteix, C., Noel, J., et al. (2011). Oxaliplatin-induced cold hypersensitivity is due to remodelling of ion channel expression in nociceptors. *EMBO Mol. Med.* *3*, 266–278.

Devilliers, M., Busserolles, J., Lolignier, S., Deval, E., Pereira, V., Alloui, A., Christin, M., Mazet, B., Delmas, P., Noel, J., et al. (2013). Activation of TREK-1 by morphine results in analgesia without adverse side effects. *Nat. Commun.* *4*, 2941.

Dichgans, M., Freilinger, T., Eckstein, G., Babini, E., Lorenz-Depiereux, B., Biskup, S., Ferrari, M.D., Herzog, J., van den Maagdenberg, A.M., Pusch, M., et al. (2005).

Mutation in the neuronal voltage-gated sodium channel SCN1A in familial hemiplegic migraine. *The Lancet* 366, 371–377.

Djillani, A., Pietri, M., Moreno, S., Heurteaux, C., Mazella, J., and Borsotto, M. (2017). Shortened Spadin Analogs Display Better TREK-1 Inhibition, In Vivo Stability and Antidepressant Activity. *Front. Pharmacol.* 8, 643.

Djillani, A., Pietri, M., Mazella, J., Heurteaux, C., and Borsotto, M. (2018). Fighting against depression with TREK-1 blockers: Past and future. A focus on spadin. *Pharmacol. Ther.*

Dobler, T., Springauf, A., Tovornik, S., Weber, M., Schmitt, A., Sedlmeier, R., Wischmeyer, E., and Döring, F. (2007). TRESK two-pore-domain K⁺ channels constitute a significant component of background potassium currents in murine dorsal root ganglion neurones. *J. Physiol.* 585, 867–879.

Dong, Y.Y., Pike, A.C.W., Mackenzie, A., McClenaghan, C., Aryal, P., Dong, L., Quigley, A., Grieben, M., Goubin, S., Mukhopadhyay, S., et al. (2015). K2P channel gating mechanisms revealed by structures of TREK-2 and a complex with Prozac. *Science* 347, 1256–1259.

Doyle, D.A., Morais Cabral, J., Pfuetzner, R.A., Kuo, A., Gulbis, J.M., Cohen, S.L., Chait, B.T., and MacKinnon, R. (1998). The structure of the potassium channel: molecular basis of K⁺ conduction and selectivity. *Science* 280, 69–77.

Du, X., and Gamper, N. (2013). Potassium Channels in Peripheral Pain Pathways: Expression, Function and Therapeutic Potential. *Curr. Neuropharmacol.* 11, 621–640.

Du, X., Wang, J., Zhu, H., Rinaldo, L., Lamar, K.-M., Palmenberg, A.C., Hansel, C., and Gomez, C.M. (2013). A second cistron in the CACNA1A gene encodes a transcription factor that mediates cerebellar development and SCA6. *Cell* 154, 118–133.

Duprat, F., Lesage, F., Fink, M., Reyes, R., Heurteaux, C., and Lazdunski, M. (1997). TASK, a human background K⁺ channel to sense external pH variations near physiological pH. *EMBO J.* 16, 5464–5471.

Duprat, F., Girard, C., Jarretou, G., and Lazdunski, M. (2005). Pancreatic two P domain K⁺ channels TALK-1 and TALK-2 are activated by nitric oxide and reactive oxygen species. *J. Physiol.* 562, 235–244.

Enyedi, P., and Czirják, G. (2015). Properties, regulation, pharmacology, and functions of the K₂p channel, TRESK. *Pflugers Arch.* 467, 945–958.

Enyedi, P., Braun, G., and Czirják, G. (2012). TRESK: The lone ranger of two-pore domain potassium channels. *Mol. Cell. Endocrinol.* 353, 75–81.

Faber, E.S.L., and Sah, P. (2003). Calcium-activated potassium channels: multiple contributions to neuronal function. *Neurosci. Rev. J. Bringing Neurobiol. Neurol. Psychiatry* 9, 181–194.

Faber, E.S.L., and Sah, P. (2007). Functions of SK channels in central neurons. *Clin. Exp. Pharmacol. Physiol.* 34, 1077–1083.

Feliciangeli, S., Bendahhou, S., Sandoz, G., Gounon, P., Reichold, M., Warth, R., Lazdunski, M., Barhanin, J., and Lesage, F. (2007). Does sumoylation control K2P1/TWIK1 background K⁺ channels? *Cell* 130, 563–569.

Feliciangeli, S., Tardy, M.P., Sandoz, G., Chatelain, F.C., Warth, R., Barhanin, J., Bendahhou, S., and Lesage, F. (2010). Potassium channel silencing by constitutive endocytosis and intracellular sequestration. *J. Biol. Chem.* 285, 4798–4805.

Fink, M., Duprat, F., Lesage, F., Reyes, R., Romey, G., Heurteaux, C., and Lazdunski, M. (1996). Cloning, functional expression and brain localization of a novel unconventional outward rectifier K⁺ channel. *EMBO J.* 15, 6854–6862.

Fink, M., Lesage, F., Duprat, F., Heurteaux, C., Reyes, R., Fosset, M., and Lazdunski, M. (1998). A neuronal two P domain K⁺ channel stimulated by arachidonic acid and polyunsaturated fatty acids. *EMBO J.* 17, 3297–3308.

Giblin, J.P., Etayo, I., Castellanos, A., Andres-Bilbe, A., and Gasull, X. (2018). Anionic Phospholipids Bind to and Modulate the Activity of Human TRESK Background K⁺ Channel. *Mol. Neurobiol.*

Girard, C., Duprat, F., Terrenoire, C., Tinel, N., Fosset, M., Romey, G., Lazdunski, M., and Lesage, F. (2001). Genomic and functional characteristics of novel human pancreatic 2P domain K(+) channels. *Biochem. Biophys. Res. Commun.* 282, 249–256.

Girard, C., Tinel, N., Terrenoire, C., Romey, G., Lazdunski, M., and Borsotto, M. (2002). p11, an annexin II subunit, an auxiliary protein associated with the background K⁺ channel, TASK-1. *EMBO J.* 21, 4439–4448.

González, A., Herrera, G., Ugarte, G., Restrepo, C., Piña, R., Pertusa, M., Orio, P., and Madrid, R. (2017). IKD Current in Cold Transduction and Damage-Triggered Cold Hypersensitivity. In *The Plastic Brain*, R. von Bernhardi, J. Eugenín, and K.J. Muller, eds. (Cham: Springer International Publishing), pp. 265–277.

Gritz, S.M., and Radcliffe, R.A. (2013). Genetic effects of ATP1A2 in familial hemiplegic migraine type II and animal models. *Hum. Genomics* 7, 8.

Guo, Z., and Cao, Y.-Q. (2014). Over-expression of TRESK K(+) channels reduces the excitability of trigeminal ganglion nociceptors. *PloS One* 9, e87029.

Gutman, G.A., Chandy, K.G., Grissmer, S., Lazdunski, M., McKinnon, D., Pardo, L.A., Robertson, G.A., Rudy, B., Sanguinetti, M.C., Stühmer, W., et al. (2005). International Union of Pharmacology. LIII. Nomenclature and molecular relationships of voltage-gated potassium channels. *Pharmacol. Rev.* 57, 473–508.

Heginbotham, L., Lu, Z., Abramson, T., and MacKinnon, R. (1994). Mutations in the K⁺ channel signature sequence. *Biophys. J.* 66, 1061–1067.

Heinrich, F., Chakravarthy, S., Nanda, H., Papa, A., Pandolfi, P.P., Ross, A.H., Harishchandra, R.K., Gericke, A., and Lösche, M. (2015). The PTEN Tumor Suppressor Forms Homodimers in Solution. *Struct. Lond. Engl.* 23, 1952–1957.

Hernández-Araiza, I., Morales-Lázaro, S.L., Canul-Sánchez, J.A., Islas, L.D., and Rosenbaum, T. (2018). Role of lysophosphatidic acid in ion channel function and disease. *J. Neurophysiol.* 120, 1198–1211.

Heurteaux, C. (2007). PUFA-induced neuroprotection against cerebral or spinal cord ischemia via the TREK-1 channel. *Ol. Corps Gras Lipides* 14, 190–193.

Heurteaux, C., Guy, N., Laigle, C., Blondeau, N., Duprat, F., Mazzuca, M., Lang-Lazdunski, L., Widmann, C., Zanzouri, M., Romey, G., et al. (2004). TREK-1, a K⁺ channel involved in neuroprotection and general anesthesia. *EMBO J.* 23, 2684–2695.

Heurteaux, C., Lucas, G., Guy, N., Yacoubi, M.E., Thümmel, S., Peng, X.-D., Noble, F., Blondeau, N., Widmann, C., Borsotto, M., et al. (2006). Deletion of the background potassium channel TREK-1 results in a depression-resistant phenotype. *Nat. Neurosci.* 9, 1134–1141.

Hibino, H., Inanobe, A., Furutani, K., Murakami, S., Findlay, I., and Kurachi, Y. (2010). Inwardly rectifying potassium channels: their structure, function, and physiological roles. *Physiol. Rev.* 90, 291–366.

Hodgkin, A.L., and Huxley, A.F. (1952). A quantitative description of membrane current and its application to conduction and excitation in nerve. *J. Physiol.* 117, 500–544.

Hodgkin, A.L., and Katz, B. (1949). The effect of sodium ions on the electrical activity of the giant axon of the squid. *J. Physiol.* 108, 37–77.

Honoré, E. (2007). The neuronal background K_{2P} channels: focus on TREK1. *Nat. Rev. Neurosci.* 8, 251–261.

Honoré, E., Maingret, F., Lazdunski, M., and Patel, A.J. (2002). An intracellular proton sensor commands lipid- and mechano-gating of the K⁺ channel TREK-1. *EMBO J.* 21, 2968–2976.

Hsieh, C.-P., Kuo, C.-C., and Huang, C.-W. (2015). Driving force-dependent block by internal Ba²⁺ on the Kir2.1 channel: Mechanistic insight into inward rectification. *Biophys. Chem.* 202, 40–57.

Hwang, E.M., Kim, E., Yarishkin, O., Woo, D.H., Han, K.-S., Park, N., Bae, Y., Woo, J., Kim, D., Park, M., et al. (2014). A disulphide-linked heterodimer of TWIK-1 and TREK-1 mediates passive conductance in astrocytes. *Nat. Commun.* 5, 3227.

Jain, A., Liu, R., Xiang, Y.K., and Ha, T. (2012). Single-molecule pull-down for studying protein interactions. *Nat. Protoc.* 7, 445–452.

Joseph, A., Thuy, T.T.T., Thanh, L.T., and Okada, M. (2018). Antidepressive and anxiolytic effects of ostruthin, a TREK-1 channel activator. *PLoS ONE* 13.

Kang, D., and Kim, D. (2006). TREK-2 (K2P10.1) and TRESK (K2P18.1) are major background K⁺ channels in dorsal root ganglion neurons. *Am. J. Physiol.-Cell Physiol.* *291*, C138–C146.

Kang, D., Mariash, E., and Kim, D. (2004a). Functional Expression of TRESK-2, a New Member of the Tandem-pore K⁺ Channel Family. *J. Biol. Chem.* *279*, 28063–28070.

Kang, D., Han, J., Talley, E.M., Bayliss, D.A., and Kim, D. (2004b). Functional expression of TASK-1/TASK-3 heteromers in cerebellar granule cells. *J. Physiol.* *554*, 64–77.

Kang, D., Choe, C., and Kim, D. (2005). Thermosensitivity of the two-pore domain K⁺ channels TREK-2 and TRAAK. *J. Physiol.* *564*, 103–116.

Kang, D., Han, J., and Kim, D. (2006). Mechanism of inhibition of TREK-2 (K2P10.1) by the Gq-coupled M3 muscarinic receptor. *Am. J. Physiol. Cell Physiol.* *291*, C649–656.

Karschin, C., Wischmeyer, E., Preisig-Müller, R., Rajan, S., Derst, C., Grzeschik, K.-H., Daut, J., and Karschin, A. (2001). Expression Pattern in Brain of TASK-1, TASK-3, and a Tandem Pore Domain K⁺ Channel Subunit, TASK-5, Associated with the Central Auditory Nervous System. *Mol. Cell. Neurosci.* *18*, 632–648.

Kelman, L. (2007). The triggers or precipitants of the acute migraine attack. *Cephalalgia Int. J. Headache* *27*, 394–402.

Kilinc, E., Guerrero-Toro, C., Zakharov, A., Vitale, C., Gubert-Olive, M., Koroleva, K., Timonina, A., Luz, L.L., Shelukhina, I., Giniatullina, R., et al. (2017). Serotonergic mechanisms of trigeminal meningeal nociception: Implications for migraine pain. *Neuropharmacology* *116*, 160–173.

Kim, D., Cavanaugh, E.J., Kim, I., and Carroll, J.L. (2009). Heteromeric TASK-1/TASK-3 is the major oxygen-sensitive background K⁺ channel in rat carotid body glomus cells. *J. Physiol.* *587*, 2963–2975.

Kim, E., Hwang, E.M., Yarishkin, O., Yoo, J.C., Kim, D., Park, N., Cho, M., Lee, Y.S., Sun, C.-H., Yi, G.-S., et al. (2010). Enhancement of TREK1 channel surface expression by protein-protein interaction with beta-COP. *Biochem. Biophys. Res. Commun.* *395*, 244–250.

Kochetov, A.V. (2008). Alternative translation start sites and hidden coding potential of eukaryotic mRNAs. *BioEssays News Rev. Mol. Cell. Dev. Biol.* *30*, 683–691.

Koesling, D., Russwurm, M., Mergia, E., Mullershausen, F., and Friebe, A. (2004). Nitric oxide-sensitive guanylyl cyclase: structure and regulation. *Neurochem. Int.* *45*, 813–819.

Kohout, S.C., Ulbrich, M.H., Bell, S.C., and Isacoff, E.Y. (2008). Subunit organization and functional transitions in Ci-VSP. *Nat. Struct. Mol. Biol.* *15*, 106–108.

Kollert, S., Dombert, B., Döring, F., and Wischmeyer, E. (2015). Activation of TRESK channels by the inflammatory mediator lysophosphatidic acid balances nociceptive signalling. *Sci. Rep.* 5, 12548.

Köpfer, D.A., Song, C., Gruene, T., Sheldrick, G.M., Zachariae, U., and Groot, B.L. de (2014). Ion permeation in K⁺ channels occurs by direct Coulomb knock-on. *Science* 346, 352–355.

Kozak, M. (1999). Initiation of translation in prokaryotes and eukaryotes. *Gene* 234, 187–208.

Kramer, D.R., Fujii, T., Ohiorhenuan, I., and Liu, C.Y. (2016). Cortical spreading depolarization: Pathophysiology, implications, and future directions. *J. Clin. Neurosci.* 24, 22–27.

Kuang, Q., Purhonen, P., and Hebert, H. (2015). Structure of potassium channels. *Cell. Mol. Life Sci.* 72, 3677–3693.

La, J.-H., and Gebhart, G.F. (2011). Colitis decreases mechanosensitive K₂P channel expression and function in mouse colon sensory neurons. *Am. J. Physiol. Gastrointest. Liver Physiol.* 301, G165-174.

Lafrenière, R.G., Cader, M.Z., Poulin, J.-F., Andres-Enguix, I., Simoneau, M., Gupta, N., Boisvert, K., Lafrenière, F., McLaughlan, S., Dubé, M.-P., et al. (2010). A dominant-negative mutation in the TRESK potassium channel is linked to familial migraine with aura. *Nat. Med.* 16, 1157–1160.

Latorre, R., Castillo, K., Carrasquel-Ursulaez, W., Sepulveda, R.V., Gonzalez-Nilo, F., Gonzalez, C., and Alvarez, O. (2016). Molecular Determinants of BK Channel Functional Diversity and Functioning. *Physiol. Rev.* 97, 39–87.

Lauritzen, M. (1994). Pathophysiology of the migraine aura. The spreading depression theory. *Brain J. Neurol.* 117 (Pt 1), 199–210.

Lauritzen, I., Zanzouri, M., Honoré, E., Duprat, F., Ehrenguber, M.U., Lazdunski, M., and Patel, A.J. (2003). K⁺-dependent cerebellar granule neuron apoptosis. Role of task leak K⁺ channels. *J. Biol. Chem.* 278, 32068–32076.

Leao, A.A.P. (1944). Spreading depression of activity in the cerebral cortex. *J. Neurophysiol.* 7, 359–390.

Lengyel, M., Czirják, G., and Enyedi, P. (2016). Formation of Functional Heterodimers by TREK-1 and TREK-2 Two-pore Domain Potassium Channel Subunits. *J. Biol. Chem.* 291, 13649–13661.

Lesage, F., and Barhanin, J. (2011). Molecular physiology of pH-sensitive background K(2P) channels. *Physiology* 26, 424–437.

Lesage, F., and Lazdunski, M. (2000). Molecular and functional properties of two-pore-domain potassium channels. *Am. J. Physiol. Renal Physiol.* 279, F793-801.

Lesage, F., Guillemare, E., Fink, M., Duprat, F., Lazdunski, M., Romey, G., and Barhanin, J. (1996). TWIK-1, a ubiquitous human weakly inward rectifying K⁺ channel with a novel structure. *EMBO J.* 15, 1004–1011.

Lesage, F., Terrenoire, C., Romey, G., and Lazdunski, M. (2000). Human TREK2, a 2P domain mechano-sensitive K⁺ channel with multiple regulations by polyunsaturated fatty acids, lysophospholipids, and Gs, Gi, and Gq protein-coupled receptors. *J. Biol. Chem.* 275, 28398–28405.

Levitz, J., Royal, P., Comoglio, Y., Wdziekonski, B., Schaub, S., Clemens, D.M., Isacoff, E.Y., and Sandoz, G. (2016). Heterodimerization within the TREK channel subfamily produces a diverse family of highly regulated potassium channels. *Proc. Natl. Acad. Sci. U. S. A.* 113, 4194–4199.

Levy, D., and Strassman, A.M. (2004). Modulation of dural nociceptor mechanosensitivity by the nitric oxide-cyclic GMP signaling cascade. *J. Neurophysiol.* 92, 766–772.

Li, X.-Y., and Toyoda, H. (2015). Role of leak potassium channels in pain signaling. *Brain Res. Bull.* 119, 73–79.

Linden, A.-M., Aller, M.I., Leppä, E., Vekovischeva, O., Aitta-aho, T., Veale, E.L., Mathie, A., Rosenberg, P., Wisden, W., and Korpi, E.R. (2006). The in Vivo Contributions of TASK-1-Containing Channels to the Actions of Inhalation Anesthetics, the α 2 Adrenergic Sedative Dexmedetomidine, and Cannabinoid Agonists. *J. Pharmacol. Exp. Ther.* 317, 615–626.

Liu, C., Au, J.D., Zou, H.L., Cotten, J.F., and Yost, C.S. (2004). Potent activation of the human tandem pore domain K channel TRESK with clinical concentrations of volatile anesthetics. *Anesth. Analg.* 99, 1715–1722, table of contents.

Liu, F., Jones, D.K., Lange, W.J. de, and Robertson, G.A. (2016). Cotranslational association of mRNA encoding subunits of heteromeric ion channels. *Proc. Natl. Acad. Sci.* 113, 4859–4864.

Liu, P., Xiao, Z., Ren, F., Guo, Z., Chen, Z., Zhao, H., and Cao, Y.-Q. (2013). Functional analysis of a migraine-associated TRESK K⁺ channel mutation. *J. Neurosci. Off. J. Soc. Neurosci.* 33, 12810–12824.

Liu, Y., Broman, J., and Edvinsson, L. (2008). Central projections of the sensory innervation of the rat middle meningeal artery. *Brain Res.* 1208, 103–110.

Lolicato, M., Riegelhaupt, P.M., Arrigoni, C., Clark, K.A., and Minor, D.L. (2014). Transmembrane helix straightening and buckling underlies activation of mechanosensitive and thermosensitive K(2P) channels. *Neuron* 84, 1198–1212.

Lolicato, M., Arrigoni, C., Mori, T., Sekioka, Y., Bryant, C., Clark, K.A., and Minor, D.L. (2018). K2P2.1 (TREK-1)-Activator Complexes Reveal a Cryptic Selectivity Filter Binding Site. *Biophys. J.* 114, 303a–304a.

Long, H., Liao, L., Zhou, Y., Shan, D., Gao, M., Huang, R., Yang, X., and Lai, W. (2017). A novel technique of delivering viral vectors to trigeminal ganglia in rats. *Eur. J. Oral Sci.* 125, 1–7.

Loots, E., and Isacoff, E.Y. (1998). Protein Rearrangements Underlying Slow Inactivation of the Shaker K⁺ Channel. *J. Gen. Physiol.* 112, 377–389.

Loots, E., and Isacoff, E.Y. (2000). Molecular coupling of S4 to a K⁽⁺⁾ channel's slow inactivation gate. *J. Gen. Physiol.* 116, 623–636.

Lopes, C.M.B., Rohács, T., Czirják, G., Balla, T., Enyedi, P., and Logothetis, D.E. (2005). PIP2 hydrolysis underlies agonist-induced inhibition and regulates voltage gating of two-pore domain K⁺ channels. *J. Physiol.* 564, 117–129.

Loucif, A.J.C., Saintot, P.-P., Liu, J., Antonio, B.M., Zellmer, S.G., Yoger, K., Veale, E.L., Wilbrey, A., Omoto, K., Cao, L., et al. (2018). GI-530159, a novel, selective, mechanosensitive two-pore-domain potassium (K2P) channel opener, reduces rat dorsal root ganglion neuron excitability. *Br. J. Pharmacol.* 175, 2272–2283.

Louter, M.A., Bosker, J.E., Oosterhout, V., J, W.P., Zwet, V., W, E., Zitman, F.G., Ferrari, M.D., and Terwindt, G.M. (2013). Cutaneous allodynia as a predictor of migraine chronification. *Brain* 136, 3489–3496.

Lüscher, C., Jan, L.Y., Stoffel, M., Malenka, R.C., and Nicoll, R.A. (1997). G protein-coupled inwardly rectifying K⁺ channels (GIRKs) mediate postsynaptic but not presynaptic transmitter actions in hippocampal neurons. *Neuron* 19, 687–695.

van den Maagdenberg, A.M.J.M., Pietrobon, D., Pizzorusso, T., Kaja, S., Broos, L.A.M., Cesetti, T., van de Ven, R.C.G., Tottene, A., van der Kaa, J., Plomp, J.J., et al. (2004). A Cacna1a Knockin Migraine Mouse Model with Increased Susceptibility to Cortical Spreading Depression. *Neuron* 41, 701–710.

MacKenzie, G., Franks, N.P., and Brickley, S.G. (2015). Two-pore domain potassium channels enable action potential generation in the absence of voltage-gated potassium channels. *Pflugers Arch.* 467, 989–999.

Maher, B.H., Taylor, M., Stuart, S., Okolicsanyi, R.K., Roy, B., Sutherland, H.G., Haupt, L.M., and Griffiths, L.R. (2013). Analysis of 3 common polymorphisms in the KCNK18 gene in an Australian Migraine case-control cohort. *Gene* 528, 343–346.

Maingret, F., Patel, A.J., Lesage, F., Lazdunski, M., and Honoré, E. (1999). Mechano- or Acid Stimulation, Two Interactive Modes of Activation of the TREK-1 Potassium Channel. *J. Biol. Chem.* 274, 26691–26696.

Maingret, F., Patel, A.J., Lesage, F., Lazdunski, M., and Honoré, E. (2000). Lysophospholipids open the two-pore domain mechano-gated K⁽⁺⁾ channels TREK-1 and TRAAK. *J. Biol. Chem.* 275, 10128–10133.

Maingret, F., Patel, A.J., Lazdunski, M., and Honoré, E. (2001). The endocannabinoid anandamide is a direct and selective blocker of the background K⁽⁺⁾ channel TASK-1. *EMBO J.* 20, 47–54.

Maingret, F., Honoré, E., Lazdunski, M., and Patel, A.J. (2002). Molecular basis of the voltage-dependent gating of TREK-1, a mechano-sensitive K(+) channel. *Biochem. Biophys. Res. Commun.* 292, 339–346.

Mannuzzu, L.M., Moronne, M.M., and Isacoff, E.Y. (1996). Direct physical measure of conformational rearrangement underlying potassium channel gating. *Science* 271, 213–216.

Mao, Q., Yuan, J., Xiong, M., Wu, S., Chen, L., Bekker, A., Tao, Y.-X., and Yang, T. (2017). Role of dorsal root ganglion K2P1.1 in peripheral nerve injury-induced neuropathic pain. *Mol. Pain* 13.

Marsh, B., Acosta, C., Djouhri, L., and Lawson, S.N. (2012). Leak K⁺ channel mRNAs in dorsal root ganglia: Relation to inflammation and spontaneous pain behaviour. *Mol. Cell. Neurosci.* 49–531, 375–386.

Mathie, A. (2010). Ion channels as novel therapeutic targets in the treatment of pain. *J. Pharm. Pharmacol.* 62, 1089–1095.

Maylie, B., Bissonnette, E., Virk, M., Adelman, J.P., and Maylie, J.G. (2002). Episodic ataxia type 1 mutations in the human Kv1.1 potassium channel alter hKvbeta 1-induced N-type inactivation. *J. Neurosci. Off. J. Soc. Neurosci.* 22, 4786–4793.

Maylie, J., Bond, C.T., Herson, P.S., Lee, W.-S., and Adelman, J.P. (2004). Small conductance Ca²⁺-activated K⁺ channels and calmodulin. *J. Physiol.* 554, 255–261.

Mazella, J., Pétrault, O., Lucas, G., Deval, E., Béraud-Dufour, S., Gandin, C., El-Yacoubi, M., Widmann, C., Guyon, A., Chevet, E., et al. (2010). Spadin, a Sortilin-Derived Peptide, Targeting Rodent TREK-1 Channels: A New Concept in the Antidepressant Drug Design. *PLOS Biol.* 8, e1000355.

McClenaghan, C., Schewe, M., Aryal, P., Carpenter, E.P., Baukowitz, T., and Tucker, S.J. (2016). Polymodal activation of the TREK-2 K2P channel produces structurally distinct open states. *J. Gen. Physiol.* 147, 497–505.

Medhurst, A.D., Rennie, G., Chapman, C.G., Meadows, H., Duckworth, M.D., Kelsell, R.E., Gloger, I.I., and Pangalos, M.N. (2001). Distribution analysis of human two pore domain potassium channels in tissues of the central nervous system and periphery. *Brain Res. Mol. Brain Res.* 86, 101–114.

Miller, A.N., and Long, S.B. (2012). Crystal structure of the human two-pore domain potassium channel K2P1. *Science* 335, 432–436.

Miyamoto, T., Dubin, A.E., Petrus, M.J., and Patapoutian, A. (2009). TRPV1 and TRPA1 Mediate Peripheral Nitric Oxide-Induced Nociception in Mice. *PLOS ONE* 4, e7596.

Morenilla-Palao, C., Luis, E., Fernández-Peña, C., Quintero, E., Weaver, J.L., Bayliss, D.A., and Viana, F. (2014). Ion channel profile of TRPM8 cold receptors reveals a role of TASK-3 potassium channels in thermosensation. *Cell Rep.* 8, 1571–1582.

- Moskowitz, M.A., Bolay, H., and Dalkara, T. (2004). Deciphering migraine mechanisms: clues from familial hemiplegic migraine genotypes. *Ann. Neurol.* *55*, 276–280.
- Murbartián, J., Lei, Q., Sando, J.J., and Bayliss, D.A. (2005). Sequential phosphorylation mediates receptor- and kinase-induced inhibition of TREK-1 background potassium channels. *J. Biol. Chem.* *280*, 30175–30184.
- Nakajo, K., Ulbrich, M.H., Kubo, Y., and Isacoff, E.Y. (2010). Stoichiometry of the KCNQ1 - KCNE1 ion channel complex. *Proc. Natl. Acad. Sci.* *107*, 18862–18867.
- Natoli, J.L., Manack, A., Dean, B., Butler, Q., Turkel, C.C., Stovner, L., and Lipton, R.B. (2010). Global prevalence of chronic migraine: a systematic review. *Cephalalgia Int. J. Headache* *30*, 599–609.
- Nieto-Posadas, A., Picazo-Juárez, G., Llorente, I., Jara-Oseguera, A., Morales-Lázaro, S., Escalante-Alcalde, D., Islas, L.D., and Rosenbaum, T. (2011). Lysophosphatidic acid directly activates TRPV1 through a C-terminal binding site. *Nat. Chem. Biol.* *8*, 78–85.
- Noël, J., Zimmermann, K., Busserolles, J., Deval, E., Alloui, A., Diochot, S., Guy, N., Borsotto, M., Reeh, P., Eschalier, A., et al. (2009). The mechano-activated K⁺ channels TRAAK and TREK-1 control both warm and cold perception. *EMBO J.* *28*, 1308–1318.
- Noël, J., Sandoz, G., and Lesage, F. (2011). Molecular regulations governing TREK and TRAAK channel functions. *Channels* *5*, 402–409.
- Olesen, J., Burstein, R., Ashina, M., and Tfelt-Hansen, P. (2009). Origin of pain in migraine: evidence for peripheral sensitisation. *Lancet Neurol.* *8*, 679–690.
- Papa, A., Wan, L., Bonora, M., Salmena, L., Song, M.S., Hobbs, R.M., Lunardi, A., Webster, K., Ng, C., Newton, R.H., et al. (2014). Cancer-associated PTEN mutants act in a dominant-negative manner to suppress PTEN protein function. *Cell* *157*, 595–610.
- Papazian, D.M., Schwarz, T.L., Tempel, B.L., Jan, Y.N., and Jan, L.Y. (1987). Cloning of genomic and complementary DNA from Shaker, a putative potassium channel gene from *Drosophila*. *Science* *237*, 749–753.
- Papreck, J.R., Martin, E.A., Lazzarini, P., Kang, D., and Kim, D. (2012). Modulation of K2P3.1 (TASK-1), K2P9.1 (TASK-3), and TASK-1/3 heteromer by reactive oxygen species. *Pflugers Arch.* *464*, 471–480.
- Park, H., Kim, E.-J., Han, J., Han, J., and Kang, D. (2016). Effects of analgesics and antidepressants on TREK-2 and TRESK currents. *Korean J. Physiol. Pharmacol. Off. J. Korean Physiol. Soc. Korean Soc. Pharmacol.* *20*, 379–385.
- Parks, C., Schwingshackl, A., and Mancarella, S. (2017). TREK-1 Has a Protective Role against Global Ischemia-Reperfusion-Induced Cardiac Injury. *Biophys. J.* *112*, 426a.

Pastor, P.D.H., Du, X., Fazal, S., Davies, A.N., and Gomez, C.M. (2018). Targeting the CACNA1A IRES as a Treatment for Spinocerebellar Ataxia Type 6. *Cerebellum Lond. Engl.* 17, 72–77.

Patel, A.J., Honoré, E., Maingret, F., Lesage, F., Fink, M., Duprat, F., and Lazdunski, M. (1998). A mammalian two pore domain mechano-gated S-like K⁺ channel. *EMBO J.* 17, 4283–4290.

Patel, A.J., Maingret, F., Magnone, V., Fosset, M., Lazdunski, M., and Honoré, E. (2000). TWIK-2, an Inactivating 2P Domain K⁺ Channel. *J. Biol. Chem.* 275, 28722–28730.

Pereira, V., Busserolles, J., Christin, M., Devilliers, M., Poupon, L., Legha, W., Alloui, A., Aissouni, Y., Bourinet, E., Lesage, F., et al. (2014). Role of the TREK2 potassium channel in cold and warm thermosensation and in pain perception. *Pain* 155, 2534–2544.

Piechotta, P.L., Rapedius, M., Stansfeld, P.J., Bollepalli, M.K., Erhlich, G., Andres-Enguix, I., Fritzenschaft, H., Decher, N., Sansom, M.S.P., Tucker, S.J., et al. (2011). The pore structure and gating mechanism of K2P channels. *EMBO J.* 30, 3607–3619.

Plant, L.D., Zuniga, L., Araki, D., Marks, J.D., and Goldstein, S.A.N. (2012). Sumoylation Silences Heterodimeric TASK Potassium Channels Containing K2P1 Subunits in Cerebellar Granule Neurons. *Sci. Signal.* 5.

Pollema-Mays, S.L., Centeno, M.V., Ashford, C.J., Apkarian, A.V., and Martina, M. (2013). Expression of background potassium channels in rat DRG is cell-specific and down-regulated in a neuropathic pain model. *Mol. Cell. Neurosci.* 57, 1–9.

Pope, L., Arrigoni, C., Lou, H., Bryant, C., Gallardo-Godoy, A., Renslo, A.R., and Minor, D.L. (2018). Protein and Chemical Determinants of BL-1249 Action and Selectivity for K2P Channels. *ACS Chem. Neurosci.*

Pradhan, A.A., Smith, M.L., McGuire, B., Tarash, I., Evans, C.J., and Charles, A. (2014). Characterization of a novel model of chronic migraine. *Pain* 155, 269–274.

Preisig-Müller, R., Schlichthörl, G., Goerge, T., Heinen, S., Brüggemann, A., Rajan, S., Derst, C., Veh, R.W., and Daut, J. (2002). Heteromerization of Kir2.x potassium channels contributes to the phenotype of Andersen's syndrome. *Proc. Natl. Acad. Sci. U. S. A.* 99, 7774–7779.

Rainero, I., Rubino, E., Gallone, S., Zavarise, P., Carli, D., Boschi, S., Fenoglio, P., Savi, L., Gentile, S., Benna, P., et al. (2014). KCNK18 (TRESK) genetic variants in Italian patients with migraine. *Headache* 54, 1515–1522.

Rajan, S., Wischmeyer, E., Karschin, C., Preisig-Müller, R., Grzeschik, K.H., Daut, J., Karschin, A., and Derst, C. (2001). THIK-1 and THIK-2, a novel subfamily of tandem pore domain K⁺ channels. *J. Biol. Chem.* 276, 7302–7311.

Rajan, S., Preisig-Müller, R., Wischmeyer, E., Nehring, R., Hanley, P.J., Renigunta, V., Musset, B., Schlichthörl, G., Derst, C., Karschin, A., et al. (2002). Interaction with

14-3-3 proteins promotes functional expression of the potassium channels TASK-1 and TASK-3. *J. Physiol.* *545*, 13–26.

Rayaprolu, V., Royal, P., Stengel, K., Sandoz, G., and Kohout, S.C. (2018). Dimerization of the voltage-sensing phosphatase controls its voltage-sensing and catalytic activity. *J. Gen. Physiol.* jgp.201812064.

Renigunta, V., Zou, X., Kling, S., Schlichthörl, G., and Daut, J. (2014). Breaking the silence: functional expression of the two-pore-domain potassium channel THIK-2. *Pflüg. Arch. - Eur. J. Physiol.* *466*, 1735–1745.

Renigunta, V., Schlichthörl, G., and Daut, J. (2015). Much more than a leak: structure and function of K₂p-channels. *Pflugers Arch.* *467*, 867–894.

Rose, F.C. (1995). The history of migraine from Mesopotamian to Medieval times. *Cephalalgia Int. J. Headache* *15 Suppl 15*, 1–3.

Ruthirago, D., Julayanont, P., and Kim, J. (2017). Chapter 7.2 - Translational Correlation: Migraine. In *Conn's Translational Neuroscience*, P.M. Conn, ed. (San Diego: Academic Press), pp. 159–165.

Salinas, M., Reyes, R., Lesage, F., Fosset, M., Heurteaux, C., Romey, G., and Lazdunski, M. (1999). Cloning of a new mouse two-P domain channel subunit and a human homologue with a unique pore structure. *J. Biol. Chem.* *274*, 11751–11760.

Samengo, I., Currò, D., Barrese, V., Tagliatela, M., and Martire, M. (2014). Large conductance calcium-activated potassium channels: their expression and modulation of glutamate release from nerve terminals isolated from rat trigeminal caudal nucleus and cerebral cortex. *Neurochem. Res.* *39*, 901–910.

Sandoz, G., and Lesage, F. (2008). Protein complex analysis of native brain potassium channels by proteomics. *Methods Mol. Biol. Clifton NJ* *491*, 113–123.

Sandoz, G., Thümmler, S., Duprat, F., Feliciangeli, S., Vinh, J., Escoubas, P., Guy, N., Lazdunski, M., and Lesage, F. (2006). AKAP150, a switch to convert mechano-, pH- and arachidonic acid-sensitive TREK K⁺ channels into open leak channels. *EMBO J.* *25*, 5864–5872.

Sandoz, G., Tardy, M.P., Thümmler, S., Feliciangeli, S., Lazdunski, M., and Lesage, F. (2008). Mtap2 Is a Constituent of the Protein Network That Regulates Twik-Related K⁺ Channel Expression and Trafficking. *J. Neurosci.* *28*, 8545–8552.

Sandoz, G., Douguet, D., Chatelain, F., Lazdunski, M., and Lesage, F. (2009). Extracellular acidification exerts opposite actions on TREK1 and TREK2 potassium channels via a single conserved histidine residue. *Proc. Natl. Acad. Sci. U. S. A.* *106*, 14628–14633.

Sandoz, G., Bell, S.C., and Isacoff, E.Y. (2011). Optical probing of a dynamic membrane interaction that regulates the TREK1 channel. *Proc. Natl. Acad. Sci. U. S. A.* *108*, 2605–2610.

Sandoz, G., Levitz, J., Kramer, R.H., and Isacoff, E.Y. (2012). Optical control of endogenous proteins with a photoswitchable conditional subunit reveals a role for TREK1 in GABA(B) signaling. *Neuron* 74, 1005–1014.

Sano, Y., Inamura, K., Miyake, A., Mochizuki, S., Kitada, C., Yokoi, H., Nozawa, K., Okada, H., Matsushime, H., and Furuichi, K. (2003). A Novel Two-pore Domain K⁺ Channel, TRESK, Is Localized in the Spinal Cord. *J. Biol. Chem.* 278, 27406–27412.

Sauter, D.R.P., Sørensen, C.E., Rapedius, M., Brüggemann, A., and Novak, I. (2016). pH-sensitive K(+) channel TREK-1 is a novel target in pancreatic cancer. *Biochim. Biophys. Acta* 1862, 1994–2003.

Scheffer, H., Brunt, E.R.P., Mol, G.J.J., van der Vlies, P., Stulp, Verlind, E., Mantel, G., Averyanov, Y.N., Hofstra, R.M.W., and Buys, C.H.C.M. (1998). Three novel KCNA1 mutations in episodic ataxia type I families. *Hum. Genet.* 102, 464–466.

Schewe, M., Nematian-Ardestani, E., Sun, H., Musinszki, M., Cordeiro, S., Bucci, G., de Groot, B.L., Tucker, S.J., Rapedius, M., and Baukrowitz, T. (2016). A Non-canonical Voltage-Sensing Mechanism Controls Gating in K2P K⁺ Channels. *Cell* 164, 937–949.

Schreiber, M., and Salkoff, L. (1997). A novel calcium-sensing domain in the BK channel. *Biophys. J.* 73, 1355–1363.

Shiber, A., Döring, K., Friedrich, U., Klann, K., Merker, D., Zedan, M., Tippmann, F., Kramer, G., and Bukau, B. (2018). Cotranslational assembly of protein complexes in eukaryotes revealed by ribosome profiling. *Nature* 561, 268–272.

Shieh, C.-C., Coghlan, M., Sullivan, J.P., and Gopalakrishnan, M. (2000). Potassium Channels: Molecular Defects, Diseases, and Therapeutic Opportunities. *Pharmacol. Rev.* 52, 557–594.

Stackman, R.W., Hammond, R.S., Linardatos, E., Gerlach, A., Maylie, J., Adelman, J.P., and Tzounopoulos, T. (2002). Small Conductance Ca²⁺-Activated K⁺ Channels Modulate Synaptic Plasticity and Memory Encoding. *J. Neurosci.* 22, 10163–10171.

Steiner, T.J., Stovner, L.J., and Birbeck, G.L. (2013). Migraine: the seventh disabler. *J. Headache Pain* 14, 1.

Sun, X.-P., Schlichter, L.C., and Stanley, E.F. (1999). Single-channel properties of BK-type calcium-activated potassium channels at a cholinergic presynaptic nerve terminal. *J. Physiol.* 518, 639–651.

Suzuki, Y., Tsutsumi, K., Miyamoto, T., Yamamura, H., and Imaizumi, Y. (2017). Heterodimerization of two pore domain K⁺ channel TASK1 and TALK2 in living heterologous expression systems. *PLoS ONE* 12.

Talley, E.M., Sirois, J.E., Lei, Q., and Bayliss, D.A. (2003). Two-Pore-Domain (Kcnk) Potassium Channels: Dynamic Roles in Neuronal Function. *The Neuroscientist* 9, 46–56.

Thomas, D., Plant, L.D., Wilkens, C.M., McCrossan, Z.A., and Goldstein, S.A.N. (2008). Alternative translation initiation in rat brain yields K2P2.1 potassium channels permeable to sodium. *Neuron* 58, 859–870.

Thomsen, L.L., Brennum, J., Iversen, H.K., and Olesen, J. (1996). Effect of a nitric oxide donor (glyceryl trinitrate) on nociceptive thresholds in man. *Cephalalgia Int. J. Headache* 16, 169–174.

Thümmler, S., Duprat, F., and Lazdunski, M. (2007). Antipsychotics inhibit TREK but not TRAAK channels. *Biochem. Biophys. Res. Commun.* 354, 284–289.

Thurber, A.E., Nelson, M., Frost, C.L., Levin, M., Brackenbury, W.J., and Kaplan, D.L. (2017). IK channel activation increases tumor growth and induces differential behavioral responses in two breast epithelial cell lines. *Oncotarget* 8, 42382–42397.

de Tommaso, M., and Scirucchio, V. (2016). Migraine and Central Sensitization: Clinical Features, Main Comorbidities and Therapeutic Perspectives. *Curr. Rheumatol. Rev.* 12, 113–126.

Trainor, D.C., and Jones, R.C. (1966). Headaches in explosive magazine workers. *Arch. Environ. Health* 12, 231–234.

Tulleuda, A., Cokic, B., Callejo, G., Saiani, B., Serra, J., and Gasull, X. (2011). TRESK channel contribution to nociceptive sensory neurons excitability: modulation by nerve injury. *Mol. Pain* 7, 30.

Ulbrich, M.H., and Isacoff, E.Y. (2007). Subunit counting in membrane-bound proteins. *Nat. Methods* 4, 319–321.

Valiyaveetil, F.I., Leonetti, M., Muir, T.W., and Mackinnon, R. (2006). Ion selectivity in a semisynthetic K⁺ channel locked in the conductive conformation. *Science* 314, 1004–1007.

Vallee, N., Meckler, C., Risso, J.-J., and Blatteau, J.-E. (2012). Neuroprotective role of the TREK-1 channel in decompression sickness. *J. Appl. Physiol. Bethesda Md* 1985 112, 1191–1196.

Vallée, N., Lambrechts, K., De Maistre, S., Royal, P., Mazella, J., Borsotto, M., Heurteaux, C., Abraini, J., Risso, J.-J., and Blatteau, J.-E. (2016). Fluoxetine Protection in Decompression Sickness in Mice is Enhanced by Blocking TREK-1 Potassium Channel with the “spadin” Antidepressant. *Front. Physiol.* 7.

Veale, E.L., Rees, K.A., Mathie, A., and Trapp, S. (2010). Dominant negative effects of a non-conducting TREK1 splice variant expressed in brain. *J. Biol. Chem.* 285, 29295–29304.

Verkest, C., Piquet, E., Diochot, S., Dauvois, M., Lanteri-Minet, M., Liguoglia, E., and Baron, A. (2018). Effects of systemic inhibitors of acid-sensing ion channels 1 (ASIC1) against acute and chronic mechanical allodynia in a rodent model of migraine. *Br. J. Pharmacol.* 175, 4154–4166.

- Vgontzas, A., and Burch, R. (2018). Episodic Migraine With and Without Aura: Key Differences and Implications for Pathophysiology, Management, and Assessing Risks. *Curr. Pain Headache Rep.* 22, 78.
- Viatchenko-Karpinski, V., Ling, J., and Gu, J.G. (2018). Characterization of temperature-sensitive leak K⁺ currents and expression of TRAAK, TREK-1, and TREK2 channels in dorsal root ganglion neurons of rats. *Mol. Brain* 11.
- Vierra, N.C., Dadi, P.K., Milian, S.C., Dickerson, M.T., Jordan, K.L., Gilon, P., and Jacobson, D.A. (2017). TALK-1 channels control β cell endoplasmic reticulum Ca²⁺ homeostasis. *Sci Signal* 10, eaan2883.
- Vilotti, S., Vana, N., Van den Maagdenberg, A.M.J.M., and Nistri, A. (2016). Expression and function of calcitonin gene-related peptide (CGRP) receptors in trigeminal ganglia of R192Q Cacna1a knock-in mice. *Neurosci. Lett.* 620, 104–110.
- Voloshyna, I., Besana, A., Castillo, M., Matos, T., Weinstein, I.B., Mansukhani, M., Robinson, R.B., Cordon-Cardo, C., and Feinmark, S.J. (2008). TREK-1 is a novel molecular target in prostate cancer. *Cancer Res.* 68, 1197–1203.
- Watkins, C.S., and Mathie, A. (1996). A non-inactivating K⁺ current sensitive to muscarinic receptor activation in rat cultured cerebellar granule neurons. *J. Physiol.* 491, 401–412.
- Waxman, S.G., and Zamponi, G.W. (2014). Regulating excitability of peripheral afferents: emerging ion channel targets. *Nat. Neurosci.* 17, 153–163.
- Wei, A., Solaro, C., Lingle, C., and Salkoff, L. (1994). Calcium sensitivity of BK-type KCa channels determined by a separable domain. *Neuron* 13, 671–681.
- Wells, J.N., Bergendahl, L.T., and Marsh, J.A. (2015). Co-translational assembly of protein complexes. *Biochem. Soc. Trans.* 43, 1221–1226.
- Wessman, M., Terwindt, G.M., Kaunisto, M.A., Palotie, A., and Ophoff, R.A. (2007). Migraine: a complex genetic disorder. *Lancet Neurol.* 6, 521–532.
- Williams, S., Bateman, A., and O'Kelly, I. (2013). Altered Expression of Two-Pore Domain Potassium (K2P) Channels in Cancer. *PLOS ONE* 8, e74589.
- Woo, D.H., Han, K.-S., Shim, J.W., Yoon, B.-E., Kim, E., Bae, J.Y., Oh, S.-J., Hwang, E.M., Marmorstein, A.D., Bae, Y.C., et al. (2012). TREK-1 and Best1 channels mediate fast and slow glutamate release in astrocytes upon GPCR activation. *Cell* 151, 25–40.
- Xiao, Y., Richter, J.A., and Hurley, J.H. (2008). Release of glutamate and CGRP from trigeminal ganglion neurons: Role of calcium channels and 5-HT₁ receptor signaling. *Mol. Pain* 4, 12.
- Yamamoto, Y., Hatakeyama, T., and Taniguchi, K. (2009). Immunohistochemical colocalization of TREK-1, TREK-2 and TRAAK with TRP channels in the trigeminal ganglion cells. *Neurosci. Lett.* 454, 129–133.

Yan, J., and Aldrich, R.W. (2010). LRRC26 auxiliary protein allows BK channel activation at resting voltage without calcium. *Nature* 466, 513–516.

Yang, S.-B., and Jan, L.Y. (2008). Thrilling Moment of an Inhibitory Channel. *Neuron* 58, 823–824.

Yoo, S., Liu, J., Sabbadini, M., Au, P., Xie, G., and Yost, C.S. (2009). Regional expression of the anesthetic-activated potassium channel TRESK in the rat nervous system. *Neurosci. Lett.* 465, 79–84.

Yoshimura, K., and Sokabe, M. (2010). Mechanosensitivity of ion channels based on protein–lipid interactions. *J. R. Soc. Interface* 7, S307–S320.

Zeng, X.-H., Yang, C., Xia, X.-M., Liu, M., and Lingle, C.J. (2015). SLO3 auxiliary subunit LRRC52 controls gating of sperm KSPER currents and is critical for normal fertility. *Proc. Natl. Acad. Sci. U. S. A.* 112, 2599–2604.

Zhang, G.-M., Wan, F.-N., Qin, X.-J., Cao, D.-L., Zhang, H.-L., Zhu, Y., Dai, B., Shi, G.-H., and Ye, D.-W. (2015). Prognostic significance of the TREK-1 K2P potassium channels in prostate cancer. *Oncotarget* 6, 18460–18468.

Zhou, J., Yang, C.-X., Zhong, J.-Y., and Wang, H.-B. (2013). Intrathecal TRESK gene recombinant adenovirus attenuates spared nerve injury-induced neuropathic pain in rats. *NeuroReport* 24, 131.

Zhou, J., Chen, H., Yang, C., Zhong, J., He, W., and Xiong, Q. (2017). Reversal of TRESK Downregulation Alleviates Neuropathic Pain by Inhibiting Activation of Gliocytes in the Spinal Cord. *Neurochem. Res.* 42, 1288–1298.

Zhou, M., Xu, G., Xie, M., Zhang, X., Schools, G.P., Ma, L., Kimelberg, H.K., and Chen, H. (2009). TWIK-1 and TREK-1 are potassium channels contributing significantly to astrocyte passive conductance in rat hippocampal slices. *J. Neurosci. Off. J. Soc. Neurosci.* 29, 8551–8564.

Zhuo, R.-G., Peng, P., Liu, X.-Y., Yan, H.-T., Xu, J.-P., Zheng, J.-Q., Wei, X.-L., and Ma, X.-Y. (2016). Allosteric coupling between proximal C-terminus and selectivity filter is facilitated by the movement of transmembrane segment 4 in TREK-2 channel. *Sci. Rep.* 6.

Zobel, C., Cho, H.C., Nguyen, T.-T., Pekhletski, R., Diaz, R.J., Wilson, G.J., and Backx, P.H. (2003). Molecular dissection of the inward rectifier potassium current (IK1) in rabbit cardiomyocytes: evidence for heteromeric co-assembly of Kir2.1 and Kir2.2. *J. Physiol.* 550, 365–372.

Migraine - Diagnosis and treatment - Mayo Clinic.